UNIVERSITY OF LEEDS

Characterising the Emission and Dispersion of Aerosols from the Toilet Plume and Quantification of the Associated Infection Risk

Ciara Angel Higham

University of Leeds

EPSRC Centre for Doctoral Training in Fluid Dynamics

Submitted in accordance with the requirements for the degree of

Doctor of Philosophy

May, 2025

Intellectual Property and Publication Statements

The candidate confirms that the work submitted is her own and that appropriate credit has been given where reference has been made to the work of others.

This work was undertaken on ARC4, part of the High Performance Computing facilities at the University of Leeds, UK.

The work in Chapters 3 and 4 of the thesis has appeared in publication as follows:

> Ciara A. Higham, Martín López-García, Catherine J. Noakes, Emma Tidswell, Louise Fletcher. A Quantitative Microbial Risk Assessment (QMRA) framework for exposure from toilet flushing using experimental aerosol concentration measurements. *Indoor Environments*. 2025, **2**(1), article no: 1000069. Available from: https://doi.org/10.1016/j.indenv.2024.100069.

For the above publication, the candidate was responsible for conceptualising the study, analysing the data, developing the experimental and mathematical modelling methodology, conducting the investigation, and overseeing project administration, as well as data validation and visualisation. The candidate also led the writing, including both the original draft and subsequent revisions. The other authors advised on the study's conceptualisation and the experimental and mathematical modelling methodology and contributed to reviewing and editing the manuscript.

Acknowledgements

I would first like to thank my supervisors, Dr Louise Fletcher, Prof. Cath Noakes, and Dr Martín López-García, for their support and insightful ideas throughout this project. Their guidance has helped shape my research, and I am incredibly grateful for their encouragement and expertise.

I am also very thankful to the Centre for Doctoral Training (CDT) in Fluid Dynamics. Their support has extended beyond academia, helping me navigate both my research and my interests in outreach and policy. A special thank you to my CDT cohort, whose friendship and support have made this journey so much more enjoyable. They have shown me that laughter truly is the best medicine when times are tough.

I would also like to express my gratitude to the laboratory staff, both past and present, in the Analytical Services Team, particularly Ms Emma Tidswell. No question ever felt too trivial, and their warm, friendly, and supportive environment made it a great place to work.

A huge thank you to my nephews, Dylan and Lucas, who have unknowingly helped me through stressful periods with their kind-hearted, humorous nature. I hope that as you grow up, I can inspire you to pursue your dreams, whatever they may be.

My deepest gratitude goes to my mum, who has been with me every step of the way. From my very first days at school to figuring out A-level choices, university applications, and eventually this PhD. We may not always have known where to start, but we have always found out what questions to ask and who to ask them to.

Finally, it is hard to imagine completing this PhD without my partner Arun, whose patience seems to have no limits, especially in these past few months. Not only has he supported me emotionally throughout this journey, but he has made every effort to understand my work, talking through my ideas and offering thoughtful conversation. He has brought sunshine to my cloudy days and celebrated my wins more than anyone.

Abstract

Toilet flushing is known to generate aerosol plumes that can contain pathogenic microorganisms, and shared toilet facilities have been implicated in the transmission of infectious diseases. However, few studies have quantified the infection risks posed by these aerosols or investigated in detail how they disperse after flushing.

This thesis presents an integrated analysis of airborne infection risks associated with toilet plume aerosols, combining controlled experimental studies, quantitative microbial risk assessment (QMRA), and computational fluid dynamics (CFD) simulations. The aim is to investigate aerosol generation, dispersion, and mitigation strategies in shared toilet settings.

Controlled chamber experiments were conducted using a gravity-flow, close-coupled toilet, with and without a cubicle enclosure over a range of ventilation rates. The generation of aerosols was characterised by flushing a salt solution, revealing a large proportion of smaller particles ($<5\,\mu m$). Particle concentrations peaked in the first 1 min after flushing and returned to background levels within 10 min. Bioaerosol sampling using *Escherichia coli* showed that most bacteria were released in the first 5 min after flushing, with ventilation rates having a modest influence on airborne concentrations. Continuous but low-level bacterial deposition suggested cumulative risks from surface contamination.

A QMRA framework was developed to assess the infection risks associated with single flushing events, accounting for transient aerosol dynamics and realistic occupancy durations. Two models were developed: one combining particle concentrations with estimated viral loads, and another using measured bioaerosol data. When applied to the experimental results, these models suggested non-negligible infection risks, particularly for pathogens present at high faecal concentrations, such as norovirus. The introduction of short delays (>1 min) between toilet users significantly reduced the estimated infection risks.

CFD simulations further examined aerosol dispersion and exposure risks, demonstrating how room layout, ventilation rate, and outlet positioning influence aerosol removal. Optimised ventilation strategies, including increased airflow and repositioned outlets, substantially reduced airborne particle concentrations.

This research provides new insights and robust methods to evaluate and mitigate airborne infection risks from toilet plume aerosols, with implications for public health guidance and the design of safer shared toilet environments.

Contents

List of Figures

List of Tables

Acronyms

ACH	Air Changes per Hour
AoA	Age of Air
ATCC	American Type Culture Collection
BLO	Bronchiolar, Laryngeal, Oral
CFD	Computational Fluid Dynamics
CFU	Colony Forming Units
DPM	Discrete Phase Model
DRW	Discrete Random Walk
EBC	Exhaled Breath Condensate
EDIS	Expiratory Droplet Investigation System
EPA	Environmental Protection Agency
FOM	Flushometer
gc	Genome Copies
HAdV	Human Adenovirus
HCW	Healthcare Workers
HEPA	High-Efficiency Particulate Air
HET	High-Efficiency Toilet
LAMP	Loop-Mediated Isothermal Amplification
MCE	Mixed Cellulose Ester
MMPD	Multiple-Path Particle Dosimetry
NHS	National Health Service
OPC	Optical Particle Counter
PAT	Pressure-Assisted Toilet
PCR	Polymerase Chain Reaction
PFU	Plaque Forming Units
PPE	Personal Protective Equipment
PVC	Polyvinyl Chloride
QMRA	Quantitative Microbial Risk Assessment

RANS Reynolds Averaged Navier-Stokes

RNA Ribonucleic Acid

RNG Renormalisation Group

RSM Reynolds Stress Model

SMA Snow Mountain Agent

SST Shear-Stress Transport

TSA Tryptone Soya Agar

TSB Tryptone Soya Broth

UK United Kingdom

US United States of America

UVGI Ultraviolet Germicidal Irradiation

VOF Volume of Fluid

WHO World Health Organization

WWTP Wastewater Treatment Plant

Chapter 1

Introduction

1.1 Background and Motivation

Flushing the toilet generates aerosols [2, 6, 7, 8, 9], referred to as the toilet plume, which can contain pathogenic microorganisms, including viruses and bacteria [10, 11, 12, 13]. These bioaerosols can remain airborne for extended periods, with the potential to be inhaled, or they can deposit on surfaces, contributing to contact transmission through hand contact with the eyes, nose, or mouth.

Faecal matter can harbour a wide range of pathogens [14], some of which remain viable in aerosolised form, raising concerns about airborne disease transmission. Transmission has been associated with exposure to faecal matter for a variety of pathogens including bacteria such as *Escherichia coli* (*E. coli*) [15] and *Clostridium difficile* (*C. difficile*) [16] and viruses such as norovirus [17], rotavirus [18], SARS-CoV [19] and SARS-CoV-2 [20]. Depending on the pathogen, exposure to these bioaerosols may result in infections ranging from asymptomatic cases to severe illness or death. Although pathogens from faecal matter are a concern, aerosols generated by flushing may also originate from vomit and can contain high concentrations of infectious viruses such as norovirus [21]. Additionally, toilets can pose a secondary exposure risk for respiratory pathogens. An infected individual may exhale particles containing infectious pathogens in a confined space in a toilet facility, highlighting the potential for exposure beyond aerosols containing faecal matter.

The specific contribution of toilet plume aerosols to disease transmission remains poorly characterised but many faecal-oral pathogens responsible for significant disease burdens can be aerosolised and transmitted through the environment. Certain populations, including young children, older adults, immunocompromised individuals and those in high-exposure environments, are particularly vulnerable to infection.

Norovirus is a leading cause of gastroenteritis, accounting for approximately one in five cases worldwide [22], and is the second largest contributor to gastrointestinal hospital burden in England [23]. Outbreaks occur frequently in healthcare settings, schools, cruise ships, and other settings where individuals are in close contact [24]. Young children, the elderly and immunocompromised individuals are considered the most vulnerable individuals for norovirus infection [24]. In the United King-

dom (UK), reported norovirus cases are increasing year on year, with laboratory confirmed cases in the first eight weeks of 2025 more than double the previous five-season average [25]. Norovirus infections tend to peak in winter, leading to significant strain on the National Health Service (NHS), ward closures, and increased bed occupancy. In late January 2025, hospital bed occupancy due to norovirus was higher than in the previous year [26], exacerbating pressures on healthcare resources. Norovirus primarily spreads through direct contact and ingestion via the faecal-oral route but it has also been detected in airborne samples in hospital toilet facilities [27], suggesting a possible airborne transmission route.

Rotavirus, another major cause of viral gastroenteritis, has seen a global decline due to widespread vaccination programmes. Before vaccination, it was the leading cause of gastroenteritis in children under the age of five years old worldwide [28]. Despite reductions in high-income countries, rotavirus remains a significant burden in developing regions, with an estimated 450,000 deaths, more than 2 million hospitalisations, and 25 million outpatient cases annually [29]. More than 90 % of deaths occur in developing countries in Asia and Africa. Direct faecal-oral transmission is considered the primary route but airborne transmission has also been suggested, with rotavirus ribonucleic acid (RNA) detected in air samples in a nursery [30].

SARS-CoV-2, the virus responsible for COVID-19, has caused more than 7 million deaths worldwide since its emergence in 2019. While infection severity and mortality rates have declined, SARS-CoV-2 is transitioning to a seasonal pattern similar to influenza [31]. In the height of the COVID-19 pandemic, hospitals were overwhelmed, reaching bed capacity limits in many regions. This led to postponed elective treatments and extended waiting lists. In the UK, the NHS waiting list increased by 2.2 million in the eight years before the pandemic, but increased by 2.6 million within just 32 months after its onset [31]. Vulnerable groups, including older adults, people with pre-existing conditions (such as diabetes, heart disease, and respiratory illnesses), those with lower incomes, and immunocompromised individuals, faced elevated risks of COVID-19 infection and mortality [32]. Multiple studies have detected SARS-CoV-2 RNA in faecal matter, with evidence of viral shedding

that continues in some individuals for several weeks following infection, even after symptoms subside [20, 33]. Faecal viral RNA does not necessarily indicate infectious virus, but several studies have successfully cultured viable SARS-CoV-2 from faeces, supporting the possibility of faecal-oral transmission [20]. Epidemiological studies have also linked aerosolised faecal matter to COVID-19 outbreaks, suggesting that the toilet plume could serve as a potential transmission route.

Bacterial pathogens such as *E. coli*, non-typhoidal *Salmonella* and *Shigella* are frequently found in faeces and are leading causes of foodborne and waterborne infections. Depending on the site of infection, a variety of symptoms can occur including diarrhoea, urinary tract infections, pneumonia and sepsis [34]. *E. coli* bloodstream infections reported by the UK Health Security Agency [35] rose from 60.4 per 100,000 in 2012–13 to 73.8 per 100,000 in 2023–24. Antibiotic resistance is thought to further increase the number of bacterial infections. An increase in *E. coli* infections can lead to excess morbidity, mortality, longer hospital stays, and higher healthcare costs [36]. *E. coli* bacteria generally exist in the body without causing disease, but exposure to certain types can lead to disease and illness [37]. *E. coli* O157:H7 can cause severe diarrhoea, abdominal cramps and in extreme cases can lead to kidney failure. *E. coli* O157:H7 has been seen to spread via the faecal-oral route [15].

If these pathogens are transmitted through exposure to toilet plume aerosols, even a modest reduction in transmission could help prevent thousands of infections annually. Given the economic burden of these infections, including healthcare costs, lost productivity, and the impact on public health services, further research into mitigation strategies is appropriate. This is particularly important for vulnerable populations, including young children, older adults, immunocompromised individuals, and those in high-exposure environments such as hospitals and care homes.

Although direct epidemiological evidence linking toilet plume aerosols to infection is limited, outbreak investigations suggest a role for airborne faecal transmission. These include an outbreak of SARS-CoV in Hong Kong in 2003 [38] and an outbreak of SARS-CoV-2 in China in 2020 [39]. Details of these and other epidemiological evidence for the transmission of faecal pathogens are discussed in Chapter 2.

Shared toilet facilities, particularly in high-occupancy settings (e.g. concerts, football matches) experience high-occupancy and high-frequency use over short periods of time [40]. These conditions create opportunities for disease transmission, with the potential for multiple infectious individuals and multiple susceptible individuals entering the facility, yet the contribution of toilet plume aerosols to infection risk remains poorly characterised. Beyond public events, toilet facilities in healthcare settings also pose a particular risk, especially for vulnerable populations such as hospital patients, immunocompromised individuals, and the elderly. Numerous studies have identified potential links between toilet use and pathogen transmission in a variety of environments [41, 42, 43, 44, 45, 46, 47, 48, 49, 50, 51].

Understanding the mechanisms of pathogen dispersal, the role of ventilation, and the risk of exposure is essential to develop effective mitigation strategies. Insights from this research could inform toilet facility design, ventilation guidelines and infection control policies, offering evidence for public health officials and policymakers looking to reduce disease burden and alleviate pressures on healthcare systems.

1.2 Research Aim and Objectives

This study aims to evaluate the infection risk associated with exposure to airborne toilet plume aerosols and to determine how room layout and ventilation influence aerosol dispersion, bioaerosol persistence, and exposure. By integrating experimental measurements, quantitative risk modelling, and Computational Fluid Dynamics (CFD) simulations, this research seeks to improve the understanding of toilet plume transmission pathways and inform practical mitigation strategies to reduce infection risks in shared toilet facilities. The objectives of this research are as follows:

1. Characterise the size distribution and concentration of aerosols generated by flushing a typical UK toilet (gravity-flow close-coupled toilet).
    - Quantify the concentration and size distribution of aerosols and bioaerosols generated by toilet flushing in a controlled chamber.
    - Evaluate how different room layouts and ventilation rates influence aerosol dispersion and bioaerosol concentrations.

2. Quantify the infection risk from exposure to airborne toilet plume particles using a stochastic risk modelling framework.
    - Estimate the infection risk for norovirus and SARS-CoV-2 based on measured aerosol concentrations and published pathogen data.
    - Assess infection risk from bioaerosols using *E. coli* as a surrogate pathogen.
3. Simulate aerosol dispersion and exposure risk in a shared toilet environment using CFD.
    - Predict the dispersion and residence time of aerosols under different ventilation conditions and room layouts over a 10 min period.
    - Estimate individual exposure risk by simulating a person entering the toilet after flushing and determining the impact of ventilation and room design on exposure.
4. Identify practical approaches to reduce exposure to airborne toilet plume aerosols in shared toilet facilities.
    - Assess the effectiveness of different mitigation strategies, such as optimising ventilation placement and adjusting entry times between users, based on insights from experimental, risk modelling, and CFD studies.

1.3 Thesis Outline

This thesis investigates aerosol generation from the toilet plume and the associated transmission risks, using experimental, computational, and risk assessment approaches. The following chapters present the research conducted in this thesis:

- Chapter 2 provides a comprehensive literature review, examining prior research on toilet plume and exhaled aerosols, their role in pathogen transmission, and methodologies used to study them experimentally, computationally, and through risk modelling.
- Chapter 3 details the experimental investigations conducted in a controlled chamber to examine toilet plume aerosol dispersion. Two scenarios were tested: one with two cubicles and one without cubicles, under different ventilation regimes. This chapter presents findings from both particle concentration mea-

surements and bioaerosol sampling using *E. coli*.

- Chapter 4 applies a Quantitative Microbial Risk Assessment (QMRA) methodology to the experimental data, estimating the probability of infection for the different scenarios and ventilation regimes. This includes risk estimates for both particle concentration data and bioaerosol data.
- Chapter 5 models the experimental setup using CFD in ANSYS Fluent, simulating aerosol dispersion and evaluating exposure risks to a susceptible individual under the same conditions.
- Chapter 6 combines the key findings of the experimental, risk assessment, and computational studies, highlighting their implications for infection control strategies and future research directions.

This structured approach provides a comprehensive evaluation of toilet plume airborne transmission, integrating multiple methodologies to assess infection risks and mitigation strategies.

Chapter 2

Literature Review

2.1 Introduction

This chapter provides a comprehensive review of the existing literature on disease transmission, with a particular focus on the potential for pathogen spread through the toilet plume. The review begins with an overview of general disease transmission mechanisms, including airborne and contact transmission routes. It then examines the evidence for aerosol and bioaerosol generation during toilet flushing, highlighting experimental studies that have quantified particle release and dispersion.

The presence of viable pathogens in faecal matter and their potential for aerosolisation are also discussed, drawing on microbiological studies that have identified bacteria and viruses in faeces and wastewater. Although faecal pathogens have been sampled from aerosols, there is limited evidence on their infectivity after airborne transport.

To assess the infection risks associated with exposure to toilet plume aerosols, this chapter reviews QMRA studies that estimate the risk of infection based on experimental data. Although QMRA has been widely applied in various settings, including healthcare facilities, transportation, and wastewater treatment plants, its application to toilet plume aerosols remains limited, with studies often relying on preexisting particle concentration data rather than controlled chamber experiments.

The use of CFD simulations in studying indoor airflows and particle dispersion is also explored. CFD methods have proven valuable in assessing airborne and fomite transmission risks, and some recent studies have applied them to model aerosol dispersion in toilet facilities. However, CFD modelling of toilet plume aerosols is still in its early stages, with few studies incorporating detailed room layouts or directly evaluating human exposure.

Finally, this chapter identifies key gaps in the literature that remain unresolved, particularly in linking toilet plume aerosols to infection risks, understanding the role of ventilation and cubicle structures in mitigating exposure, and refining experimental and computational methods to improve risk assessments. Addressing these gaps will contribute to a better understanding of disease transmission dynamics in toilet facilities and inform strategies to reduce infection risks in shared toilet environments.

2.2 Dynamics of Disease Transmission

When a susceptible individual enters an environment, such as a toilet facility or another shared space, there are multiple pathways through which they can be exposed to infectious pathogens. If exposure leads to infection, the susceptible individual can develop disease, with symptoms varying in severity. This section outlines the mechanisms by which an environment can become contaminated by an infected individual and how a susceptible individual can then be exposed to these pathogens.

2.2.1 Types of Emission

Emission Through the Toilet Plume

When an infected individual uses a toilet facility, aerosols containing pathogens can be released into the environment during flushing. These pathogens can originate from the individual's faecal matter or vomit (see Section 2.3). Contamination of the flush water can also contribute to aerosolised pathogens (e.g. *Legionella* and non-tuberculous mycobacteria) however, this pathway is not considered in this thesis.

Johnson et al. [2] investigated the amount of particles generated by flushing various modern toilets and found that up to 145,000 droplets were produced per flush. Of these, 95 % were less than 2 µm, and more than 99 % were less than 5 µm. Other studies have also quantified the number of particles released by flushing the toilet, further confirming the generation of airborne droplets [2, 6, 7, 8, 9].

Beyond particle quantification, Crimaldi et al. [52] provided visual evidence of the toilet plume using laser imaging techniques, capturing its dispersion over time. This direct visualisation reinforces the role of flushing in aerosol generation and potential pathogen transmission in shared toilet environments.

Multiple studies have demonstrated that droplets and aerosols generated by toilet flushing can contain pathogens as large as bacteria [10, 11, 53, 54]. Jessen [53] was the first to show that aerosols from the toilet plume could carry pathogens. In their study, toilets containing *Serratia marcescens* (*S. marcescens*) were flushed, and agar plates were used to capture settling aerosols, while a slit impactor collected airborne particles. Positive bioaerosol counts were detected for at least 8 min. Similarly,

Darlow and Bale [11] flushed toilets seeded with *S. marcescens* and used a slit sampler and a liquid impinger to assess contamination. Their findings showed that viable bacteria were still present in the air 12 min after flushing.

Gerba, Wallis, and Melnick [10] further explored disease transmission through the toilet plume. Their experiments involved seeding household toilets with either *E. coli* or MS2 bacteriophage (a viral surrogate) before flushing. Pathogens were detected on surfaces 4 h to 6 h after flushing, suggesting airborne persistence long enough for deposition throughout the bathroom. Within 0 h to 2 h of flushing, bacterial contamination was concentrated on plates closest to the toilet, but at later times pathogens were found across the room. This indicated that droplets could remain airborne for extended periods and travel throughout the space.

Emission Through Expiratory Activities

Although expired pathogens are not explicitly linked to toilet plume aerosols, an infected individual using a shared toilet facility may exhale particles containing pathogens, which can contaminate the air and surfaces. This could contribute to disease transmission alongside aerosolisation from toilet flushing.

Droplets and aerosols are released from the oral and nasal cavities during human expiratory activities, including breathing, coughing, sneezing, laughing, and talking. The concept that such activities generate fine airborne particles containing bacteria was first proposed in the late 19th century by Flügge [55], who described the release of fine 'dust' particles containing bacteria during speech, coughing, and sneezing.

Expiratory activities produce droplets of varying sizes that originate in distinct regions of the respiratory tract. Morawska et al. [56] used a novel Expiratory Droplet Investigation System (EDIS) to measure the size distributions of droplets generated during breathing, speech, and coughing. Their study identified distinct droplet size modes associated with different expiratory activities with each mode linked to specific physiological processes within the respiratory system.

Johnson et al. [57] classified expiratory aerosol generation into three primary mechanisms: bronchiolar film burst (B), laryngeal vibration (L), and oral cavity ejection (O). Bronchiolar aerosols are typically smaller, whereas larger droplets tend

to originate in the oral cavity. This classification, known as the BLO model, has been widely used in studies that model droplet release from expiratory activities [58, 59, 60, 61, 62]. Most aerosols in exhaled breath tend to be less than 4 µm with a median of 0.7 µm to 1 µm [63, 64].

Gregson et al. [65] investigated aerosol production across various expiratory activities using 25 professional singers. Their study measured particles ranging from 500 nm to 20 µm, sampling emissions during singing at different volumes, as well as breathing and coughing. They found that speaking and singing produced particle numbers that were similar orders of magnitude, while increasing vocal volume led to a significant increase in particle counts. Based on these findings, the authors recommended that public health organisations assess transmission risks at events based on sound volume rather than the specific type of expiratory activity. This study quantified the number and size of the particles, without measuring the actual viral load in exhaled breath.

Although particle size distributions from expiratory activities have been well documented, determining the presence and viability of pathogens within these particles is more complex. In addition, the distribution of pathogens across different particle sizes likely depends on the pathogen itself and its site of infection within the respiratory tract. Several studies have successfully recovered viral RNA and culturable virus from exhaled breath. Yan et al. [66] isolated both viral RNA and viable influenza virus from symptomatic volunteers with acute respiratory illness. Similarly, Lindsley et al. [67] detected viable influenza virus in aerosols generated by coughing, with the virus predominantly found in the smallest particle size fraction (0.3 µm to 0.8 µm).

During the COVID-19 pandemic, extensive research efforts focused on characterising the distribution of SARS-CoV-2 across particle sizes, leading to a large number of recent studies on this topic. Coleman et al. [68] investigated viral loads in coarse (> 5 µm) and fine (≤ 5 µm) expiratory aerosols. Patients with COVID-19 performed various activities (including breathing, talking, and singing) while facing a G-II exhaled breath collector, a cone shaped inlet that draws air around a partic-

ipant's head for sampling. SARS-CoV-2 RNA was detected in 13 participants, with substantial variation in viral load between individuals and across different activities. They found that 7 participants had a higher viral load from talking than from singing, which challenges recommendations that event transmission risks should be assessed based on sound volume rather than activity type. Viral load was also highest in participants in earlier stages of illness. Fine aerosols produced during talking and singing accounted for 85 % of the total viral load detected, suggesting that fine aerosols may play a more significant role in the transmission of SARS-CoV-2 than coarse ones.

Malik and Kunze [69] detected SARS-CoV-2 RNA in the exhaled breath of both asymptomatic and symptomatic individuals using an exhaled breath collection device. Their study found that asymptomatic individuals could exhibit greater viral shedding than symptomatic cases and that viral shedding did not necessarily correlate with the severity of symptoms.

Similarly, Lane et al. [70] collected SARS-CoV-2 RNA from exhaled breath in patients with COVID-19. They reported that viral RNA levels remained relatively high until at least day 8 of infection. In addition to SARS-CoV-2 and influenza, viral RNA has also been isolated from exhaled breath for rhinoviruses [71, 72].

Although multiple studies have successfully detected SARS-CoV-2 RNA in exhaled breath [68, 69, 70, 73], the isolation of viable virus remains more limited. The most recent successful culturing of SARS-CoV-2 from exhaled breath was reported by Alsved et al. [27], who isolated viable virus from three individuals and found that the viral source strength was highest during singing. Prior to this, both Lai et al. [74] and Adenaiye et al. [75] successfully cultured viable SARS-CoV-2 from exhaled breath.

Beyond viral pathogens, bacterial pathogens have also been detected in exhaled breath. Zheng et al. [76] developed a protocol that combined an exhaled breath condensate (EBC) device with loop-mediated isothermal amplification (LAMP) to detect bacterial pathogens. Their study identified *Haemophilus influenzae* (*H. influenzae*), *Pseudomonas aeruginosa* (*P. aeruginosa*), *E. coli*, *Staphylococcus aureus*

(*S. aureus*), and methicillin-resistant *S. aureus* (MRSA), with *H. influenzae* being the most frequently detected pathogen.

Fomite Contamination

A fomite is an object (surface, hand, floor, clothing, etc.) that is capable of carrying infectious pathogens [77]. In shared toilet settings, surface contamination is often considered in the context of pathogen transfer to a susceptible individual's hands. However, contamination can also occur when an individual enters the facility with already contaminated hands, clothing, or shoes. This contamination may originate from the individual's own infection or from prior contact with contaminated surfaces or infected individuals outside of the toilet facility.

If an individual's hands are contaminated, the extent of pathogen transfer to a surface depends on the transfer efficiency during hand-to-surface contact. This efficiency is influenced by factors such as type of contact, pressure, duration, hand surface area, relative humidity, surface type, and pathogen characteristics [5]. Textiles can also harbour both bacteria and viruses, with the potential for aerosolisation when disturbed [78]. In a toilet facility, disturbance of clothing, such as the removal of trousers and underwear, could release pathogens into the air or deposit them on nearby surfaces. In addition, shoe soles can act as a vector for the introduction of pathogens into the toilet environment [79].

2.2.2 Modes of Transmission

Modern Understanding of Transmission

Once particles containing pathogens are released into the environment from a contaminated or infected individual, they can be transmitted to others through various routes. The World Health Organization [1] (WHO) highlighted that during the COVID-19 pandemic, there was significant confusion about terminology used to describe transmission routes, particularly the term airborne transmission, due to a lack of consensus across disciplines, organisations, and the general public. They published a report in 2024 [1] to address this to establish a standardised terminology across disciplines. They defined the key modes of transmission as:

Through the air, illustrated in Fig. 2.1.

- *Airborne* - When particles containing pathogens remain suspended in the air or travel with airflows, they can be inhaled by a susceptible individual. This form of transmission can occur at both short and long distances from the source. Inhaled particles may deposit anywhere along the respiratory tract.
- *Direct deposition* - At short ranges, particles containing pathogens can follow semi-ballistic trajectories and deposit directly on the mucosa of the mouth, nose, or eyes.

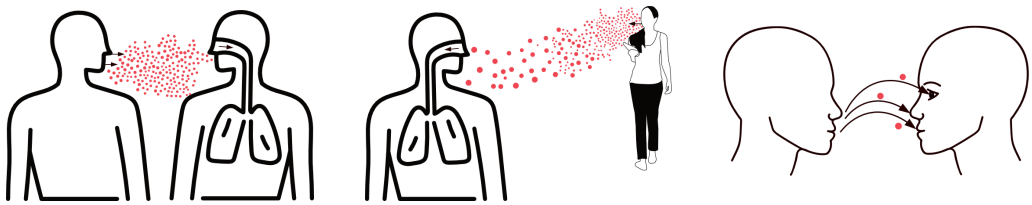

(a) Short-range airborne (b) Long-range airborne (c) Direct deposition

Figure 2.1: Illustrations adapted from World Health Organization [1] for 'through the air' modes of transmission.

Contact, illustrated in Fig. 2.2.

- *Direct contact* - Pathogen transfer occurs when a susceptible individual touches an infected source (usually with their hands), such as by shaking hands. The pathogen is transmitted when they touch their mouth, nose, or eyes.
- *Indirect contact* - Pathogen transfer occurs through an intermediate contaminated object (e.g. a door handle). The object may have become contaminated through direct fomite contact or aerosol deposition. Once a susceptible individual touches the contaminated surface, transmission occurs when they subsequently touch their mouth, nose, or eyes.

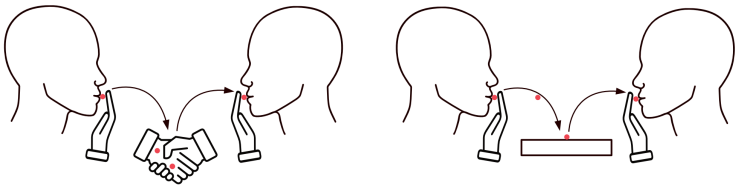

(a) Direct contact (b) Indirect contact

Figure 2.2: Illustrations adapted from World Health Organization [1] for 'contact' modes of transmission.

While these definitions have been suggested, communication of how transmission occurs is complex. These suggestions are relatively new, and there are still misunderstandings between different types of transmission. For example, short-range airborne transmission can often be neglected or categorised as direct deposition, with the incorrect assumption that exposure is through larger ballistic particles only.

Historical Understanding of Transmission

Wells [80] introduced the concept of distinct transmission routes based on droplet size. Their study determined that for droplets released from a height of 2 m, a critical size of 100 µm characterised their behaviour. They suggested that droplets larger than this size would settle as a result of gravity, while smaller droplets would evaporate, leaving behind droplet nuclei that could remain airborne for hours. This model is now known as the Wells curve. Although the study suggested a critical size of 100 µm, an arbitrary cut-off value of 5 µm is frequently cited to distinguish smaller airborne aerosols from larger ballistic droplets.

Randall et al. [81] reviewed the historical context of this 5 µm threshold in relation to transmission routes (airborne vs. contact transmission) and found that recommendations based on this value are not supported by contemporary scientific understanding. They traced the origin of this cut-off values to industrial hygiene studies from the 1930s and 1940s, including work by Sayers and Jones [82] and Wijk and Patterson [83], which suggested that only particles smaller than 5 µm could reach the deepest regions of the lungs. This led to an association between particle size and infectiousness.

Langmuir [84] further reinforced this threshold, arguing that particles larger than 5 µm are almost completely removed in the nose and upper respiratory tract, whereas smaller particles are more likely to reach the bronchioles and alveoli. Wells [85] later popularised this cut-off in the context of airborne transmission, focusing on the ability of particles smaller than 5 µm to reach the lungs. However, Randall et al. [81] found that modern interpretations often conflate understandings of this size cut-off. They found that what was originally a distinction based on which particles could reach the deeper regions of the lungs has since been misinterpreted

as a threshold to determine whether particles remain airborne.

Bourouiba [86] also highlighted issues with the arbitrary 5 µm cut-off. They argued that exhalation in particular should be modelled as a turbulent multiphase cloud, where initial particle trajectories are determined not by droplet size but by the characteristics of the warm, moist respiratory cloud. The subsequent dispersal of this cloud is then influenced by ambient background conditions.

It is crucial to consider particles larger than 5 µm when evaluating airborne transmission. In particular, Hou et al. [87] found that SARS-CoV-2 infection can be initiated in the nose and upper respiratory tract by particles exceeding 5 µm.

2.2.3 Factors Affecting Transmission

Several factors influence pathogen transmission in indoor environments, including environmental conditions, human behaviour, and pathogen characteristics. This section outlines the key factors that impact transmission risk.

Environmental Factors

Temperature - Temperature affects both pathogen viability and particle transport. Both Chin et al. [88] and Biryukov et al. [89] found that increasing the temperature reduced the survival time of SARS-CoV-2. Similarly, McEldowney and Fletcher [90] investigated bacterial (*Pseudomonas* sp., *Acinetobacter calcoaceticus*, a coryneform, *Staphylococcus* sp., and *S. aureus*) survival at 4 °C, 15 °C, and 25 °C, finding that survival was shortest at 25 °C and longest at 4 °C, suggesting increased viability at lower temperatures. Temperature also influences droplet evaporation and transport. Pal, Sarkar, and Mukhopadhyay [91] developed a model to study the effects of ambient temperature and relative humidity on respiratory droplet transport. The model showed that higher temperatures increase droplet evaporation, causing larger droplets to shrink into smaller sizes that can travel further in airflow as a result of increased buoyancy effects. Consequently, increased temperatures can reduce transmission via contact routes by promoting evaporation, but could also decrease pathogen viability in the environment and lead to increased airborne transmission.

Relative humidity - Pal, Sarkar, and Mukhopadhyay [91] also examined the role

of relative humidity in droplet transport, finding that lower humidity increased evaporation rates. This could enhance airborne transmission while reducing contact transmission. Similarly, Biryukov et al. [89] found that the survival times of SARS-CoV-2 were longer at lower humidity levels, suggesting that humidity may influence both pathogen persistence and transmission dynamics. Increasing relative humidity has also been shown to increase transfer efficiency [92] for contact transmission.

Airflow patterns - Airflow patterns determine how particles disperse within a space. When ambient airflows are minimal, particle trajectories follow the Wells curve [80], where larger particles settle quickly due to gravity, while smaller particles remain airborne due to buoyancy effects. However, in real-world environments, airflow dynamics influence these trajectories. Airflows can transport smaller particles over longer distances [93, 94], which usually reduces the risk in close proximity of the source. However, there can be an increased risk of exposure beyond the immediate vicinity of the source. Ventilation systems and air currents (e.g. wind) can alter particle transport, either dispersing particles throughout a room [95] or directing them away from susceptible individuals (discussed in Section 2.2.4). Thermal effects, such as plumes generated by body heat or differences in temperature between rooms [96], can create convective flows that impact particle dispersion.

Sunlight exposure - Sunlight (along with artificial ultraviolet radiation, discussed in Section 2.2.4), can inactivate pathogens and reduce transmission risk. Natural sunlight contains UV radiation, which has been shown to inactivate a variety of bacteria, including *Bacillus spp.*, *S. aureus*, *Mycobacterium tuberculosis*, and *Staphylococci* [97], as well as viruses such as SARS-CoV-2 [98] and influenza [99]. The effectiveness of sunlight in pathogen inactivation depends on factors such as UV intensity, duration of exposure, and pathogen type.

Behavioural Factors

Human behaviour plays an important role in transmission. In situations where exposure may occur, individual actions can either prevent or facilitate pathogen spread. Touching the face, particularly the nose, mouth and eyes, increases the

likelihood of transmission by transferring pathogens from contaminated surfaces to mucous membranes [100]. The frequency and nature of social interactions also influence transmission risks, as individuals with a higher number of social contacts or frequenting high-occupancy environments are more likely to be exposed to infectious agents [101].

Pathogen Specific Factors

Pathogen load - The viral or bacterial load of an infected individual is a key determinant of transmission risk. Higher viral loads have been associated with increased transmission for several viruses [102, 103, 104, 105, 106].

Pathogen survival - Pathogen survival depends on structural properties, environmental conditions, and surface type. Enveloped viruses, such as SARS-CoV-2 and influenza, are generally less stable, remaining infectious for hours to days [107]. In contrast, non-enveloped viruses like norovirus can persist for weeks to months [108]. Bacteria also exhibit varying survival times. Katzenberger, Rösel, and Vonberg [109] found that gram-positive bacteria, such as *S. aureus*, remained viable on inanimate surfaces for up to a week, whereas gram-negative bacteria, such as *E. coli*, were inactivated within two days.

2.2.4 Mitigation Strategies

When transmission is likely to occur, mitigation strategies can be used with the aim of reducing transmission. This section will outline a variety of mitigation measures that have been identified.

Environmental Controls

Ventilation - Ventilation is a recognised strategy for reducing transmission, achieved through mechanical or natural means by supplying or removing air from a given space [110]. Effective ventilation helps to remove particles containing pathogens, thereby reducing airborne transmission and surface contamination through aerosol deposition [111]. Lipinski et al. [112] reviewed ventilation strategies in high-occupancy buildings and found that systems relying on centralised air distribution and ceiling-

level air supply or recirculation provide optimal conditions for reducing transmission. However, natural or naturally assisted ventilation can also be effective in some settings. According to the UK Department for Levelling Up, Housing and Communities [113], bathrooms should be equipped with mechanical ventilation, although a window may suffice if the bathroom contains only a toilet. Despite these regulations, there is little data available on the compliance of ventilation standards in public toilets. One of the few investigations on ventilation performance in public toilet facilities, conducted by Roberts et al. [114], used carbon dioxide measurements as a proxy for ventilation and found that average air quality in toilets was good at most events, though there were peaks where air quality was considered poor during intervals or half-time breaks. However, this study focused on prestigious venues, which makes it unclear how representative these findings are for everyday settings. Poorly ventilated toilets have been associated with increased bacterial contamination. Lee and Tham [115] performed environmental sampling in toilet facilities and reported higher airborne and surface bacterial counts in settings with inadequate ventilation, suggesting that bacterial contamination is influenced by ventilation effectiveness. Furthermore, inadequate ventilation in hospital bathrooms has been linked to outbreaks, with Jung et al. [116] associating SARS-CoV-2 transmission to a ventilation system failure in a hospital ward toilet. This highlights the need for further research on ventilation compliance and performance in public toilets, particularly in high-occupancy settings where airborne and contact transmission risks can be elevated.

Portable air cleaners - Portable air cleaners have been shown to reduce airborne transmission of pathogens. Li et al. [117] highlighted a variety of studies to support their effectiveness [118, 119, 120, 121, 122]. Evidence suggests that portable air filters can effectively remove respiratory-sized particles from the air, and they have been shown to reduce SARS-CoV-2 RNA concentrations in the air [123, 124, 125, 126]. In addition to reducing airborne transmission, portable air cleaners can also reduce fomite contamination by capturing particles that would otherwise settle on surfaces. Boswell and Fox [127] found that the use of a portable High-Efficiency

Particulate Air (HEPA) filtration device led to a reduction in MRSA surface contamination, suggesting that air filtration can play a role in reducing both airborne and contact transmission risks.

Ultraviolet-C (UVC) radiation - Ultraviolet Germicidal Irradiation (UVGI) is a form of UV-C radiation that inactivates microorganisms by inducing photochemical damage to their nucleic acids, preventing replication [128]. The germicidal effectiveness of UVGI peaks at 254 nm. However, exposure to these wavelengths can be harmful to human skin and eyes [129, 130]. Recent research has focused on Far-UVC, a specific wavelength of 222 nm, which is mostly absorbed before reaching the deeper layers of the skin or the eye lens, reducing the risk of harm [131]. Studies have demonstrated that Far-UVC effectively inactivates airborne pathogens [129, 132, 133], and one study has shown its ability to deactivate SARS-CoV-2 on surfaces [134]. Furthermore, Kaple et al. [135], Bang et al. [136], and Kitagawa et al. [137] have shown that Far-UVC can reduce airborne and surface pathogen contamination in toilet facilities. Although Far-UVC shows promise as a transmission mitigation strategy, more research is needed, particularly on long-term safety and practical implementation, before widespread adoption.

Cleaning surfaces - Surface cleaning can reduce transmission by removing pathogens and lowering the risk of contact transmission. Cleaning refers to the physical removal of dirt, oils, and debris using soap or detergent wipes, while disinfection is an enhanced cleaning method that eliminates or reduces pathogens on surfaces [138]. A review by Donskey [139] found strong evidence supporting environmental disinfection as an effective strategy for infection control. Targeted cleaning measures in toilet environments have also been shown to reduce contamination. Sassi et al. [140] found that the addition of disinfectant to the toilet bowl before flushing reduced surface contamination both inside the bowl and on surfaces in the surrounding environment. Similarly, Goforth et al. [43] reported that scrubbing the toilet bowl with a brush together with disinfectant reduced contamination in both the bowl water and on the toilet brush itself. However, it has been proposed that cleaning tools in toilet facilities can act as vectors for pathogen spread. Abney et al. [46] highlighted

the potential for sponges, cloths, and other cleaning tools to transfer faecal bacteria onto surrounding surfaces in toilet facilities, emphasising the importance of proper hygiene practices when handling cleaning materials.

Behavioural Interventions

Face masks - Face masks can reduce the transmission of airborne particles containing pathogens by blocking their entry into or release from the oral and nasal cavity of the respiratory tract [141]. They serve two primary functions. As a source control, they limit the number of particles containing pathogens that are exhaled by an infected individual, and as personal protection, they can reduce the inhalation of particles containing pathogens by a susceptible individual. There are a variety of face masks including cloth face masks, medical or surgical face masks and respirators [142]. A systematic review by MacIntyre and Chughtai [143] identified five studies supporting the use of face masks to reduce environmental contamination by individuals with respiratory illnesses [71, 144, 145, 146, 147]. Additionally, a meta-analysis by Liang et al. [148] found that the use of face masks reduced respiratory viral infections by 80 % among healthcare workers and 47 % among non-healthcare workers.

Closing the toilet lid before flushing - There are varying views on whether closing the toilet lid reduces transmission through the toilet plume. Best, Sandoe, and Wilcox [45] found that lidless toilets increased airborne and surface contamination, with a higher risk of *C. difficile* transmission. Similarly, Cai et al. [9] observed a reduction in particle counts when the toilet was flushed with the lid closed compared to the lid open. Li, Zhang, and Zhang [8] found a reduction in particle counts in the breathing zone after flushing a toilet with the lid closed compared to open. However, more recent research by Goforth et al. [43] reported that closing the lid before flushing a toilet filled with an MS2 bacteriophage solution did not significantly reduce viral contamination of bathroom surfaces.

Hand hygiene - Hand hygiene is widely regarded as one of the most effective measures to interrupt the fomite transmission of microorganisms that cause infections [149]. It encompasses both handwashing and the use of antiseptic hand rubs, in

order to remove contaminating microorganisms from the hands. A meta-analysis by Aiello et al. [150] that examined disease risk in community settings found that better hand hygiene was associated with a 31 % reduction in gastrointestinal illnesses and a 21 % reduction in respiratory illnesses. Girou et al. [151] compared the effectiveness of alcohol-based hand rubs with handwashing and found that hand rubs achieved a higher median percentage reduction (83 %) in bacterial contamination compared to handwashing (58 %). Despite the well established benefits of hand hygiene in both community and healthcare settings, compliance remains a challenge. A systematic review by Mouajou et al. [152] reported hand hygiene compliance rates among healthcare workers ranging from 60 % to 70 %. Increased compliance has been associated with a reduction in healthcare associated infections [153], while educational interventions have been shown to improve compliance [154].

2.3 The Toilet Plume

2.3.1 Types of Flushing Mechanisms

Internationally, toilets use different flushing mechanisms, which can influence the generation of aerosols and droplets. Examples of the types of toilets discussed are illustrated in Fig. 2.3. This section outlines the main types of flush toilets.

Gravity-Flow Flush From a Cistern

In this type of flush system, a cistern is located above the toilet bowl and releases water into the bowl when a handle or button is pressed [155]. Pressing the lever or button lifts a stopper, allowing water to rush into the bowl under gravity. As the flush ends, the cold water supply refills the cistern.

This flushing mechanism is the most common in the UK and includes several variations: siphon, high-level, back-to-wall, and close-coupled toilets. Siphon toilets are rare in the UK, although they externally look identical to close-coupled toilets (Fig. 2.3a), and high-level cistern toilets (Fig. 2.3c were predominantly used during the Victorian era. Close-coupled and back-to-wall toilets are now the most common (Figs. 2.3a and 2.3b).

Siphon toilets feature an additional port that directs water into the drainage pipe and the toilet bowl. The drainage pipe is designed with an upward curve, creating a siphon effect that transfers water and waste from the bowl to the drainage system [156]. Siphon toilets are common in households in the United States of America (US).

(a) Close-coupled/siphon [157].

(b) Back to wall [158].

(c) High-level [159].

(d) Flushometer [160].

(e) Pressure-assisted [161].

(f) Vacuum [162].

Figure 2.3: Images of different types of flush toilets.

Flushometer Valve

Flushometer toilets operate without a cistern. When the flush lever is pressed, a valve opens, allowing water from the mains supply to enter the bowl at high-pressure [163]. The design leverages a balance of pressure inside the valve, ensuring a controlled amount of water is released per flush. Flushometer toilets are commonly found in non-residential buildings in the US.

Pressure-Assisted Flush

A pressure-assisted toilet (Fig. 2.3e) uses a tank with a small pressure chamber that compresses air to deliver a more powerful flush [164].

Vacuum Flush

Vacuum flush systems use minimal water and rely on a vacuum to remove waste from the toilet bowl. A vacuum station connected to a collection tank generates suction, rapidly drawing waste into the system [165]. This type of flush is typically used in settings where water conservation is a priority, such as on aircraft or trains.

2.3.2 Fluid Dynamics of Toilet Flushing

The fluid dynamics involved in toilet flushing is complex, and there is limited research detailing the exact mechanisms by which droplets and aerosols are generated. This section does not aim to define the full physical processes governing water flow and aerosol production from flushing the toilet, but instead introduces relevant non-dimensional parameters: the Reynolds number and the Weber number.

Water Flow in the Toilet Bowl

Toilet flushing is a multiphase process that involves both water and air. In most toilets, excluding vacuum-operated systems, flushing releases water into the bowl at a pressure determined by the toilet design. Upon impact with the walls of the bowl, the water flow induces splashing and disturbs the surrounding air, both inside and above the bowl. This air disturbance leads to air vortices rising above the toilet seat [166].

The Reynolds number (Re) is used to quantify the ratio of inertial forces to viscous forces in fluid flow [167]. It is defined as

$$\mathrm{Re} = \frac{\rho D v}{\mu} \tag{2.1}$$

where

ρ = density of the fluid [$\mathrm{kg\,m^{-3}}$],

D = characteristic length [m],

v = velocity of the fluid [$\mathrm{m\,s^{-1}}$] and

μ = viscosity of the fluid [$\mathrm{kg\,m^{-1}\,s^{-1}}$].

Due to the high velocity at which water enters the toilet bowl, the flow is highly turbulent, indicating that inertial forces dominate viscous forces. As a result, the Reynolds number is large, indicating that turbulence plays a significant role in the movement of water within the bowl.

Aerosolisation Mechanisms

As water enters the bowl, Johnson et al. [2] suggested that droplets and aerosols are generated through two primary mechanisms: splashing (which produces larger droplets) and bubble bursting (which leads to finer droplets). The Weber number (We) is used to assess the balance between inertial forces and surface tension in the splashing process [168] and is defined as

$$\mathrm{We} = \frac{\rho v^2 D}{\lambda} \tag{2.2}$$

where

λ = surface tension [$\mathrm{N\,m^{-1}}$].

The aerosolisation of toilet bowl water occurs in several ways. When water collides with the walls of the bowl or with the water in the bowl, it can result in splash formation. Dandekar et al. [169] examined the dynamics of liquid splashes and described a process in which an impacting droplet first creates a cavity below the liquid surface, while a cylindrical liquid sheet rises above it. As this sheet expands, instabilities develop, forming ligaments that eventually break apart into smaller droplets. When the sheet reaches peak height, it begins to collapse, leading to the closure of the cavity. Depending on the energy of the impact, this process may result in either a crown splash or alternatively the cavity closes and a bubble and jet droplet are formed. This aligns with previous suggestions of Johnson et al. [2] that splashing and bubble bursting contribute to aerosol generation during flushing.

The way in which water interacts with the walls of the toilet bowl can also influence the type of splashing that occurs. Zhang et al. [170] identified two distinct types of droplet splashes: i) corona splashes, which are influenced by surrounding air conditions and tend to occur on smooth surfaces and ii) prompt splashes, which are driven by surface roughness and typically occur on rough surfaces.

2.3.3 Experimental Techniques to Measure the Toilet Plume

As discussed in Section 2.2.1, toilet flushing release particles into the environment, some of which may contain viruses and bacteria. This section outlines the experimental techniques used to quantify and investigate the toilet plume, with a focus on the equipment and methodologies employed in recent studies. Modern experimental approaches are emphasised to highlight contemporary measurement techniques.

Particle Concentration Measurements

Johnson et al. [2] measured the initial droplet size distribution of toilet flush aerosols using a 15-channel optical particle counter (OPC) (Grimm Model 1.108 aerosol spectrometer), which detected particles ranging from 0.3 µm to 20 µm in size. The experiments were carried out in a controlled chamber designed to simulate the size of a typical 'powder room'. To minimise the effects of humidity, the toilet bowl was covered with a plastic plate, with a particle sampler and hygrometer inserted through a small hole. The spectrometer was activated while the room was ventilated at 18 air changes per hour (ACH) for 45 min. The ventilation was then turned off and the toilet was flushed, with aerosol sampling continuing for 15 min. To quantify total droplet counts, particle concentrations were measured 15 s after flushing and multiplied by the air volume between the bowl water level and the cover plate. The study tested high-efficiency (HET), pressure-assisted high-efficiency (PAT), and flushometer (FOM) toilets, finding that up to 145,000 particles could be produced per flush, with aerosol generation increasing with flush energy.

Lai et al. [6] measured particle concentrations generated during flushing using an Optical Particle Sizer 3330 (TSI) with a 1 s sampling rate. The counter recorded particles in six size bins ranging from 0.3 µm to 10 µm, with air sampled through

a tube positioned inside an acrylic box surrounding the toilet bowl. Background levels were measured for 5 min before flushing. They showed that flushometer toilets produced significantly more droplets than cistern toilets, regardless of the water pressure or tank height. Droplet emission began immediately after flushing, reaching a peak concentration within 15 s. The maximum recorded particle count was 287,400 droplets. Zhang et al. [171] used the same methodology in their study.

Several other studies have quantified particle concentrations in various settings using OPCs. Zhang et al. [7] used an AeroTrak Portable Particle Counter 9310 (TSI) to measure the concentrations near the surface of a squat toilet in a laboratory setting. The same type of counter was used by Li, Zhang, and Zhang [8] to measure particle concentrations from toilet flushing on a commercial aircraft, comparing the levels near the toilet region and in the breathing zone. Their findings indicated an increase in concentrations after flushing in the breathing zone, although the concentration was lower than that in the immediate toilet region.

Cai et al. [9] used an AeroTrak Portable Particle Counter 9306 (TSI) to measure particle concentrations in a hospital toilet facility, specifically testing the effectiveness of a portable toilet cover in reducing aerosol release.

The use of OPCs is therefore a well-established method for quantifying particle concentrations after toilet flushing in indoor air research.

Biological Measurements

Lai et al. [6] measured the strength of bacterial emission during toilet flushing by inoculating a toilet bowl with *Staphylococcus epidermidis* (*S. epidermidis*), *E. coli*, and *Pseudomonas alcaligenes* (*P. alcaligenes*). The bacteria were added to the bowl using a syringe prior to flushing. Airborne bacterial emissions were collected using an Andersen sampler with nutrient agar plates. The collected samples were then incubated and the colony forming units (CFUs) were manually counted. Background levels were assessed by flushing the toilet without bacteria. To prevent cross-contamination between trials, the toilet was disinfected with bleach and neutralised using sodium thiosulfate. The results showed that a higher initial bacterial concentration in the bowl led to an increase in bacterial emission. In addition,

smaller bacteria were more likely to become airborne, with *S. epidermidis* exhibiting the highest emission strength. Zhang et al. [171] applied the same methodology but expanded the study to include viruses (bacteriophages MS2 and P22) along with *Salmonella enterica* (*S. enterica*) bacteria. Their findings showed that viral emission rates were higher than bacterial emission rates.

Knowlton et al. [12] investigated bioaerosol emissions from toilet flushing using human faeces in hospital wards. They used bioaerosol impactor samplers with tryptone soy agar (TSA) plates. Air sampling was performed before and after flushing. Plates were incubated at 37 °C for 24 h, and CFU were counted to calculate bioaerosol concentrations (CFU m^{-3}). They found higher levels of bioaerosols when faecal waste was present.

Bioaerosol emissions from toilet flushing using a specially constructed toilet cubicle with controlled ventilation were investigated by Paddy, Afolabi, and Sohail [13] following a Design of Experiments approach. *C. difficile* was cultured and prepared at 10^7 CFU mL^{-1} before being added to the toilet bowl. A MicroBio MB1 bioaerosol sampler (100 L min^{-1}) was positioned at a height of 0.8 m and distances of 0 m or 1 m laterally from the toilet. The samples were taken immediately or 1 h after flushing. The experimental variables included lid position and ventilation, without human presence to control external influences. The agar plates were incubated at 37 °C for 48 h, and the positive hole count correction method [172] was used. The results showed higher concentrations of bioaerosols near the toilet and immediately after flushing, with mechanical ventilation aiding dispersal over time.

Microorganism Surrogates

Johnson et al. [2] investigated bioaerosol generation from toilet flushing using fluorescent polymer microspheres as microbial surrogates. A microsphere suspension was introduced into the toilet bowl and air sampling was performed using mixed cellulose ester (MCE) filters (0.2 µm pore size). The filters were attached to open-face air cassettes connected to air sampling pumps placed at multiple locations. To maintain controlled conditions, the chamber was first ventilated for 45 min, followed by a 5 min pause. The toilet was flushed, after which another 5 min pause was ob-

served while a fan was used to mix the air in the chamber for another 5 min, and the air samplers were subsequently turned on for 30 min at a flow rate of 1.5 L min^{-1}. The captured particles were analysed using fluorescence microscopy. The results showed that the mean number of fluorescent droplet nuclei aerosolised and remaining airborne increased with flush energy. Additionally, the number of fluorescent droplet nuclei per flush decreased as the particle size increased.

Cai et al. [9] used fluorescein to investigate contamination from toilet flushing. A 1 % fluorescein solution was mixed into the toilet bowl before each flush, and a high-speed camera recorded droplet generation and trajectories for 10 s after flushing. Surface contamination was measured by wiping the toilet lid, divided into four quadrants. The wipes were extracted in distilled water and fluorescein concentration quantified using an ultraviolet-visible spectrophotometer and calibration curve. The results showed significant differences in contamination between lid sections, with higher concentrations in front sections than back sections.

2.4 Prevalence of Pathogens in Faecal Matter

A variety of pathogens, including viruses and bacteria, are present in faecal matter and can contribute to disease transmission. This section explores the range of microorganisms found in faeces, their typical concentrations, and their relevance to public health.

2.4.1 Bacterial Pathogens

Faecal Coliforms

Coliform bacteria are a group of facultatively anaerobic, gram-negative, non-spore-forming rods that ferment lactose vigorously, producing acid and gas at 35 °C± 2 °C within 24 h to 48 h [173]. Faecal coliforms are a subset of coliform bacteria associated with animal or human waste. Unlike total coliforms, faecal coliforms can ferment lactose at higher temperatures, typically 44.5 °C to 45.5 °C [174].

In faeces, coliform concentrations generally range from 10^7 CFU g^{-1} to 10^9 CFU g^{-1}, while faecal coliform concentrations generally fall between 10^6 CFU g^{-1} to 10^9 CFU g^{-1}

[14]. *E. coli* is a subset of faecal coliforms and is widely considered a more reliable faecal indicator organism than total coliforms or faecal coliforms [175]. *E. coli* bacteria generally exist in the body without causing disease but exposure to certain types can lead to disease and illness [37]. *E. coli* O157:H7 can cause severe diarrhoea, abdominal cramps and in extreme cases can lead to kidney failure. *E. coli* O157:H7 has been seen to spread through the faecal-oral route [15]. Faecal coliforms, particularly *E. coli*, are commonly used as indicators of faecal contamination in water, helping to assess associated health risks. Although other pathogens may be present in faeces and of interest, Holcomb and Stewart [176] suggest that the high concentrations of faecal coliforms and their ease of culturing make them practical and effective indicators of faecal contamination.

Other Bacterial Pathogens

Salmonella can be found in faeces at concentrations ranging from $10^4\,\mathrm{CFU\,g^{-1}}$ to $10^{10}\,\mathrm{CFU\,g^{-1}}$ [14]. Infection with *Salmonella* primarily causes diarrhoea, but symptoms can also include abdominal pain, fever and vomiting [177]. The species *S. enterica* is transmitted through the faecal-oral route in humans [178]. *Shigella* is a bacterial pathogen that causes shigellosis and is present in faecal matter at concentrations ranging from $10^5\,\mathrm{CFU\,g^{-1}}$ to $10^9\,\mathrm{CFU\,g^{-1}}$ [14]. Symptoms of the disease include abdominal pain, tenesmus, diarrhoea, and dysentery, and is transmitted through the faecal-oral route [179]. *C. difficile* is a bacterial pathogen that causes diarrhoea and is strongly associated with antibiotic use and healthcare environments [180]. Transmission of *C. difficile* occurs through the faecal-oral route.

2.4.2 Viruses

Norovirus

Norovirus is one of the leading causes of gastroenteritis worldwide. It is a single-stranded, non-enveloped RNA virus with a diameter of 38 nm [177]. Symptoms include vomiting, diarrhoea, and nausea, usually lasting 48 h to 72 h. Norovirus has a low infectious dose and is environmentally stable, with faecal concentrations ranging from $10^6\,\mathrm{gc\,g^{-1}}$ to $10^{11}\,\mathrm{gc\,g^{-1}}$ [181, 182]. These qualities contribute to its

high transmission potential. It is transmitted primarily through the faecal-oral route by contact. However, Tan et al. [21] found evidence for aerosol transmission, with more cases linked to vomiting than faecal exposure.

Rotavirus

Rotavirus is a double-stranded RNA virus that causes symptoms such as fever, vomiting, and diarrhoea. Symptoms typically last 2 days to 3 days, although diarrhoea may persist for 5 days to 8 days. The virus mainly affects children under 5 years of age [18]. Faecal concentrations in infected children are approximately $10^6\,\mathrm{gc\,g^{-1}}$ (genome copies per gram) [183]. Transmission occurs through the faecal-oral route by contact transmission, but there is evidence suggesting the possibility of airborne transmission [30, 184].

SARS-CoV-2

SARS-CoV-2 is a single-stranded RNA virus with a diameter of 70 nm [185]. The concentration of SARS-CoV-2 RNA in faecal matter ranges from 10^3 $\mathrm{gc\,g^{-1}}$ to $10^7\,\mathrm{gc\,g^{-1}}$ [186, 187]. While numerous studies have detected viral RNA in faecal matter, there is less evidence to confirm whether this corresponds to infectious virus.

A systematic review by Termansen and Frische [20] identified 13 studies that successfully cultured infectious SARS-CoV-2 from faecal samples using cell, tissue, organoid or animal models. Of these, 2/13 studies used rectal swabs [188, 189], while 11/13 studies used faecal matter [190, 191, 192, 193, 194, 195, 196, 197, 198, 199, 200]. In addition, 9/13 studies used human samples, while 4/13 studies used samples from various animal species [188, 189, 196, 198]. However, to date, there is no evidence that viable SARS-CoV-2 persists in wastewater, leaving the associated transmission risk uncertain.

2.5 Risk Modelling

Risk modelling is a valuable tool for assessing disease transmission and informing decision-makers in healthcare and public policy. Quantifying the probability of infection allows different mitigation strategies to be compared, helping to inform

regulatory and policy decisions. This section outlines key risk modelling techniques used to evaluate disease transmission risks.

2.5.1 The Wells-Riley Model

Traditional Model

The Wells-Riley model combines a Poisson distribution with the concept of a quantum of infection to estimate the probability of infection from airborne pathogens [201]. A quantum of infection was first introduced by Wells [85] and represents the number of infectious doses required to infect an individual with probability $1 - e^{-1}$. This metric accounts for both the number of airborne infectious particles and the dose-response relationship. In the Wells-Riley model, the probability, P, of an individual becoming infected during a time interval $[0, t]$ is given by

$$P = \frac{C}{S} = 1 - \exp\left(-\frac{Iqpt}{Q}\right), \tag{2.3}$$

where

C = number of infections during $[0, t]$,
S = number of susceptible individuals,
I = number of infectors,
p = pulmonary ventilation rate $[\mathrm{m^3\,h^{-1}}]$,
q = quanta generation rate [quanta $\mathrm{h^{-1}}$],
t = exposure time [h] and
Q = room ventilation rate $[\mathrm{m^3\,h^{-1}}]$.

The quanta generation rate can be estimated using a backward calculation from outbreak data, allowing for risk assessments of future events. However, this approach does not distinguish whether a higher quanta rate is due to increased pathogen infectivity or higher emission rates. Some studies have attempted to quantify quanta generation by integrating data on exhaled particle emissions and viral loads in respiratory fluids [202].

The traditional Wells-Riley model assumes that the air in the indoor environment is well mixed, which means that the pathogen concentration is uniform throughout

the space. This assumption can lead to an underestimation of risk for individuals closer to the infectious source [203]. Additionally, the model is based on steady-state conditions for both airflow and pathogen concentration, which may not reflect real-world scenarios where there are transient behaviours [204]. Despite these limitations, the Wells-Riley model has been widely used in airborne disease risk assessments, with early applications focusing on tuberculosis transmission [205, 206, 207].

Extensions of the Wells-Riley Model

To address the limitations of the traditional Wells-Riley model, a variety of modifications and extensions have been proposed. Edwards et al. [204] reviewed several adaptations, including the incorporation of CFD modelling [208, 209, 210, 211]. Other modifications have introduced spatial adaptations [212, 213, 214], incorporated quanta variation using transport equations [209, 215, 216, 217, 218, 219] and linked quanta conservation principles with epidemic models [220]. Edwards et al. [204] also introduced a stochastic formulation of the Wells-Riley model and further incorporated transient behaviours, randomness, and population heterogeneity.

2.5.2 Quantitative Microbial Risk Assessment Principles

QMRA is a framework used to determine the risk of infection caused by microorganisms [14]. An outline of the QMRA framework is detailed in Fig. 2.4. The Wells-Riley model can be classified as a type of QMRA model which incorporates the exposure and dose-response model in one step. The QMRA framework was first

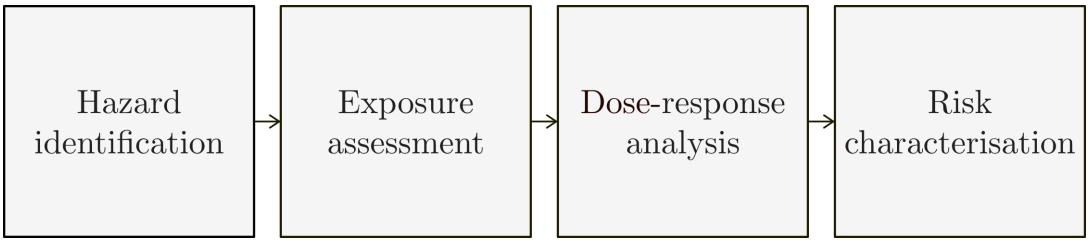

Figure 2.4: The Quantitative Microbial Risk Assessment (QMRA) framework [14].

formally detailed by Haas, Rose, and Gerba [221] in 1999 but was first applied to waterborne hazards in 1991 by Rose, Haas, and Regli [222]. QMRA methods are based on frameworks for risk assessments of chemical agents [14].

Hazard Identification

Haas, Rose, and Gerba [14] define hazard identification as the process of identifying microbial agents and the human diseases they cause, which can range from asymptomatic infections to fatal outcomes. This can be based on clinical, microbiological, and veterinary studies. Key considerations include pathogen virulence, host immune response, and the reliability of animal models in representing human infection. Haas, Rose, and Gerba [14] also highlight the importance of epidemiological studies in understanding disease patterns, with transmission routes varying between pathogens.

Exposure Assessment

Haas, Rose, and Gerba [14] define exposure assessment as the process of identifying the population at risk of infection and their characteristics, such as age and location. This step also involves determining the routes of exposure, assessing pathogen concentrations, and analysing pathogen spatial and temporal distribution. It includes evaluating the prevalence of pathogens in specific environments and understanding their fate over time. In cases where pathogen recovery, detection, or quantification is not feasible, exposure estimates may rely on existing databases. Haas, Rose, and Gerba [14] emphasise that understanding a pathogen's sources, transport mechanisms, survival, and inactivation is critical for exposure assessment.

Dose-Response Analysis

Dose-response models describe the probability of infection after exposure to a given dose of a pathogen [14]. The dose is expressed in the standard laboratory unit used to quantify the pathogen, such as CFU for bacteria and plaque forming units (PFU) for viruses. These models are typically based on experimental data, in which humans or animals are exposed to varying doses through natural routes of exposure, such as inhalation, ingestion, or contact. The endpoint of the model relates the dose to the probability of either disease or death.

A key discussion in dose-response modelling is whether a threshold dose exists. This threshold refers to the minimum dose required to initiate infection. The de-

bate concerns whether a single pathogen can cause infection or whether multiple pathogens are required. Haas, Rose, and Gerba [14] suggest that scientific evidence supports the independent-action theory, as proposed by Schmid-Hempel [223]. According to this theory, a single pathogen can theoretically initiate infection, but the probability of evading host immune defenses is low, which means that infection is more likely when multiple pathogens are present.

Additional support for the independent-action theory comes from dose-response models fitted to experimental data. Haas, Rose, and Gerba [14] suggest that the beta-Poisson and exponential models provide a better fit to the dose-response data than the log-normal model [224]. If a threshold dose existed, the log-normal model would be expected to fit the data more appropriately.

For the exponential dose-response model, the response probability for a given dose D, $P_{\text{response}}(D)$, is given by

$$P_{\text{response}}(D) = 1 - \exp(-rD), \tag{2.4}$$

where

D = intake dose [pathogen unit] and

r = probability to reach and infect an appropriate site [1/pathogen unit].

In the beta-Poisson dose-response model, the parameter r in the exponential model is considered as a distribution rather than a fixed value, and the response probability is given by

$$P_{\text{response}}(\mathrm{D}) = 1 - \left(1 + \frac{D}{\beta}\right)^{-\alpha}, \tag{2.5}$$

where α and β [pathogen unit] are the fitted parameters in the model to be estimated from experimental data [225].

A limitation of dose-response models is that they need experimental data to determine which model best fits the observed infection probabilities. In some cases, data from animal studies are extrapolated to humans, but this approach does not always account for differences in respiratory or immune system responses. For some pathogens, there can be significant risks in the laboratory that require strict safety

precautions when conducting experiments involving aerosolised pathogens.

There are instances where dose-response models have been directly calibrated for humans. If a pathogen is not highly dangerous, human challenge studies can be conducted under controlled conditions. Historically, before modern ethical and safety regulations, some potentially hazardous experiments were carried out on human subjects. One such example is Operation Whitecoat [226], a US military research program conducted between 1954 and 1973, in which volunteers were intentionally exposed to infectious agents, including *Francisella tularensis*, to study disease progression and immune responses. Exceptions were also granted for conducting controlled human exposure studies for research during the COVID-19 pandemic [227]. Human challenge studies have also been performed for *Salmonella* [228], *Shigella* [229] and rotavirus [230]. In contrast to dose-response models, the Wells-Riley model always derives the quanta generation rate from human outbreak data, making it directly applicable to human transmission risk assessments [225].

Examples of fitted parameters for both the exponential and beta-Poisson dose-response models are provided in Table 2.1 and Table 2.2, respectively. Dose-response models can be used to evaluate the risk associated with both airborne and fomite transmission, unlike the Wells-Riley model which is used only for airborne transmission.

Risk Characterisation

Risk characterisation is the final step in the framework, integrating the results of hazard identification, exposure assessment, and dose-response analysis [14]. A point estimate probability can be used to determine the likelihood of infection or disease following exposure. However, QMRA typically employs probabilistic techniques, such as Monte Carlo methods, that account for variability and uncertainty in risk estimates. Monte Carlo simulations involve repeatedly sampling from probability distributions of input parameters to generate a distribution of risk outcomes, rather than a single deterministic value. This approach provides a better representation of infection risk by incorporating natural variability in pathogen concentrations, exposure levels, and host susceptibility. Risk characterisation includes an assessment of

Table 2.1: Estimated values of r in Eqn. (2.4) for various pathogens in the exponential dose-response model.

Pathogen	r	Study	Method	Response
SARS-CoV-2	6.4×10^{-4}–9.8×10^{-5}	Zhang and Wang [231]	A combination of data from experiments on mice, a meta-analysis, and viral shedding in exhaled breath.	Infection
SARS-CoV	2.46×10^{-3}	Dediego et al. [232]	Intranasal administration to mice and monitoring survival for 13 days.	Death
Poliovirus	4.91×10^{-1}	Koprowski [233]	Oral administration to nine human volunteers.	Infection
Enterovirus	3.74×10^{-3}	Cliver [234]	Oral administration to pigs.	Infection
Bacillus anthracis	6.4×10^{-5}	Toth et al. [235]	An extension of existing risks model using non-human primate data and human epidemiological data to refine parameter values.	Infection (leading to death)

Table 2.2: Values of α and β in Eqn. (2.5) for various pathogens in the beta-Poisson dose-response model.

Pathogen	α	β	Study	Method	Response
H1N1 Influenza	9.04×10^{-1}	1.08×10^{6}	Murphy et al. [236]	Nasal adminisration to human volunteers.	Infection
Rotavirus	2.53×10^{-1}	4.26×10^{-1}	Ward et al. [230]	Oral administration to male human volunteers aged 8 to 45 years old.	Infection
Rhinovirus	2.21×10^{-1}	8.22×10^{-2}	Hendley, Edmondson, and Gwaltney [237]	Nasal administration to human volunteers over the age of 21.	Infection
E. coli	1.55×10^{-1}	2.44×10^{4}	DuPont et al. [238]	Oral administration to human volunteers.	Positive stool sample
Salmonella anatum	3.18×10^{-1}	4.73×10^{3}	McCullogh and Eisele [228]	Oral administration to human volunteers.	Positive stool sample

the magnitude of the risk, the likelihood of occurrence, and the associated variability and uncertainty in these estimates. This step is essential to inform risk management

decisions, evaluate mitigation strategies and guide public health policies.

2.5.3 Fomite Transmission Modelling Tools

When modelling contact transmission, additional tools can be integrated into QMRA modelling to estimate transmission dynamics.

Markov Chain Models

A Markov chain model can be used to estimate intake dose from contaminated surfaces. A Markov chain is a stochastic process $\{X(t) : t \in [0, \infty)\}$ that satisfies the memoryless property, expressed as

$$P\{X_{n+1} = i_{n+1} | X_0 = i_0, X_1 = i_1, ..., X_n = i_n\} = P\{X_{n+1} = i_{n+1} | X_n = i_n\} \quad (2.6)$$

where $0 \leq t_0 < t_1 < ... < t_n < t_{n+1}$ and $X(t_n) = X_n$ and for states $i_0, i_1, ..., i_{n+1}$ [239]. Eqn. (2.6) states that in a Markov process, the probability of the system being in state i_{n+1} at time t_{n+1} depends only on the current state i_n at time t_n and not on any previous states. For any two time points $s < t$ a probability transition matrix, $p_{ji}(t, s)$, can be defined as

$$p_{ji}(t, s) = P\{X(t) = j | X(s) = i\}. \quad (2.7)$$

King, Noakes, and Sleigh [240] applied a Markov chain approach to model contamination dynamics in single-bed and four-bed hospital rooms. In this study, various surfaces in the hospital room were assigned a numerical value between 1 and 5, and the movement of healthcare workers (HCWs) between these surfaces was modelled as a Markov chain. The probability of an HCW contacting a specific surface depended only on their current contact and not on previous interactions. This approach used discrete-time Markov chains, rather than continuous-time models. To determine transition probabilities, observational data were collected in an NHS single-bed hospital room, with more than 400 care episodes recorded. This data was used to quantify HCW movement patterns and refine the Markov chain model.

Pathogen Accretion

The amount of pathogen transferred to an individual upon contact with a contaminated fomite depends on several factors, as summarised in Table 2.3. King, Noakes, and Sleigh [240] defined the hand pathogen loading at any time step after contact with any one surface, Y, using a recurrence relation given by

$$Y_i = \lambda V_i A_i + \beta Y_{i-1}, \tag{2.8}$$

where $i = 0, 1, ...n$ represents the surface count. Transfer efficiencies, λ and β, are derived from experimental studies and vary depending on the type of pathogen, surface material, and glove usage.

Table 2.3: Parameters affecting pathogen accumulation on an individual's hands [240, 241].

Parameter	Description
n	Number of surfaces touched by the individual
A	Contact area between the hand and surface touched (cm^2)
V	Surface contamination (CFU/cm^2)
λ	Surface-to-hand transfer efficiency
β	Hand-to-surface transfer efficiency

Lopez et al. [5] conducted experimental studies to determine transfer efficiencies on different surfaces for three bacterial species, *E. coli, S. aureus, Bacillus thuringiensis* (*B. thuringiensis*), and the MS2 coliphage virus. For MS2 virus, PFU were counted using the double-agar overlay method in TSA. The study investigated two relative humidity conditions, high (45 % to 60 %) and low (15 % to 32 %), and compared porous versus non-porous surfaces. The results suggested that higher relative humidity generally led to greater transfer efficiencies, and non-porous surfaces facilitated greater pathogen transfer compared to porous surfaces. The transfer efficiencies measured under high relative humidity (40 % to 65 %) for non-porous surfaces are presented in Table 2.4.

Walker et al. [92], evaluated the effect of touch transfer of aerosol-deposited material on various high-touch surfaces. They found that at relative humidity levels below 40 %, transfer efficiency remained low on all surfaces, typically below 10 %. However, the transfer efficiency increased substantially as humidity exceeded 40 %,

reaching a maximum of approximately 50 %. Surface roughness also influenced transfer rates, with smoother surfaces exhibiting higher transfer efficiencies compared to a textured surface. They found that pooled human saliva demonstrated lower transfer efficiency than artificial saliva.

Table 2.4: Values for transfer efficiency for four different pathogens on different non-porous surfaces found by Lopez et al. [5]. Relative humidity was 40 % to 65 %.

Pathogen	Surface type	Average % TE	Standard deviation
E. coli	Acrylic	53.3	27.5
	Glass	78.6	27.1
	Ceramic tile	60.7	45.4
	Laminate	27.4	30.2
	Stainless steel	54.1	23.5
	Granite	36.5	39.3
S. aureus	Acrylic	47.2	17.9
	Glass	45.5	15.5
	Ceramic tile	54.7	18.8
	Laminate	61.9	24.7
	Stainless steel	48.3	25.4
	Granite	39.6	41.5
B. thuringiensis	Acrylic	65.6	15.9
	Glass	<33.8	24.0
	Ceramic tile	<21.2	28.2
	Laminate	53.5	19.6
	Stainless steel	57.0	9.7
	Granite	12.8	19.8
MS2	Acrylic	79.5	21.2
	Glass	67.3	25.0
	Ceramic tile	41.2	18.8
	Laminate	63.5	24.0
	Stainless steel	37.4	16.0
	Granite	30.0	24.3

2.5.4 Relevant QMRA Studies

The QMRA methodology has been widely applied in research to assess the infection risks associated with airborne and contact transmission. This section provides an overview of QMRA studies for both transmission routes, with a discussion on studies that examine toilet facilities. The main objectives of QMRA studies are to quantify infection risk in a given setting and to compare the results with established infection risk benchmarks. Wilson et al. [242] reviewed current risk evaluation thresholds,

including the 1 in 10,000 annual risk threshold commonly used in QMRA studies [243]. However, they discuss limitations of arbitrary thresholds and propose an alternative framework that integrates individual risk perception into risk assessment.

Contact Transmission

QMRA methods have been applied to estimate contact transmission infection risks for a variety of bacterial pathogens, including *Salmonella* [244, 245], *E. coli* [245], *Pseudomonas* spp. [245], and *S. aureus* [245]. A variety of viral pathogens have also been studied in the context of contact transmission using QMRA. Following the COVID-19 pandemic, interest in modelling SARS-CoV-2 transmission increased, leading to numerous studies on contact risks for this virus [51, 246, 247, 248, 249, 250]. QMRA studies have been conducted for other viruses, including rhinovirus [244, 251, 252], rotavirus [244, 251, 252], norovirus [245, 252, 253], and influenza [251].

QMRA contact transmission models have been applied in various environments and activities. Studies have evaluated the infection risk associated with household environments, including laundry practices [244], as well as healthcare settings, where the risks of personal protective equipment (PPE) removal have been examined [246] and the effects of room layout on pathogen transfer [253]. QMRA has also been used to assess the effectiveness of disinfectants in reducing infection risks [245, 251] and has been applied in public transportation settings [249, 250]. Several studies have attempted to quantify infection risk in toilet facilities using QMRA.

Abney et al. [46] applied Monte Carlo simulations to estimate the infection risks of high-touch toilet facility surfaces (e.g. toilet seat, entrance/exit door) for SARS-CoV-2, adenovirus, and norovirus in eight exposure scenarios reflecting different user behaviours. Their study quantified risk reduction with hand sanitiser after using the toilet and found that norovirus had the highest infection risk. The use of automatic hand sanitiser reduced the probability of infection by up to 99.75 %, making it more effective than handwashing in achieving lower risk thresholds.

Amoah et al. [51] investigated SARS-CoV-2 contamination in shared toilet facilities in peri-urban South Africa, collecting swabs from key contact surfaces (e.g.

toilet seat, cistern handle, door latch, tap, and floor). RNA copies were detected and quantified using qPCR, and infection risks were estimated using an exponential dose-response model. Their findings showed that 54 % to 69 % of the surfaces were contaminated, with toilet seats carrying the highest viral loads (28.1 gc cm^{-2} to 132.7 gc cm^{-2}). Cleaning interventions significantly reduced contamination levels, highlighting the importance of hygiene interventions in shared toilet facilities to mitigate infection risks.

Airborne transmission

QMRA has been widely applied to assess infection risks for airborne transmission for a variety of pathogens and environments. Many studies have focused on bacterial transmission, particularly *Legionella*, which is responsible for Legionnaires disease [254, 255, 256, 257, 258, 259, 260, 261, 262, 263, 264, 265, 266]. Other bacterial pathogens investigated using QMRA include *S. aureus* [50, 267, 268, 269, 270, 271, 272], *E. coli* [268, 270], and *P. aeruginosa* [273]. For viral pathogens, QMRA has been widely applied to SARS-CoV-2 in the context of airborne transmission [42, 187, 247, 249, 250, 274, 275, 276, 277, 278, 279, 280, 281, 282, 283, 284, 285], again following the COVID-19 pandemic, as well as adenovirus [286, 287] and influenza [288, 289].

QMRA has been applied to assess airborne infection risks in a variety of settings. Studies have evaluated reclaimed water use and rainwater harvesting [256, 259, 261, 262, 264, 266], residential indoor water use [260], and high-pressure water devices in dental offices [258]. Other applications include laboratory and office spaces, where QMRA has been used to determine the effectiveness of precautionary measures to maintain low infection risks [274].

Transportation settings have been investigated, with studies assessing airborne transmission risks on buses [249, 250, 280]. Similar approaches have assessed risks in classrooms, weddings, exercise settings [281], restaurants [285], and orchestras [279].

A significant focus of QMRA research has been on airborne transmission risks in wastewater treatment plants (WWTPs), highlighting potential infection risks from

aerosolised faecal matter across various pathogens [268, 269, 270, 271, 272, 286].

Carducci et al. [286] applied QMRA to estimate human adenovirus (HAdV) infection risks from bioaerosol exposure in a WWTP. Their model incorporated HAdV concentrations measured in different areas of the facility and an inhalation dose-response model. The sensitivity analysis identified viral concentration as the dominant risk factor. The results indicated that the highest infection risks were associated with the sewage influent and biological oxidation tanks, with probabilities of 15.64 % and 12.73 % for 3 min exposure periods.

Chen et al. [268] conducted a QMRA study to assess worker exposure to *S. aureus* and *E. coli* bioaerosols in two WWTPs with different aeration modes. Without PPE, annual infection risks exceeded US Environmental Protection Agency (EPA) benchmarks [243], but the use of PPE effectively reduced risks to acceptable levels.

More recently, Dada and Gyawali [187] estimated occupational health risks for WWTP operators exposed to aerosolised SARS-CoV-2 through inhalation. Their model incorporated factors such as population infection rate, virus concentration in wastewater, inhaled aerosol volume, and environmental conditions affecting viral viability. Using an exponential dose-response model, risk was assessed in low (0.03 %), moderate (0.3 %), and aggressive (3 %) outbreak scenarios. Results indicated that accidental occupational exposure to SARS-CoV-2 in wastewater was negligible.

A growing number of studies have applied QMRA modelling to airborne transmission in toilet environments. Denpetkul et al. [42] used QMRA to assess the risk of infection in a shared toilet due to an infected individual performing expiratory activities such as breathing, coughing and sneezing.

A few studies have applied QMRA to estimate infection risks from inhalation of toilet plume aerosols in toilet facilities. Lim, Hamilton, and Jiang [290] were the first to apply QMRA for toilet plume aerosols, estimating infection risks for norovirus and adenovirus for exposure to aerosolised stormwater. Their approach relied on previously published data for 2.5 µm droplets generated from flushing, with pathogen concentrations taken from the literature. The inhaled dose was estimated by assuming spherical droplets and calculating the inhaled particle volume. Annual

infection risk was estimated using best case (1 min exposure) and worst case (5 min exposure) exposure times per toilet flush. The annual median risks were found to be below the US EPA guidelines [243].

Hamilton et al. [259] evaluated *Legionella* infection risks from toilet flushing with reclaimed water. They compared three QMRA approaches, including a partitioning coefficient method and also two variations of the approach used by Lim, Hamilton, and Jiang [290], using experimental particle concentration data from Johnson et al. [2] which had a larger range of particle size bins (0.3 µm to 10 µm). Their findings indicated that the median annual infection risks from toilet flushing exceeded the US EPA benchmark [243], although the clinical severity risk remained low.

Ali et al. [267] measured *S. aureus* bioaerosols in a real-world toilet facility after flushing the water that was part of the water supply. Using an Andersen sampler, bioaerosol samples were collected at 5 min intervals under different ventilation scenarios. QMRA was applied, assuming that an individual spent 5 min per day in the toilet facility, with age and gender accounted for using different breathing rates for each. Again, annual infection risks were calculated and the study found that the infection risk exceeded the US EPA benchmarks [243] for up to 15 min after flushing but dropped to acceptable levels after 35 min.

Ali et al. [50] extended this research by comparing *S. aureus* bioaerosol emissions in squat and bidet toilet facilities. Bioaerosols were sampled at different heights to simulate defecation (squat height for squat toilets, sitting height for bidet toilets) and handwashing (standing height). Their results showed that bioaerosol concentrations were higher in squat toilets, with infection risks 8.43 % to 59.11 % higher than in bidet toilets. Poor ventilation significantly increased risks, while the risks became acceptable 35 min after flushing.

Ali et al. [41] then built on this by investigating both *S. aureus* and *E. coli*, comparing two flushing scenarios: one with only water from the building water supply in the bowl and another with human faecal matter. QMRA was applied using a uniform distribution for daily exposure time (5 min to 10 min), with an annual infection risk calculated. The results showed that squat toilets produced 1.7

to 2.6 times more *S. aureus* and 1.2 to 1.4 times more *E. coli* than bidet toilets. The second flush generated more fine bioaerosols ($< 4.7\,\mu m$), leading to higher airborne risks. Ventilation with an active exhaust fan significantly reduced risk, reducing disease burden by an order of magnitude.

Previous QMRA studies of toilet plume aerosols have been limited to specific pathogens (*S. aureus*, *E. coli*, *Legionella*, adenovirus, and norovirus). The studies by Ali et al. [41, 50, 267] used the same squat and bidet toilet facilities, while Hamilton et al. [259] and Lim, Hamilton, and Jiang [290] relied on particle concentration data from prior studies without accounting for toilet facility layout effects. Furthermore, risk estimates in these studies were based on annual exposure using point estimates or uniform distributions for daily exposure time, which appeared to be arbitrarily chosen rather than based on behavioural data. Hamilton et al. [259] and Lim, Hamilton, and Jiang [290] did not assess risks from faecal matter in the toilet bowl, but instead focused on pathogen exposure from reclaimed water and stormwater, which do not reflect faecal concentrations from a bowel movement in real-world settings. Moreover, the data in Ali et al. [41, 50, 267] were collected in real-world toilet facilities, where background bioaerosol concentrations may have contributed to overall exposure. Although these studies accounted for background contamination, no QMRA study has used a controlled chamber data set. However, existing controlled experimental studies have not explicitly investigated how varying ventilation rates influence toilet plume aerosol generation and dispersion. Additionally, previous studies have not compared aerosol dispersion between a toilet located in an open space versus one enclosed within cubicles.

No existing study has evaluated how the infection risk evolves over time after flushing for a single event. Addressing this gap would provide a more detailed understanding of exposure risk dynamics in toilet facilities.

2.6 Computational Airflow Modelling

Understanding and modelling airflow in indoor environments is essential for various applications, including mechanical ventilation design, window opening strategies,

airborne and contact transmission mitigation, pollution control, thermal comfort and energy consumption. Experimental modelling of airflow is limited by the number and location of sensors and can be impractical and expensive [291]. As a result, computational airflow modelling provides a faster and more cost-effective alternative for predicting airflow behaviour.

This section discusses two common computational approaches: multi-zonal modelling and CFD. Multi-zonal models provide a simplified representation of airflow across connected zones, while CFD simulations offer more detailed spatial and temporal resolution. CFD models tend to be more accurate but are computationally expensive, creating a trade-off between precision and efficiency.

2.6.1 Multi-Zonal Modelling

Multi-zonal airflow models estimate airflows between indoor zones and outdoor environments by taking into account pressure-driven forces such as wind, buoyancy, and mechanical ventilation [292]. These models use a network-based approach, treating air in each zone as well-mixed (as in the Wells-Riley model) and connecting them through inter-zonal airflow pathways (e.g. cracks, windows, and ducts). Airflows are determined by solving non-linear mass conservation equations.

To model contaminant transport, multi-zonal models track concentration changes over time based on airflow rates, source emissions, and removal mechanisms. They can provide insights into contaminant concentration distribution and inhaled dose estimation.

Applications of Multi-Zonal Modelling

Noakes and Sleigh [293] developed a stochastic Wells–Riley model integrated with a multi-zonal ventilation model to assess proximity-based infection risks in healthcare settings. The study showed that neglecting stochastic effects underestimated infection risk by at least 15 %, and that assuming fully mixed air could incorrectly estimate infection probabilities, with quanta values being less than half of the actual source values.

López-García, King, and Noakes [294] combined a deterministic multi-zonal ven-

tilation model with a stochastic Markovian Susceptible-Infectious-Susceptible (SIS) model to study airborne transmission in hospital wards. Their model incorporated patient arrival and discharge, outbreak detection, and variations in ventilation rate to assess the impact on epidemic dynamics. The results indicated that ventilation significantly affects infection spread, particularly in overcrowded wards or slow detection scenarios, and that reducing overall ward risk could increase localised risks in certain areas.

CONTAM, a multi-zonal indoor air quality and ventilation analysis tool, has been widely used in airflow modelling studies [295]. Edwards et al. [296] used CONTAM to estimate airborne virus concentrations by incorporating a transient infectious individual into an adapted Wells–Riley model. The study compared steady-state and transient approaches in a hospital ward and found that steady-state models tend to overestimate infection risk or underestimate quanta emission, particularly for short-duration exposures.

Other studies have applied CONTAM to model airflow in office buildings [297, 298] and healthcare settings [299, 300], demonstrating its versatility in the assessment of infection risk.

2.6.2 Computational Fluid Dynamics Modelling

CFD is a powerful tool for solving the governing equations of fluid flow at multiple points within a given domain [301]. Advances in computing power have made CFD widely accessible, with various commercial and open-source software available. In indoor air environments, CFD enables detailed analysis of airflow patterns and particle dispersion, allowing for the quantification of airborne contamination by tracking particle transport over time and space. Additionally, contact transmission can be assessed by modelling particle deposition from airborne sources under the influence of airflow.

Setting up a CFD simulation requires data on the geometry and boundary conditions, which are usually determined through experimental measurements or estimations. A common approach in indoor air studies for particle tracking is the Euler-Lagrange method, where airflow is modelled using an Eulerian reference frame, while

discrete particles (e.g. respiratory droplets) are tracked using a Lagrangian reference frame.

Applications in Indoor Air Settings

CFD is frequently used to study aerosol transport and deposition in healthcare environments [4, 116, 253, 302, 303, 304, 305]. Wilson et al. [253] conducted CFD simulations of a hospital room to investigate the deposition of particles that contained norovirus from a breathing patient. The study used ANSYS Fluent [306] with the Discrete Phase Model (DPM) for Lagrangian particle tracking. The boundary conditions for patient breathing were taken from literature. Two hospital room layouts were tested (left and right facing bed positions), with particle concentrations on surfaces quantified to assess deposition. A Markov chain model was used to estimate viral accretion on hands, and a QMRA model calculated risk using the CFD results for the exposure analysis. The results showed that doctors' rounds posed the highest infection risk, and room layout influenced particle deposition and healthcare worker exposure.

Jung et al. [116] performed CFD simulations to retrospectively investigate a COVID-19 outbreak in a hospital ward in Seoul, Korea. Using STAR-CCM+ [307], a passive tracer was used to simulate viral spread. The outbreak involved a patient who became infected after a COVID-19 patient had used a shared bathroom with a malfunctioning ventilation system. Simulations revealed that positive pressure in the bathroom combined with poor ventilation caused air to spread into the adjacent patient's room, providing a likely transmission route.

King et al. [4] validated CFD simulations against bioaerosol deposition patterns in a hospital test room. Using ANSYS Fluent, the study applied a Reynolds-Averaged Navier–Stokes (RANS) turbulence model and Lagrangian particle tracking with stochastic discrete random walk (DRW). The Reynolds Stress Model (RSM) provided the best agreement with the experimental anemometry data. Simulations showed that small bioaerosols deposited throughout the room with no clear spatial pattern, but physical partitions significantly reduced cross-contamination between patients.

CFD models are also widely used to study airborne transmission in educational environments [308, 309, 310, 311, 312, 313]. Mirzaie et al. [308] simulated SARS-CoV-2 droplet dispersion from coughing in a classroom using ANSYS Fluent. A RANS turbulence model, renormalisation group (RNG) $k-\epsilon$, and Lagrangian particle tracking were applied. The study analysed ventilation speeds and the impact of partitions between classroom seats on particle spread. Higher ventilation speeds increased particle velocity but reduced surface deposition time. Seat partitions reduced infection risk by limiting dispersion, while in the absence of partitions, seats cloest to the infected individual had the highest droplet concentrations.

Abuhegazy et al. [309] used CFD to simulate the dispersion of exhaled particles in a classroom, considering ventilation, air conditioning, and window openings. Using ANSYS Fluent, the study applied a RANS turbulence model (RNG $k-\epsilon$) and Lagrangian particle tracking for aerosol dispersion and deposition analysis across a range of particle sizes (1 µm to 50 µm). They found that 24 % to 50 % of particles smaller than 15 µm exited through ventilation within 15 min, while larger particles deposited on surfaces. Glass barriers reduced aerosol transmission by 92 % at 2.4 m separation, and window openings increased particle removal by 38 %.

Coldrick et al. [61] developed a CFD model to simulate the dispersion of droplets and aerosols from exhalation, incorporating a warm, humid carrier airflow and saliva-based Lagrangian particle tracking. Simulations were carried out in ANSYS Fluent [306], using a species transport model for air, water vapour, and carbon dioxide, with the $k-\omega$ shear stress transport (SST) turbulence model. Exhalation was modelled using transient velocity profiles for coughing, speaking, and singing, with droplet size distributions based on the BLO model. The results showed that particles smaller than 10 µm remained airborne beyond 2 m, and bacterial deposition was highest within 1 m of the source. Strong agreement between simulated and experimental deposition patterns demonstrated the ability of the CFD model to predict airborne microbial dispersion.

CFD modelling has also been used to study aerosol dispersion in aircraft cabins [314, 315, 316].

2.6.3 Toilet Flush Modelling

There are a limited number of studies that have used CFD to model toilet flushing. Two primary approaches are employed: the Volume of Fluid (VOF) method and the DPM method. The VOF simulations tend to focus on the movement of water within the toilet bowl during flushing to optimise toilet design, while DPM simulations examine the dispersion of aerosolised particles into the surrounding environment.

Volume of Fluid Method

The VOF method has been used mainly to study and optimise the design of water drainage dynamics for siphon toilets. The details of these toilet designs were previously discussed in Section 2.3.1. The VOF approach tracks the interface between two immiscible fluids, in this case, air and water, by assigning a phase volume fraction to each fluid [317]. A cell fully occupied by water has a water phase fraction of 1 and an air phase fraction of 0, while a cell containing equal parts water and air has a phase fraction of 0.5 for each.

Ge et al. [318] used the VOF method to simulate the flushing dynamics of a siphon jet toilet, modelling the multiphase flow in ANSYS Fluent [306]. The realisable $k - \epsilon$ turbulence model was used. The boundary conditions included one pressure inlet in the toilet cistern and two pressure outlets in the waste pipe and toilet bowl. The flushing process was analysed by recording the velocity, pressure, and mass flow rate inside the siphon pipe. The simulation domain was limited to the toilet itself, without modelling water breakup or aerosol formation.

Other studies have used similar multiphase VOF CFD methods to optimise siphon toilet designs using ANSYS Fluent [319, 320, 321]. Like Ge et al. [318], these studies focused on the flow of water in the toilet bowl and did not incorporate droplet breakup or simulate particle dispersion in the external environment.

Discrete Phase Model Method

Recent studies have increasingly used DPM methods in CFD simulations to investigate the toilet plume and its potential for aerosol dispersion.

Li, Wang, and Chen [166] and Wu et al. [322] employed a combined VOF-DPM

approach to simulate toilet flushing and aerosol release in a two dimensional siphon toilet model, with the latter study incorporating a mitigation strategy. The VOF model tracked the air-water interface, while the DPM model simulated the movement of aerosolised particles using Lagrangian particle tracking. The simulations were conducted in ANSYS Fluent, using the RNG $k-\epsilon$ turbulence model. Results showed that air vortices formed within the toilet bowl during flushing, generating high airflow speeds. This turbulence disturbed airflow above the toilet bowl after flushing, with upward air velocities reaching $5\,\mathrm{m\,s^{-1}}$. Between 40 % to 60 % of aerosolised particles rose above the toilet seat, some reaching heights of 106.5 cm. Double-port flushing resulted in greater aerosol dispersion, despite using the same water volume and gravitational potential energy as single-port flushing.

Wan et al. [323] simulated particle dispersion in a compact toilet facility equipped with a vacuum toilet, considering both flushing and coughing scenarios. The model, developed in ANSYS Fluent, used the $k-\omega$ SST turbulence model with Lagrangian particle tracking (DPM). The simulation incorporated airflow from the ceiling exhaust, suction from the toilet, and a standing or seated manikin. Toilet suction was modelled as a 4 s flow rate profile, while coughing was represented by a 6 s velocity profile. The results indicated rapid aerosol decay, with fine particles ($< 10\,\mu\mathrm{m}$) taking 315 s to 348 s to drop to 5 % of initial levels, while larger particles (50 µm to 100 µm) settled within 11 s. The toilet seat, bowl, and walls were the most contaminated surfaces, while the thermal plumes from the standing manikin increased the aerosol dispersion. Droplets from the seated manikin's cough deposited primarily on the floor, legs, and feet.

Li, Liu, and Zhang [324] also investigated the dispersion in a vacuum toilet within a compact aircraft toilet facility using COMSOL [325]. The study used the $k-\omega$ turbulence model with Lagrangian particle tracking (DPM). The toilet flush was modelled with a triangular negative pressure profile and airflow was supplied from the aircraft cabin. Flushing lasted 4 s, releasing 8,822 aerosol particles, with emission rates proportional to local air velocity. Coarse particles (greater than 1 µm) resuspended from the floor were also included in the simulation. The results showed

that more than 70 % of particles were drained into the sewage but that particles dispersed in the air when flushed with an open lid, remaining airborne for more than 5 min. Closing the lid reduced dispersion but increased deposition on the lid and seat. An inhalation exposure risk persisted for up to 3 min after flushing with a closed lid.

Liu et al. [326] developed a three dimensional CFD model in ANSYS Fluent to simulate toilet plume aerosol dispersion and particle residence time in a public toilet. The study used the $k-\omega$ SST turbulence model with Lagrangian particle tracking (DPM). To validate the model, in-situ droplet measurements were taken using an optical particle counter (TSI AeroTrak 9306-V2), which recorded particle size distributions (0.3 µm to 10 µm) at various heights (1 cm to 15 cm above the toilet bowl). These measurements were used as input to the CFD model, where 30,000 particles were injected at the toilet surface (0.4 m) to replicate aerosol dispersion from flushing. Six different toilet cubicles were tested to analyse spatial dispersion patterns. The ventilation system was modelled with an exhaust outlet positioned according to commercial designs, with ventilation rates ranging from 3 ACH to 20 ACH. Six different vent locations were examined to assess their effect on aerosol dispersion. The residence time distribution was used to determine how long droplets remained airborne, while the Age of Air (AoA) metric was applied to evaluate ventilation efficiency. The results showed that higher ventilation rates significantly reduced particle residence time, which lowered the risk of prolonged aerosol persistence in the toilet environment.

2.7 Epidemiological Evidence

A small number of epidemiological studies have provided evidence of associations between disease and toilet facilities, with wastewater and aerosols from the toilet plume being a likely cause.

Ho et al. [327] investigated a gastroenteritis outbreak aboard a transatlantic cruise ship, which was linked to toilet usage. The outbreak was attributed to Snow Mountain Agent (SMA), a type of virus. The study compared infection risk between

passengers who used shared toilet facilities and those with private ones. They found that individuals using shared toilets had twice the risk of developing gastroenteritis compared to those with private ones. Although the exact transmission route was unclear, the findings suggest that shared toilet facilities pose a higher risk of pathogen transmission. Transmission could have occurred if aerosolised faecal matter remained airborne and was inhaled, or through surface contamination if particles settled and were later touched. However, alternative contamination routes, such as infectious expiratory aerosols or transfer of virus to surfaces through touch, cannot be ruled out.

Yu et al. [38] conducted a retrospective analysis of a SARS-CoV outbreak at Amoy Gardens, a residential complex in Hong Kong. The outbreak resulted in 341 infections and 42 deaths. Amoy Gardens consisted of 19 apartment towers, each with 33 floors and eight apartments per floor. In particular, 45 % of the cases occurred in 'block E', where a known index case had experienced diarrhoea. The sanitary plumbing system in the complex connected apartments through vertical drainage pipes, with each bathroom linked to the system. U-traps or P-traps are used to create a seal between drainage pipes and bathrooms that prevents sewage gases, insects, and rodents from entering apartments. However, investigators found that many traps in block E were faulty and had dried out, rendering them ineffective since there was no seal. This created an entry point for aerosolised wastewater, allowing airborne particles containing viruses to enter apartments through the drainage system. In addition, many residents used window-mounted exhaust fans, which generated negative pressure in bathrooms. This drew contaminated air from the drainage system into living spaces, increasing the exposure to airborne SARS-CoV.

A similar but smaller-scale outbreak was identified by Kang et al. [39] during the COVID-19 pandemic in a high-rise residential building in Guangzhou, China. A family returning from Wuhan, where the first known infections had been recorded, became infected. Shortly afterward, two other families in the same building also tested positive for SARS-CoV-2. All three families lived in vertically aligned apartments connected by a shared drainage system in their bathrooms. To investigate

potential transmission routes, researchers collected surface and air samples using quantitative polymerase chain reaction (qPCR) and conducted tracer gas experiments to simulate the movement of aerosols through the drainage pipes. Their findings indicated that airborne transmission through aerosolised faecal matter was the likely route of infection. However, unlike Yu et al. [38], they could not confirm that faulty U-traps contributed to the spread.

A separate investigation by Widdowson et al. [328] examined a norovirus outbreak aboard an 8 h flight from London to Philadelphia in 2002. During the flight, eight out of fourteen crew members developed gastroenteritis symptoms, including vomiting and diarrhoea. The study aimed to determine whether passengers also became infected after the flight and to identify possible transmission routes. Among the 83 complete surveys from passengers (out of 191 onboard), five were found to have probable norovirus gastroenteritis. These passengers had used the toilet more frequently than those who did not become ill, suggesting that the toilet facility played a role in transmission. However, it remains unclear whether airborne transmission or contact transmission was the primary mode of transmission.

2.8 Conclusion

This chapter has reviewed the existing literature on the potential for disease transmission in toilet facilities, focusing on aerosol generation, the presence of pathogens in faecal matter, experimental methods, risk assessment approaches and computational airflow modelling techniques. The evidence highlights the role of toilet plume aerosols in pathogen transmission and the need for further research to fully understand infection risks. Key findings from the literature include:

- Experimental studies demonstrate that toilet flushing generates aerosols and bioaerosols, some of which remain airborne for long periods of time and may contain viable pathogens. However, studies differ in their methodologies and there is a lack of standardised approaches to assessing toilet generated aerosol risks in toilet facilities.
- Epidemiological studies have identified toilet facilities as potential transmission

environments, although distinguishing between airborne and contact transmission remains a challenge. Cases such as Amoy Gardens (SARS-CoV) and outbreaks on aircraft and cruise ships suggest that aerosols may play a role, but direct evidence is limited.

- Pathogens are present in faecal matter at varying concentrations, and some have been shown to remain viable in faecal aerosols. However, there is less evidence to confirm whether these pathogens retain infectivity after aerosolisation.
- QMRA has been widely used to estimate infection risks for both airborne and contact transmission. Studies have applied QMRA to toilets, healthcare settings, transportation, and wastewater treatment plants, reinforcing its utility in assessing disease transmission risks.
- CFD simulations are widely used to study airborne and contact transmission in indoor environments. CFD studies focused on toilet plume aerosols show that particles remain airborne for extended periods of time.

Despite significant research on bioaerosols and transmission dynamics, gaps remain, particularly in linking toilet plume aerosols to infection risks and in assessing different types of exposure scenarios. Addressing the following gaps would improve understanding of potential risks and enhance mitigation strategies:

- Experimental studies on aerosol and bioaerosol dispersion in toilet facilities remain limited, particularly in controlled chamber investigations that examine the impact of room layout. There is little experimental evidence exploring the effects of cubicle structures on aerosol dispersion in a mechanically ventilated setting.
- QMRA studies on toilet plume aerosols are scarce and often rely on preexisting particle concentration data rather than direct measurements that incorporate different ventilation rates and room configurations. Existing studies have been limited to specific toilet configurations and have not used controlled seeding of toilet water.
- CFD modelling of toilet plume aerosols has been relatively limited, with few

studies applying the DPM method. Only one study has investigated a shared toilet facility and no studies have explicitly examined human exposure in such environments.

Chapter 3

Experimental Study Investigating Flush-Generated Aerosols

3.1 Introduction

As discussed in Chapter 2, flushing the toilet can generate airborne particles that can contain infectious microorganisms, which can disperse and remain airborne for extended periods or settle on surfaces [10, 11, 49, 52, 53]. Quantifying the generation and dispersion of such particles provides the data needed to evaluate environmental exposure risks. This chapter describes a series of controlled experiments in a mechanically ventilated chamber designed to characterise the aerosolisation of particles and bacteria during toilet flushing under different conditions.

Two different solutions were used in the toilet bowl for flushing: (i) a sodium chloride (NaCl) solution used to model the aerosolisation of non-biological particles and (ii) a suspension of *E. coli* as a microbial contaminant. *E. coli* was selected as a biological surrogate due to its relevance as an indicator organism for faecal contamination, as discussed in Chapter 2, Section 2.4.

The objective of this work was to assess how different ventilation rates and cubicle configurations influence airborne particle concentrations and microbial dispersion for a toilet typical of the UK (gravity-flow close-coupled). Ventilation is a crucial factor in mitigating airborne disease transmission, and understanding its role in reducing particle and bioaerosol persistence is essential for improving infection control measures in shared toilet facilities. In the experiments a cubicle structure was included to allow for a direct comparison between open and enclosed toilet environments, reflecting real-world scenarios where confined spaces may affect particle dispersion and bioaerosol exposure.

The following sections describe the materials, experimental setup, and methodologies used to quantify airborne particles and *E. coli* bacterial concentrations in the controlled chamber after a toilet flushing event. This data informs the subsequent risk assessment of environmental exposure.

3.2 Materials

The following sections describe the preparation of materials used in the experimental work. This includes the growth of *E. coli* cultures, the preparation of media

and solutions to quantify biological contamination and the formulation of the NaCl solution used to assess the concentration of particles generated by toilet flushing.

3.2.1 Bacterial Strains

The strain of *E. coli* used in this study was the American Type Culture Collection (ATCC) 10536 strain. *E. coli* was selected for its relevance as an indicator organism for faecal contamination [329]. *E. coli* is a gram-negative, non-spore-forming bacterium with rod-shaped cells measuring 2.0 µm to 6.0 µm in length and 1.0 µm to 1.5 µm in width [330]. Fig. 3.1 provides an illustration of an *E. coli* cell.

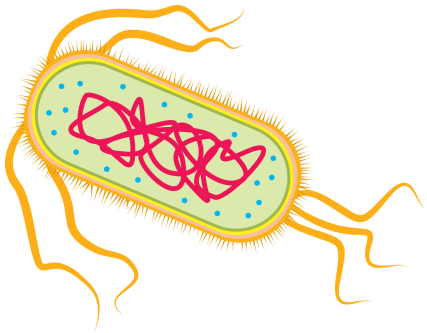

Figure 3.1: Illustration of an *E. coli* cell, a rod-shaped, Gram-negative bacterium used in this study.

3.2.2 Preparation of Suspension Liquids

Preparation of Ringer's Solution

A quarter-strength Ringer's solution was used as a suspension medium for *E. coli*. Ringer's solution is an isotonic solution, meaning that there is no net flow of water across cell membranes. This prevents cells from shrinking or swelling [331]. A total of 0.9 L of quarter-strength Ringer's solution was prepared by dissolving two Oxoid™ Ringer's solution tablets (Thermo Scientific™) in 1 L of deionised water. After thorough mixing, 0.1 L was removed before sealing the container. The solution was then autoclaved at 121 °C for 15 min. These quantities were selected according to the measured capacity of the toilet bowl, which could hold approximately 1 L of fluid. Thus, 0.9 L of quarter-strength Ringer's solution was prepared, with 0.1 L of liquid *E. coli* culture added before each experiment. The preparation of the liquid *E. coli* culture is discussed in Section 3.2.5.

For the serial dilutions, discussed in detail in Section 3.2.6, 9 mL units of quarter-strength Ringer's solution were required. To prepare these, 1 L of the solution was made by dissolving two Oxoid™ Ringer's solution tablets (Thermo Scientific™) in 1 L of deionised water. The solution was thoroughly mixed and 9 mL aliquots were dispensed in McCartney bottles. The bottles were then autoclaved at 121 °C for 15 min and cooled to room temperature before use.

Preparation of Sodium Chloride Solution

For particle concentration measurements, a 5 % sodium chloride (NaCl) in a water solution was used in the toilet bowl. This created a safe aerosol, and salt solutions have previously been shown to behave in a similar way to microbial aerosols in the air [332, 333]. The solution was prepared by dissolving 50 g of sodium chloride (99.5 % purity, Scientific Laboratory Supplies) in 1 L of deionised water, in a sterile container. The solution was mixed thoroughly by shaking.

3.2.3 Preparation of Agar Plates

TSA plates were used as a growth medium for bacterial cultures, including fresh *E. coli* cultures, serial dilutions, bioaerosol sampling and settle plates. TSA is commonly used in environmental microbial studies [132, 334, 335, 336].

For small batches, 40 g of TSA powder (Oxoid™ Cold Filterable Tryptone Soya Agar Dehydrated, Thermo Scientific™) was dissolved in 1 L of deionised water and autoclaved at 121 °C for 15 min. After being cooled to approximately 60 °C, the medium was poured into 90 mm petri dishes using aseptic technique and left to cool to room temperature. Aseptic technique was used to prevent microbial contamination during media preparation. This technique involves working near a Bunsen burner, which creates an upward convection current that reduces the risk of airborne microorganisms settling on the agar [331].

For larger batches, TSA preparation was automated using the Masterclave 09 (Don Whitley Scientific) and the APS One: Fully Automated Pourer Stacker (Don Whitley Scientific). The Masterclave 09 stirred the TSA powder and deionised water for 5 min, then heated the mixture to 121 °C for 15 min to sterilise it. The mixture

was cooled to 45 °C and kept at this temperature until dispensed into 90 mm petri dishes by the APS One.

3.2.4 Preparation of Liquid Growth Media

To grow the *E. coli* from a single culture, a Tryptone Soya Broth (TSB) was used as a liquid medium for bacterial growth prior to adding it to the toilet bowl. TSB contains enzymatic digests of casein and soybean meal, supplying amino acids and nitrogenous compounds essential for bacterial growth [337]. It is used for cultivating both aerobic and anaerobic bacteria.

To prepare the TSB, 15 g of TSB powder (Oxoid™ Cold Filterable Tryptone Soya Broth Dehydrated, Thermo Scientific™) was dissolved in 0.5 L of deionised water. The solution was divided into 0.1 L portions in five conical flasks, each with a foam bung inserted and loosely covered with foil. They were autoclaved at 121 °C for 15 min, then cooled to room temperature and refrigerated at 3 °C until use.

3.2.5 Preparation of Bacterial Cultures

Bacterial cultures of *E. coli* were required for the biological experiments. Agar cultures were prepared to ensure that colonies were readily available for inoculation of the TSB. Once inoculated, 0.1 L of liquid culture was grown and subsequently added to 0.9 L of quarter-strength Ringer's solution. This method is similar to that of Zhang et al. [171] such that an amount of *E. coli* (50 mL) was added to the toilet bowl water, but in their study the mixture was added to the water that was already in the toilet bowl. In this current study, the *E. coli* solution and toilet bowl water were thoroughly mixed before being added to the toilet bowl. This section details the preparation of both the agar and liquid cultures.

Agar Culture

Using aseptic technique, a sterile inoculation loop was used to transfer a frozen *E. coli* colony onto a TSA plate. The loop was streaked horizontally across a section of the plate to create a dense streak (streak 1). A fresh loop was then used to drag through streak 1 and spread across another section, forming a less dense streak

(streak 2). This process was repeated to create four streaks, each progressively decreasing in bacterial density. Fig. 3.2 illustrates the streak plate method.

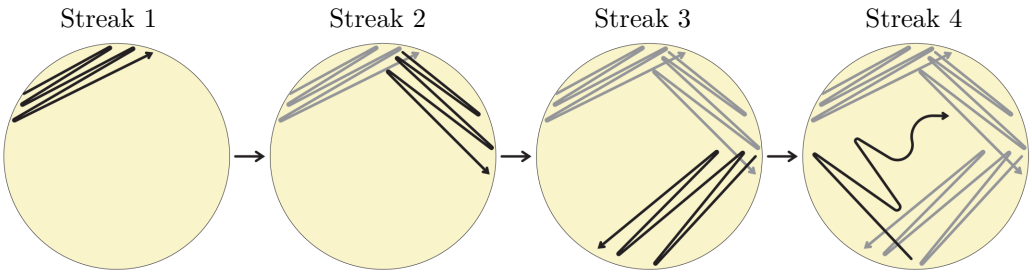

Figure 3.2: Illustration of the streak plate method for *E. coli* isolation. Bacterial density decreases progressively across four streaks to obtain single colonies.

The agar plate was incubated at 37 °C for 24 h, allowing single visible colonies to form, as shown in Fig. 3.3.

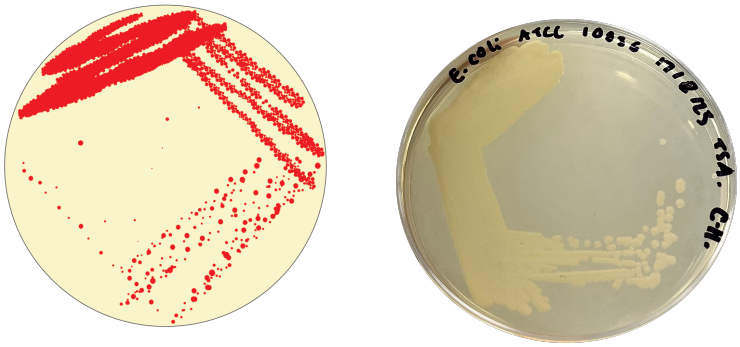

(a) Schematic representation of the streaking process.

(b) TSA plate showing isolated *E. coli* colonies.

Figure 3.3: Formation of *E. coli* colonies on TSA plates after incubation at 37 °C for 24 h. The streaking process results in areas of high and low bacterial density, enabling colony isolation.

Once healthy *E. coli* colonies were established, additional cultures were prepared by selecting a single colony and streaking it onto a new agar plate using the same technique. Subsequently, these isolated colonies were used to inoculate TSB to prepare liquid culture.

Liquid Culture

To prepare the 0.1 L liquid culture of *E. coli*, a sterile 0.1 L TSB solution was prepared in a conical flask, as detailed in Section 3.2.4. Using aseptic technique, a single *E. coli* colony was transferred from an agar plate to the broth using a sterile

inoculation loop. The loop was swirled in the broth to ensure that the colony was fully transferred.

The flask, fitted with a foam bung, was then placed in an incubator with an orbital shaker and incubated at 37 °C for 24 h. After incubation, the culture was cooled to room temperature and refrigerated until use. Before the experiment, the 0.1 L liquid culture was added aseptically to 0.9 L of quarter-strength Ringer's solution (prepared as described in Section 3.2.2). The mixture was shaken throughly to create a 1 L *E. coli* suspension.

The density of faecal coliforms in faeces typically ranges from 10^6 CFU g^{-1} to 10^9 CFU g^{-1} [14]. The average human stool weighs approximately 100 g [46] which results in a typical bacterial count of 10^9 CFU to 10^{12} CFU per bowel movement.

The methods used in the present study produced a 1 L suspension of *E. coli* with a total bacterial count on the order of 10^{12} CFU. While Zhang et al. [171] used bacterial quantities of 10^{11} CFU in the toilet bowl per flush, the decision was made to use the upper bound of faecal coliform concentrations. As faecal coliforms encompass a broader range of bacterial species beyond *E. coli*, it should be noted that this approach may overestimate *E. coli* concentrations in faecal matter.

3.2.6 Serial Dilutions and Enumeration of Bacterial Cultures

Serial dilutions are used to determine the concentration of a bacterial solution by systematically reducing its concentration by an order of magnitude. In this study, serial dilutions were performed to quantify the initial concentration of the 1 L *E. coli* solution used in the toilet bowl experiments. The dilution process is illustrated in Fig. 3.4. To prepare the dilutions, 1 mL of the *E. coli* solution was pipetted into a McCartney bottle (bottle A) containing 9 mL of quarter-strength Ringer's solution (prepared as described in Section 3.2.2), creating a 10^{-1} dilution. Bottle A was thoroughly shaken, and 1 mL of its contents was transferred to another McCartney bottle (bottle B) containing 9 mL of quarter-strength Ringer's solution, producing a 10^{-2} dilution. This step was repeated sequentially to generate a series of solutions, each diluted by an order of magnitude from the previous one. All dilution steps were

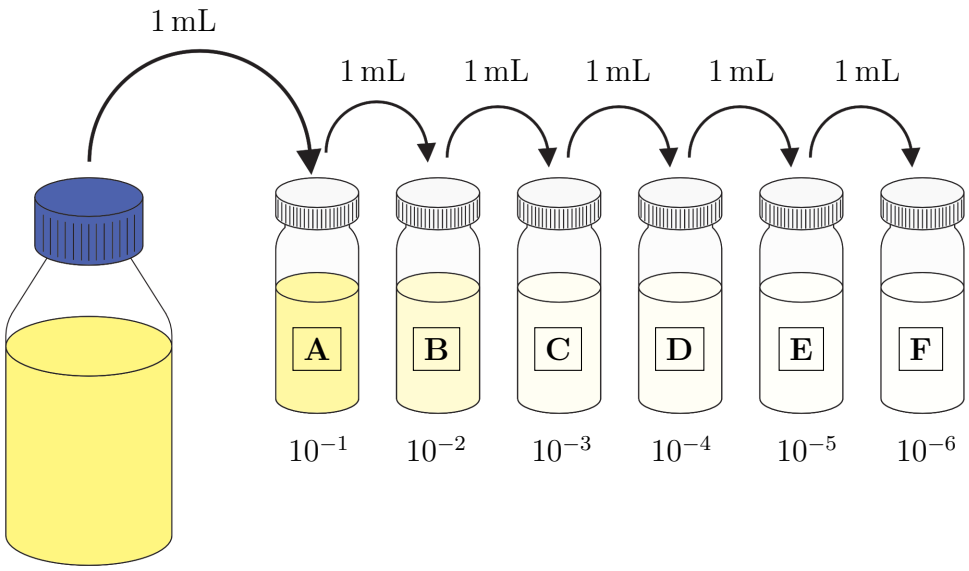

Figure 3.4: Illustration of the serial dilution process used to quantify *E. coli* concentrations by dilution in quarter-strength Ringer's solution.

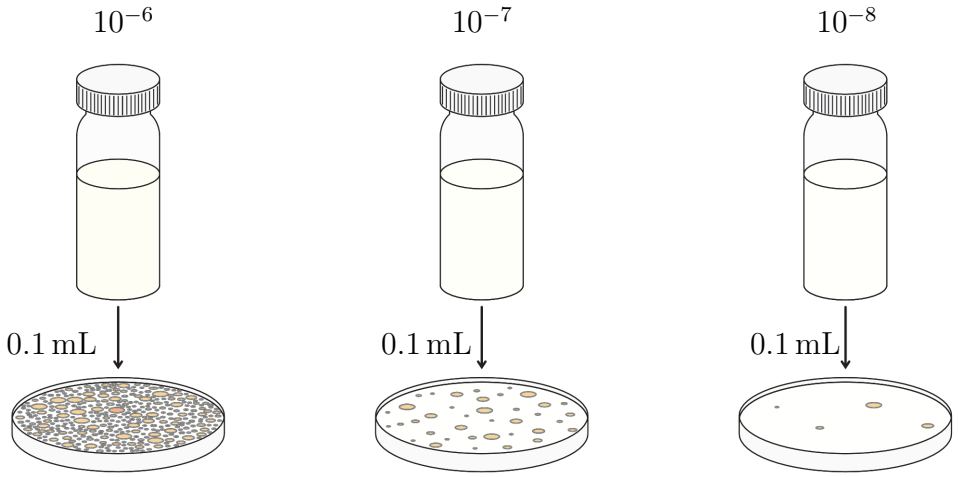

Figure 3.5: The plating out process following on from serial dilutions. The 10^{-7} dilution plate has a countable number of colonies, the 10^{-6} dilution plate has too many to count and the 10^{-8} dilution plate has too few to count.

performed using aseptic techniques to prevent contamination and ensure accuracy.

Following serial dilution, each dilution was plated onto TSA plates (prepared as detailed in Section 3.2.3). Fig. 3.5 provides an overview of this process. For each dilution, 0.1 mL was pipetted onto a TSA plate and spread using a plate spreader. This was done in duplicate for accuracy. The plates were incubated at 37 °C for 24 h, after which colony counts were performed.

Plates containing more than 300 colonies were considered too numerous to count accurately, while those with less than 30 colonies were insufficient for reliable estima-

tion. The colony count of plates containing between 30 and 300 colonies (countable plates) was averaged across duplicates to calculate the mean colony count. The initial concentration of the 1 L *E. coli* solution was then determined using Eqn. (3.1).

$$C_{\text{initial}} = \frac{n_{\text{colonies}}}{V_{\text{plate}}} \times \frac{1}{F_{\text{dilution}}}, \tag{3.1}$$

where,

C_{initial} = initial concentration of *E. coli* stock [CFUmL^{-1}],
n_{colonies} = mean number of colonies on the countable plates [CFU],
V_{plate} = volume of solution pipetted onto the TSA plate [mL] and
F_{dilution} = dilution factor (e.g. 10^{-7}).

For example, if 50 colonies were counted on a plate from the 10^{-7} dilution, applying Eqn. (3.1) gives an initial solution concentration of 5.0×10^{9} CFU mL^{-1}. This corresponds to a total of 5.0×10^{12} CFU in the 1 L solution.

3.3 Experimental Setup

3.3.1 Aerobiology Chamber

The controlled experiments were performed in a mechanically ventilated chamber measuring 4.26 m × 3.35 m × 2.26 m based at the University of Leeds, with well-insulated adiabatic walls to minimise heat exchange with the environment. This particular chamber has previously been used for experimental investigations of bioaerosol and surface sampling [4, 132, 338, 339, 340]. A schematic of the chamber is shown in Fig. 3.6.

The chamber door, which leads to an anteroom, remained closed during the experiments. Air was supplied through a high-level diffuser with an area of 0.110 m^2, filtered using a HEPA filter. Although HEPA filters are not common in toilet facilities, one was used here to eliminate the influence of particles external to the chamber on particle concentration results. The air exited through a low-level diffuser outlet with an area of 0.113 m^2, positioned diagonally opposite the inlet.

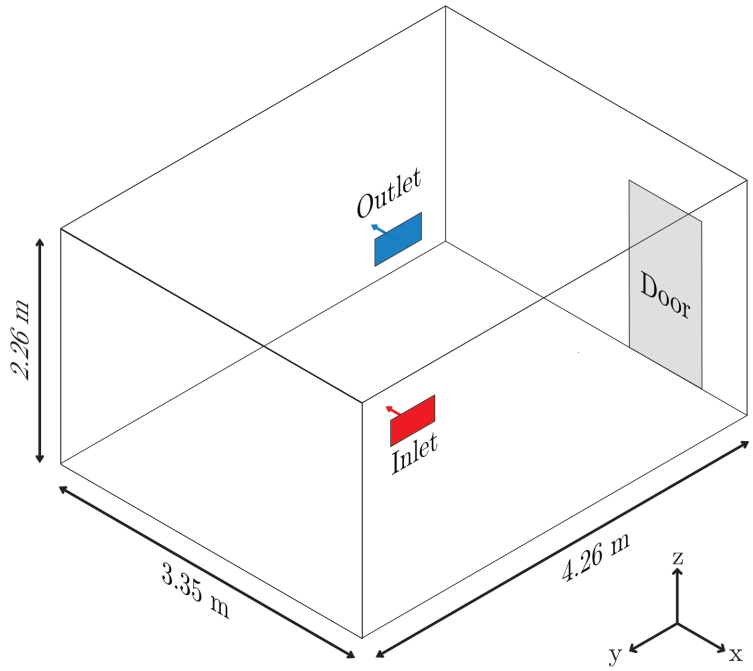

(a) The empty aerobiology chamber.

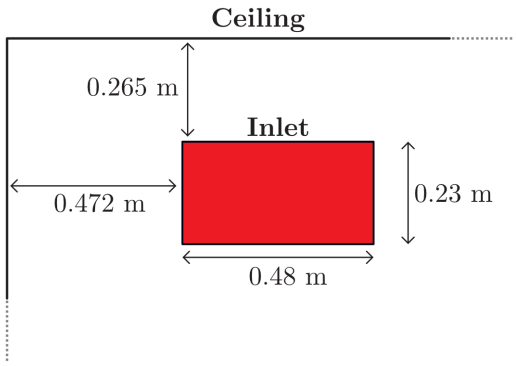

(b) The dimensions of the inlet.

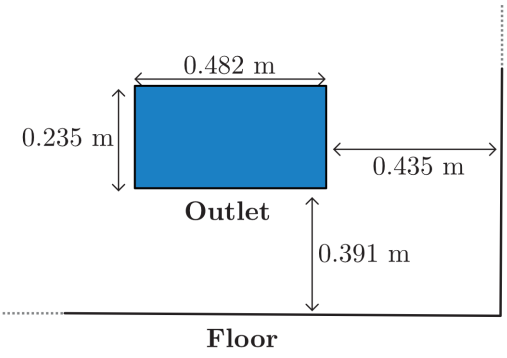

(c) The dimensions of the outlet.

Figure 3.6: A schematic diagram of the mechanically ventilated aerobiology chamber based at the University of Leeds used for the experimental work.

Ventilation Rate Set-up

Three ventilation rates were investigated: 1.5, 3 and 6 ACH. These rates were based on guidance from NHS England, which recommends 3 ACH for single-room toilet facilities and 6 ACH for communal ward toilets [341]. A 1.5 ACH condition was used to represent a poorly ventilated scenario. The mass flow rate at the ventilation outlet was calculated using Eqn. (3.2) to determine the settings for the extract and inlet fans.

$$Q = \frac{V_{\text{chamber}} \times \text{ACH}}{3.6} \tag{3.2}$$

where

Q = mass flow at the outlet [$\mathrm{L\,s^{-1}}$],

ACH = required ventilation rate [$\mathrm{h^{-1}}$] and

V_{chamber} = volume of the chamber [$\mathrm{m^3}$].

Table 3.1 lists the mass flow rates required at the outlet for a given ventilation rate, based on the volume of the chamber. The extract fan settings were adjusted while measuring the mass flow rate at the outlet with a balometer (Model PH721, TSI Incorporated, Shoreview, MN) to achieve the desired ventilation rate. The inlet fan was then adjusted to maintain a negative pressure of approximately 10 Pa to 12 Pa to prevent contamination from the external environment.

Table 3.1: Mass flow rates required at the chamber outlet for the ventilation rates in the aerobiology chamber.

Ventilation rate [ACH]	**Q** [$\mathrm{L\,s^{-1}}$]
1.5	13.44
3	26.88
6	53.75

3.3.2 Toilet Rig

Toilet

A Portland close-coupled toilet pan, cistern and seat (Wickes), typical of the UK, was used. The cistern was 390 mm × 320 mm × 180 mm, and the toilet pan was 400 mm × 350 mm × 660 mm, with a total weight of 35 kg. The maximum capacity of the cistern was 6 L, and water was added manually for each experiment. Wastewater was collected in an external 15 L bucket connected with two flexible pipes (Euroflo Flexible Long Pan Connector, Fluidmaster), linking the toilet waste pipe to the bucket. The connection between the pipe and the bucket was sealed to prevent leakage and minimise secondary aerosolisation.

Toilet Mount

To ensure proper drainage, the toilet was positioned on a custom mount that directed the waste pipe to the collection bucket below. The mount frame was constructed from steel, while the platform and back were made of polyvinyl chloride (PVC), both

chosen for their durability and ease of cleaning. The mount was mobile, equipped with wheels for easy relocation within the chamber and between laboratories. Fig. 3.7 provides a schematic of the toilet mount.

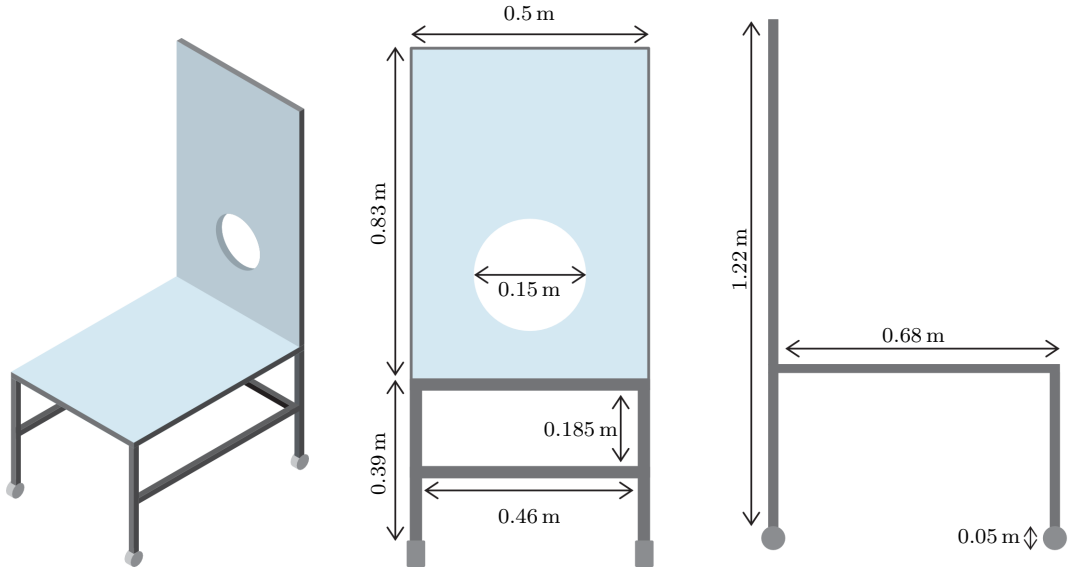

(a) A three dimensional view of the toilet mount.

(b) A two dimensional front view with dimensions.

(c) A two dimensional side view with dimensions.

Figure 3.7: Schematic of the toilet mount used in the experimental setup.

Flushing Mechanism

The toilet was modified to flush remotely from outside the chamber using a cable-operated flush valve (Skylo Dual Flush Valve Long Cable, Viva) to minimise external influence. The cable was extended and secured to the ceiling above the toilet with a cable tie and threaded through a chamber port. Pulling the cable from outside the chamber lifted the valve, releasing water from the cistern into the bowl and initiating the flush.

3.3.3 Bioaerosol Sampling

Bioaerosol sampling was conducted using two Microbio MB2 samplers (Cantium Scientific), each fitted with a 220-hole head and 90 mm TSA plates (prepared as described in Section 3.2.3). The samplers operated at a flow rate of 100 L min^{-1} and had a d50 cut-off of 1.7 µm. Previous work by Paddy, Afolabi, and Sohail [13] used a similar device, the Microbio MB1, to sample bioaerosols from the toilet plume.

Positive Hole Correction

To account for the likelihood that multiple microorganisms enter the same sampling hole and form a single colony, positive hole correction was applied. For the Microbio MB2, the corrected colony count [172, 342], N_c, is given by

$$N_c = N_f \left(\frac{1.075}{1.052 - \frac{N_f}{N_h}} \right)^{0.483}, \tag{3.3}$$

where

N_f – number of counted colonies and

N_h – number of holes in the sampling head.

3.3.4 Particle Concentration Measurement

During salt solution experiments, two OPCs (Handheld Particle Counter 3889, Kanomax) were used, mounted on tripods, to measure particles with diameters of 0.3, 0.5, 1, 3, 5, and 10 µm. These particle sizes are size bins such that the 0.3 µm measurement corresponds to the number of particles with size 0.3 µm to 0.5 µm, the 0.5 µm size is then particles of size 0.5 µm to 1 µm and the 10 µm size is particles ≥10 µm. Each device operated at a sampling flow rate of 2.83 L min^{-1}.

3.3.5 Indoor Air Quality Measurements

Temperature and relative humidity were monitored using an indoor air quality monitor (AirVisual Pro, IQAir) for both the non-biological and biological experiments.

3.4 Overview of Experimental Scenarios

3.4.1 Aerosolisation Experiments Using Sodium Chloride Solution

For each experiment, 6 L of tap water was manually added to the cistern. Any water accumulated in the bowl was siphoned into the waste bucket. The toilet seat and lid were positioned upright and the toilet bowl was filled with 1 L of a 5 % NaCl solution, prepared as described in Section 3.2.2. Two tripods supporting the OPCs

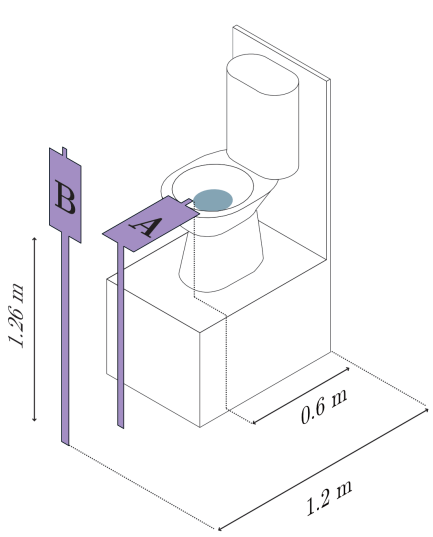

(a) The distances of the OPCs relative to the toilet and toilet mount.

(b) A photograph of the OPCs, toilet and toilet mount inside the chamber.

Figure 3.8: Optical particle counter A and B used for the non-biological particle concentrations.

Table 3.2: Details of scenario 1 (NC) and scenario 2 (2C) used for the non-biological particle concentration measurements using a sodium chloride solution in the toilet bowl.

Scenario	**Abbreviation**	**Details**	**Particle counter locations**
1	NC (no cubicle)	Toilet inside the chamber, against one wall.	A: directly above toilet, horizontally B: next to the toilet, vertically
2	2C (two cubicles)	Toilet in the same location as scenario 1 (NC), but with the addition of two cubicles. One cubicle surrounded the toilet, the other was the same size and adjacent to the first cubicle.	A: inside toilet cubicle, directly above toilet, horizontally B: inside toilet cubicle, next to the toilet, vertically

were used. Particle counter A was positioned directly above the toilet in a horizontal orientation, while particle counter B was placed in front of the toilet in a vertical orientation. The distances of these counters relative to the toilet and mount are shown in Fig. 3.8a and a photograph of the OPCs, the toilet and the toilet mount are shown in Fig. 3.8b. Two scenarios were considered, detailed in Table 3.2 and illustrated in Fig. 3.9. In scenario 2 (2C), the cubicles were constructed using lab

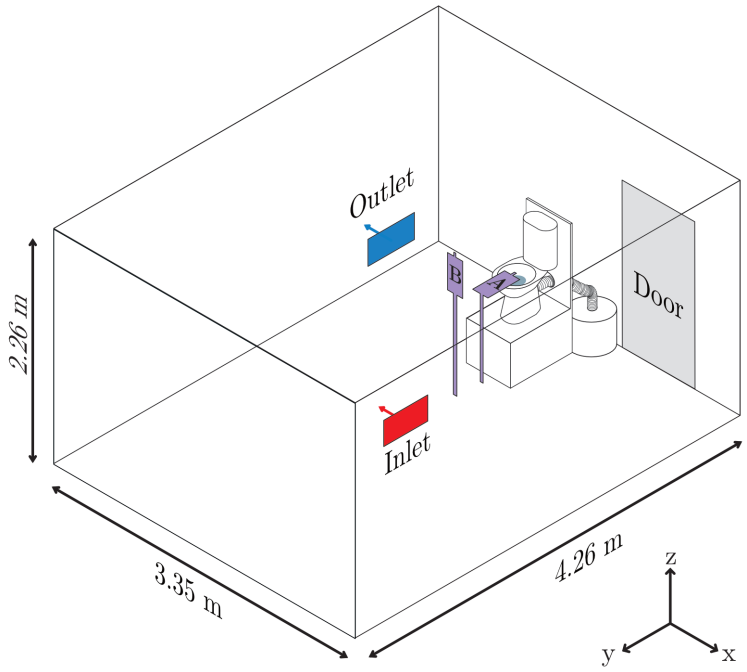

(a) Scenario 1 (NC).

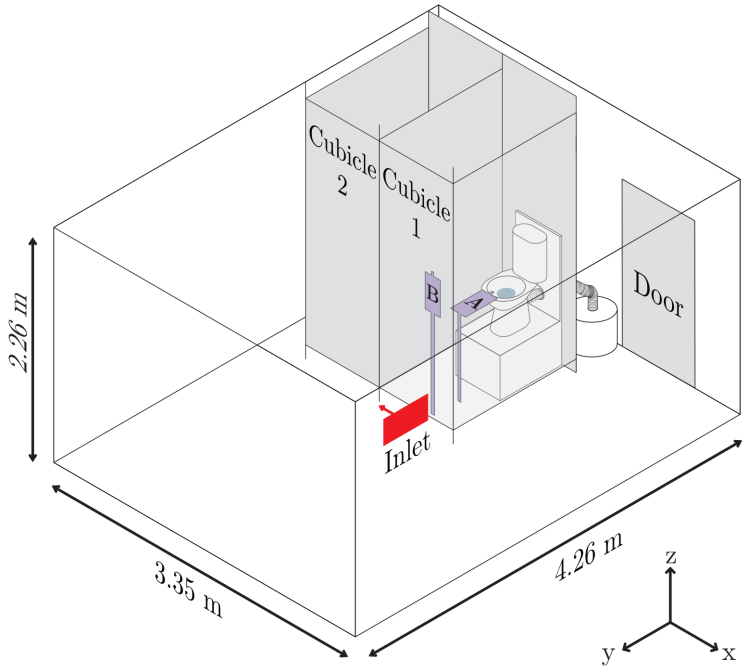

(b) Scenario 2 (2C).

Figure 3.9: Experimental set up for the two scenarios inside the aerobiology chamber.

scaffolding and plastic sheet, with dimensions informed by British Standards [343]. However, it is important to note that cubicle design standards vary internationally. The cubicle dimensions are shown in Fig. 3.10. A small gap existed below the cubicle of 0.11 m and a gap above the cubicle of 0.31 m.

Each experiment measured particle concentrations in the air during a single flush scenario. At the beginning of the experiment, the particle counters were set to run

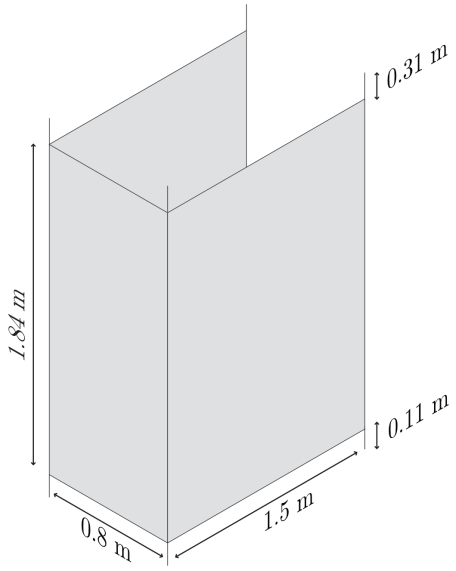

Figure 3.10: The dimensions of the toilet cubicle used in scenario 2 (2C) for the experimental work.

with a 10 s sample interval time, measuring the average concentration of particles over this period. The room was then vacated and left to ventilate at 11 ACH for 30 min aimed at removing any particles generated during the process of entering the room and filling the toilet. The required ventilation rate for the experiment was set and left for 45 min, allowing the room to reach a steady-state background level of particles. The toilet was flushed remotely from outside the room and, after 10 min, the particle counters were stopped. The experiments were performed in triplicate for each ventilation rate. The waste bucket was emptied and the experiment was repeated following the same process for the required ventilation.

Data Processing

The experimental data were extracted from the particle counters and analysed using R (R version 4.3.2 [344], run using RStudio 2023.12.0). A time series for the particle concentrations was generated by averaging the concentrations over the three replicate experiments. The standard error was included as a shaded range in the plots, calculated from the standard deviation of the experimental replicates.

For a given ventilation rate, particle size i, and experimental replicate j, the increase in concentration associated with flushing $c_{i,j,t}$ [m^{-3}] was calculated as

$$c_{i,j,t} = {c_{i,j,t}}^{\text{raw}} - {c_{i,j}}^{\text{background}}, \tag{3.4}$$

where

$c_{i,j,t}^{\text{raw}}$ = average concentration over the 10 s sample [m^{-3}] and

$c_{i,j}^{\text{background}}$ = median concentration in the 5 min prior to flushing [m^{-3}].

If $c_{i,j,t}$, was returned as a negative value, it was set to zero. This analysis enabled a determination of the relative change in concentration over time as a result of the flush, accounting for the background concentration measured before the flush.

The results were also compared with published literature. A comparison was made between the particle size distributions observed in the current study and those reported in previous experimental work by Johnson et al. [2] that quantified droplet production from various types of toilet flush. This comparison used the mean concentration results from scenario 1 (NC) at 1.5 ACH, where external airflows were minimal, reducing the likelihood of external influences on particle dispersion. This concentration was taken from the first 2 min of the current experimental data, with the background count removed. The 2 min period was chosen to minimise the influence of positive fluctuations in background concentration beyond this time. The toilet most comparable in the previous study was a high-efficiency gravity-flow toilet, which was used as a benchmark for this analysis.

3.4.2 Aerosolisation Experiments Using *E. coli*

A similar experimental methodology was used for the *E. coli* experiments as for the sodium chloride experiments (Section 3.4.1). 6 L of tap water was added to the toilet cistern, and any water collected in the bowl was siphoned into the waste bucket. The toilet seat and lid were placed in the upright position and the bowl was filled with 1 L of a liquid culture of *E. coli*, prepared as detailed in Section 3.2.5. Serial dilutions were performed and plated to determine the initial *E. coli* concentration. To disinfect the wastewater as it entered the bucket, two disinfectant tablets were added to the bucket.

Two tripods, each supporting a Microbio MB2 sampler, were positioned in front of the toilet. Each sampler contained a TSA plate, as prepared in Section 3.2.3. The distances of these bioaerosol samplers relative to the toilet and mount are shown in Fig. 3.11. Initial preliminary experiments were performed at locations further away

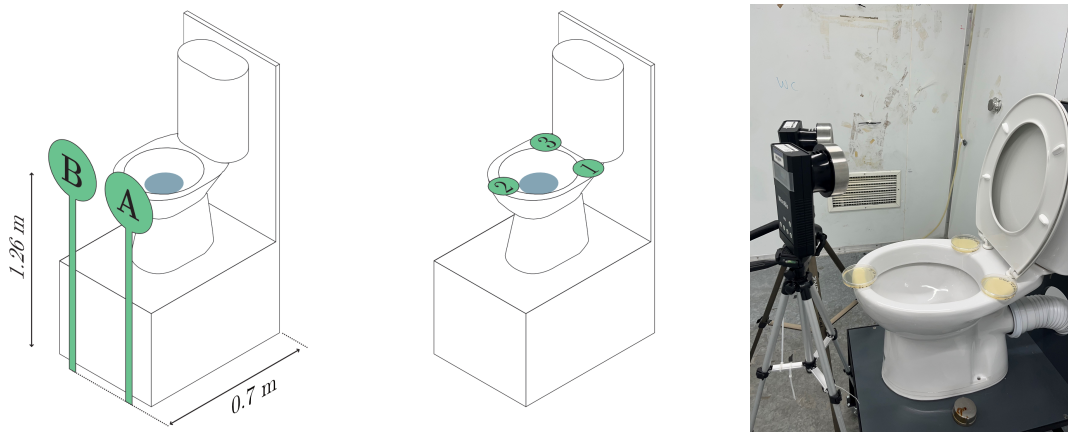

(a) Bioaerosol sampler A and B relative to the toilet mount.

(b) TSA settle plate locations on the toilet rim.

(c) An image of the toilet, toilet mount, settle plates and bioaerosol samplers.

Figure 3.11: Locations of sampling equipment relative to the toilet and mount for the biological toilet flush experiments using *E. coli*.

from the bowl, but no colonies were detected when sampling at these distances. Previous work found that at a lateral distance of 1 m from the centre of a toilet bowl no colonies were collected when flushing *C. difficile* in a toilet bowl using a bioaerosol sampler and that decreasing the distance from the sampler and the bowl resulted in an increase in the bioaerosol concentration [13].

The samplers were set to run for 5 min at a flow rate of 100 L min^{-1}, such that each sampler collected a total volume of 500 L. In addition to bioaerosol samples, deposition samples were collected using TSA settle plates. Three settle plates were placed around the rim of the toilet bowl, and their lids were initially kept on. The experiments were performed in triplicate.

As in the sodium chloride experiments, two scenarios were considered, one with a cubicle arrangement and one without. These scenarios are detailed in Table 3.3 and follow the same arrangement illustrated in Fig. 3.9, but with bioaerosol samplers positioned as shown in Fig. 3.11a. The chamber was ventilated at 11 ACH for 30 min prior to each experiment. After this period, the settle plate lids were removed and the bioaerosol samplers were activated with delayed start times. Bioaerosol sampler A was set to start after 30 min, while bioaerosol sampler B had a delayed start time of 35 min. Ventilation at 11 ACH continued for another 20 min before being reduced to the required ventilation rate.

Table 3.3: Details of scenario 1 (NC) and scenario 2 (2C) used for the bioaerosol and deposition measurements using an *E. coli* solution in the toilet bowl.

Scenario	Abbreviation	Details	Particle counter locations
1	NC	Toilet inside the chamber, against one wall.	A: next to the toilet, vertically B: next to the toilet, vertically
2	2C	Toilet in the same location as scenario 1, but with the addition of 2 cubicles. One cubicle is around the toilet, the other is adjacent to the first cubicle.	A: inside toilet cubicle, next to the toilet, vertically B: inside toilet cubicle, next to the toilet, vertically

Flushing was scheduled to coincide with the start of bioaerosol sampler A. 10 min after flushing, aligning with the end of bioaerosol sampling, the ventilation rate was increased to 11 ACH to ensure the removal of any remaining *E. coli*. The lids were placed back onto all TSA plates (both bioaerosol and settle plates) before being removed from the room. The disinfected wastewater was disposed of 24 h later.

After collection, the samples were incubated at 37 °C for 24 h. The number of colonies grown on the plates was counted both for the bioaerosol samples and the settle plates. For the bioaerosol samples, the counts were adjusted using positive hole correction. The final counts were converted into CFU m^{-3} based on the sampled volume of 500 L (0.5 m^3).

3.5 Results and Discussion

3.5.1 Non-biological Flushing Particle Measurements

Time Evolution of Particle Concentrations

The mean measured particle concentrations with background levels removed for particle counter A and B are shown in Fig. 3.12 and Fig. 3.13, respectively. The mean was calculated as an average of the three experiments for each ventilation rate and scenario.

At particle counter A, there was a rapid initial increase in particle concentra-

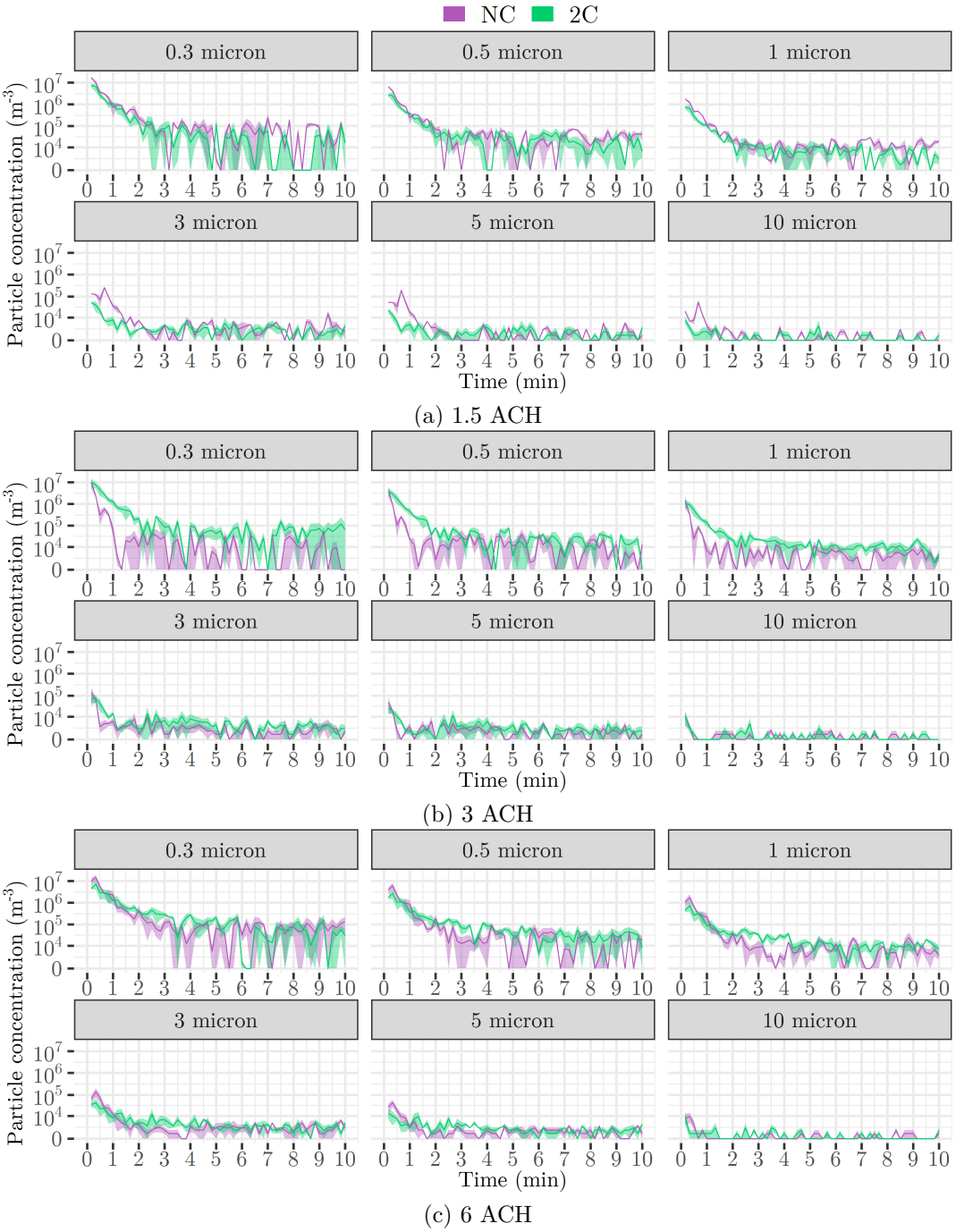

(a) 1.5 ACH

(b) 3 ACH

(c) 6 ACH

Figure 3.12: Particle concentrations at particle counter A, with background concentration removed (median concentration 5 min before flushing), during the 10 min post-flush. Shaded areas denote standard error across replicates.

tions across all particle sizes. This peak decayed to background levels as the flushed particles dispersed within the room and were subsequently removed by ventilation. After this decay, fluctuations in concentration were observed above zero, reflecting variations around the background level. The time series was positively skewed as concentrations below the background threshold were set to zero. During the first 10 s of flushing, higher particle concentrations were observed in scenario 1 (NC)

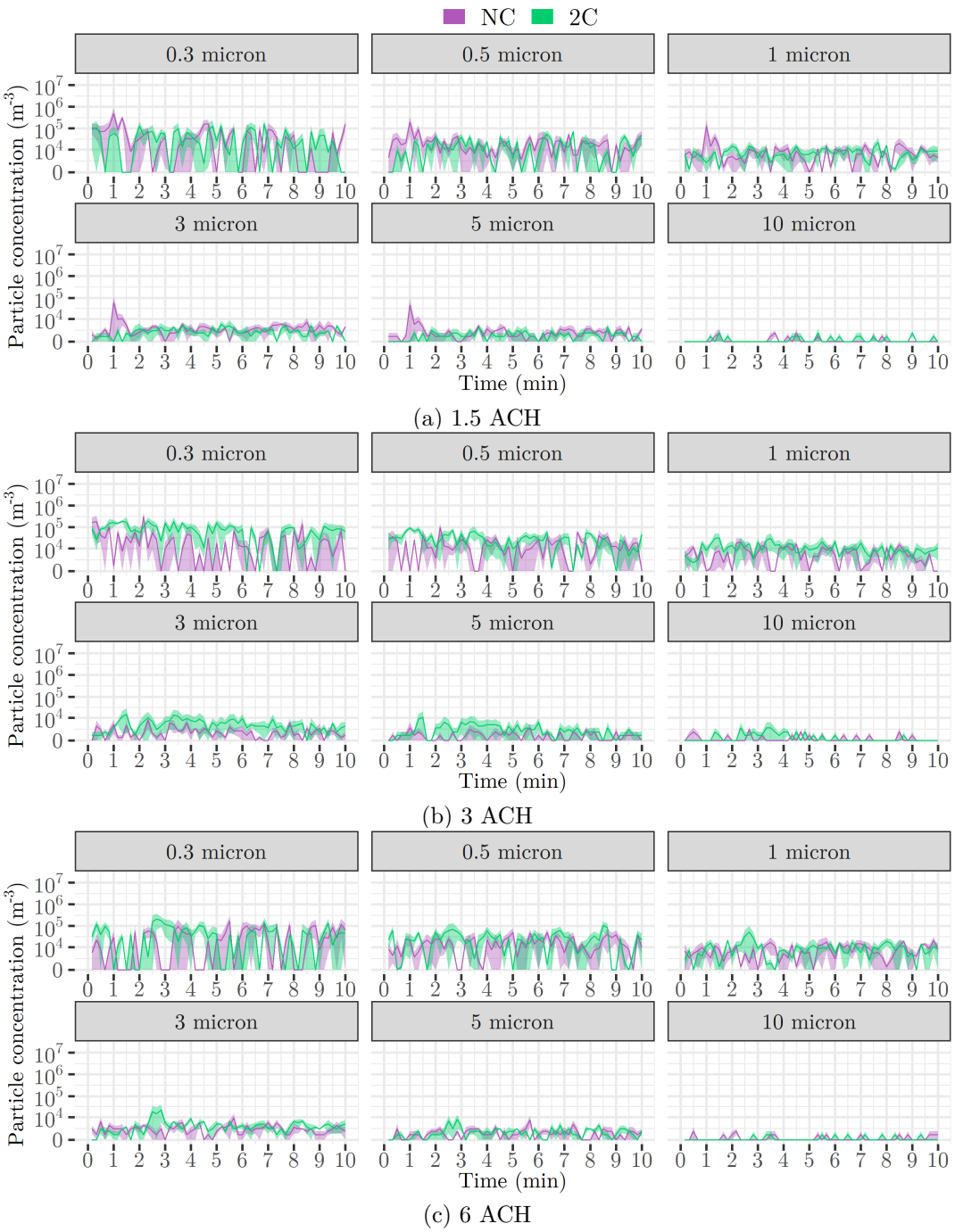

(a) 1.5 ACH

(b) 3 ACH

(c) 6 ACH

Figure 3.13: Particle concentrations at particle counter B, with background concentration removed (median concentration 5 min before flushing), during the 10 min post-flush. Shaded areas denote standard error across replicates.

compared to scenario 2 (2C) at ventilation rates of 1.5 and 6 ACH. However, at 3 ACH, concentrations were similar between the scenarios. Differences in concentration between ventilation rates may be influenced by airflow patterns within the room, potentially enhancing particle aerosolisation in this region.

At particle counter B, no clear initial spike in concentration was observed. While a spike occurred at particle counter A, which was closer to the source, any increase

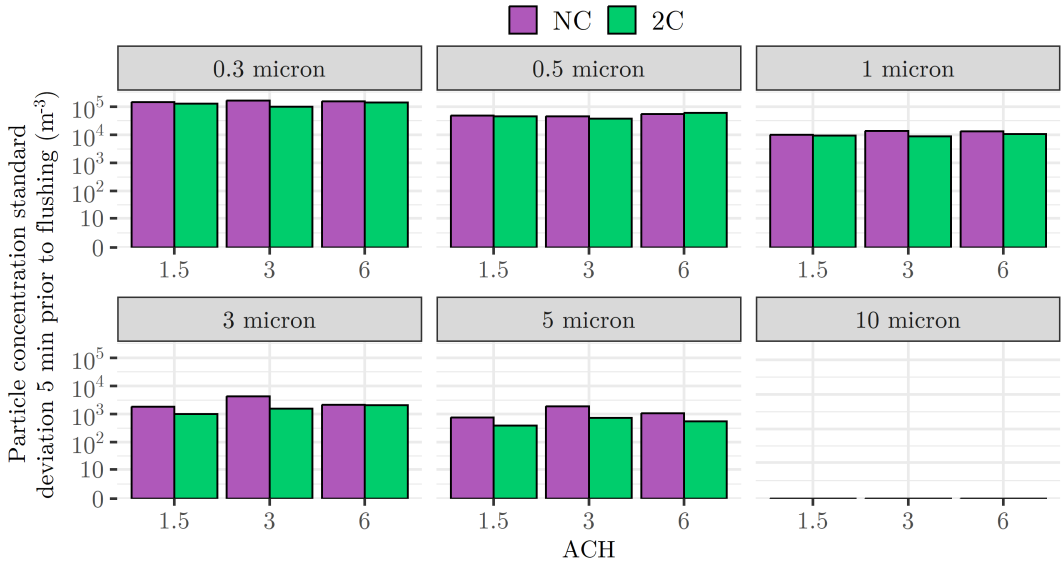

Figure 3.14: Standard deviations of particle concentrations at particle counter B in the 5 min prior to flushing for scenario 1 (NC) and scenario 2 (2C) at the three different ventilation rates.

at particle counter B remained below the detection limit due to background fluctuations. As particles dispersed throughout the room, the resulting concentration increase was less pronounced compared to particle counter A. Fig. 3.14 shows the standard deviation in particle concentrations at particle counter B during the 5 min before flushing. Across all particle sizes, these variations are of the same order of magnitude as the variations in Fig. 3.13, highlighting the challenge of distinguishing toilet flush generated particles from the background variations.

For particle sizes 3 µm and 5 µm, a small spike occurred at 1 min in Fig. 3.13a and at 2.5 min in Fig. 3.13c. These increases were likely influenced by airflow patterns. Such fluctuations could be significant, as an individual in the toilet facility at these times may have inhaled a large quantity of particles.

Total Particle Counts From Flushing

Fig. 3.15 shows the normalised particle concentrations using the experimental data for the first 2 min after flushing, compared to those reported by Johnson et al. [2] for a high-efficiency gravity-flow toilet, which were measured over the first 15 s. The term $\Delta\ln(d)$ represents the logarithmic difference between the upper and lower bounds of the size bin. The 10 µm particle bin is not included, as it represents particles greater than 10 µm, which makes $\Delta\ln(d)$ undefined.

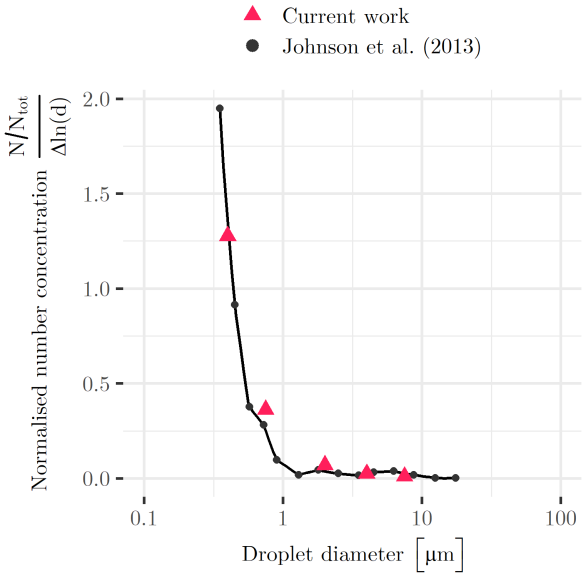

Figure 3.15: Normalised particle concentrations in the current study compared to a high-efficiency gravity-flow toilet in the work by Johnson et al. [2].

Table 3.4: Estimated total number of particles generated by the toilet flush for each particle diameter, calculated using Optical Particle Counter (OPC) counts and an estimation of the volume occupied by the toilet plume.

Particle diameter [µm]	**Proportion (%)**	**Total number of particles**
0.3	65	23,179
0.5	25	8,923
1	7.7	2,744
3	1.3	448
5	0.69	245
10	0.19	67

The study by Johnson et al. [2] used a 15-channel particle counter, which provided a larger number of data points for comparison. The results of the current study show good agreement with previous experimental data, suggesting that the use of the 2 min period is appropriate when considering the relative weights of each particle size. The estimated total number of particles generated by the toilet flush for each particle diameter is detailed in Table 3.4.

The total number of particles released by the toilet was estimated to be 35,607. The study by Johnson et al. [2] found that 10,620 particles were released for the high-efficiency toilet. This may be due to the larger volume of the toilet cistern in this current study (6 L vs. 4.9 L) or other differences in the toilet itself such as the shape of the bowl or the exact flushing mechanism. The total number of droplets released in the study by Johnson et al. [2] ranged from 8,220 to 145,214

so the quantity estimated here is within the same order of magnitude. From Table 3.4 it can be seen that 99 % of particles released have a diameter of less than 5 µm, aligning with the findings of Johnson et al. [2] who found that for all toilet types and flush conditions, more than 99 % of droplets were less than 5 µm.

3.5.2 Aerosolisation Experiments Using *E. coli*

Bioaerosol Samples

The concentration of airborne bacteria measured by the bioaerosol samplers is shown in Fig. 3.16. Bacterial counts were recorded in CFU m^{-3} of air.

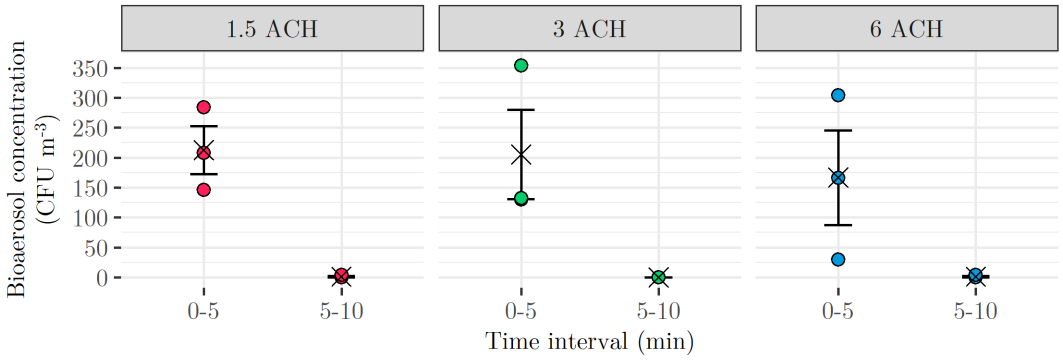

(a) Scenario 1 (NC).

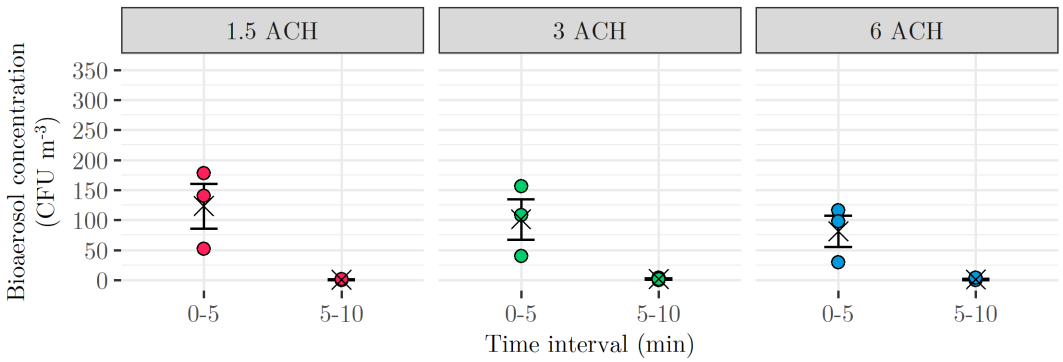

(b) Scenario 2 (2C).

Figure 3.16: Bioaerosol concentrations measured by the bioaerosol samplers (Microbio MB2) for the three ventilation rates and two experimental scenarios. The mean count is indicated by a cross, with standard error bars representing variability across replicates. Each time period and ventilation rate was tested in triplicate.

The results shown in Fig. 3.16 reveal trends in bioaerosol concentrations under different ventilation rates and experimental scenarios. There is an absence of bacteria in the 5 min to 10 min sampling period which suggests that no further bacteria were aerosolised from the toilet plume or transported to this region of the chamber in this time. The lack of airborne bacteria in this period indicates that most

bioaerosol generation occurs within the first few minutes after flushing, with little to no release after at this location. This aligns with the particle concentration findings from Section 3.5.1 where there was a sharp increase in particle concentrations in the first few minutes which then decrease back to background. This finding supports the idea that toilet plume generated bioaerosols are highly transient.

The results also show that increasing the ventilation rate lead to a small reduction in mean bacterial concentration. This reduction could be due to the removal of airborne bacteria through the ventilation system, preventing their build-up in the chamber. Another possibility is that higher airflow velocities increase deposition onto surfaces, reducing the number of bacteria that remain airborne. Additionally, higher airflow velocities could transport the plume away from the sampler zone more rapidly and promote greater dispersion in the air, leading to lower measured concentrations at the sampling location. Increasing ventilation from 1.5 ACH to 3 ACH resulted in a decrease of 7 CFU m^{-3} for scenario 1 (NC) and 22 CFU m^{-3} for scenario 2 (2C). Increasing ventilation from 1.5 ACH to 6 ACH led to a further decrease of 46 CFU m^{-3} for scenario 1 (NC) and 42 CFU m^{-3} for scenario 2 (2C). The larger reduction at higher ventilation rates suggests that increased air exchange may be more effective in removing airborne bacteria in regions close to the toilet.

Another notable trend is the difference in bioaerosol concentrations between the two experimental scenarios. Across all ventilation rates, the mean bioaerosol concentration in the 0 min to 5 min sampling period was lower in scenario 2 with the cubicle (2C) compared to the open room in scenario 1 (NC). One possible explanation is variability in the initial *E. coli* concentration in the toilet bowl, as it was not possible to achieve identical bacterial concentrations for each experiment. The exact relationship between initial bacterial concentration and bioaerosol release remains uncertain. However, Paddy, Afolabi, and Sohail [13] found that higher bacterial concentrations in the toilet bowl led to higher bioaerosol concentrations, the extent of this effect depending on the sampling time and lateral sampling location. Similarly, Zhang et al. [171] identified a linear relationship between total bacterial count and bioaerosol release during flushing.

In scenario 1 (NC), the average initial *E. coli* concentration in the toilet bowl was 6.3×10^9 CFU mL^{-1}, 6.1×10^9 CFU mL^{-1}, and 7.6×10^9 CFU mL^{-1} for ventilation rates of 1.5 ACH, 3 ACH, and 6 ACH, respectively. In scenario 2 (2C), these values were 3.2×10^9 CFU mL^{-1}, 7.0×10^9 CFU mL^{-1}, and 6.9×10^9 CFU mL^{-1}. For 1.5 ACH and 6 ACH, the initial bacterial concentration was lower in scenario 2 (2C), which could contribute to the observed reduction in bioaerosol concentrations.

Another possible explanation is the influence of airflow dynamics. In scenario 1 (NC), the absence of cubicle walls may have resulted in higher airflow velocities near the bioaerosol samplers, increasing the likelihood of particles containing bacteria becoming airborne. Additionally, variations in the flushing process itself could have played a role, as small differences in flush dynamics can influence the number of bacteria aerosolised.

Zhang et al. [171] found that the total release of bioaerosol from toilet flushing was approximately 0.2 CFU per 10^9 initial CFU in the toilet bowl for *E. coli*. This was determined by dividing the total bioaerosol counts by the initial bacterial concentration in the bowl, multiplying by 10^9, and averaging over repeated experiments. The equivalent values for the current data set are presented in Fig. 3.17. The normalisation process followed the same approach, with bioaerosol counts divided by the initial bacterial concentration in the bowl, scaled to 10^9, and averaged over three experimental repetitions.

The results in Fig. 3.17 are approximately an order of magnitude lower than those reported by Zhang et al. [171], where the normalised values ranged from 0.1 to 0.3. The lower bioaerosol release observed in this study, particularly in scenario 2 (2C), may be attributed to differences in toilet type, room layout, or ventilation conditions, all of which influence aerosolisation and particle transport. Furthermore, Zhang et al. [171] used an Andersen sampler, while the present study used a Microbio MB2, making direct comparisons between studies challenging. However, despite methodological differences, the normalised values remain within a comparable range.

The mean normalised value decreases as ventilation rate increases. This is most noticeable in scenario 2 (2C) between 1.5 and 3 ACH and in scenario 1 between 3

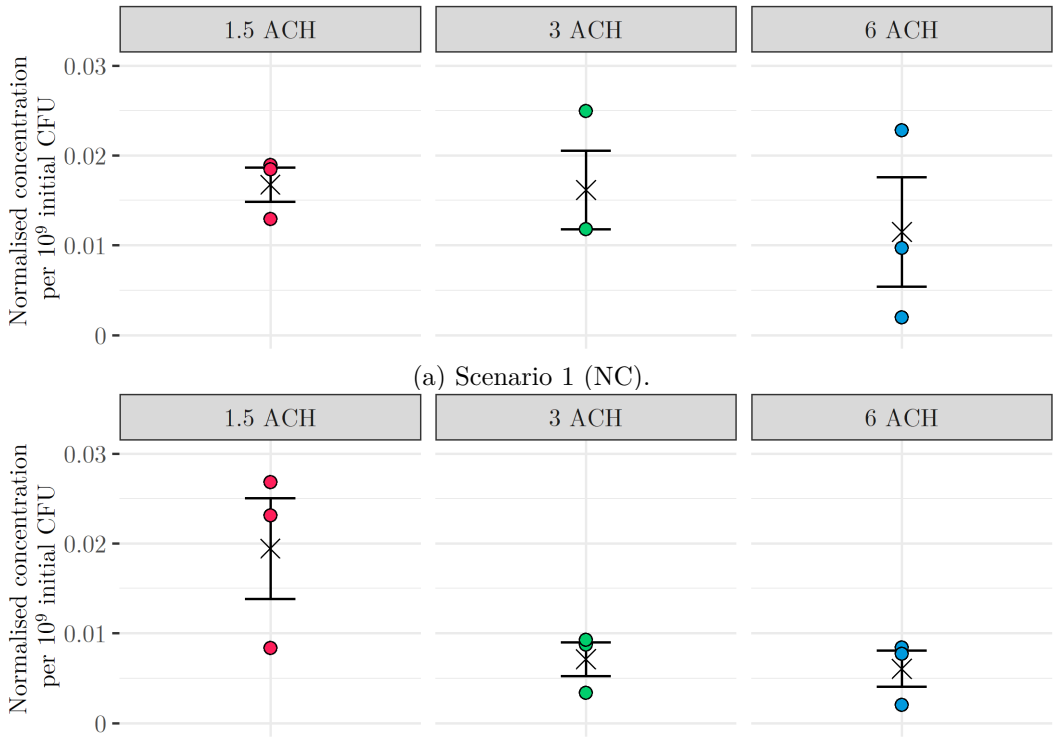

(a) Scenario 1 (NC).

(b) Scenario 2 (2C).

Figure 3.17: Normalised *E. coli* bioaerosol release following toilet flushing, calculated as CFU per 10^9 initial CFU in the toilet bowl over the total 10 min sample for the three ventilation rates and two experimental scenarios. The mean count is indicated by a cross, with standard error bars representing variability across replicates. Each ventilation rate was tested in triplicate.

and 6 ACH.

These results highlight the role of ventilation in reducing airborne bacterial concentrations and suggest that bioaerosols from the toilet plume are primarily released within the first few minutes after flushing. The differences between the two scenarios indicate that airflow patterns within the space may influence bioaerosol dispersion, which could have implications for infection control in shared toilet environments. More research is needed to better understand the mechanisms driving these differences and the impact of cubicle enclosures on bioaerosol transport.

Deposition Samples

The bacterial deposition on settle plates positioned around the toilet bowl, shown in Fig. 3.18, reveals spatial trends in microbial surface contamination after flushing.

A consistent observation across all scenarios and ventilation rates is that plate 3 has a higher mean bacterial concentration than plate 2. Since plate 3 is located

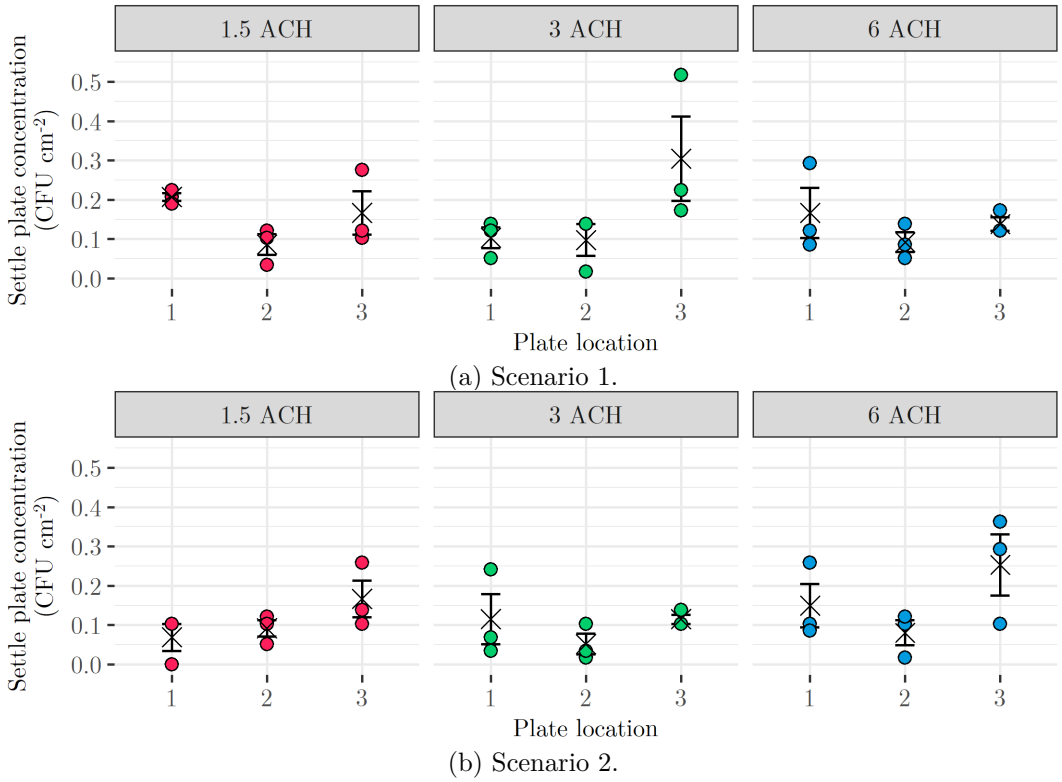

(a) Scenario 1.

(b) Scenario 2.

Figure 3.18: Concentration of bacteria deposited on the settle plates around the bowl of the toilet. Results shown for the three ventilation rates and the two scenarios with mean count depicted by a cross and standard deviation. Plate locations are shown in Fig. 3.11b.

nearest to the ventilation outlet, this suggests that airborne bacteria may be influenced by the airflow patterns within the room, potentially being drawn toward this plate before settling. This aligns with the understanding that airflow can transport bioaerosols before they deposit onto surfaces. The trend highlights the potential role of deposition due to ventilation in toilet facilities.

In contrast, plate 2 shows a relatively stable bacterial concentration of approximately 0.1 CFU cm^{-2} across all ventilation rates and scenarios. This suggests that its location is less influenced by airflows inside the chamber. The consistency in bacterial deposition on this plate implies that proximity to the toilet and gravitational settling alone may be the dominant factors that govern bacterial deposition at this position, rather than room layout or ventilation rate.

To assess potential contact exposure risks, the highest observed bacterial concentration of 0.54 CFU cm^{-2} was considered. Using an estimated maximum hand surface area of 535 cm^2, a maximum fraction of hand surface contact of 0.04, and a toilet seat surface-to-hand transfer efficiency of 0.55 [48], the estimated bacterial

transfer from a single hand touch would result in a maximum hand contamination of 6 CFU. Although *E. coli* has been reported to have a low infectious dose of approximately 10 CFU [345], it is unlikely that all 6 CFU transferred to the hand would subsequently be ingested. This suggests that, under the conditions tested, the infection risk of a single flush is low in all scenarios and ventilation rates. However, multiple flushes over time could lead to an accumulation of *E. coli* on the toilet seat, potentially increasing exposure risk in real-world settings. Additionally, while deposition was only measured on the toilet seat, aerosolised bacteria may settle on other surfaces that are frequently touched, such as the toilet paper dispenser, flush button, and door handle. These surfaces may pose a greater risk of indirect transmission, particularly in settings with high-occupancy and limited cleaning frequency.

A study carried out in a community ablution block in South Africa found toilet seat contamination levels of 10^5 CFU cm^{-2} when sampled with sterile swab sticks [346]. This highlights the potential for higher bacterial loads in real-world environments compared to controlled experimental settings. Differences in sampling methodology can also influence measured bacterial concentrations, as swabbing may capture bacteria embedded in surface biofilms, whereas settle plates collect recently deposited bacteria. These findings underscore the need to carefully interpret laboratory contamination assessments in the context of real-world exposure scenarios.

These findings highlight the role of ventilation in influencing bacterial deposition patterns, with bioaerosols potentially being directed towards specific locations before settling. The results also reinforce the importance of surface contact in potential pathogen transfer. Understanding these deposition mechanisms is crucial to improve hygiene practices and risk mitigation strategies in shared toilet facilities.

3.6 Conclusions

This study examined the generation, dispersion, and deposition of particles and bacteria during toilet flushing, considering different ventilation rates and room layouts. The results highlight the transient nature of toilet plume aerosols, the dominance of smaller particle diameters, and the role of ventilation in reducing airborne

bioaerosols. In addition, challenges in quantifying particle concentrations at distances further from the toilet were identified due to background variations in particle counts. The key findings are summarised below:

- Toilet plume aerosol release is highly transient, with a sharp increase in particle concentrations immediately after flushing, followed by a rapid decay to background levels in several minutes. When sampling near to the toilet bowl surface, ventilation rate and room layout had little effect on this initial release.
- Smaller sized particles dominated the aerosol distribution, with 99 % of measured particles smaller than 5 µm and 90 % smaller than 1 µm. An estimated 35,607 droplets were released per flush.
- Background variations in particle concentrations can make it difficult to isolate toilet plume particles at sampling locations further from the toilet bowl. Fluctuations were largest for smaller particle diameters, with 0.3 µm standard deviations of particles at 10^5 m^{-3} 5 min prior to flushing. CFD analysis (see Chapter 5) can help resolve this issue by isolating toilet plume particles without interference from background concentrations.
- Higher ventilation rates slightly reduced airborne *E. coli* concentrations, which may be due to increased removal through the ventilation system. However, bioaerosol concentrations were unexpectedly higher in the non-cubicle scenario 1 (NC) compared to the cubicle scenario 2 (2C). This difference may be due to lower airflow velocities inside the cubicle reducing airborne transport or variations in the initial *E. coli* concentrations used in each experiment.
- Toilet plume *E. coli* bioaerosols were greatest in the first 0 min to 5 min, with two thirds of 5 min to 10 min sampling period results containing no detectable airborne *E. coli* and the other third containing less than 4 CFU m^{-3}. This aligns with the particle concentration data, suggesting that bioaerosol release occurs almost entirely within the first few minutes after flushing.
- Bacterial deposition occurred at low levels but may accumulate over time. Settle plates placed around the toilet consistently detected bacterial deposition, but concentrations were relatively low (a maximum of 0.54 CFU cm^{-2}).

While this does not indicate a high risk of contamination from a single flush, repeated flushing events could lead to bacterial accumulation on surfaces. Multiple touches of contaminated surfaces may further increase exposure risks.

These findings reinforce the importance of adequate ventilation in shared toilet facilities to reduce airborne bioaerosol exposure. They also highlight the potential for bacterial deposition on surfaces, which could contribute to contact transmission risks. Future studies should investigate the cumulative impact of multiple flushes and the effectiveness of cleaning interventions in mitigating contamination.

Chapter 4

A Quantitative Microbial Risk Assessment Using Experimental Data From Toilet-Flush Generated Aerosols

4.1 Introduction

This chapter details the development of a QMRA model based on experimental measurements of the toilet plume. The model aims to provide a framework for evaluating the possible infection risk to a second susceptible individual entering a toilet facility after an infected individual has flushed the toilet after a bowel movement. By integrating experimental data with stochastic modelling, this approach allows the assessment of airborne exposure and the influence of key parameters on infection risk, supporting a better understanding of transmission dynamics from airborne toilet plume particles in shared toilet facilities. Two distinct models are introduced: (i) one using non-biological particle concentration data from an OPC and (ii) another using airborne *E. coli* concentration data.

Some previous studies have investigated the infection risk associated with toilet flush aerosols using QMRA, but the literature in this area is limited and significant gaps remain. Five prior studies [41, 50, 259, 267, 290], as discussed in Chapter 2, have attempted to quantify infection risk from inhalation exposure to aerosols generated by toilet flushing using QMRA methods. However, two of these studies [259, 290] focused on contaminated water (stormwater and reclaimed water) rather than toilet bowl water contaminated by faecal matter from a bowel movement. These studies also relied on particle concentrations from previous research rather than direct measurements and did not account for the potential evaporation of droplets, which may initially have been larger and carried a greater viral load.

The remaining three studies [41, 50, 267] were conducted in real-world toilet environments. Ali et al. [50] and Ali et al. [267] examined bioaerosol exposure to *S. aureus* but only flushed water from the building's water supply rather than water contaminated with faecal waste. Ali et al. [41] extended the approach by studying *E. coli* and used human faecal matter.

In all five studies, infection risk was estimated on an annual basis using either point or uniform distribution values for exposure time, often based on arbitrary assumptions (e.g. exposure times ranging from 1 min to 5 min). In reality, exposure times are more complex and vary based on factors such as gender and behaviour.

No previous study has quantified the infection risk from a single toilet flushing event while explicitly examining how the concentrations of aerosols and bioaerosols vary over time per event. This study aims to address this gap by evaluating the decay of particle concentrations over time for an individual flushing event, examining how the entry time of a second susceptible individual influences their exposure. In addition to this, behavioural data for occupancy exposure time (time spent in the toilet facility) is applied in this model. Furthermore, this study introduces a novel approach by fitting experimental particle concentration data to an exponential model and subsequently applying bioaerosol data to this fitted model. This allows for an estimation of infection risk per event with temporal detail.

Both the non-biological data and the biological data models enable the evaluation of infection risks across different scenarios and ventilation regimes, supporting evidence-based recommendations on toilet entry and occupancy times to mitigate infection risk. The particle data from Chapter 3 and the QMRA model framework from this chapter are published in Higham et al. [347].

4.2 Methodology

An outline of the methodology for the QMRA model, using experimental data from either the non-biological particle concentrations or the *E. coli* bioaerosol concentrations is shown in Fig. 4.1.

4.2.1 Risk Modelling Using Non-biological Experimental Particle Concentrations

Experimental data from Chapter 3, specifically scenarios 1 (NC) and 2 (2C) (detailed in Section 3.4), were used alongside published data on viral concentrations in faecal matter, toilet facility occupancy times, and aerosol physics to develop a QMRA model. This model was applied to two viruses: SARS-CoV-2 and norovirus. Norovirus was included due to its common presence in faecal matter [24] and SARS-CoV-2 was selected based on epidemiological evidence suggesting its transmission through bioaerosols generated by toilet flushing [19]. The model assesses the prob-

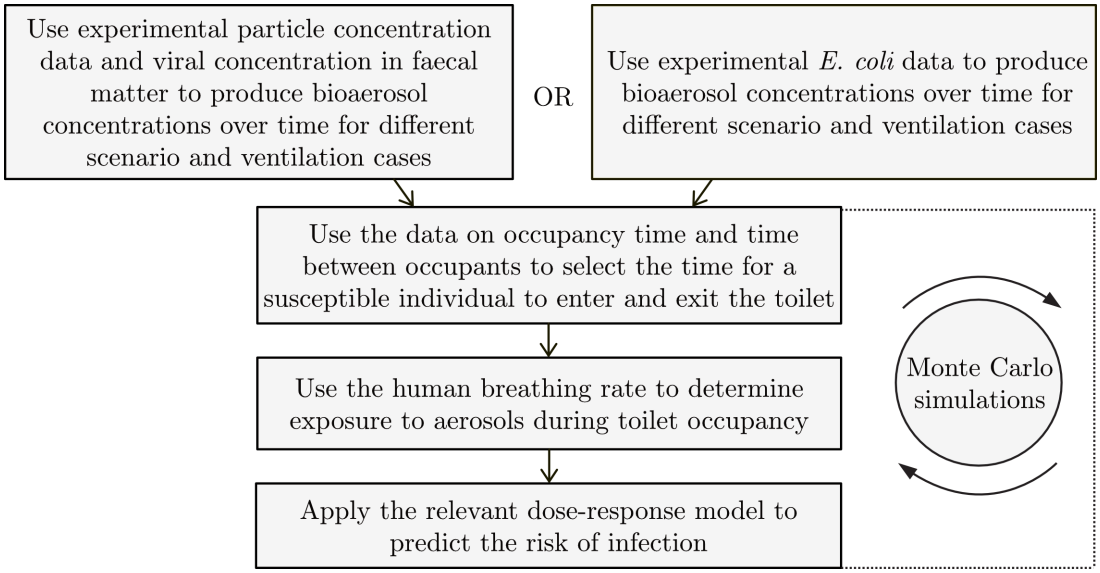

Figure 4.1: A flow chart detailing the methodology for the QMRA work from initial experimental measurements through to evaluating the probability of infection.

ability of infection for a second individual entering the toilet facility after a flushing event (with a bowel movement) by an infected person. It also explores the behavioural and environmental factors that influence this risk.

Gender-Specific Occupancy Times

Infection risk was evaluated using gender-specific cubicle occupancy times, t_{dur} [s], under various cubicle and ventilation scenarios observed in the experiments (Fig. 4.2). These occupancy times were taken from a study conducted in a shopping plaza in Canada during Autumn 1972 and Spring 1973 [3]. Although there are more recent studies that exist [348, 349, 350], they primarily report total bathroom occupancy rather than cubicle-specific times, including handwashing and drying. Since handwashing duration varies by gender [351], the shopping plaza data set was chosen because it specifically reports cubicle occupancy times. A 1976 study on office buildings [352] included raw data for female cubicle occupancy, but lacked male occupancy times.

The model considered scenarios in which a second individual entered the facility immediately (0 s), after 60 s, or after 240 s following a flush, using the corresponding experimental particle concentrations. For each t_{enter} value, 999 simulations were performed (333 random samples of t_{dur} from Fig. 4.2 for each of the three replicates).

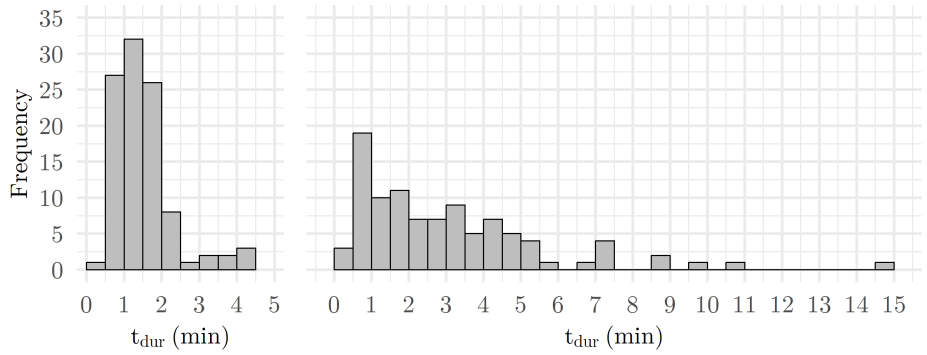

(a) Female (b) Male

Figure 4.2: Cubicle occupancy times for a) females and b) males for an enclosed mall-type suburban shopping plaza during Autumn of 1972 and Spring of 1973. Observations were made on Thursday and Friday evenings and during the day on Saturdays (i.e. the busiest times of the week). The figure has been generated based on observational data reported in Henning [3].

Uniformly Distributed Occupancy Times

It was recognised that gender-specific bathroom behaviours measured in the Canadian study represent a limited data set from a particular setting and time period, with cubicle occupancy times potentially varying. To account for this, a sensitivity analysis was performed to investigate the relationship between toilet facility occupancy time, t_{dur} [s], the time for a second individual to enter the toilet facility post-flush, t_{enter} [s], and corresponding normalised infection risk. In this part of the study, the cubicle occupancy time was sampled from a uniform distribution between [1,900] s in 1 s intervals (i.e., 900 values). These occupancy times were simulated with $t_{\text{enter}} \in$ [0,599] s in 1 s intervals (i.e., 600 values), resulting in 540,000 (900×600) values of normalised infection risk. The results of this section are presented in units of minutes for t_{enter} and t_{dur}. This investigation was independent of the observational occupancy times in Fig. 4.2, allowing a broader sensitivity analysis.

Exposure Modelling

The model framework employed a stochastic Monte Carlo approach to estimate exposure, selecting parameters from realistic ranges and running multiple simulations to evaluate risk variability. The number of particles inhaled by the second individual

was first calculated, followed by an estimation of the viral load in these particles to determine likely exposure. Parameters and their distributions used in the QMRA model are detailed in Table 4.1.

The concentrations of SARS-CoV-2 and norovirus in faecal matter, as shown in Table 4.1, were derived from hospitalised cases. SARS-CoV-2 concentrations were based on samples collected on the first day of hospitalisation, while norovirus concentrations were based on samples from individuals hospitalised with gastroenteritis, with stool samples collected within 96 h of the onset of symptoms. Individuals in this stage of illness are unlikely to use shared public toilet facilities but may use shared toilet facilities in a hospital, which may lead to an overestimation of concentrations in this model for public toilet facilities. Those with mild symptoms who are not hospitalised are likely to shed lower concentrations of the viruses. For SARS-CoV-2, the peak concentration in faeces has been estimated to occur at 0.34 days after the onset of symptoms [353], while for norovirus, peak concentrations are observed within a few days of infection onset [17]. For both viruses, there is significant temporal variation in faecal concentrations between individuals, which could result in an overestimation or underestimation in the model.

Recall in Section 3.4, Chapter 3 that for a given ventilation rate, particle size i, and experimental replicate j, the increase in concentration over time associated with flushing, $c_{i,j,t}$ [m^{-3}], was defined by Eqn. (3.4), with $c_{i,j,t}$ set to zero when a negative value was returned. For each experimental replicate j, the number of particles of size i, $i \in \{0.3, 0.5, 1, 3, 5, 10\}$ µm, inhaled by a second susceptible individual, $N_{i,j}$, was estimated as

$$N_{i,j} = \int_{t_{\text{enter}}}^{t_{\text{enter}}+t_{\text{dur}}} c_{i,j,t} \times B dt \tag{4.1}$$

where

B = breathing rate [$\mathrm{m}^3\,\mathrm{s}^{-1}$].

In practice, Eqn. (4.1) was implemented as a summation, as $c_{i,j,t}$ was a piecewise function.

Table 4.1: Parameters used for the QMRA exposure model.

Parameter	Parameter	Unit	Distribution	Parameters	Source
Inhalation rate[1]	B	$\mathrm{m^3\,s^{-1}}$	Normal (truncated)	$\mu = 2.00 \times 10^{-4}$ $\sigma = 4.17 \times 10^{-5}$ $\min = 9.26 \times 10^{-5}$ max $\sigma = 2.69 \times 10^{-4}$	[354, 355]
SARS-CoV-2 concentration in faeces	$\rho_{\text{SARS-CoV-2}}$	$\mathrm{gc\,L^{-1}}$	Hockey-stick	$\min = 5.00 \times 10^{6}$ median $= 1.30 \times 10^{8}$ $\max = 3.98 \times 10^{10}$	[186, 187, 356, 357]
Norovirus concentration in faeces[2]	$\rho_{\text{norovirus}}$	$\mathrm{gc\,L^{-1}}$	Hockey-stick	$\min = 2.30 \times 10^{9}$ median $= 9.02 \times 10^{11}$ $\max = 6.10 \times 10^{14}$	[181, 182, 356, 357]
Ratio of genome copies corresponding to infectious virus	f	$\mathrm{gc\ PFU^{-1}}$	Uniform	$\min = 100$ $\max = 1000$	[358]
Volume of faecal matter[3]	V_{faeces}	L	Normal (left-truncated at zero)	$\mu = 1.84 \times 10^{-1}$ $\sigma = 1.51 \times 10^{-1}$	[359]

[1] Men and women combined breathing rate for short exposure. Normal distribution assumed and standard deviation estimated by halving the difference of the 95th percentile and mean. Divided by 60 for volume per second.
[2] Density of faecal matter, $= 1.06 \times 10^{3}$ g $\mathrm{L^{-1}}$ multiplied by viral load per gram.
[3] Mean diarrhoeal stool volume divided by number of stools for placebo group. Standard error propagated and standard deviation found using $n = 11$ placebo group participants.

In the experiments, it was assumed that the particles measured just above the toilet after flushing had completely evaporated, possibly leading to a smaller measured diameter d_i^{measured}. This may have corresponded to an initial larger diameter, d_i, when released. The model incorporated an initial droplet size derived from the measured droplet size, relative humidity, and the distance between the water in the bowl and the toilet surface. An approximation of the time-dependent radius of an evaporating droplet [360], $R(t)$ [m], was given by

$$R(t) = \sqrt{R_0^2 - \theta(1 - \text{RH})t} \tag{4.2}$$

where

R_0 = initial radius [m],
RH = relative humidity and
θ = 1.1×10^{-9} [$\text{m}^2\,\text{s}^{-1}$].

The velocity of the droplet at the surface of the bowl, v_{surface}, was assumed to be $1\,\text{m}\,\text{s}^{-1}$ to $2\,\text{m}\,\text{s}^{-1}$ [52], and the distance between the water in the bowl and the surface of the bowl was measured to be 0.2 m. Using kinematics equations, with the droplet accelerating downwards due to gravity, the time for the droplets to reach the surface of the toilet bowl was assumed to be 0.083 s to 0.124 s. The relative humidity in the room was assumed 40 % to 50 %, as the experimental measurements were in this range. For each experiment, a relative humidity and v_{surface} were randomly sampled from a uniform distribution between 0.4 to 0.5 and $1\,\text{m}\,\text{s}^{-1}$ to $2\,\text{m}\,\text{s}^{-1}$ respectively. Table 4.2 summarises the maximum and minimum estimated initial droplet diameters using this method for each measured diameter. The ini-

Table 4.2: Estimated initial droplet diameter ranges for each measured diameter, based on extreme values of relative humidity and surface velocity.

Measured diameter [µm]	**Estimated initial diameter range** [µm]
0.3	13.5 to 18.1
0.5	13.5 to 18.1
1	13.5 to 18.1
3	13.9 to 18.4
5	14.4 to 18.8
10	16.8 to 20.7

tial droplet size was used to estimate its volume and the potential viral load before evaporation. Assuming the droplets were spherical, their volume, V_i^{droplet} [L], was calculated as

$$V_i^{\text{droplet}} = \frac{\pi}{6} d_i^3 \times 1000. \tag{4.3}$$

The factor of 1000 accounted for the unit conversion from m^3 to L. The exposure dose was then estimated using the droplet volume, viral concentrations in faecal matter, and the values of $N_{i,j}$ from Eqn. (4.1) to determine the number of PFU per droplet.

The dose in genome copies for each replicate j, ${D_j}^{\text{gc}}$ [gc], was given by

$${D_j}^{\text{gc}} = \sum_i N_{i,j} \times V_i^{\text{droplet}} \times \frac{V_{\text{faeces}}}{V_{\text{bowl}} + V_{\text{faeces}}} \times \rho_{\text{pathogen}}, \tag{4.4}$$

where

V_{faeces} = volume of faecal matter per bowel movement [L],
V_{bowl} = volume of water in the toilet bowl [L] and
ρ_{pathogen} = density of genomic copies [gc L^{-1}].

The corresponding infectious virus dose, ${D_j}^{\text{PFU}}$, was

$${D_j}^{\text{PFU}} = \frac{{D_j}^{\text{gc}}}{f}, \tag{4.5}$$

where

f = ratio of genome copies to infectious pathogen [gc PFU^{-1}].

Eqn. (4.4) assumes a homogeneous distribution of faecal matter within the bowl, maintaining a uniform ratio of faecal matter to bowl water throughout. This assumption is more applicable to diarrhoeal stool, which disperses easily, while solid stool likely settles at the bottom. However, this assumption is supported by a study in which flushing a toilet with *E. coli* in the bowl showed no significant difference in bacteria generation between solid and homogenised stool [10]. Additionally, it was assumed that the virus is uniformly distributed by volume within the initial droplet size. Although studies have shown the potential for viral enrichment in

certain aerosol sizes [361], there is no data available that would be appropriate to use in this scenario.

Dose-response Model

A quantitative microbial dose-response relationship was then used to estimate the probability of infection for the second individual given a specific dose. Such models are typically derived from human outbreak or animal data and are widely used to assess infection risks in air, water, and food [14]. For SARS-CoV-2, the probability of infection, $P_{\text{infection}}(D^{\text{PFU}})$, was modelled using an exponential function [362] such that

$$P_{\text{infection}}\left(D^{\text{PFU}}\right) = 1 - \exp\left(-k \times D^{\text{PFU}}\right) \tag{4.6}$$

where

$k = 5.39 \times 10^{-2}$ [PFU^{-1}].

For norovirus, a Beta-Poisson model is commonly used to estimate infection probability [253, 363]. This model was applied as follows

$$P_{\text{infection}}\left(D^{\text{gc}}\right) = 1 - \left(1 + \frac{\lambda \times D^{\text{gc}}}{\beta}\right)^{-\alpha} \tag{4.7}$$

where

$\alpha = 0.104$ and

$\beta = 32.3$ [gc].

Here, α and β are the fitted Beta-Poisson parameters. Unlike the SARS-CoV-2 dose-response model, the dose is expressed in genome copies rather than in PFU. A reduction factor, λ, is included in Eqn. (4.7) to account for the capture of particles in the upper respiratory tract, where they are assumed to be removed by ciliary action and transferred to the digestive tract through the pharynx. A range of 10 % to 50 % was applied for λ, based on previous work [364], and implemented using Monte Carlo simulations.

Recognising the inherent uncertainties in these estimates, both from experimental measurements and parameter distributions, the infection risk was calculated as a normalised infection risk for comparison across scenarios.

For gender-specific occupancy times (using the t_{dur} distributions in Fig. 4.2), a normalised infection risk was visualised as violin plots for $t_{\text{enter}} \in \{0, 60, 240\}$ s across different scenarios and ventilation rates. The normalisation factor used was the maximum infection risk across both viruses, scenarios, ventilation rates, and entry times, allowing a direct comparison between SARS-CoV-2 and norovirus.

For uniformly distributed occupancy times, a normalised infection risk was plotted as a heat map as a function of t_{enter} and t_{dur}. The normalisation factor applied was the median infection risk, $\widetilde{P}_{\text{infection}}$, for each virus across the two scenarios and ventilation rates. To assess the monotonic relationship between infection risk and parameters, bivariate Spearman rank correlation coefficients were calculated using the R package `cor()`. The correlation coefficients were calculated for two subsets of infection risk: (i) $0\,\text{min} < t\text{enter} \leq 1\,\text{min}$, and (ii) $1\,\text{min} < t_{\text{enter}} \leq 10\,\text{min}$. The strength of the correlation based on Spearman coefficients is categorised in Table 4.3.

Table 4.3: Classification of correlation strength based on Spearman correlation coefficients.

Spearman correlation value	**Strength of correlation relationship**	**Colour**
$\lvert r_s \rvert \geq 0.70$	Very strong	
$0.40 \leq \lvert r_s \rvert < 0.70$	Strong	
$0.30 \leq \lvert r_s \rvert < 0.40$	Moderate	
$0.20 \leq \lvert r_s \rvert < 0.30$	Weak	
$\lvert r_s \rvert < 0.20$	Negligible	

4.2.2 Risk Modelling Using Experimental Bioaerosol Concentrations

A QMRA model was developed using the *E. coli* experimental data presented in Section 3.5.2, Chapter 3, in combination with the inhalation rate parameter outlined in Table 4.1. Unlike the approach in Section 4.2.1, this method did not require assumptions about the quantity of pathogen aerosolised by the toilet flush, as the bioaerosol sampler provided direct measurements of CFU present in the air following a flushing event.

For each experimental replicate j, two air samples were collected: (i) from 0 min to 5 min and (ii) from 5 min to 10 min. These samples were used to estimate the concentration of bacteria over time, providing a direct assessment of bioaerosol dispersion dynamics.

Concentration Estimation

Two methods were used to estimate the bacterial concentration. The first approach involved a simplified estimation, assuming a constant bacterial release within each sampling interval. Under this assumption, the bacterial concentration for a given experiment, C_j, sampled over the 10 min period, was represented as a piecewise function such that

$$C_j(t) = \begin{cases} C_1, & \text{if } 0 \leq t < 300\,\text{s}, \\ C_2, & \text{if } 300\,\text{s} \leq t < 600\,\text{s} \end{cases} \tag{4.8}$$

where

C_1 – concentration of bacteria sampled over 0 s to 300 s [CFU m^{-3}] and

C_2 – concentration of bacteria sampled over 300 s to 600 s [CFU m^{-3}].

The values of C_1 and C_2 can be related to the total cumulative bacteria count over the 5 min sampled by

$$\int_0^{300} C_t \times Q dt = B_1 \tag{4.9a}$$

$$C_1 = \frac{B_1}{300Q} \tag{4.9b}$$

and

$$\int_{300}^{600} C_t \times Q dt = B_2 \tag{4.10a}$$

$$C_2 = \frac{B_2}{300Q} \tag{4.10b}$$

where

B_1 – average total cumulative bacteria count over the 0 s to 300 s sample [CFU],

B_2 – average total cumulative bacteria count over the 300 s to 600 s sample [CFU] and

Q – flow rate of the bioaerosol sampler [m^3 s^{-1}]

This piecewise concentration estimate for the two scenarios and ventilation rates is shown in Fig. 4.3.

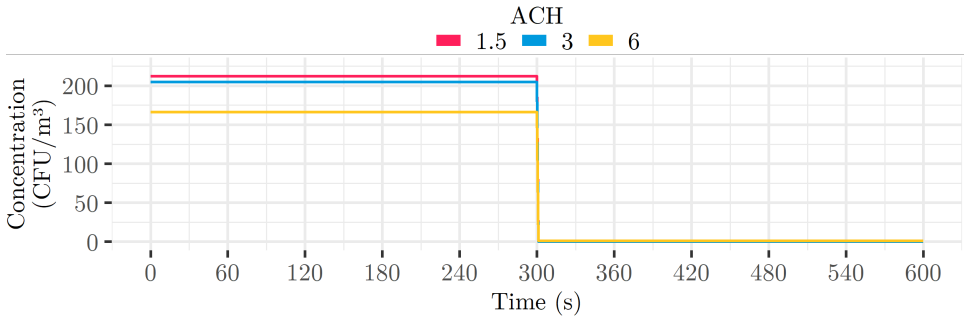

(a) Scenario 1 (NC).

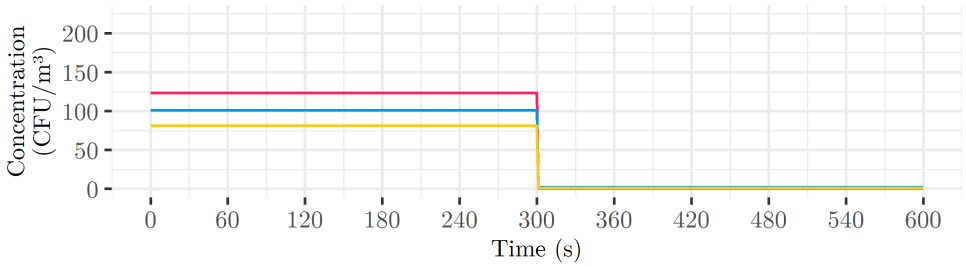

(b) Scenario 2 (2C).

Figure 4.3: Piecewise bacterial concentrations estimated for each scenario and ventilation rate based on bioaerosol experimental data. NC and 2C are detailed in Fig. 3.9, Chapter 3 and correspond to different experimental conditions, with variations in bioaerosol release and dispersion dynamics.

This approach provides a simplified estimate but it does not account for the dynamically changing nature of bacterial aerosol concentrations following a flushing event. To improve this estimation, a second approach was developed using OPC measurements. Based on observed trends in particle concentrations, bacterial release over the 10 min period was assumed to follow an exponential decay model. The decay constant for particle concentrations was determined using nonlinear least squares regression (`nls()`) in R, applied separately for each particle size, scenario, and ventilation rate. As the exact distribution of *E. coli* across particle sizes was not directly measurable, an average decay constant was calculated across all particle sizes. The initial bacterial concentration for the exponential model was determined for each experimental data set by ensuring that the area under the curve matched the total colony count obtained from the experiments. Under this assumption, the bacterial concentration for a given experiment, C_j, sampled over the 10 min period, was represented as:

$$C_j(t) = C_0 \exp(-kt) \tag{4.11}$$

where

C_0 – initial concentration [CFU] and

k – fitted decay constant [s^{-1}].

After fitting the exponential function to different particle sizes, scenarios, and ventilation rates, 36 decay rates were calculated, resulting in an average decay constant of $k = 0.049\,s^{-1}$. The values of C_0 were determined by using the integral of the concentration curve such that

$$\int_0^{600} C_t \times Q dt = B_1 + B_2 \tag{a}$$

$$C_0 = \frac{B_1 + B_2}{Q(1 - \exp(-600k))} \tag{b}$$

The resulting concentration curves are shown in Fig. 4.4. The concentration is the average concentration over a 1 s interval. This refined estimation method

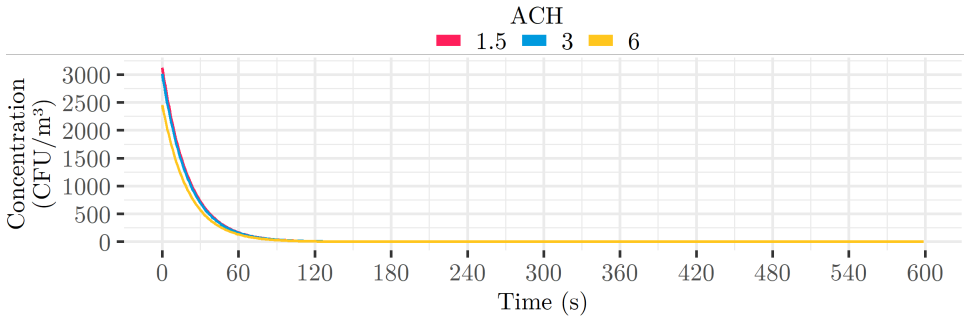

(a) Scenario 1 (NC).

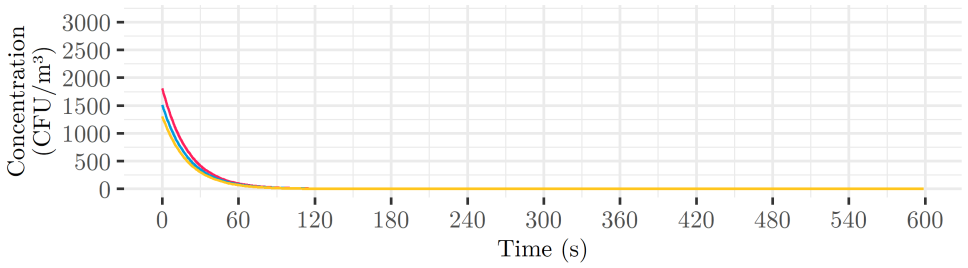

(b) Scenario 2 (2C).

Figure 4.4: Estimated bacterial concentrations for each scenario and ventilation rate, based on the exponential function fitted to OPC particle count data and bioaerosol experimental data. NC and 2C are detailed in Table 3.2 and Fig, 3.9, Chapter 3 and correspond to different experimental conditions, with variations in bioaerosol release and dispersion dynamics.

provides a more accurate representation of bacterial concentration dynamics over time, capturing the rapid release and subsequent decay of aerosols after flushing the toilet. Future work could improve this model by incorporating direct measurements of bacterial loads across particle sizes within the toilet plume.

Dose-response

The dose in terms of CFU for each replicate j, D_j^{CFU} [CFU], was calculated as

$$D_j{}^{\text{CFU}} = \int_{t_{\text{enter}}}^{t_{\text{enter}}+t_{\text{dur}}} C_j(t) \times B dt \tag{4.13}$$

A quantitative microbial dose-response relationship was then applied to estimate the probability of infection from *E. coli* exposure. A beta-Poisson model [238] was used, defined as

$$P_{\text{infection}}(D^{\text{CFU}}) = 1 - \left(1 + \frac{D^{\text{CFU}}}{\beta}\right)^{-\alpha}, \tag{4.14}$$

where

$\alpha = 0.155$ and

$\beta = 24{,}386$ [CFU].

Although this model was originally calibrated using a different strain of *E. coli* (EIEC 1624), it has been widely adopted in previous QMRA studies involving ATCC 10536 [365] and other strains. It has also been applied in bioaerosol models [271, 366] and in various exposure assessment contexts [367, 368].

As in Section 4.2.1, two models were implemented. The first used gender-specific occupancy times based on the distributions in Fig. 4.2. In this approach, the second person entered the toilet facility at 0 s, 60 s, or 240 s after flushing, with 999 Monte Carlo simulations conducted for each entry time. The second model applied uniformly distributed occupancy times, where cubicle durations were sampled from a uniform distribution between [1,900] s in 1 s intervals (i.e., 900 values). These occupancy durations were combined with entrance times sampled uniformly from $t_{\text{enter}} \in [0, 599]$ s, also in 1 s intervals (i.e., 600 values). For this part of the study using *E. coli*, absolute risk was calculated instead of a normalised risk. As discussed in Section 3.2.5 the bacterial concentration in the bowl was based on the typical amounts found in faeces. Therefore, it was assumed that the aerosolised quantity accurately represented the amount released during toilet use involving faeces.

4.3 Results and Discussion

4.3.1 Risk Modelling Using Non-biological Particle Concentrations

Gender-Specific Occupancy Times

The normalised infection risk for the two scenarios, with a susceptible individual entering a toilet facility after an infected individual flushed the toilet, is illustrated in Fig. 4.5.

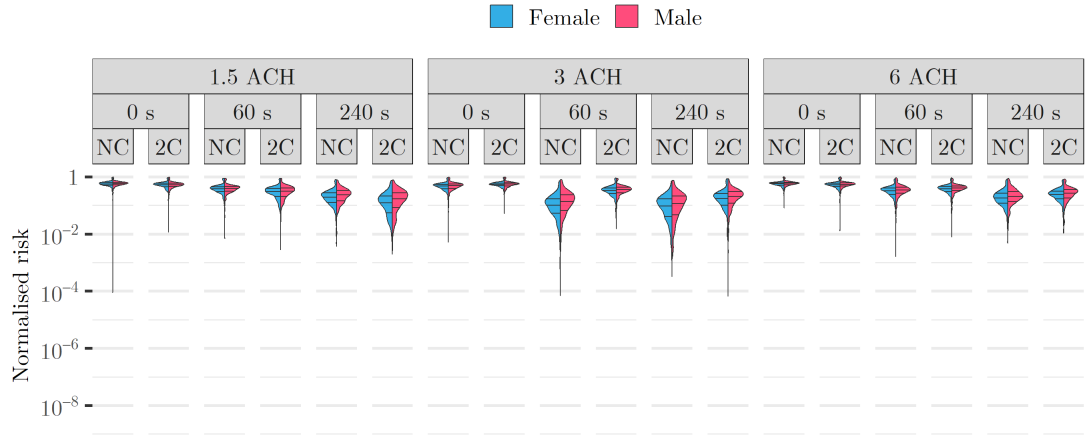

(a) Norovirus.

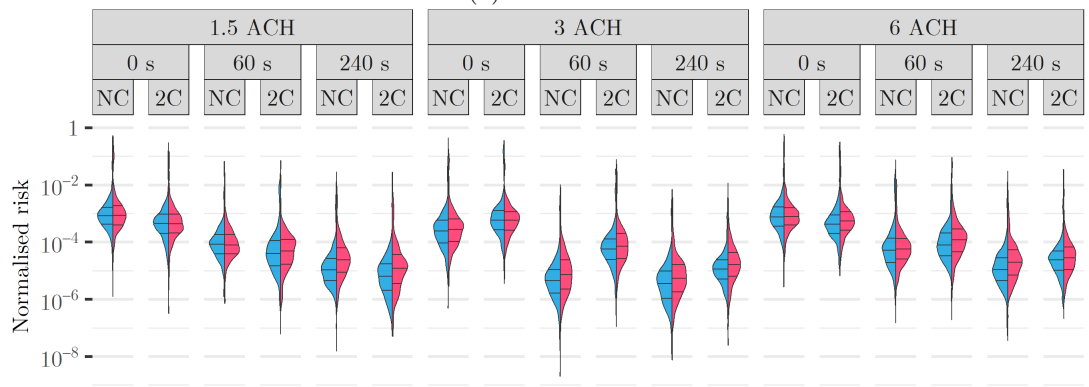

(b) SARS-CoV-2.

Figure 4.5: Violin plots corresponding to the normalised risk for particle counter A. Infection risk was normalised by the maximum value across all virus, scenario and ventilation rates (this was obtained for norovirus, NC, $t_{\text{enter}} = 0\,\text{s}$, 1.5 ACH). The times referred to indicate the moment when the susceptible individual entered post-flush, t_{enter}. NC and 2C refer to scenarios as described in Table I (Section 3.4, Chapter 3). Horizontal lines represent the 25th, 50th, and 75th quantiles.

Table 4.4 provides the absolute mean and median infection risk values for each scenario for reference. The indicated times correspond to the moment when the susceptible individual was exposed to the aerosols following a toilet flush, denoted t_{enter}. This represents the time at which the second individual enters the toilet facil-

Table 4.4: Absolute median and mean risk infection values for SARS-CoV-2 and norovirus at $t_{\text{enter}} \in \{0, 60, 240\}$ s. The risks are shown for the three ventilation rates: 1.5, 3 and 6 ACH with a comparison between scenario 1 (NC) and scenario 2 (2C).

ACH	t_{enter}(s)	**Scenario**	**Gender**	**SARS-CoV-2**		**Norovirus**	
				Mean (%)	**Median (%)**	**Median (%)**	**Mean (%)**
1.5	0	NC	Female	6.2e-02	4.0e-01	4.2e+01	4.2e+01
			Male	6.4e-02	8.2e-01	4.3e+01	4.3e+01
		2C	Female	3.4e-02	2.8e-01	3.9e+01	3.9e+01
			Male	3.2e-02	2.4e-01	3.9e+01	3.9e+01
	60	NC	Female	6.4e-03	8.1e-02	2.8e+01	2.9e+01
			Male	5.9e-03	3.4e-02	2.9e+01	2.9e+01
		2C	Female	2.9e-03	3.8e-02	2.2e+01	2.3e+01
			Male	3.7e-03	4.0e-02	2.3e+01	2.3e+01
	240	NC	Female	8.4e-04	1.4e-03	1.4e+01	1.6e+01
			Male	1.7e-03	2.1e-02	1.7e+01	1.9e+01
		2C	Female	4.6e-04	4.3e-02	9.4e+00	1.1e+01
			Male	9.7e-04	2.3e-03	1.3e+01	1.4e+01
3	0	NC	Female	1.7e-02	2.2e-01	3.6e+01	3.5e+01
			Male	2.1e-02	2.1e-01	3.6e+01	3.6e+01
		2C	Female	4.4e-02	5.4e-01	4.0e+01	4.0e+01
			Male	4.3e-02	2.2e-01	4.1e+01	4.1e+01
	60	NC	Female	3.3e-04	3.9e-03	7.7e+00	9.5e+01
			Male	5.5e-04	7.8e-03	1.0e+01	1.3e+01
		2C	Female	4.3e-03	4.6e-02	2.5e+01	2.5e+01
			Male	5.4e-03	9.1e-02	2.6e+01	2.7e+01
	240	NC	Female	2.7e-04	3.3e-03	7.2e+00	8.8e+01
			Male	4.1e-04	5.7e-03	8.6e+00	1.1e+01
		2C	Female	8.6e-04	7.3e-03	1.3e+01	1.5e+01
			Male	1.2e-03	5.6e-03	1.6e+01	1.7e+01
6	0	NC	Female	5.7e-02	3.0e-01	4.2e+01	4.2e+01
			Male	5.5e-02	6.0e-01	4.4e+01	4.3e+01
		2C	Female	3.0e-02	3.4e-01	3.9e+01	3.9e+01
			Male	4.0e-02	3.2e-01	4.0e+01	4.0e+01
	60	NC	Female	4.0e-03	7.2e-01	2.5e+01	2.5e+01
			Male	4.3e-03	2.8e-02	2.5e+01	2.6e+01
		2C	Female	5.7e-03	4.6e-02	2.9e+01	2.8e+01
			Male	9.3e-03	9.1e-02	3.0e+01	3.0e+01
	240	NC	Female	7.9e-04	9.8e-03	1.4e+01	1.6e+01
			Male	1.5e-03	1.6e-02	1.5e+01	1.8e+01
		2C	Female	1.8e-03	2.1e-02	1.8e+01	1.9e+01
			Male	2.1e-03	1.7e-02	2.1e+01	2.1e+01

ity. While an entry time of zero seconds may be considered unrealistic, it is included for comparative analysis. Across the two scenarios, virus types, and entry times $t_{\text{enter}} \in \{0, 60, 240\}$ s, the estimated absolute infection risk ranged from 1.4×10^{-7} %

to 74 %. These values represent extreme cases, with low-density estimates indicating their lower likelihood. The high infection risk values corresponded to the highest inhaled doses, which, as described in Eqns. (4.1) and (4.4), depended on factors such as occupancy duration and breathing rate. There may be an overestimation in the infection risk values, as any increase above the background concentration in the data was assumed to contain infectious particles. In reality, some non-zero concentrations may have resulted from background fluctuations rather than aerosolised particles from the flush. This effect was more pronounced for smaller particles, which exhibited greater variability in background concentrations.

The normalised infection risk associated with norovirus exposure was higher, with a maximum infection risk approximately twice that of SARS-CoV-2. This difference arose from differences in viral concentrations in faeces [181, 182, 186, 187] (see Table 4.1) and variations in dose-response models [253, 362, 363] (see Eqns. (4.6) and (4.7)). However, both the infectious dose and faecal viral load for SARS-CoV-2 are less understood than those for norovirus, which leads to uncertainty in the estimates.

Differences in normalised infection risk between male and female occupancy patterns were observed in all scenarios. The variation in occupancy times (Fig. 4.2) was derived from observational data, with mean occupancy times of 173 s for men and 95 s for women. As shown in Fig. 4.5, for a given scenario, the mean normalised infection risk decreased as the time to enter the cubicle after flushing increased. For example, in the 1.5 ACH cubicle scenario (2C) with norovirus (Fig. 4.5a), the mean normalised infection risk across both genders decreased by 41 % between $t_{\text{enter}} = 0$ and 60 s, and by 67 % between $t_{\text{enter}} = 0$ and 240 s. In the same scenario using SARS-CoV-2 (Fig. 4.5b), the corresponding reductions were 85 % and 95 %, respectively. This highlights the importance of allowing aerosol removal through ventilation and deposition before exposure to reduce infection risk. Among the 36 cases in Fig. 4.5, 72 % (26/36) showed a higher normalised mean infection risk for men. However, empirical data on gender-specific toilet occupancy times were obtained from a suburban shopping plaza in Canada and may not be representative of other settings

such as hospitals, workplaces, or public events. Additional behavioural data specific to different environments and populations would improve the understanding of exposure risks.

For both viruses, at 3 ACH and for $t_{\text{enter}} \in \{0, 60, 240\}$ s, the estimated mean normalised infection risk was higher for scenario 2 (2C) than for scenario 1 (NC). At 6 ACH, this trend was consistent for $t_{\text{enter}} \in \{60, 240\}$ s, while at $t_{\text{enter}} = 0$ s, scenario 1 (NC) had a higher infection risk. This suggests that cubicle enclosures may affect particle removal from the air, leading to higher exposure. However, at 1.5 ACH, scenario 2 (2C) exhibited lower mean infection risks in all cases. Airflow dynamics likely play a crucial role in determining droplet dispersion patterns in these scenarios.

The difference in normalised mean infection risk between males and females was smaller compared to other variables, such as entry time (t_{enter}). This may be attributed to the transient nature of particle release, with most aerosols detected as a spike within the first 2 min after flushing, as discussed in Chapter 3, Section 3.5.1, indicating that occupancy duration may have a less impact on the infection risk.

Uniformly Distributed Occupancy Times

Figs. 4.6 and 4.7 illustrate the variation in normalised infection risk for SARS-CoV-2 and norovirus as a function of t_{enter} and t_{dur}, respectively. The infection risk retained a degree of stochasticity due to the random selection of dose values from the experimental replicates.

The red regions, indicating higher infection risk, are concentrated in areas where the entry time (t_{enter}) was less than 60 s, and in some cases, even less than 30 s. These areas exhibited the highest relative risks. Even for shorter occupancy times, the infection risk remained significantly higher compared to when t_{enter} exceeded 60 s. This suggests that a delay in entry into the toilet facility may be more effective in reducing infection risk than simply limiting occupancy duration.

Waiting at least 60 s before entering the toilet facility is recommended, based on a comparison of normalised infection risks for $t_{\text{enter}} < 1$ min and 1 min $\leq t_{\text{enter}} < 10$ min. For norovirus in scenario 1 (NC), 79 % of normalised infection risks exceeded the me-

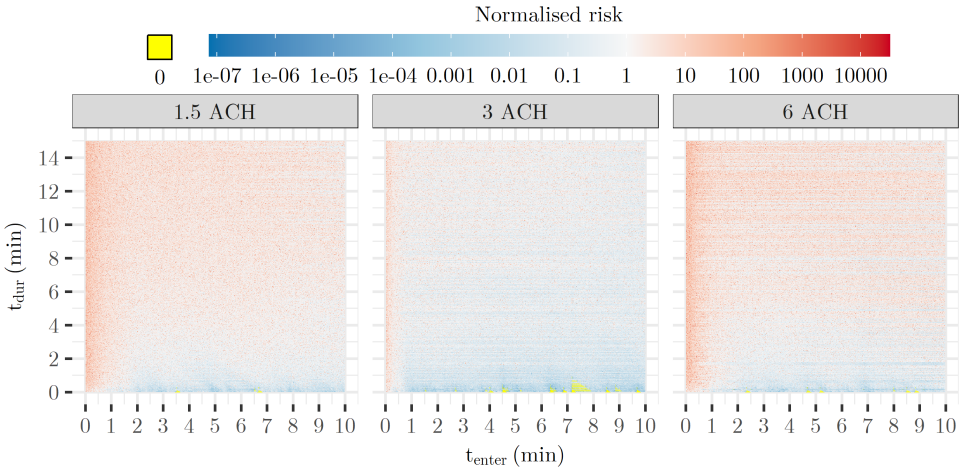

(a) Scenario 1 (NC).

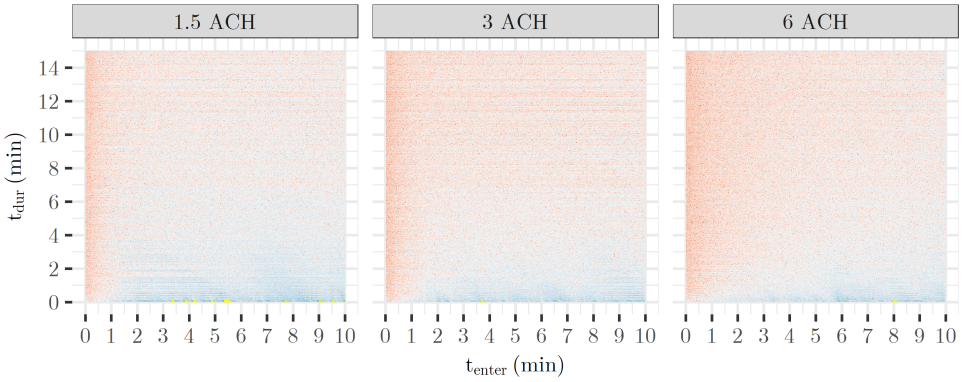

(b) Scenario 2 (2C).

Figure 4.6: Heat maps showing the relationship between $t_{\text{enter}}, t_{\text{dur}}$ and normalised SARS-CoV-2 risk infection. The particle counter was at location A and infection risk was normalised by the median value across the two scenarios and ventilation rates for SARS-CoV-2, $\widetilde{P}_{\text{infection}} = 2.6 \times 10^{-5}\,\%$.

dian infection risk when $t_{\text{enter}} < 1\,\text{min}$, compared to 89 % in scenario 2 (2C). When $1\,\text{min} \leq t_{\text{enter}} < 10\,\text{min}$, 47 % and 53 % of risks exceeded the median infection risk for scenarios 1 (NC) and scenario 2 (2C), respectively.

For SARS-CoV-2, 79 % of normalised infection risks exceeded the median infection risk in scenario 1 (NC) when $t_{\text{enter}} < 1\,\text{min}$, compared to 89 % in scenario 2 (2C). In contrast, when $1\,\text{min} \leq t_{\text{enter}} < 10\,\text{min}$, only 47 % and 53 % of risks exceeded the median infection risk for scenarios 1 (NC) and scenario 2 (2C), respectively. These findings highlight the effectiveness of increasing t_{enter} in reducing exposure risk.

Providing adequate toilet facilities and cubicles can help reduce the need for individuals to enter immediately after a flush, thereby lowering the risk of exposure to the toilet plume. However, expanding toilet infrastructure entails economic costs associated with construction, planning and spatial requirements.

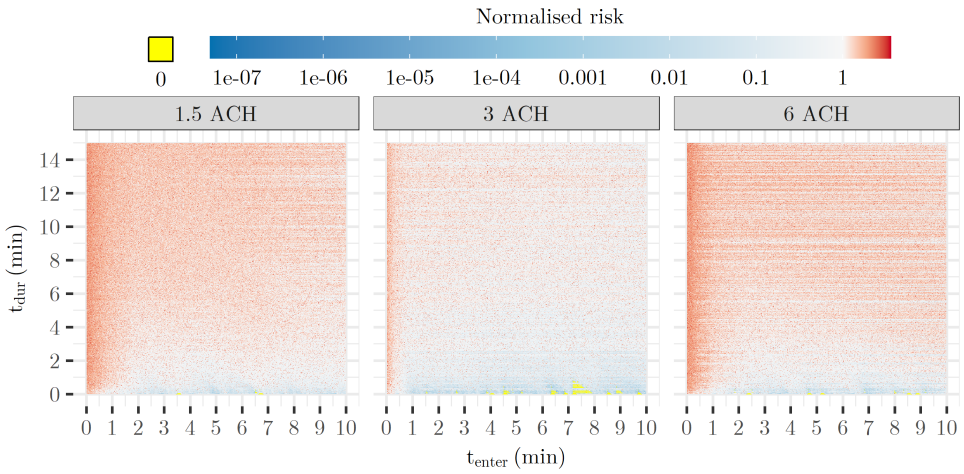

(a) Scenario 1 (NC).

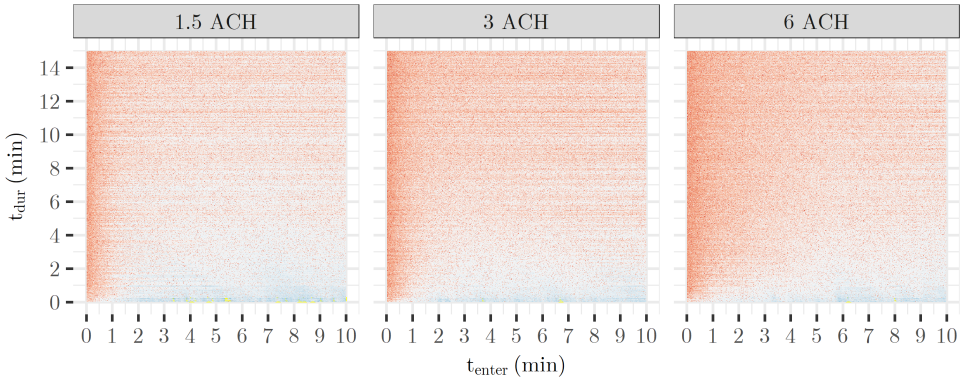

(b) Scenario 2 (2C).

Figure 4.7: Heat maps showing the relationship between $t_{\text{enter}}, t_{\text{dur}}$ and normalised norovirus risk infection. The particle counter was at location A and infection risk was normalised by the median value across the two scenarios and ventilation rates for norovirus, $\widetilde{P}_{\text{infection}} = 22\,\%$.

The values of the Spearman correlation coefficients for SARS-CoV-2 and norovirus, calculated using the R package `cor()`, can be seen in Table 4.5 and 4.6. The associated strength of the correlation was previously described in Table 4.3. This analysis is used to explore the relative importance of different parameters in the model.

For the narrower range of $0\,\text{min} < t_{\text{enter}} \leq 1\,\text{min}$, the relationship between infection risk and occupancy time (t_{dur}) was negligible to weak, as infection risk during this period was primarily driven by t_{enter}. The correlation between infection risk and the time of entry (t_{enter}) was strong in most cases, with one moderate case observed within this 0 min to 1 min window.

For $1\,\text{min} \leq t_{\text{enter}} \leq 10\,\text{min}$, the influence of t_{enter} on the infection risk was negligible or, in two cases, moderate, whereas the relationship with occupancy time (t_{dur}) was strong or in one case moderate. This suggests that if the second individual enters

Table 4.5: Spearman correlation coefficients, r_s, between respective parameters and SARS-CoV-2 infection risk.

Very strong	Strong	Moderate	Weak	Negligible

Parameter	t_{enter} **(s)**	**Scenario 1**			**Scenario 2**		
		1.5 ACH	**3 ACH**	**6 ACH**	**1.5 ACH**	**3 ACH**	**6 ACH**
t_{dur}	0-1	0.17	0.22	0.15	0.15	0.17	0.18
	1-10	0.43	0.42	0.40	0.45	0.45	0.40
t_{enter}	0-1	-0.40	-0.46	-0.44	-0.39	-0.37	-0.30
	1-10	-0.15	-0.11	-0.08	-0.13	-0.13	-0.28
f	0-10	-0.36	-0.32	-0.30	-0.32	-0.34	-0.34
ρ	0-10	0.39	0.37	0.34	0.36	0.38	0.39
B	0-10	0.12	0.11	0.10	0.11	0.11	0.11
V_{faeces}	0-10	0.40	0.37	0.33	0.37	0.38	0.38
RH	0-10	-0.05	-0.04	-0.04	-0.04	-0.05	-0.05
v_{surface}	0-10	-0.11	-0.10	-0.09	-0.10	-0.10	-0.11

Table 4.6: Spearman correlation coefficients, r_s, between respective parameters and norovirus infection risk.

Very strong	Strong	Moderate	Weak	Negligible

Parameter	t_{enter} **(s)**	**Scenario 1**			**Scenario 2**		
		1.5 ACH	**3 ACH**	**6 ACH**	**1.5 ACH**	**3 ACH**	**6 ACH**
t_{dur}	0-1	0.17	0.22	0.15	0.15	0.18	0.19
	1-10	0.45	0.41	0.39	0.47	0.47	0.41
t_{enter}	0-1	-0.42	-0.46	-0.46	-0.40	-0.39	-0.30
	1-10	-0.16	-0.12	-0.08	-0.13	-0.13	-0.29
λ	0-10	-0.27	-0.25	-0.22	-0.24	-0.26	-0.27
ρ	0-10	0.42	0.39	0.37	0.39	0.40	0.41
B	0-10	0.12	0.11	0.10	0.11	0.12	0.12
V_{faeces}	0-10	0.41	0.37	0.34	0.37	0.39	0.39
RH	0-10	-0.05	-0.05	-0.04	-0.04	-0.05	-0.05
v_{surface}	0-10	-0.11	-0.10	-0.09	-0.10	-0.10	-0.11

the toilet facility within the first 1 min after flushing, the infection risk is determined primarily by the timing of entry. Specifically, the negative correlation indicates that the risk decreases as the entry delay increases. During this early period, the risk was less affected by the duration of occupancy, suggesting that reducing the time spent in the cubicle would have minimal impact on infection risk in this timeframe. In contrast, if the second individual enters after the first 1 min, infection risk becomes strongly dependent on how long they remain in the toilet facility.

The relationship between infection risk and factors such as (i) breathing rate, (ii)

relative humidity, and (iii) the velocity of droplets at the toilet surface was negligible within the model. However, the volume of faecal matter (V_{faeces}) showed a moderate to strong correlation with infection risk. The density of genome copies per litre of faecal matter (ρ), the ratio of genome copies corresponding to infectious virus (f), and the reduction factor (λ) exhibited moderate to strong, moderate and weak correlation with infection risk, respectively.

Given the data available in the literature, these findings suggest that further research should prioritise collecting data on the volume of faecal matter per bowel movement and the density of genome copies per litre of faecal matter, as these factors have the most significant impact on estimated infection risks.

4.3.2 Risk Modelling Using Experimental Bioaerosol Concentrations

The risk of infection to a second susceptible individual from exposure to aerosolised *E. coli* due to toilet flushing, using gender-specific occupancy times, is presented in Fig. 4.8. Results are shown for both the piecewise estimation and the exponential estimation of concentration. The mean and median infection risks for the various scenarios and entry times are summarised in Table 4.7.

Across the two scenarios, both concentration models, and entry times $t_{\text{enter}} \in \{0, 60, 240\}$ s, the estimated infection risk ranged from 0 % to 1.8×10^{-2} %. Various per-event risk thresholds have been proposed in the literature when applying QMRA models [242]. These thresholds aim to define an acceptable level of risk for a given activity. Some studies adopt more conservative thresholds, such as 1.0×10^{-4} % [244, 245, 369], while others use higher values, such as 0.10 % [370]. Although these thresholds have been applied primarily to fomite transmission, others, such as a 0.010 % annual risk [243], are used in drinking water risk assessments. The acceptable level of risk depends on multiple factors, including the vulnerability of the exposed individuals. The maximum infection risk observed in this study exceeds the conservative threshold of 1.0×10^{-4} %, suggesting that mitigation measures may be necessary in high-risk environments where toilet facilities are located.

Differences in infection risk between males and females were observed in all

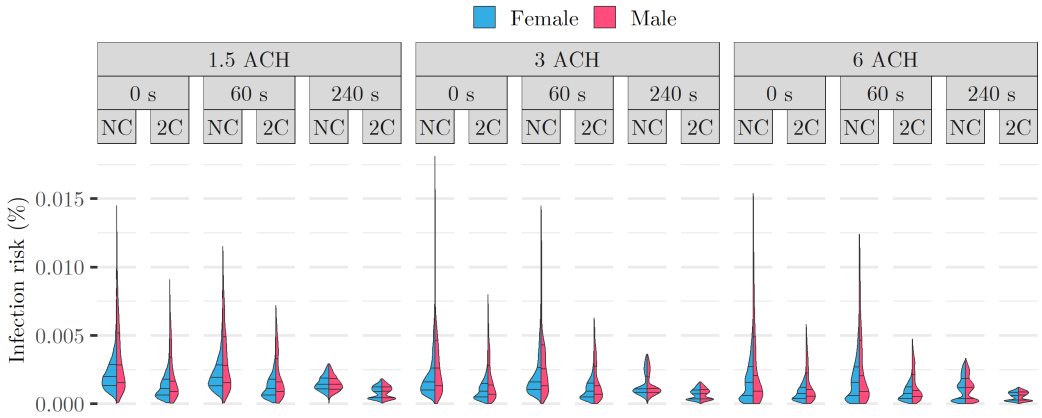

(a) Modelling the concentration with a piecewise function.

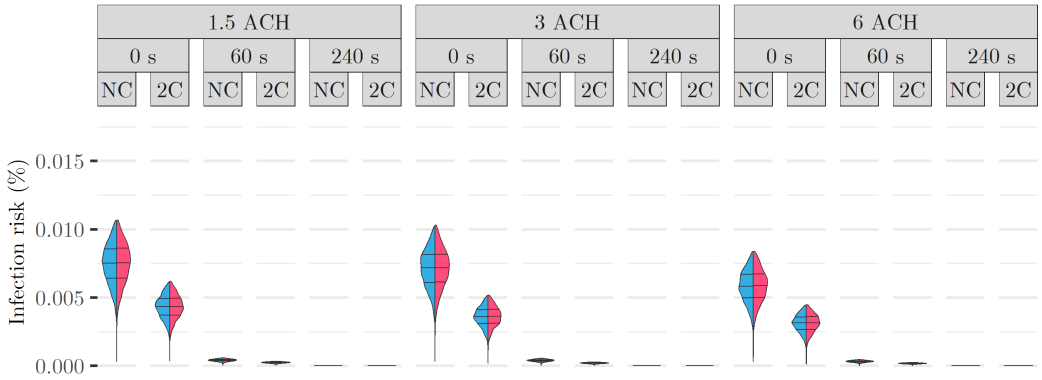

(b) Modelling the concentration with an exponential function.

Figure 4.8: Violin plots corresponding to the absolute risk for the *E. coli* experiments. The times referred to indicate the moment when the susceptible individual entered post-flush, t_{enter}. NC and 2C refer to scenarios as described in Table I (Section 3.4, Chapter 3). Horizontal lines represent the 25th, 50th, and 75th quantiles.

scenarios, primarily due to variations in occupancy times based on observational data shown in Fig. 4.2. Of the 18 cases presented for the piecewise model in Table 4.7, 89 % (16/18) showed a higher mean infection risk for males compared to females. For the exponential model, this was 75 % (12/18).

When considering combined risks between genders, the mean infection risk decreased as the entry time increased for both the piecewise and exponential concentration models. For example, in scenario 1 (NC) at 3 ACH, the mean infection risk across both genders decreased by 3.6 % when the second individual entered 60 s after flushing, compared to entering immediately (0 s). When the entry time was delayed to 240 s after flushing, the infection risk decreased by 50 % compared to immediate entry. The differences were less pronounced for the infection risk in the piecewise model than those observed using the exponential model. For the same case using the exponential model, the infection risk decreased by 95 % when the second in-

Table 4.7: Absolute median and mean infection risk values from exposure to *E. coli* at $t_{\text{enter}} \in \{0, 60, 240\}$ s. The results are shown using both a piecewise and an exponential function to estimate the concentration of bacteria inhaled based on experimental data. The risks are shown for the three ventilation rates: 1.5, 3 and 6 ACH with a comparison between scenario 1 (NC) and 2 (2C).

ACH	t_{enter} (s)	**Scenario**	**Gender**	**Piecewise C_j**		**Exponential C_j**	
				Mean (%)	**Median (%)**	**Median (%)**	**Mean (%)**
1.5	0	NC	Female	2.0e-03	2.3e-03	7.5e-03	7.5e-03
			Male	2.7e-03	3.6e-03	7.6e-03	7.5e-03
		2C	Female	1.0e-03	1.3e-03	4.3e-03	4.3e-03
			Male	1.5e-03	2.2e-03	4.3e-03	4.3e-03
	60	NC	Female	1.9e-03	2.3e-03	4.0e-04	4.0e-04
			Male	2.8e-03	3.4e-03	4.1e-04	4.0e-04
		2C	Female	1.1e-03	1.3e-03	2.3e-04	2.3e-04
			Male	1.5e-03	2.1e-03	2.3e-04	2.3e-04
	240	NC	Female	1.4e-03	1.5e-03	6.2e-08	6.1e-08
			Male	1.4e-03	1.5e-03	6.1e-08	6.1e-08
		2C	Female	9.0e-04	8.6e-04	3.5e-08	3.5e-08
			Male	9.2e-04	8.7e-04	3.6e-08	3.6e-08
3	0	NC	Female	1.6e-03	2.1e-03	7.2e-03	7.1e-03
			Male	2.5e-03	3.6e-03	7.2e-03	7.1e-03
		2C	Female	9.1e-04	1.1e-03	3.6e-03	3.6e-03
			Male	1.3e-03	1.9e-03	3.9e-03	3.6e-03
	60	NC	Female	1.6e-03	2.1e-03	3.9e-04	3.8e-04
			Male	2.5e-03	3.4e-03	2.0e-04	3.8e-04
		2C	Female	9.0e-04	1.1e-03	1.9e-04	1.9e-04
			Male	1.2e-03	1.7e-03	5.9e-04	1.9e-04
	240	NC	Female	1.1e-03	1.4e-03	5.9e-08	5.8e-08
			Male	1.1e-03	1.4e-03	3.0e-08	5.9e-08
		2C	Female	7.2e-04	7.1e-04	3.0e-08	2.9e-08
			Male	7.4e-04	7.2e-04	5.8e-08	2.9e-08
6	0	NC	Female	1.4e-03	1.8e-03	5.8e-03	5.8e-03
			Male	1.7e-03	3.1e-03	5.9e-03	5.9e-03
		2C	Female	7.2e-04	8.6e-04	3.1e-03	3.1e-03
			Male	9.5e-04	1.4e-03	3.2e-03	3.1e-03
	60	NC	Female	1.4e-03	1.8e-03	3.1e-03	3.1e-04
			Male	1.7e-03	2.9e-03	3.2e-04	3.1e-04
		2C	Female	7.2e-04	8.6e-04	1.7e-04	1.7e-04
			Male	8.9e-04	1.3e-03	1.7e-04	1.7e-04
	240	NC	Female	1.2e-03	1.2e-03	4.8e-08	4.8e-08
			Male	1.2e-03	1.2e-03	4.8e-08	4.8e-08
		2C	Female	6.1e-04	5.6e-04	2.5e-08	2.5e-08
			Male	6.3e-04	5.8e-04	2.6e-08	2.5e-08

dividual entered 60 s after flushing compared to entering immediately (0 s). This decrease was larger at 100 % when comparing 240 s entry to 0 s. The differences between the piecewise and exponential results arise from the assumption that the

bacterial concentration remains constant over the two 5 min sampling intervals in the piecewise model. Consequently, variations in infection risk for different entry times were primarily due to the fact that the later entry times overlapped more with the 5 min to 10 min sampling period, where no bacteria or a minimal quantity of bacteria was detected. In contrast, for the exponential concentration model, the highest risk occurred within the first 60 s, meaning that avoiding this initial period significantly reduced the infection risk. Across different ventilation rates and entry times, scenario 1 (NC) exhibited a higher mean infection risk than scenario 2 (2C). This may be due to variations in the initial concentration of *E. coli* in the toilet bowl, although the relationship between the bowl concentration and aerosolised bacteria remains uncertain. Alternatively, the absence of a cubicle in the room could lead

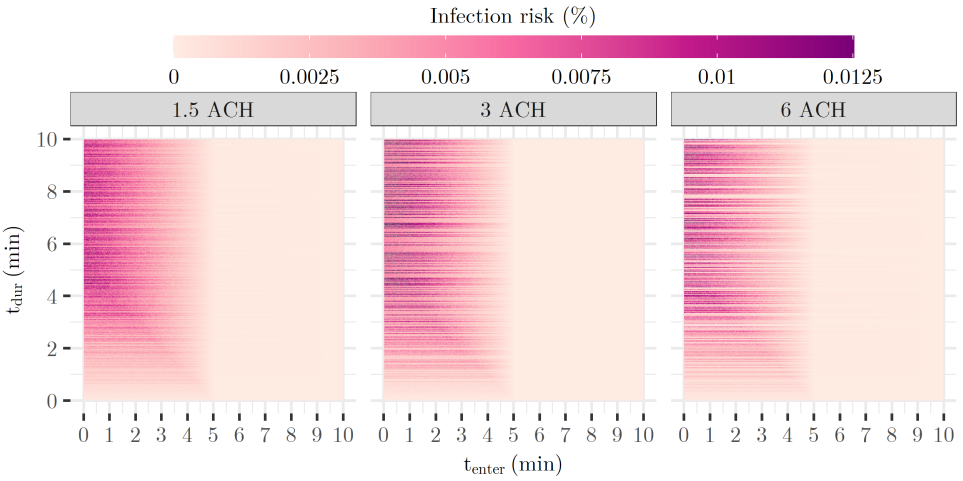

(a) Scenario 1 (NC).

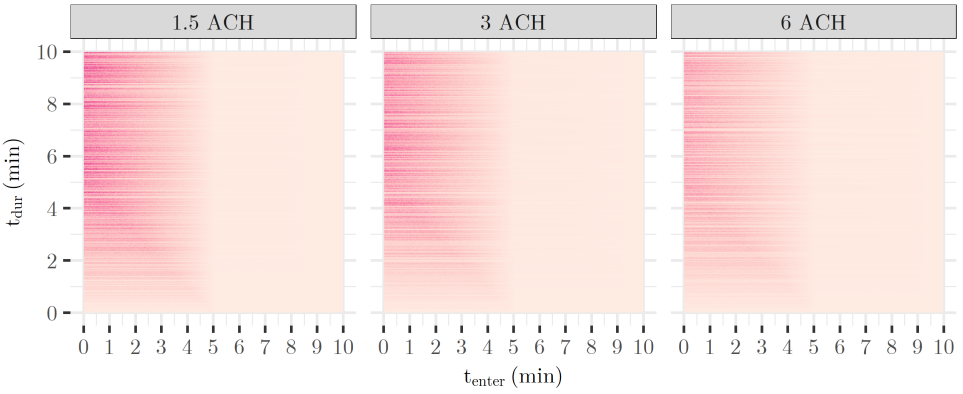

(b) Scenario 2 (2C).

Figure 4.9: Heat maps illustrating the relationship between entry time (t_{enter}), occupancy duration (t_{dur}), and absolute *E. coli* infection risk under the piecewise concentration model. Scenario 1 (NC) represents a setting without a cubicle, while scenario 2 (2C) includes two cubicles.

to higher airflow velocities near the toilet and the sampler, increasing the likelihood that aerosols are captured during the 5 min sampling period. Higher airflow velocities might also prevent bioaerosols from settling on surfaces, keeping them airborne and subsequently sampled at a higher rate. Additionally, the stochastic nature of the toilet flush may contribute to these differences, suggesting that further studies on the repeatability of toilet flush dynamics could provide more insight.

The infection risk as a function of t_{enter} and t_{dur} using uniformly distributed occupancy times is shown in Figs. 4.9 and 4.10, using the uniform distribution for occupancy time.

For the piecewise estimation of concentration, $C_j(t)$, higher infection risks are observed when $t_{\text{enter}} < 5\,\text{min}$, as indicated by the darker regions in Fig. 4.9. The mean infection risk for $t_{\text{enter}} \geq 5\,\text{min}$ in all scenarios and ventilation rates was

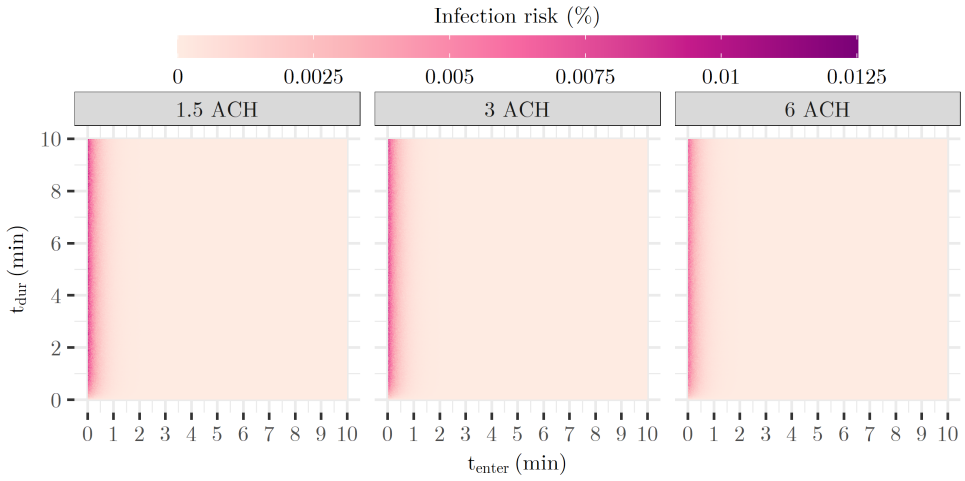

(a) Scenario 1 (NC).

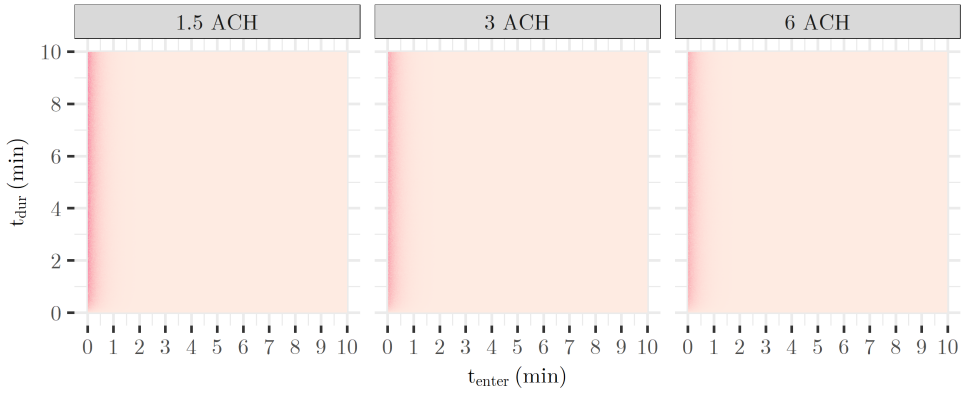

(b) Scenario 2 (2C).

Figure 4.10: Heat maps illustrating the relationship between entry time (t_{enter}), occupancy duration (t_{dur}), and absolute *E. coli* infection risk under the exponential concentration model. Scenario 1 (NC) represents a setting without a cubicle, while scenario 2 (2C) includes two cubicles.

1.8×10^{-5} %. This value is below the conservative risk threshold of 1.0×10^{-4} %, as discussed earlier, suggesting that the infection risk from aerosolised *E. coli* in the toilet plume beyond 5 min after flushing is negligible.

For the exponential concentration estimation, the highest risks occur when $t_{\text{enter}} <$ 1 min, shown by the darker regions in Fig. 4.10. The mean infection risk for $t_{\text{enter}} \geq 1$ min is 1.1×10^{-5} %, which is an order of magnitude lower than the conservative threshold, suggesting that the risk is negligible beyond this period.

The results indicate that the breathing rate and occupancy time have negligible effects on the infection risk, whereas the post-flush entry time has a strong influence. These findings highlight the importance of allowing sufficient time to pass between successive toilet users to reduce the risk of infection from aerosolised pathogens.

Tables 4.8 and 4.9 present the Spearman correlation coefficients (r_s) between post-flush entry time, occupancy time, breathing rate, and *E. coli* infection risk for the piecewise and exponential concentration models, respectively.

Table 4.8: Spearman correlation coefficients, r_s, between respective parameters and *E. coli* infection risk using a piecewise function for the concentration.

Very strong	Strong	Moderate	Weak	Negligible

Parameter	t_{enter} **(s)**	**Scenario 1**			**Scenario 2**		
		1.5 ACH	**3 ACH**	**6 ACH**	**1.5 ACH**	**3 ACH**	**6 ACH**
t_{dur}	0-10	0.08	0.06	0.04	0.06	0.09	0.06
t_{enter}	0-10	-0.87	-0.89	-0.83	-0.86	-0.86	-0.85
B	0-10	0.06	0.05	0.05	0.05	0.07	0.06

Table 4.9: Spearman correlation coefficients, r_s, between respective parameters and *E. coli* infection risk using an exponential function for the concentration.

Very strong	Strong	Moderate	Weak	Negligible

Parameter	t_{enter} **(min)**	**Scenario 1**			**Scenario 2**		
		1.5 ACH	**3 ACH**	**6 ACH**	**1.5 ACH**	**3 ACH**	**6 ACH**
t_{dur}	0-10	0.01	0.01	0.01	0.01	0.01	0.01
t_{enter}	0-10	-1.00	-1.00	-1.00	-1.00	-1.00	-1.00
B	0-10	0.02	0.02	0.02	0.02	0.02	0.02

For both models, the parameter with the greatest influence on infection risk is the time at which the second individual enters the toilet facility (t_{enter}). There is a very

strong relationship between infection risk and t_{enter}, which is even more pronounced in the exponential model. In contrast, both breathing rate and occupancy time have a negligible effect on infection risk.

4.4 Implications of Findings

This study presents a quantitative framework for assessing airborne transmission risks from toilet plume aerosols using controlled experimental data. It is the first application of a QMRA model in such detail to airborne transmission from toilet plume aerosols in a controlled setting. While prior studies have estimated annual infection risk, none have examined infection risk per exposure event. This is crucial, as exposure to hazardous pathogens in large quantities is unlikely to occur each time an individual uses the toilet but rather sporadically. By considering time-dependent exposure risks, rather than annualised estimates, this study provides a more realistic assessment of transmission risks for individuals entering a toilet after a flush. This makes the model particularly relevant for high-occupancy events, such as those in stadiums, concerts, and other events, where airborne pathogen concentrations may be temporarily elevated. The approach presented here formalises infection risk assessment per exposure event and quantifies how increasing entry time after a flush influences risk. Unlike previous studies, this model also incorporates occupancy behaviours. The model is adaptable as new data on aerosols, human behaviours, exposure patterns, viral concentrations, and dose-response relationships become available. It could be applied to any emerging pathogens, particularly if there is indication of contamination in faecal matter.

By integrating the experimental measurements with stochastic modelling, this framework evaluates how different factors influence infection risk. This structured methodology is valuable for identifying key exposure contributions. This can support toilet facility design, occupancy management, and future experimental studies. The ability to explore ventilation rates, exposure durations, and aerosol decay makes it a flexible tool for assessing mitigation strategies. The findings emphasise the importance of minimising exposure during peak aerosol dispersion periods, which

can help inform mitigation strategies.

The study employs two distinct models to quantify risk. The non-biological particle concentration model provides a more refined temporal resolution, as data are collected at shorter intervals. This makes it particularly useful for assessing exposure dynamics across different time points, making it applicable to a variety of other pathogens with known faecal concentrations and dose-response models. Additionally, it is more feasible in non-laboratory settings, where biological sampling may not be practical.

In contrast, the bioaerosol-based model provides a direct estimate of absolute infection risk as it quantifies viable bacteria in aerosol samples. Although the piecewise concentration model has lower temporal resolution due to longer sampling intervals, it provides stronger biological relevance for evaluating absolute exposure risks. The exponential decay model using bioaerosol concentrations, which integrates both particle concentration and bioaerosol data, offers a novel approach that better represents pathogen exposure over a period of time compared to the piecewise concentration model.

This structured methodology establishes a scalable framework for future risk assessments, allowing adaptation to different pathogens, new aerosol data, and evolving occupancy behaviours.

4.5 Study Limitations and Areas for Further Research

In both studies, distinctions between droplet sizes and their deposition sites within the respiratory tract were not considered. Different particle sizes, which vary between toilet plumes and exhaled breath, deposit in different regions of the respiratory tract. For the same number of virions, variations in droplet size could influence infection risk and severity of the illness depending on the deposition site. Additionally, the presence and distribution of virus receptors determine whether deposition leads to infection and the severity of illness [371]. Incorporating dose-response models specific to upper and lower respiratory tract infections [372, 373], alongside tools

such as the Multiple-Path Particle Dosimetry Model (MPPD) [374], could enhance future iterations of this model.

The toilet occupancy times used in this study were based on data from 1972. Changes in behaviour since then, such as increased smartphone use, could lead to longer cubicle occupancy times [375]. More recent behavioural data, potentially collected through observational studies or automated door sensors, would improve occupancy time estimates and enhance model accuracy.

This study modelled idealised scenarios with mechanical ventilation and two specific toilet facility layouts. However, real-world variations in ventilation performance and facility design can influence aerosol dispersion and experimental measurements. Most toilet facilities do not use HEPA filters, as implemented in this study, which could result in exposure to external contaminants. A CFD model of toilet flushing in the aerobiology chamber, discussed in Chapter 5, provides further insight into airflow patterns within the ventilation system and the influence of cubicle structures on aerosol dispersion.

Uncertainty remains in dose-response models, particularly with regard to infection risks associated with different exposure routes. Further calibration of these models could refine guidance on t_{enter}, particularly when the infector and pathogen type are known. This would be especially beneficial for individuals with increased susceptibility to infection.

4.5.1 Risk Modelling Using Non-biological Experimental Particle Concentrations

The sodium chloride experiments assumed a proportional viral load distribution by volume, which is unlikely to reflect real-world conditions. In real-world conditions, viral load distribution will vary with particle size and will differ between exhaled breath and toilet plumes.

The aerosol transmission of norovirus has been explored in recent studies [21], with more cases linked to vomiting than to diarrhoea. One recommendation of this research was the need for further investigation of the role of diarrhoea and toilet flushing in aerosol transmission. Expanding research in this area would complement

the present study and enhance the applicability of norovirus as a model pathogen.

Exposure was modelled through inhalation with a reduction factor to account for ingestion. Respiratory activities are likely to contribute to ingestion, as particles deposited in the upper respiratory tract may be transported to the digestive system through mucus and saliva. The actual airborne exposure mechanism for norovirus is more complex than the approach considered here, meaning that the modelled infection risks may be overestimated or underestimated. As understanding of pathogen exposure routes improves, models such as the one presented here can be refined to incorporate more complex exposure pathways.

Recent modelling has identified where viruses predominantly deposit after inhalation, showing, for example, that SARS-CoV-2 deposits primarily in the nasal region [371]. A similar approach could be applied to norovirus to estimate the proportion of inhaled virus that deposits in the nasal region and subsequently is ingested. This would refine the assumption of the current study of a uniform 10 % to 50 % reduction factor.

Although normalising infection risk allowed relative comparisons, further calibration using pathogen-specific concentration data from toilet flushing, along with factors such as the ratio of solid faeces to water, would improve the reliability of absolute infection risk estimates. In cases where the infectious dose of a pathogen is particularly high, the maximum infection risk from the toilet plume may be negligible, making additional mitigation measures unnecessary.

4.5.2 Risk Modelling Using Bioaerosol Concentrations

This study highlights the importance of concentration modelling in assessing infection risk. By modelling *E. coli* concentration as a piecewise function, there may be an overestimation of risk in the region of $1\,\text{min} < t_{\text{enter}} < 5\,\text{min}$. However, it should be noted that the particle counter A data may not accurately represent particle concentrations at breathing height. Ideally, measurements at breathing height would be used, but as discussed in Section 3, background variation in this region was greater than the increase attributed to the toilet flush.

A key limitation of the piecewise model is the assumption that bacterial con-

centration remains constant across the two 5 min intervals. Particle concentration time series data in Chapter 3, Section 3.5.1 indicate a significant peak within the first 1 min. The exponential model addressed this by assuming that the bacterial concentration followed an exponential decay. A mean decay rate was determined, but, in reality, the decay rates varied by the particle diameter. The actual decay profile is likely to align more closely with a specific particle size, depending on how bacteria are distributed across particle diameters. For example, if most bacteria were associated with 10 µm particles, then the decay profile could be expected to follow that of these larger particles.

Future research should focus on developing a more refined time series of bacterial concentration in the 10 min interval, with particular emphasis on the first 5 min. Conducting such studies is challenging because they require extensive experimental bioaerosol sampling under controlled conditions that realistically simulate the interactions between stool and water. These measurements are difficult to obtain, as the transient nature of toilet flushing means that the time evolution of airborne pathogens occurs more rapidly than the sampling time of current bioaerosol collection techniques.

4.6 Conclusions

This study presents a quantitative framework for estimating infection risk following a toilet flush and exposure to aerosolised pathogens. The model was applied to two types of experimental data (bioaerosol measurements and particle counts) across several ventilation and occupancy scenarios, based on data from controlled chamber experiments. The QMRA framework can be extended to other experimental settings, such as different toilet facility configurations or assessing the impact of closing the toilet lid. The findings lead to the following conclusions:

- The combined experimental and QMRA approach indicates that infection risk from the toilet plume is highly variable but may be non-negligible, particularly for pathogens with high faecal concentrations, such as norovirus.
- The model framework provides a method to assess the factors that influence

risk and possible mitigation strategies. The results suggest that allowing time for ventilation after toilet use significantly reduces the infection risk. Even a short delay of 60 s between occupants can substantially reduce the risk of exposure.

- When considering mitigation strategies, increasing the time between toilet use after a flush (t_{enter}) to at least 60 s appears to be a more effective approach than reducing occupancy time (t_{dur}).
- The method used to model aerosol concentration has a substantial impact on infection risk estimates. The exponential decay model provided a more realistic representation of bioaerosol concentration over time compared to the piecewise function, which may overestimate risks in certain time intervals.
- The spatial distribution of aerosols within the toilet environment remains a key uncertainty. Particle measurements were primarily taken from a fixed location, meaning airflow patterns and particle transport dynamics require further investigation through additional experimental and computational modelling studies.
- The study highlights the need for more refined bioaerosol sampling techniques capable of capturing transient aerosol dynamics following a toilet flush. Current sampling methods may not adequately resolve rapid changes in concentration, particularly in the first 1 min after flushing.
- Further quantitative data are required to refine the accuracy of absolute risk estimates. Key areas for improvement include detailed toilet cubicle occupancy times across different settings (e.g. hospitals, workplaces, and public events), virus concentrations in faeces, particle generation rates from different toilet types, and pathogen-specific dose-response relationships.

Chapter 5

Numerical Modelling of the Fate of Droplets Generated by a Toilet Using Computational Fluid Dynamics

5.1 Introduction

Understanding the transport and fate of aerosols generated by flushing the toilet is crucial for assessing infection risks in indoor environments, particularly toilet facilities. Few studies have specifically modelled the toilet plume using CFD [166, 322, 323, 324, 326]. Although research on respiratory emissions has leveraged CFD to understand airflow dynamics and droplet dispersion, the modelling of toilet plume aerosols remains underexplored. The complexity of simulating turbulent multiphase flows, combined with the challenges of replicating real-world flushing mechanisms, has limited detailed numerical investigations in this area. This study aims to address this gap by employing a CFD model to assess the fate of aerosols generated during flushing events.

In this chapter, a CFD model is developed to simulate the toilet flushing experiments described in Chapter 3. As in Chapter 3, two scenarios are modelled: (1) the toilet flushing on its own within the aerobiology chamber, and (2) the toilet flushing in the aerobiology chamber with two cubicles. Simulations are conducted for three ventilation rates: 1.5, 3, and 6 ACH.

The primary aim of this chapter is to qualitatively and quantitatively analyse the airflow patterns and particle trajectories generated by toilet flushing. These simulations provide insight into the influence of room layout and ventilation rates on the dispersion and fate of particles released during flushing events.

Previous studies have demonstrated the use of CFD techniques to model airflow in indoor spaces, often focusing on respiratory emissions, such as coughing and sneezing, and their associated droplet dispersion. The DPM is commonly used in these studies to simulate droplet behaviour. While most research has concentrated on respiratory emissions, limited and recent studies [166, 323, 324, 326], as discussed in Chapter 2, have applied CFD modelling using DPM modelling to investigate particle dispersion specifically related to toilet plumes. This approach represents a developing methodology, with research into the dispersion of toilet plume aerosols through CFD modelling still in its early stages. These recent studies highlight the growing recognition of the need to understand and quantify the risks associated with

airborne particles generated by toilet flushing using CFD methods.

This chapter builds on these approaches by simulating the trajectory of particles released during flushing events to assess whether they remain airborne or deposit on surfaces. The influence of ventilation rates on airflow patterns and their subsequent impact on particle behaviour is also examined. These analyses provide critical insight on the potential for airborne exposure and help inform strategies to mitigate risks associated with toilet plume aerosols in shared facilities.

5.2 Methodology

A CFD model was developed in ANSYS Fluent (version 2023, R2) [306] to simulate the dispersion of droplets generated by toilet flushing. As discussed in Chapter 2, the fluid dynamics of a toilet flush involves complex multiphase interactions, including droplet breakup driven by inertial and surface tension forces. Direct modelling of the full multiphase dynamics of the flush, including droplet formation and fragmentation, would be computationally prohibitive because of the metre-scale dimensions of the chamber and the minute-scale simulation durations. Instead, this study focused on droplet dispersion using Lagrangian particle tracking, with the toilet flush represented as an injection of particles at the toilet surface.

Previous studies have used VOF models to simulate toilet flushing [319, 320, 321, 376], but these have mainly focused on evaluating toilet performance rather than aerosol generation. One study [166] has combined a VOF model with a DPM to simulate both the flushing process and aerosol dispersion. However, this modelling was limited to two dimensions. Incorporating this level of detail into a full-scale chamber simulation remains computationally prohibitive.

The simulation workflow is outlined in Fig. 5.1, covering domain definition, meshing, boundary conditions, solver setup, and post-processing.

Each step in the workflow was designed to ensure that the model adequately represented the experimental setup and provided meaningful insight on the behaviour of particles under different ventilation conditions. The process begins with defining the physical geometry and boundary conditions of the system to replicate the aer-

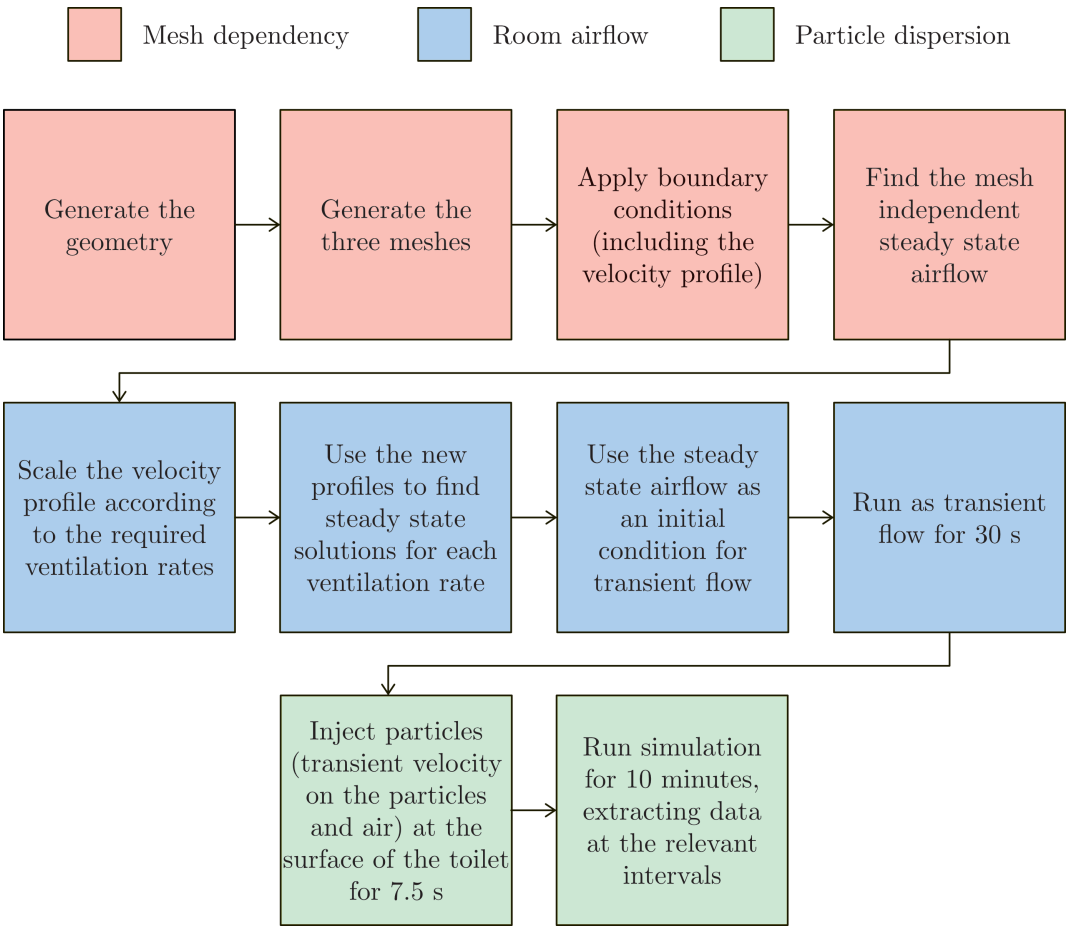

Figure 5.1: A workflow for the CFD simulation process.

obiology chamber and toilet setup used in the experiments. Following this, a mesh independence study ensured an appropriate spatial resolution to capture airflow and particle trajectories. Initial simulations were performed using the ventilation strategy applied in the aerobiology chamber, with three ventilation rates (1.5, 3, and 6 ACH) to evaluate the impact of ventilation on particle fate. In addition, further simulations were conducted to explore the effect of introducing ventilation extracts above cubicles, assessing their potential to enhance aerosol removal and reduce airborne particle concentration.

5.2.1 Geometry Generation

The aerobiology chamber was modelled to match the experimental conditions using ANSYS DesignModeler (version 2023, R2) [377]. The geometry of the chamber, including its dimensions, has previously been detailed in Chapter 3, Section 3.3.1 (Fig. 3.6a). The sizes of the ventilation inlet and outlet, which were based on the

actual chamber, have previously been illustrated in Figs. 3.6b and 3.6c.

A simplified version of the toilet on the plinth was included, created by extruding it from the geometry. Simplified geometries are commonly used in CFD studies of indoor environments, such as classrooms and hospitals [253, 308], to balance computational efficiency with accuracy. The simplified version allows for improved mesh convergence. In this case, the plinth was modelled as a solid block, while the toilet was constructed using a combination of cuboid and elliptical shapes. The resulting geometry of the toilet is shown in Fig. 5.2a, with the dimensions of the particle injection surface illustrated in Fig. 5.2b.

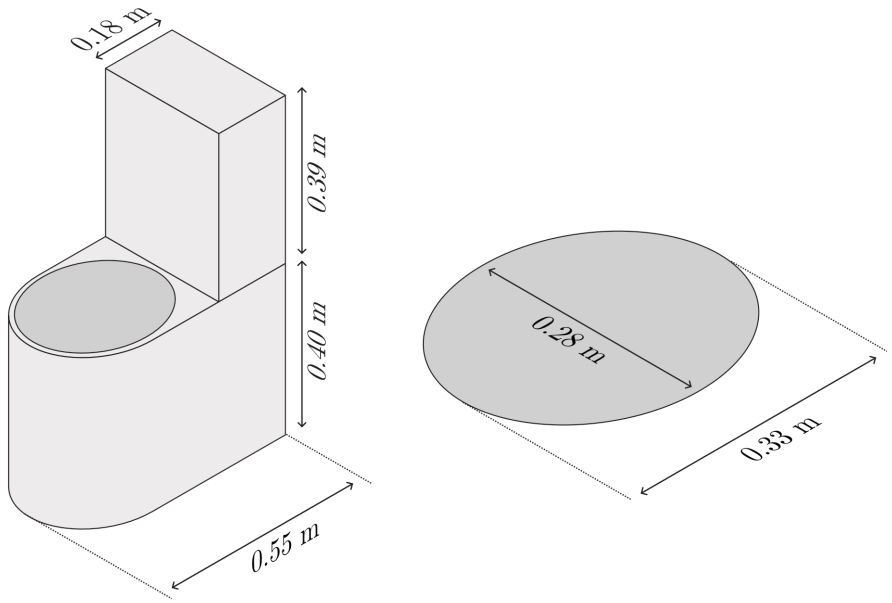

(a) The simplified toilet geometry. (b) The injection surface.

Figure 5.2: The dimensions of the simplified toilet geometry used for the CFD simulations.

For scenario 2 (recall from Chapter 3 that this is the two cubicle (2C) scenario), cubicles were added as thin walls with a thickness of 0.02 m, using the same dimensions as those in the experimental setup (Fig. 3.10, Section 3.4).

5.2.2 Mesh Generation

Mesh generation was performed using ANSYS Fluent Meshing (version 2023, R2) [306]. A poly-hexcore mesh structure was used to generate the mesh, consisting of octree hexahedral elements in the bulk region, polyhedral buffer layers in the

transition region and prism layers near the boundary walls [378]. This type of mesh is known to decrease the number of elements by 20 % to 50 %, compared to conventional hexahedral meshing [379]. The poly-hexcore mesh has been applied in previous studies of airflow in indoor spaces [380, 381, 382, 383]. For both scenario 1 (NC) and scenario 2 (2C), three levels of mesh refinement (coarse, medium, and fine) were generated, resulting in a total of six meshes.

Face sizing was applied to the walls of the chamber, including the floor and ceiling, as well as the walls of the toilet and plinth. A body of influence was introduced within a cylindrical region that extended 0.39 m from the particle injection surface of the toilet to enhance the resolution of the mesh in this area. Inflation layers were also added to the chamber walls and the toilet surfaces to better capture boundary layer effects.

During the mesh refinement process, the maximum cell length and the sizing within the body of influence were systematically reduced. Adjustments were made to the face sizing and inflation layer parameters to ensure mesh quality was maintained across all refinement levels. Details of global and local sizing parameters, as well as inflation layers, are summarised in Tables 5.1, 5.2, and 5.3 for both scenarios. The total number of elements and the orthogonal cell quality for each mesh configuration are provided in Table 5.4. The total number of elements of the coarse, medium and fine meshes and the corresponding minimum and average orthogonal cell quality are detailed in Table 5.4. A minimum mesh quality of greater than 0.1 is considered acceptable and all three meshes fit this criterion. A mesh independence study was conducted using the three generated meshes to ensure that the model output was not influenced by the size of the mesh. The results of this study are detailed in Section 5.2.7.

Table 5.1: The global sizing used to generate the bulk volume mesh for scenario 1 (NC) and scenario 2 (2C).

Scenario	Mesh	Max cell length (m)
1 and 2	Coarse	0.13
	Medium	0.07
	Fine	0.03

Table 5.2: The local sizing for the coarse, medium and fine meshes in scenario 1 (NC) and scenario 2 (2C). All settings had a growth rate of 1.2.

Scenario	Mesh	Location	Type	Size (m)
1	Coarse	Chamber walls	Face sizing	0.07
		Toilet walls	Face sizing	0.05
		Cylinder above toilet	Body of influence	0.05
	Medium	Chamber walls	Face sizing	0.05
		Toilet walls	Face sizing	0.03
		Cylinder above toilet	Body of influence	0.03
	Fine	Chamber walls	Face sizing	0.05
		Toilet walls	Face sizing	0.03
		Cylinder above toilet	Body of influence	0.02
2	Coarse	Chamber walls	Face sizing	0.07
		Toilet walls	Face sizing	0.05
		Cylinder above toilet	Body of influence	0.05
		Cubicle walls	Face sizing	0.05
	Medium	Chamber walls	Face sizing	0.05
		Toilet walls	Face sizing	0.03
		Cylinder above toilet	Body of influence	0.03
		Cubicle walls	Face sizing	0.03
	Fine	Chamber walls	Face sizing	0.05
		Toilet walls	Face sizing	0.03
		Cubicle walls	Face sizing	0.02
		Cylinder above toilet	Body of influence	0.02

Table 5.3: Details of the inflation layers used to generate the meshes for scenario 1 (NC) and scenario 2 (2C).

Scenario	Mesh	Location	First layer thickness (m)	Number of layers
1	Coarse	Chamber walls	0.0005	10
		Toilet walls	0.001	3
	Medium	Chamber walls	0.0005	10
		Toilet walls	0.001	3
	Fine	Chamber walls	0.0005	10
		Toilet walls	0.001	3
2	Coarse	Chamber walls	0.0005	10
		Toilet and cubicle walls	0.001	3
	Medium	Chamber walls	0.0005	10
		Toilet and cubicle walls	0.001	3
	Fine	Chamber walls	0.0005	10
		Toilet and cubicle walls	0.001	3

5.2.3 Boundary Conditions

After creating the meshes, ANSYS Fluent (version 2023, R2) [306] was used to configure the CFD model. A no-slip boundary condition was applied to all chamber walls, including the four vertical walls, ceiling and floor, as well as to the walls of the

Table 5.4: The total number of elements and the corresponding minimum and average orthogonal cell quality in the meshes for scenario 1 (NC) and scenario 2 (2C).

Scenario	Mesh	Total number of elements	Minimum orthogonal cell quality	Average orthogonal cell quality
1	Coarse	234,853	0.15	0.94
	Medium	483,996	0.15	0.99
	Fine	1,160,220	0.15	0.99
2	Coarse	479,992	0.14	0.94
	Medium	862,580	0.15	0.97
	Fine	1,917,054	0.14	0.98

toilet and plinth. The surface of the toilet also had a no-slip boundary condition, other than simulations involving toilet flushing.

The ventilation outlet of the chamber was defined as a pressure outlet (set at 0 Pa), while a velocity profile, previously used in CFD models of the University of Leeds aerobiology chamber [4], was applied at the inlet to represent airflow through the louvred diffuser. This profile, derived from anemometer measurements, was established in the earlier study (King et al. [4]) by defining velocities at 66 points arranged in an 11-by-6 grid 4 cm from the inlet. Inverse distance interpolation in ANSYS Fluent was used to apply the profile to the mesh at the inlet. The initial velocity profile corresponded to a ventilation rate of 6.5 ACH and was therefore scaled to match the required ventilation rates after the mesh independence study, which was performed with the velocity profile corresponding to the 6.5 ACH ventilation rate. The velocity profile for the medium mesh at 6 ACH is shown in Fig. 5.3.

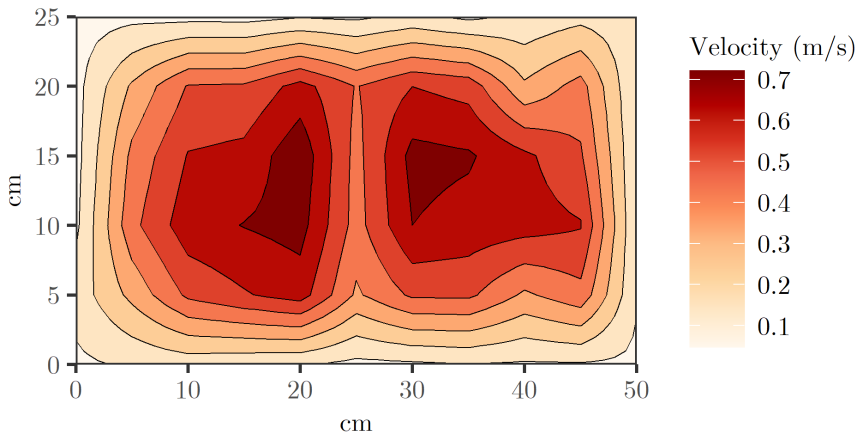

Figure 5.3: Velocity contours for the anemometer measurements 4 cm from the inlet used for the velocity profile in the chamber CFD model. Produced using measurements taken from King et al. [4].

To determine particle exposure, a small mass flow outlet was positioned at a height of 1.46 m from the floor, approximately breathing height, with a mass flow rate of $2.00 \times 10^{-4}\,\mathrm{m^3\,s^{-1}}$ to represent light-intensity human breathing [354, 355]. Additionally, a small outlet was included to simulate the OPC, with a mass flow rate of $4.78 \times 10^{-5}\,\mathrm{m^3\,s^{-1}}$, representing particle counter A from the experimental work in Chapter 3. The mesh was refined around these outlets to ensure that the particle results were not influenced by mesh resolution. The locations of these outlets relative to the toilet and mount are shown in Fig. 5.4. The number of particles that escaped through these outlets was analysed to assess exposure and support model validation. The human exposure outlet provided an estimate of the potential number of particles a person could inhale when entering the toilet facility over a 10 min period. The OPC outlet allowed for a direct comparison between the CFD simulations and the experimental data from Chapter 3, Section 3.5.1.

All simulations were conducted under isothermal conditions, as there were no significant heat sources in the experimental setup. This assumption meant that thermal buoyancy effects did not influence airflow patterns, with the focus on ventilation-driven aerosol transport.

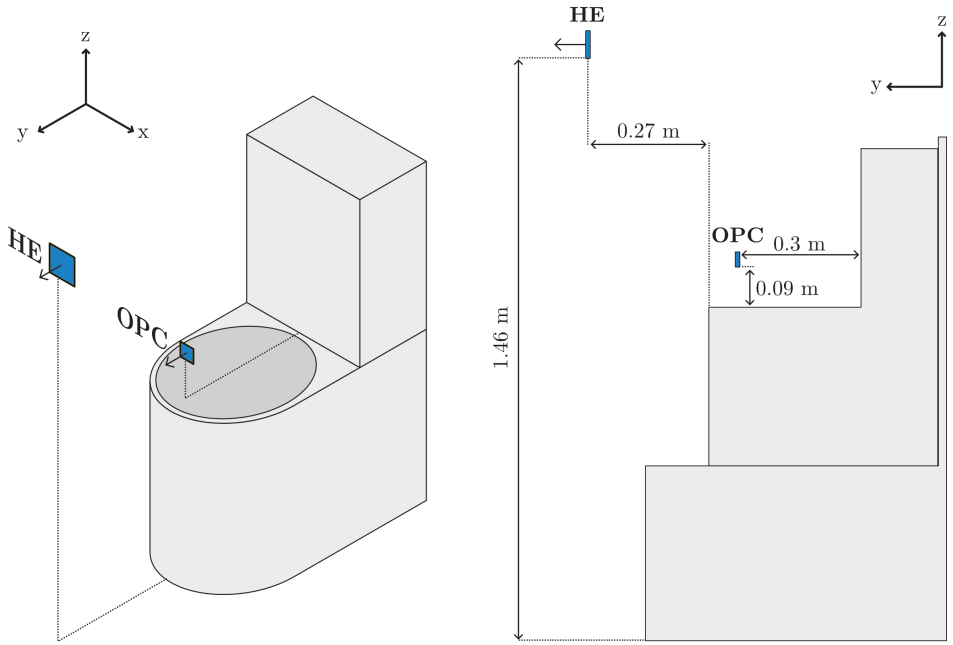

(a) A three dimensional visualisation. (b) Locations in the $y - z$ plane.

Figure 5.4: The locations of the human exposure outlet (HE) and the OPC outlet relative to the toilet and plinth.

5.2.4 Solver

Before modelling the dispersion of the particles that are released from a toilet flush, a steady-state flow was established in the chamber for the bulk airflow, using the boundary conditions described in Section 5.2.3. This was used as an initial condition for the transient flow that occurs during particle release. The steady-state solution was calculated in ANSYS Fluent [306] using the coupled algorithm with second-order upwind discretisation for all variables, with a pseudo-transient time-stepping method.

5.2.5 Turbulence Model

The flow was simulated using a RANS model, specifically the $k-\omega$ SST (Standard Shear Turbulence) model [384]. This model is a low-Reynolds model and combines the strengths of the $k-\omega$ model and the $k-\epsilon$ model. The $k-\omega$ model performs well in predicting flow behaviour near walls, and the $k-\epsilon$ model is more accurate in the bulk flow. The $k-\omega$ SST model therefore uses a blending function to activate the $k-\omega$ model in the near-wall region and then activates the $k-\epsilon$ model in the bulk flow [385].

Since this study considered the deposition of particles on surfaces as well as airborne particles, the $k-\omega$ SST model provides a more reliable representation of the near-wall region. For this model, the near-wall mesh resolution must be fine (i.e., $y^+ \approx 1$) [386] such that there are a few cells in the viscous sub-layer [387]. Previous studies have demonstrated good agreement between experimental measurements and CFD simulations when the $k-\omega$ SST model is applied to airflow in indoor environments [385, 387, 388, 389, 390, 391] and the $k-\omega$ SST model has been used specifically for toilet flushing models [323, 326].

For all of the simulations in this study, the mesh was created to keep the maximum y^+ value at 5.5, with the majority of the y^+ values less than 1. The distributions of the y^+ values for the medium mesh in both scenario 1 (NC) and scenario 2 (2C), along with their frequencies and locations where they occur, are presented in Fig. 5.5.

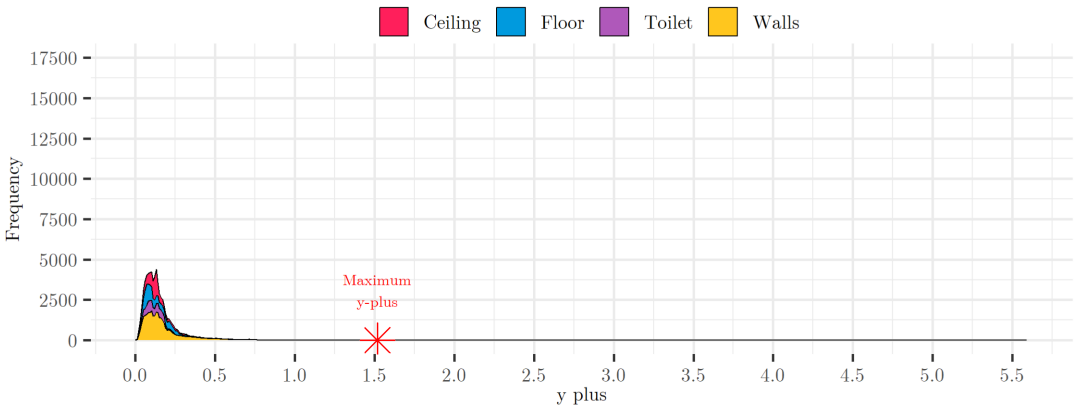

(a) Scenario 1 (NC).

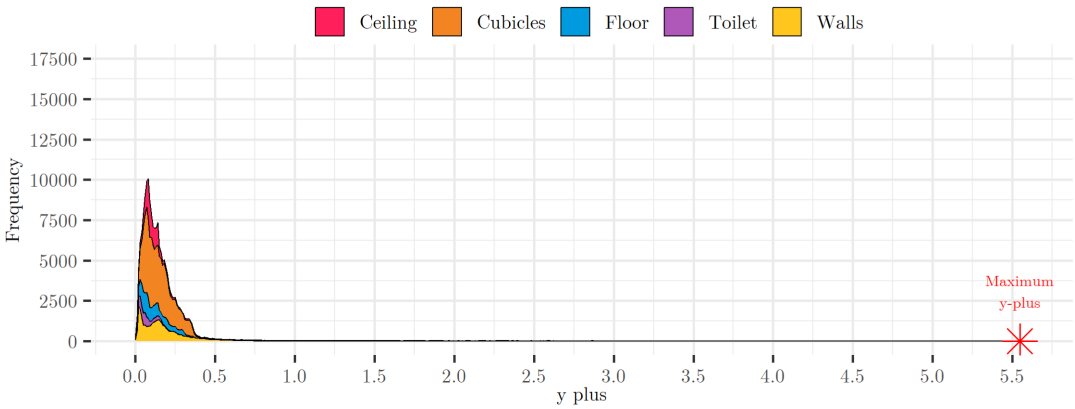

(b) Scenario 2 (2C).

Figure 5.5: The y^+ values and their frequencies for the medium mesh and the using the unscaled velocity profile (6.5 ACH).

5.2.6 Convergence

Each steady-state simulation was run until it converged. The residuals for continuity and the x, y and z velocities were monitored, with all final steady-state solutions showing residuals below 5×10^{-4}. The net mass flow between the ventilation inlet and the ventilation outlet was below $1 \times 10^{-5}\,\mathrm{kg\,s^{-1}}$. This process was performed for both scenarios, with the inlet velocity profile scaled to represent three ventilation rates (1.5, 3, and 6 ACH), resulting in six steady-state initial conditions, one for each ventilation rate in both scenarios.

5.2.7 Mesh Independence

A mesh independence study was conducted using the coarse, medium and fine meshes for scenario 1 (NC) and scenario 2 (2C), as described in Section 5.2.2. The velocity profile from Section 5.2.3 was applied, and the simulation was run with the

solver and turbulence models detailed in Sections 5.2.4 and 5.2.5 until it converged.

The velocity magnitude was monitored along five virtual poles defined within the room, following a setup similar to previous work in the University of Leeds chamber [4]. These velocity profiles were compared to select the most suitable mesh. The poles spanned the height of the room (2.26 m), with their x and y locations detailed in Fig. 5.6. This process was done for both scenarios, with the inlet velocity profile

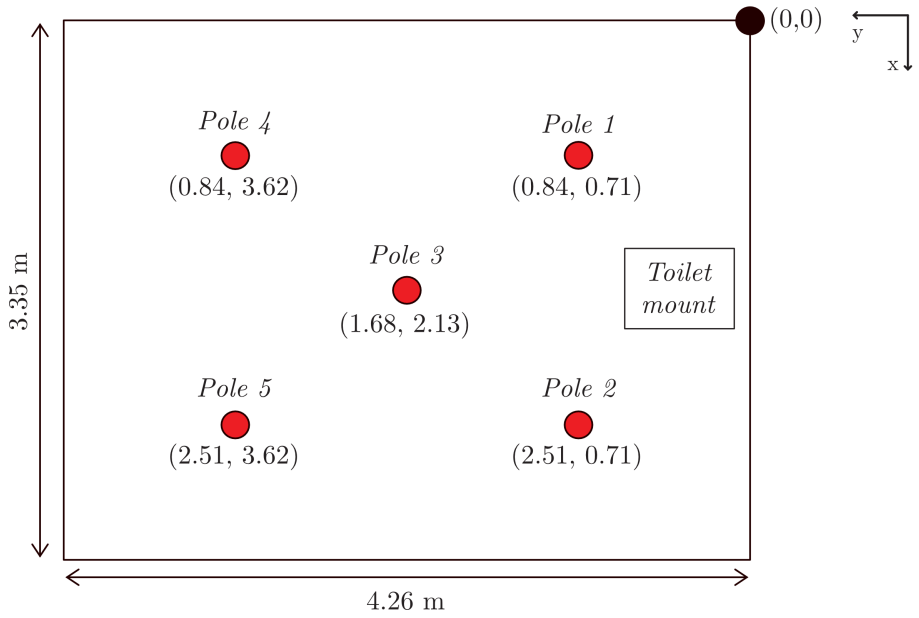

Figure 5.6: The x and y locations for the poles used in the mesh independence study.

scaled to represent three ventilation rates (1.5, 3, and 6 ACH), creating 18 steady-state initial conditions, one for each mesh type, ventilation rate and scenario.

5.2.8 Modelling the Toilet Flush

To model the toilet flush as an injection of particles at the toilet surface, a Euler-Lagrange approach was implemented through the DPM in ANSYS Fluent. This allowed for detailed tracking of particle trajectories and interactions within the chamber environment.

Euler-Lagrange Approach

The Euler-Lagrange approach models a continuous and a dispersed phase. The continuous phase, air in this case, is solved using a Eulerian frame of reference. It is solved using the RANS approach detailed previously in Section 5.2.5. This approach

is common for modelling particle dispersion in indoor environments [4, 61, 253, 308, 309, 314, 316] and has recently been applied to particle dispersion from the toilet plume [166, 322, 323, 324, 326]. The dispersed phase, water in this case, is treated using a Lagrangian frame of reference, where individual particle trajectories can be found by integrating the particle force balance equation [317] (Eqn. (5.1))

$$m_p \frac{d\vec{\mathbf{u}}_p}{dt} = m_p \frac{\vec{\mathbf{u}} - \vec{\mathbf{u}}_p}{\tau_r} + m_p \frac{\vec{\mathbf{g}}(\rho_p - \rho)}{\rho_p} + \vec{\mathbf{F}}, \tag{5.1}$$

where

$\vec{\mathbf{u}}$ – velocity of the continuous phase [$\mathrm{m\,s^{-1}}$],

ρ – density of the continuous phase [$\mathrm{kg\,m^{-3}}$],

m_p – mass of the discrete phase [kg]

$\vec{\mathbf{g}}$ – gravitational force [$\mathrm{m\,s^{-2}}$],

$\vec{\mathbf{u}}_p$ – velocity of the discrete phase [$\mathrm{m\,s^{-1}}$],

ρ_p – density of the discrete phase [$\mathrm{kg\,m^{-3}}$],

$\vec{\mathbf{F}}$ – additional force [$\mathrm{m\,s^{-2}}$] and

τ_r – particle relaxation time [s].

The relaxation time in Eqn. (5.1) is given by

$$\tau_r = \frac{\rho_p {d_p}^2}{18\mu} \frac{24}{C_d \mathrm{Re}} \tag{5.2}$$

such that

$$\mathrm{Re} = \frac{\rho d_p \left|\vec{\mathbf{u}}_p - \vec{\mathbf{u}}\right|}{\mu} \tag{5.3}$$

where

μ – kinematic viscosity of the continuous phase [$\mathrm{m^2\,s^{-1}}$],

d_p – particle diameter [m] and

C_d – drag coefficient.

The three terms on the right-hand side of Eqn. (5.1) represent the forces that act on the particle: drag, gravitational forces, and other external forces. This modelling approach is appropriate when the dispersed phase occupies a low volume fraction of the computational cells, which was the case in this study. Micron-sized particles were modelled within a mesh consisting of centimetre-sized elements.

A one-way coupling approach was adopted. This meant that the dispersed phase did not influence the momentum of the continuous phase. This method was chosen because the micron-sized droplets were unlikely to significantly affect airflow patterns within the room.

In RANS models, such as $k-\omega$ SST, particles follow the mean airflow velocity with fluctuations around the mean caused by turbulence. These fluctuations can be modelled stochastically using the DRW model in ANSYS Fluent. The DRW model better represents the impact of turbulence on particle trajectories and captures the turbulent nature of particle dispersion. Without the DRW model, particle trajectories appear smooth and deterministic, failing to account for the randomness introduced by turbulent airflow.

Discrete Phase Model Parameters

Previous CFD studies have made different assumptions regarding particle release in toilet plume modelling. Liu et al. [326] provided no details on injection velocity but assumed 30,000 droplets of each particle size, injected as a cone with a 120° angle under steady-state airflow conditions on the surface of the toilet bowl. Wan et al. [323] and Li, Wang, and Chen [166] used a pressure profile to simulate the toilet flush, where the disturbances in airflow induced by the pressure change drove particle motion, with particles themselves assigned zero initial velocity. Li, Wang, and Chen [166] developed a two dimensional model combining a VOF model with a DPM model, where water entered the bowl from a tank and mixed with the water seal, generating turbulent motions that induced airflow patterns.

In the current study, an approach most similar to Liu et al. [326] was taken where the toilet flush was modelled as an injection of particles at the surface of the toilet over a 7.5 s period. This duration was selected because previous experimental measurements of the toilet plume showed that the intensity of the flush dropped to zero after 7.5 s [52]. Particles were injected using the face normal, with injections occurring at each cell on the injection surface.

For the particle injection velocity, a transient function was applied. The velocity started at zero, increased linearly to a maximum value at 0.5 s, remained constant

for 5 s, and then decreased linearly back to zero at the end of the 7.5 s period. The air velocity at the injection surface was also assigned a transient profile, with a maximum value of 0.125 m s^{-1}, corresponding to ambient airflow conditions reported in the same study. The study by Crimaldi et al. [52] found that particle velocities ranged from 1 m s^{-1} to 2 m s^{-1}. Initial simulations were conducted with maximum particle velocities of 0.5 m s^{-1}, 1 m s^{-1}, and 2 m s^{-1}. These simulations did not reveal significant differences in the particle trajectories after 10 min. Consequently, a maximum velocity of 1 m s^{-1} was chosen. All velocities were applied normal to the surface injection at each cell on the surface. The transient velocity profiles used for these simulations are shown in Fig. 5.7.

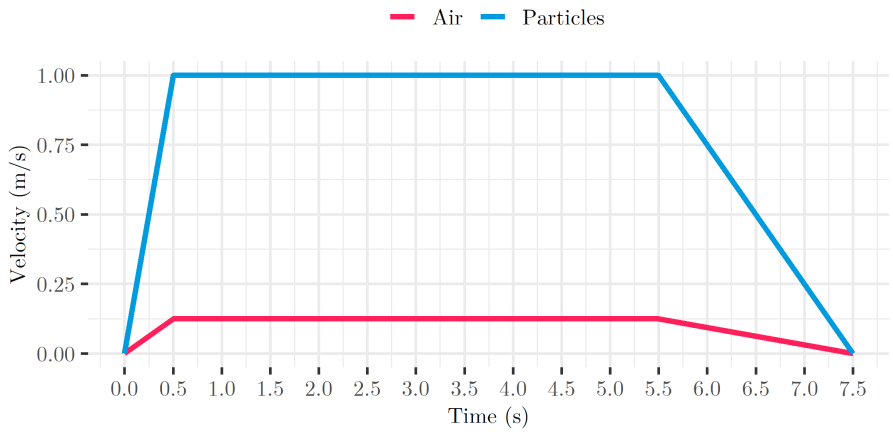

Figure 5.7: Velocity profiles for the transient toilet flush injection.

Using the DPM in ANSYS Fluent, particles with diameters of 0.3, 0.5, 1, 3, 5, and 10 µm were injected at the surface. These sizes correspond to the particle sizes sampled in the experimental work. The density of the particles was set to water, $\rho_p = 998.2\,\mathrm{kg\,m^{-3}}$, while the density of air was set to $\rho = 1.225\,\mathrm{kg\,m^{-3}}$. In reality, droplets may also contain faecal matter and other biological materials. However, water was assumed as the particle phase in this study, as it represents the bulk of the liquid in the toilet and aligns with the the experimental measurements.

All walls and the surface injection were assigned a DPM boundary condition type of “trap”, meaning particles that reached these surfaces were considered deposited and removed from the flow. The chamber ventilation outlet and the human exposure outlet were assigned a DPM boundary condition type of “escape” that allowed the particles that reach these locations to exit the domain.

Particle Sensitivity

ANSYS Fluent allows multiple particles to be represented by a single parcel to improve computational efficiency. Even when each parcel represents exactly one particle, the results may still lack statistical significance if the number of particles injected is insufficient [392].

In this study, the number of particles injected was increased by an order of magnitude from the initial number. The quantities of particles that escaped from the human exposure outlet were then analysed to ensure that a sufficient number of particles were injected to achieve statistically significant results. This method has been used in previous studies to ensure particle count independence [4, 61].

For scenario 1 (NC) at 6 ACH, the initial number of particles injected at the surface of the toilet for each size was on the order of 100. This number was increased consecutively by a factor of 10, leading to simulations with approximately 1,000, 10,000, 100,000, 1,000,000 and 10,000,000 particles for each size. The proportions of particles escaping from the human exposure outlet, the OPC outlet and the ventilation at the end of the full simulation were quantified, and the number of particles depositing on surfaces was also quantified. These results informed the decision on the number of particles to inject for further simulations.

5.3 Full Simulations

After reaching steady-state solutions for each ventilation rate and scenario, transient simulations were initialised using the steady-state results. Unsteady particle tracking was enabled, allowing the dispersed phase to be updated at the start of each time step. The continuous phase was then solved within that same time step, with a specified number of iterations per time step. In this study, the maximum number of iterations per time step was set to 20. According to previous work [61], a 30 s initialisation phase with a 1 s time step was used. For the 7.5 s flushing activity, a time step of 0.1 s was used, and the following 10 min used a 1 s time step. In each phase, the time step was reduced by half with no difference in the results.

During each time step, the number of particles that escaped through the hu-

man exposure outlet and the OPC outlet were monitored as a proportion of those injected. At the end of each full simulation, the total number of particles that escaped (through the chamber ventilation outlet, the human exposure outlet and the OPC outlet), deposited on surfaces, or remained airborne was recorded. The locations of all particles in the simulation were tracked, and they were represented visually using CFD-Post (version 2023, R2) [393].

5.3.1 Rescaling the Injection

For each particle size, a sufficient number of particles were selected in the CFD simulation to ensure sensitivity in the analysis. However, this number did not directly correspond to the actual number of particles emitted at the toilet bowl surface. To establish a relationship between the number of particles injected in the CFD model and the number observed experimentally, the particle concentration recorded by particle counter A for scenario 1 (NC) at a ventilation rate of 1.5 ACH (see Chapter 3) was used. The total number of particles injected in the CFD model for each particle diameter corresponded to the estimated total of the experimental data in Table 3.4, Section 3.5.1. The relative weighting of each particle size in the CFD model was then determined based on this experimental measured concentration and the total particle count for each size from the experiment. This count may underestimate the actual number of particles generated by the flush, as the OPC was unlikely to detect every aerosolised particle. The number of particles injected for each diameter in the CFD simulations, as well as subsequent results such as deposition, were then adjusted accordingly to align with these total estimates. The quantities of particles in Table 3.4 were used to scale the CFD results, allowing the approximation of absolute quantities rather than relative proportions for outcomes such as particle deposition on surfaces or particles escaping through an outlet. This rescaling is particularly important as the total number of particles decreases with increasing particle diameter. For example, even if a large proportion of 10 µm droplets escaped through the human exposure outlet, their overall contribution to exposure may be relatively low due to the smaller initial number of particles released.

5.4 Verification of the Model

5.4.1 Mesh Independence for Bulk Flow

The velocity magnitudes at the five poles for the unscaled velocity profile (6.5 ACH) located in the chamber for scenario 1 (NC) and scenario 2 (2C) can be seen in Fig. 5.8 and 5.9 respectively.

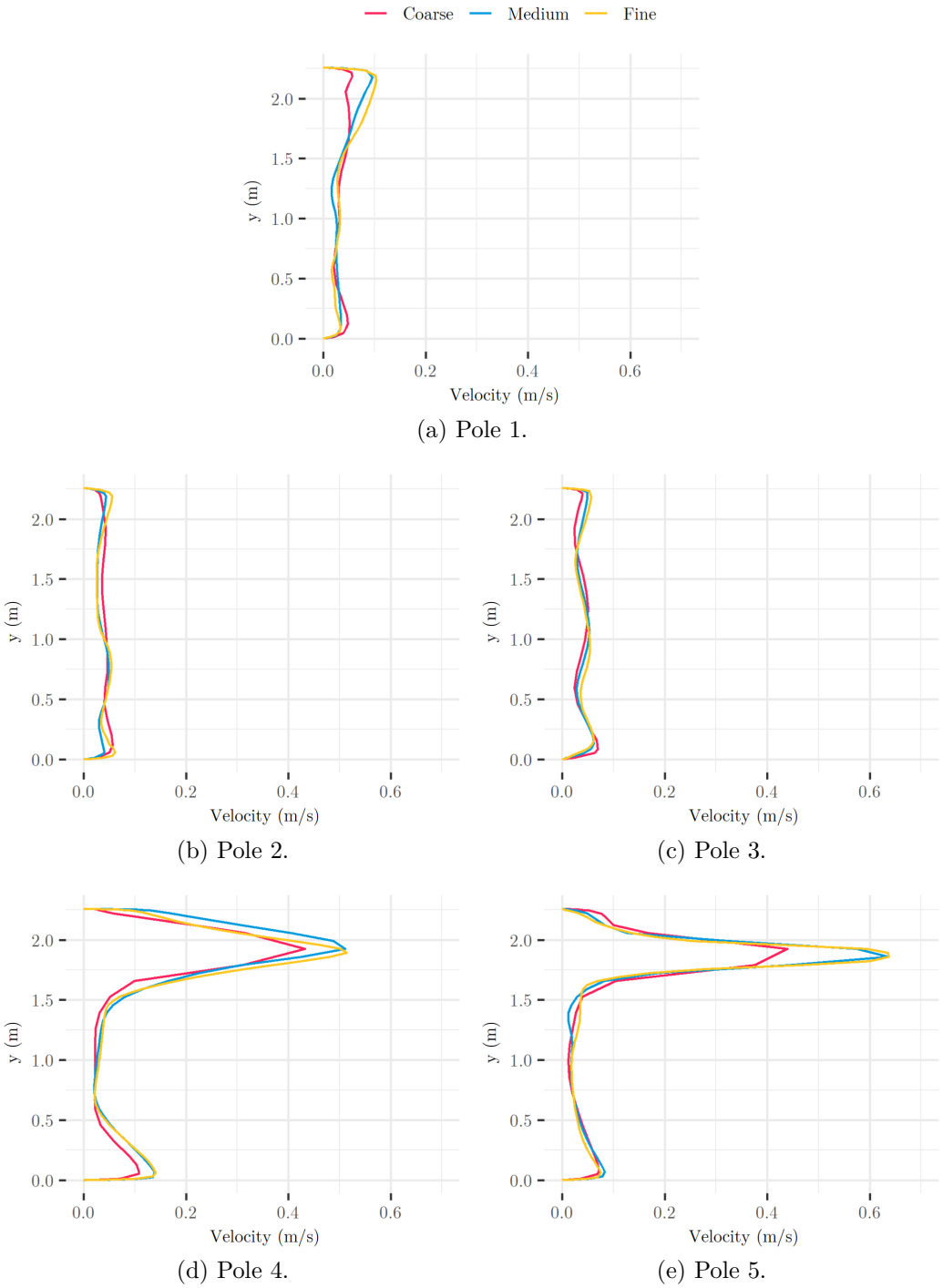

(a) Pole 1.

(b) Pole 2.

(c) Pole 3.

(d) Pole 4.

(e) Pole 5.

Figure 5.8: Velocity magnitude at the various pole locations for the coarse (234,853 elements), medium (483,996 elements) and fine (1,160,220 elements) meshes using the unscaled velocity profile (6.5 ACH in scenario 1 (NC)).

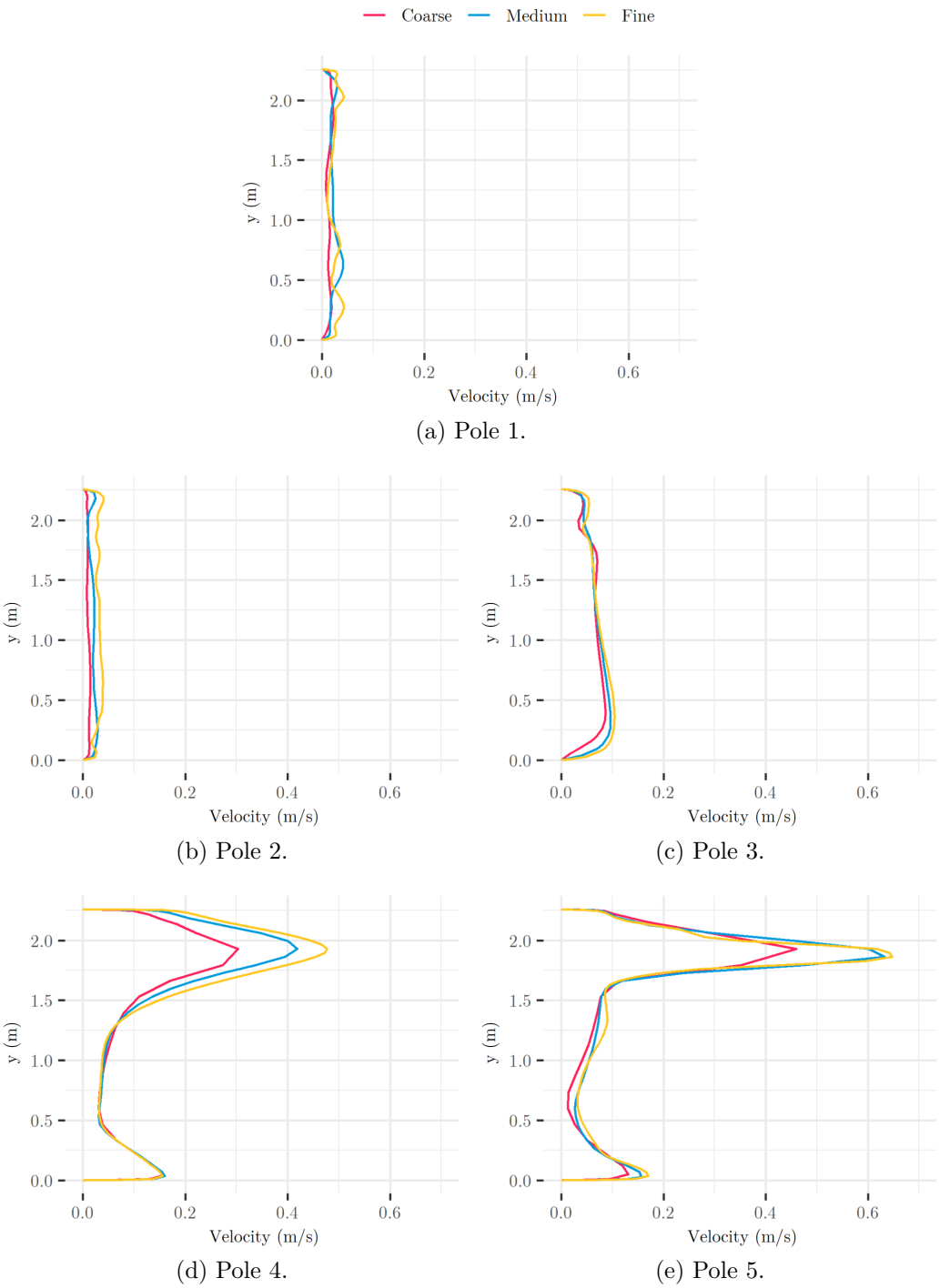

(a) Pole 1.

(b) Pole 2.

(c) Pole 3.

(d) Pole 4.

(e) Pole 5.

Figure 5.9: Velocity magnitude at the various pole locations for the coarse (479,992 elements), medium (862,580 elements) and fine (1,917,054 elements) meshes using the unscaled velocity profile (6.5 ACH) in scenario 2 (2C).

The differences in velocity magnitudes between the medium and fine meshes, as shown in Fig. 5.8 and Fig. 5.9, were generally less than $0.025\,\mathrm{m\,s^{-1}}$. The differences at poles 4 and 5 in scenario 2 (2C) remained below $0.05\,\mathrm{m\,s^{-1}}$, while differences at pole 4 in scenario 1 (NC) were below $0.1\,\mathrm{m\,s^{-1}}$. Although some differences larger than $0.05\,\mathrm{m\,s^{-1}}$ were observed at pole 4 in scenario 1 (NC), Fig. 5.8d shows that

the airflow patterns were consistent between the medium and fine meshes. These differences can be attributed to variations in the centre of the mesh cells. These velocity magnitudes and variations fall within the range of measurement and uncertainty observed in previous anemometer readings taken in the bioaerosol chamber [4]. Based on these findings, the medium mesh was selected for further simulations.

5.4.2 Particle Sensitivity

The results of the particle sensitivity study are presented in Fig. 5.10. Fig. 5.10b shows the proportion of injected droplets that deposit on surfaces during the simulation (scenario 1 at 6 ACH) as the number of injected particles increases, while Fig. 5.10c shows the proportion that are removed through the ventilation outlet of the aerobiology chamber. Fig. 5.10a shows the proportion that escape through the human exposure outlet and the OPC outlet. The injection speed corresponds to the maximum velocity used in the transient velocity profile shown in Fig. 5.7.

The particle injection velocity, as shown in Fig. 5.10, had minimal impact on particle sensitivity. Based on these results, an injection velocity of $1\,\mathrm{m\,s^{-1}}$ was selected for the remaining simulations. Fig. 5.10b shows that increasing the number of particle injections beyond 10,000 did not significantly improve the accuracy of deposition results. This was similar for the ventilation outlet seen in Fig. 5.10c, with an increase beyond 10,000 seeing no significant improvement in the results. For the larger particles of 3, 5 and 10 µm, Fig. 5.10a indicated that injecting 1,000,000 particles was needed to achieve reliable results.

5.4.3 Adapted Scenario 2 (2C*)

To examine the effect of the location of the ventilation outlet on particle dispersion, two new pressure ventilation outlets were introduced in the model to replace the previous ventilation outlet. These outlets were positioned on the ceiling, centred within each cubicle, and had half the area of the original aerobiology chamber ventilation outlet. Consequently, each new ventilation outlet had half the mass flow rate of the original ventilation outlet. This configuration maintained the total ventilation rate of the chamber while altering the airflow distribution within the room. The

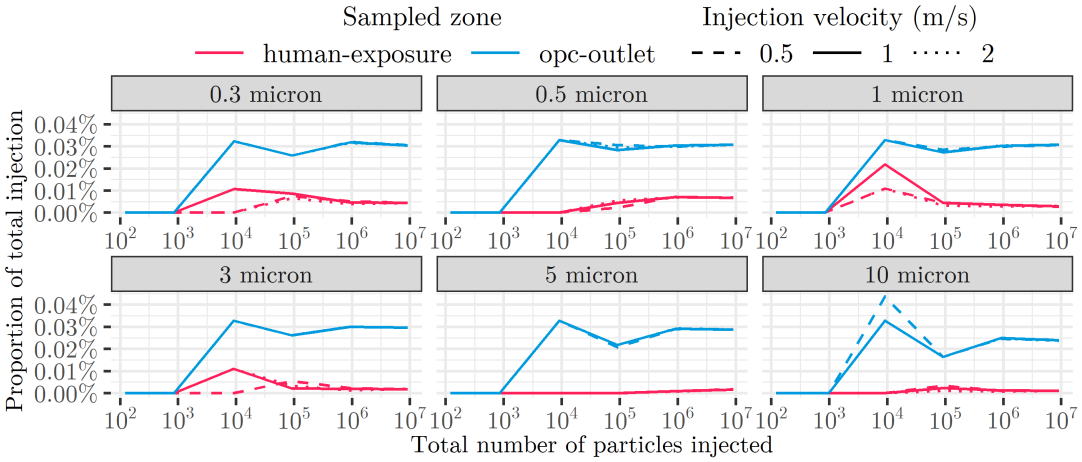

(a) Escaped particles through the human exposure outlet and OPC outlet.

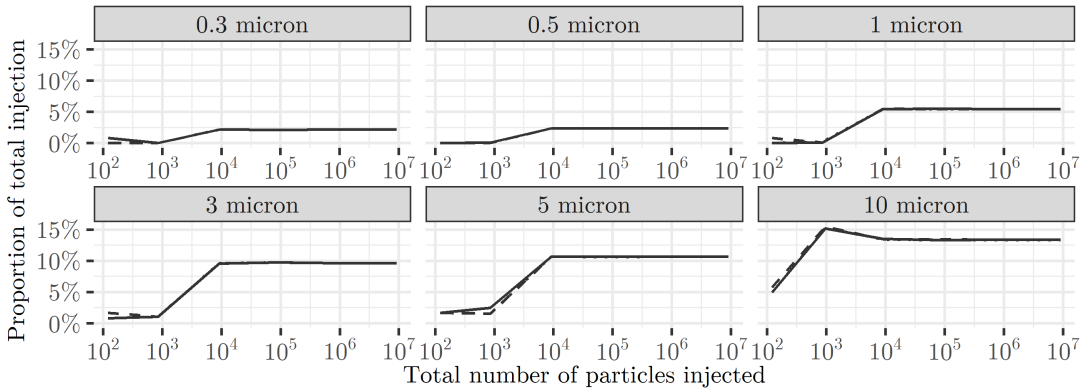

(b) Deposited particles.

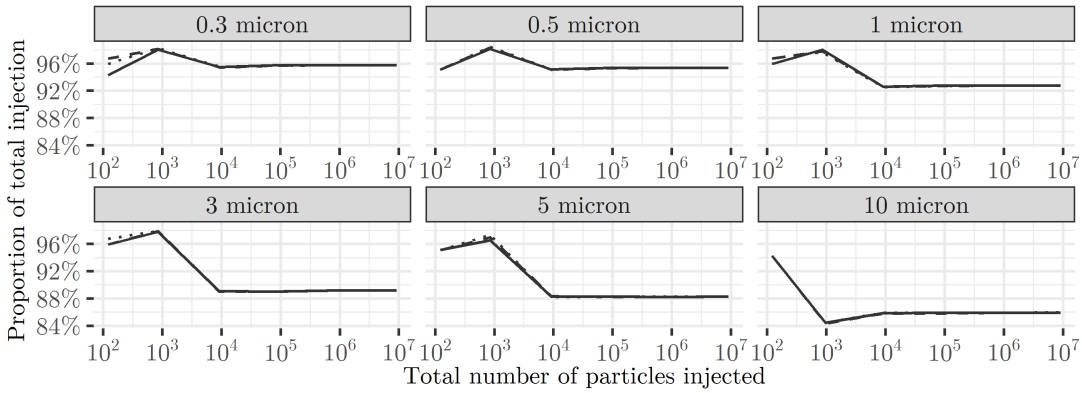

(c) Escaped particles through the chamber ventilation outlet.

Figure 5.10: Particle sensitivity study for scenario 1 (NC) at 6 ACH, detailing the proportion of particles sampled at relevant zones at the end of the 10 min simulation period for three injection velocities.

abbreviation for this adapted scenario is 2C*.

The mesh sizing parameters of Tables 5.1 and 5.2 were applied to this adapted scenario, with the primary modification being the removal of the original ventilation outlet and the introduction of two new ventilation outlets, O1 and O2. This arrangement is illustrated in Fig. 5.11.

Using the methods described in Section 5.2.8, the toilet flush was simulated as

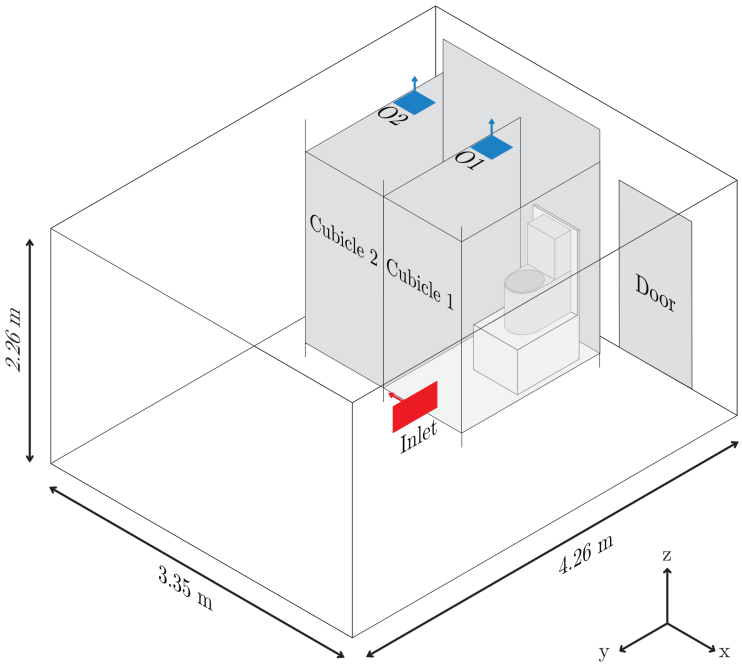

Figure 5.11: The geometry of the chamber used in the CFD simulations for adapted scenario 2 (2C*).

an injection of inert water particles, which were then rescaled to obtain absolute results. The proportion of particles within each zone was extracted over a 10 min period, and their locations at six different time steps were monitored and visualised.

5.5 Results and Discussion

5.5.1 Modelling the Experimental Scenarios

Optical Particle Counter Experimental Comparison

A time series of the particle concentration sampled at the OPC outlet in the CFD, along with the mean experimental data for scenario 1 (NC) and scenario 2 (2C), is shown in Fig. 5.12. The CFD results are approximately one to two orders of magnitude lower than the experimental measurements. However, the overall decay pattern is consistent across all ventilation rates. To further examine this trend, an exponential decay curve was fitted to the experimental data, following the approach described in Chapter 4. The fitting was performed separately for each particle size using the mean experimental concentrations. This approach allows for a direct comparison of the decay rate observed in the experiments with the decay trend predicted by the CFD model. A normalised time series of the CFD and experimental

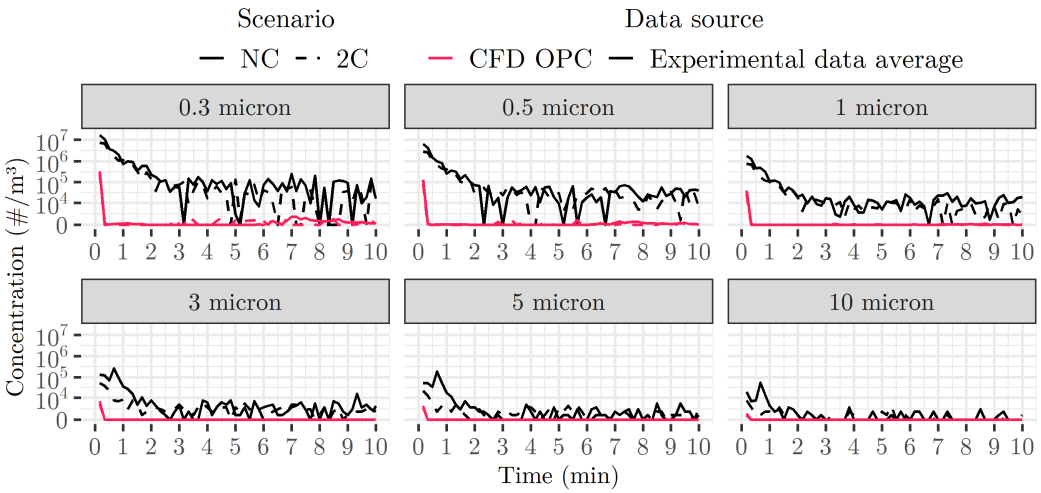

(a) 1.5 ACH.

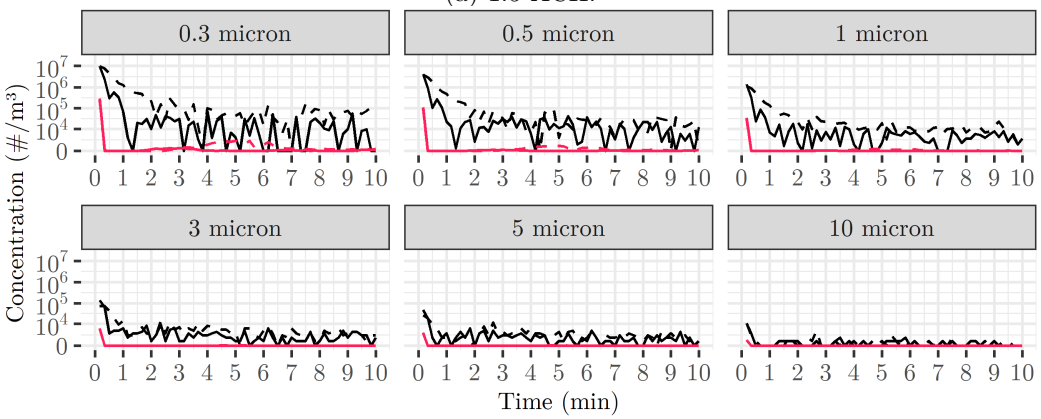

(b) 3 ACH.

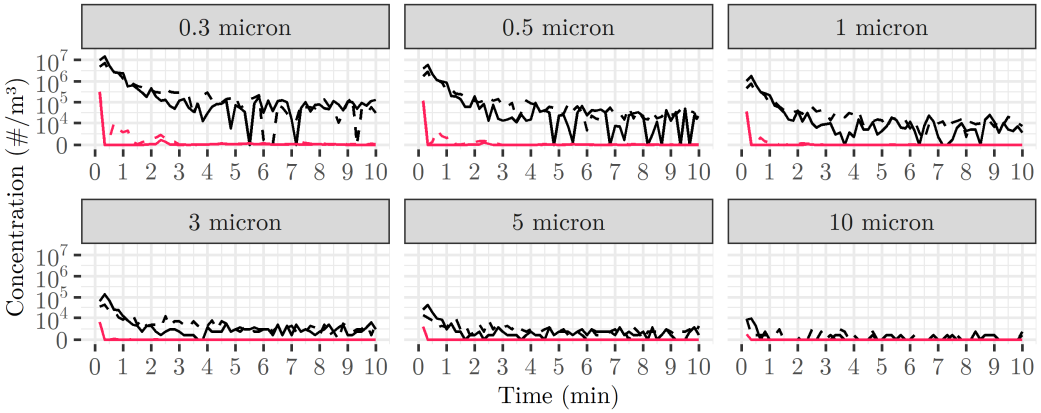

(c) 6 ACH.

Figure 5.12: Comparison of the time series of particle concentrations at the OPC outlet from CFD simulations and experimental data at different ventilation rates for scenario 1 (NC) and scenario 2 (2C).

results for each ventilation rate and scenario is shown in Fig. 5.13. The values are normalised by the maximum concentration, enabling a clearer comparison of the relative decay trends between the two data sets.

The normalised results show a distinct initial increase in concentration in the first 10 s, followed by a gradual decline. This increase is due to the transient nature of

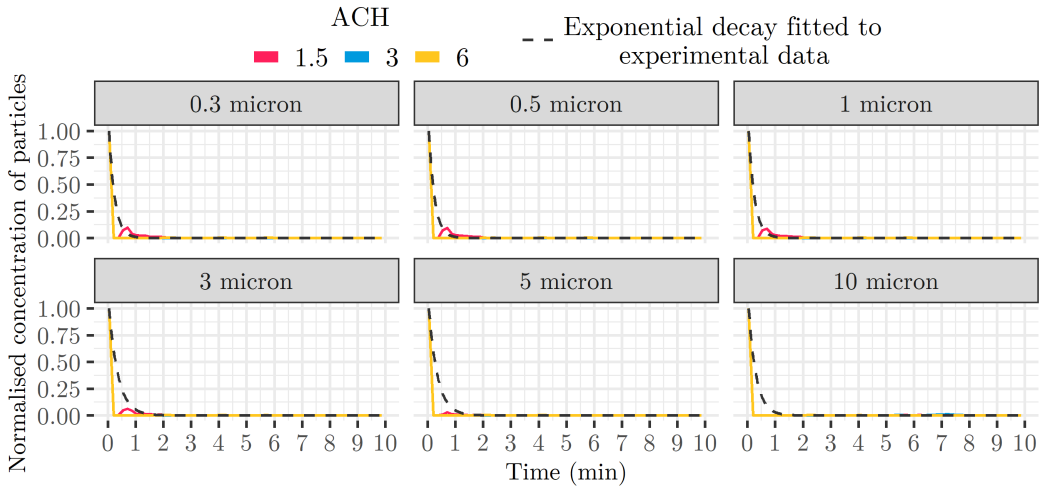

(a) Scenario 1 (NC).

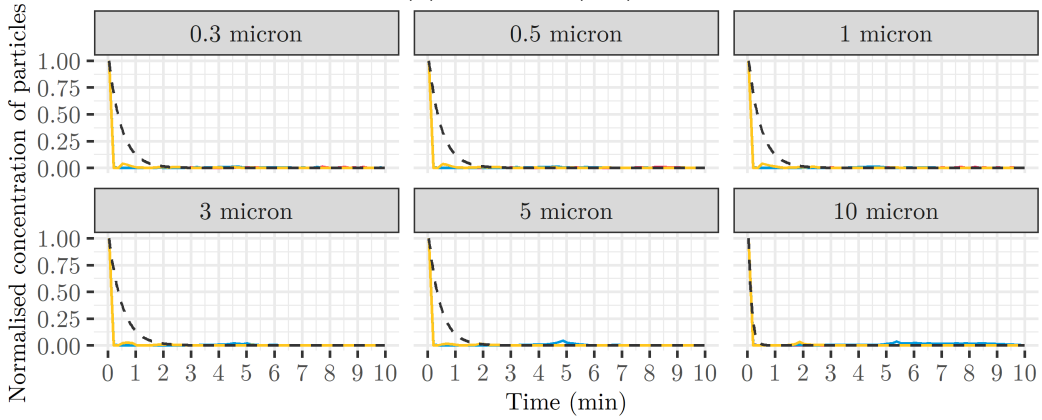

(b) Scenario 2 (2C).

Figure 5.13: Normalised time series of particle concentrations from CFD simulations and experimental data for each scenario. Experimental results are fitted with an exponential decay curve.

particle dispersion at the onset of sampling, as particles generated by the toilet flush are transported towards the OPC outlet. After this brief peak, the concentration decreases, which aligns with observations from the experimental data.

There is qualitative agreement between the CFD model and the experimental data in that both show a rapid decrease in particle concentration within the first 2 min. However, the CFD simulations predict a faster decline compared to the experimental data. This discrepancy may arise due to differences in the way ventilation is modelled in the CFD versus the experimental airflows, potential underrepresentation of particle aerosolisation from the toilet plume in the CFD model, or uncertainties in the exact positioning and sampling efficiency of the OPC in the experimental setup. Despite these differences, the CFD model qualitatively captures the overall trend of particle removal, supporting its utility in assessing exposure risks.

One approach to reducing this discrepancy would be to rescale the CFD injection to better match the OPC measurements. However, this would require injecting an unrealistically high number of particles at the toilet surface, which is not consistent with the number of particles released from a toilet flush in prior studies [2]. Additionally, there is considerable uncertainty in the measurement at the OPC outlet, and refinements to the emission method, such as an improved velocity profile, may be necessary to improve agreement between the CFD and experimental results.

Another potential source of discrepancy is the representation of the OPC outlet in the CFD model. The current mass flow outlet is modelled as a small two-dimensional square, which may not fully capture the particle sampling dynamics of the OPC. More accurately replicating the dimensions and flow characteristics of the OPC in the CFD setup could improve the estimated particle concentrations.

Airflow Patterns

Cross-sections of the velocity magnitude contours were plotted in both the $y-z$ and $x-z$ planes. These velocity contours are plotted from the steady-state airflow simulation, prior to the toilet being flushed. The velocity magnitude was clipped to $0.05\,\mathrm{m\,s^{-1}}$ to improve visualisation of the differences in the region around the toilet. The maximum velocity magnitude was consistently observed near the ventilation inlet. In scenario 1 (NC) with a ventilation rate of 6 ACH, the maximum velocity magnitude in the $y-z$ plane reached $0.6\,\mathrm{m\,s^{-1}}$.

In scenario 1 (NC), shown in Fig. 5.14, the highest velocity regions are concentrated near the ventilation inlet and the ventilation outlet. This is expected as the ventilation system drives airflow into the chamber through the inlet and removes it through the ventilation outlet. As the ventilation rate increases, the high-velocity zones expand, particularly around these regions. The lowest velocity regions are located around the toilet itself, where airflow disturbances are minimal. This suggests that for lower ventilation rates, particles released from the flush can experience reduced advection, leading to particles that become airborne for prolonged periods before settling or being removed by ventilation.

Introducing two cubicles in scenario 2 (2C), shown in Fig. 5.15, significantly

alters airflow patterns. The addition of cubicle walls creates more localised high-velocity regions, particularly within the cubicles themselves. This occurs because the partitions restrict airflow, forcing it through narrower pathways. For the same ventilation rate, the reduced cross-sectional area available for airflow leads to an increase in velocity, consistent with the Bernoulli principle. This effect results in higher airflow speeds within and around cubicles, particularly near the ventilation outlet, where the air is drawn out of the chamber.

The second cubicle (closest to the ventilation outlet) experiences higher velocities than the first cubicle where the experimental data were collected. This is due to the airflow being drawn toward the ventilation outlet, resulting in stronger air movement in this region as the distance between the ventilation outlet and the cubicle is less compared to the distance between the ventilation outlet and the first cubicle.

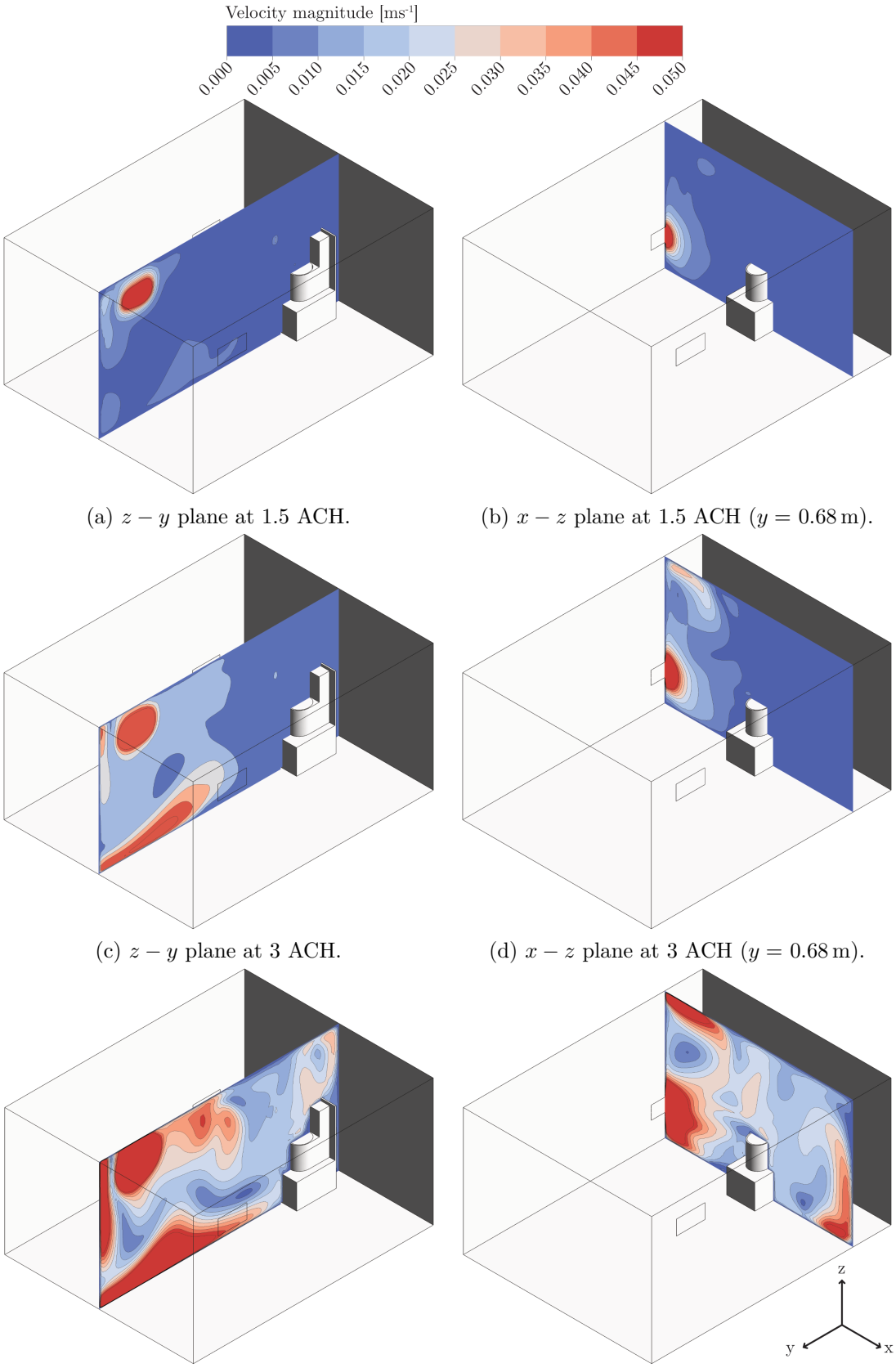

(a) $z-y$ plane at 1.5 ACH.

(b) $x-z$ plane at 1.5 ACH ($y = 0.68\,\mathrm{m}$).

(c) $z-y$ plane at 3 ACH.

(d) $x-z$ plane at 3 ACH ($y = 0.68\,\mathrm{m}$).

(e) $z-y$ plane at 6 ACH.

(f) $x-z$ plane at 6 ACH ($y = 0.68\,\mathrm{m}$).

Figure 5.14: Steady-state velocity magnitude contours for scenario 1 (NC). The range is clipped to $0.05\,\mathrm{m\,s^{-1}}$.

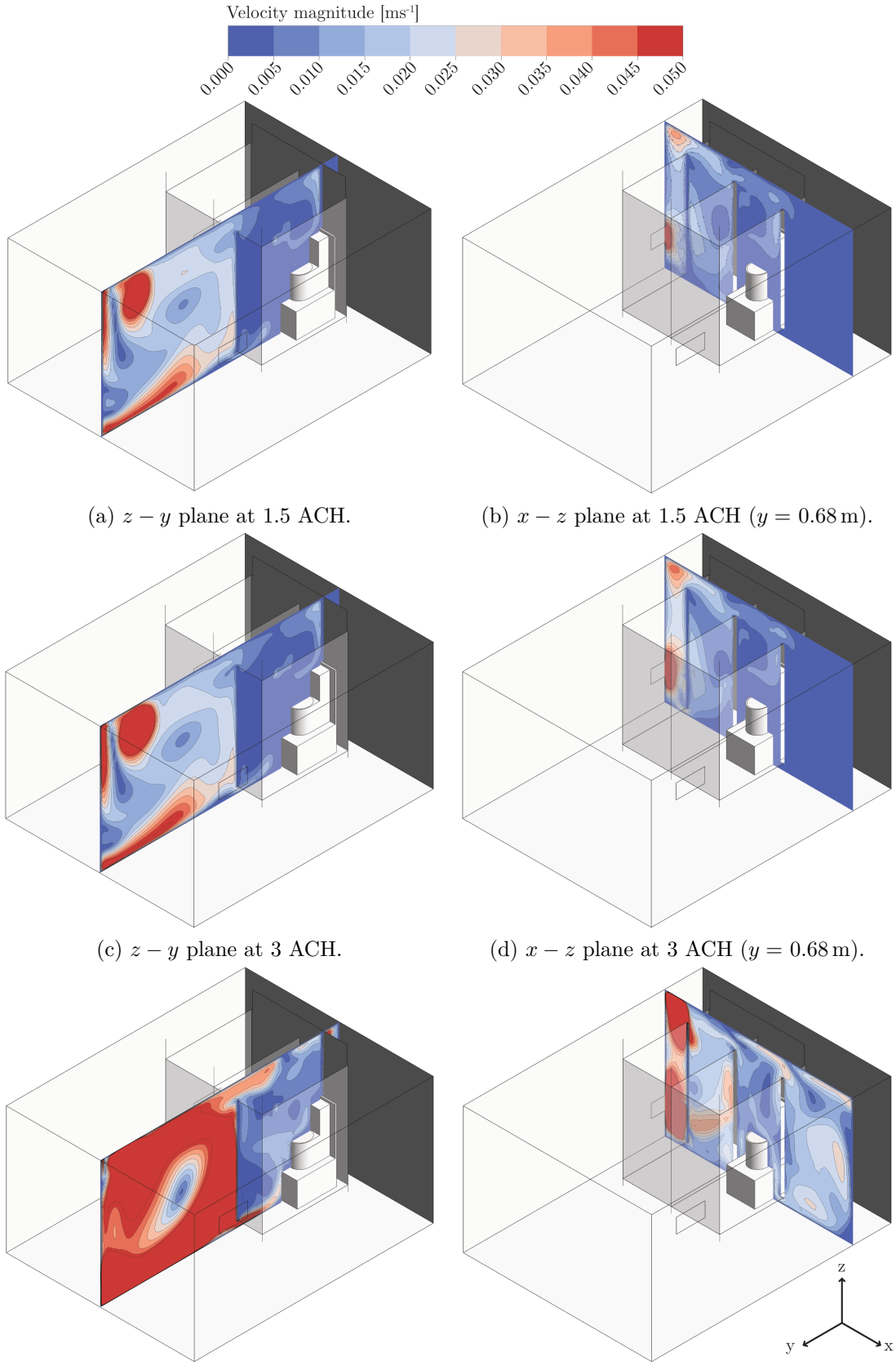

(a) $z - y$ plane at 1.5 ACH.

(b) $x - z$ plane at 1.5 ACH ($y = 0.68\,\mathrm{m}$).

(c) $z - y$ plane at 3 ACH.

(d) $x - z$ plane at 3 ACH ($y = 0.68\,\mathrm{m}$).

(e) $z - y$ plane at 6 ACH.

(f) $x - z$ plane at 6 ACH ($y = 0.68\,\mathrm{m}$).

Figure 5.15: Steady-state velocity magnitude contours for scenario 2 (2C). The range is clipped to $0.05\,\mathrm{m\,s^{-1}}$.

Table 5.5: The average and maximum velocity in the aerobiology chamber for the CFD simulations for the three ventilation rates and two scenarios prior to the toilet being flushed.

Scenario	**Ventilation rate (ACH)**	**Average velocity** ($\mathrm{m\,s^{-1}}$)	**Maximum velocity** ($\mathrm{m\,s^{-1}}$)
Scenario 1 (NC)	1.5	0.015	0.173
	3	0.022	0.346
	6	0.049	0.691
Scenario 2 (2C)	1.5	0.008	0.595
	3	0.020	0.644
	6	0.051	0.689

Table 5.5 summarises the average velocity in the chamber for both scenarios at different ventilation rates. As expected, there is a trend in which an increase in the ventilation rate results in an increase in the average velocity. At 1.5 ACH, airflow velocities remain low, with an average velocity ranging from $0.008\,\mathrm{m\,s^{-1}}$ to $0.015\,\mathrm{m\,s^{-1}}$. At 3 ACH, the average velocity almost doubles, reaching $0.020\,\mathrm{m\,s^{-1}}$ to $0.022\,\mathrm{m\,s^{-1}}$ in scenario 2 (2C) and scenario 1 (NC), respectively, indicating a stronger airflow circulation. At 6 ACH, velocities further increase, with a maximum average velocity of $0.051\,\mathrm{m\,s^{-1}}$ in scenario 2 (2C).

Velocity contours reveal localised high-velocity regions, suggesting increased airflow variability within the chamber. Maximum velocities increase with higher ventilation rates. In scenario 1 (NC), these peak velocities occur at the ventilation inlet. In scenario 2 (2C), the highest velocities are found within the second cubicle at 1.5 ACH and 3 ACH, while at 6 ACH, the maximum velocity is in the region of the ventilation inlet.

Figs. 5.16, 5.17, 5.18 show the velocity vectors for the 1.5, 3 and 6 ACH ventilation rates, respectively, in the $x - z$ plane for both scenarios. Again, these vectors are taken before the toilet is flushed. It can be clearly seen that for scenario 1 (Figs. 5.16a, 5.17a, and 5.18a), the airflow direction moves air from the toilet to the ventilation outlet. This effect is strongest at 6 ACH, where airflow is more direct and less recirculated. At 1.5 ACH, although the flow is still directed toward the outlet, some air is initially drawn upward before circulating downward. For scenario 2 (Figs. 5.16b, 5.17b, and 5.18b), the airflow at 6 ACH is primarily directed upward

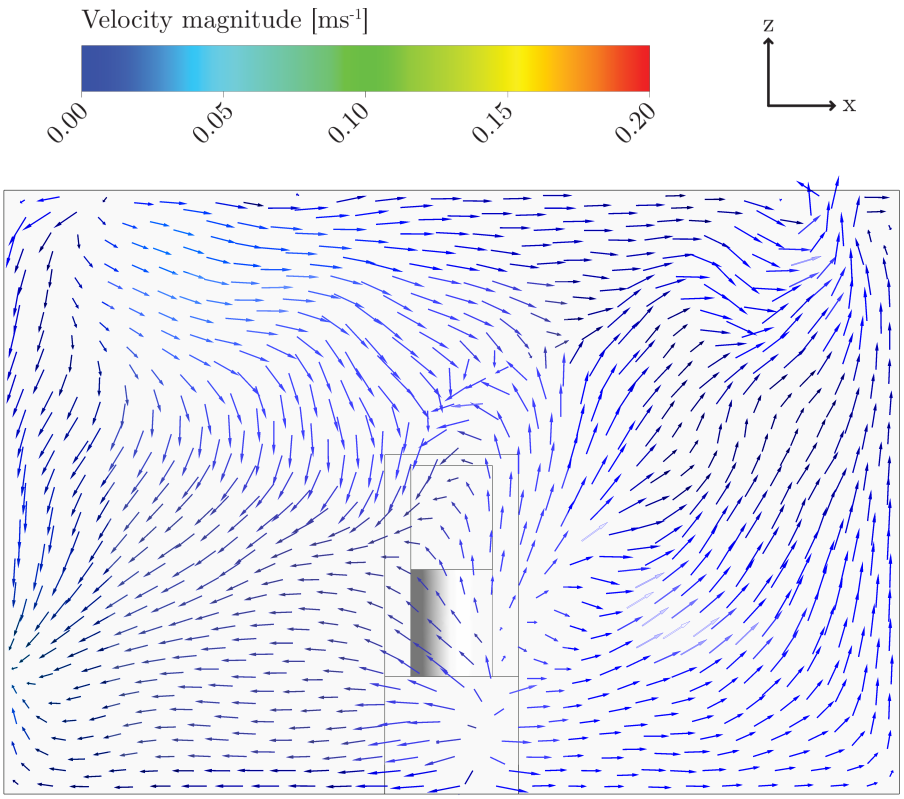

(a) Scenario 1 (NC).

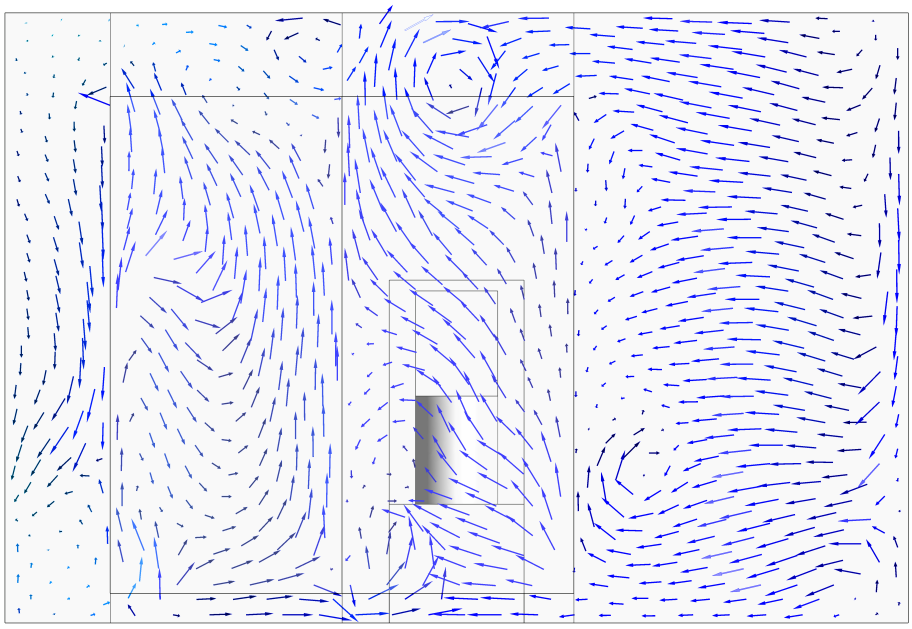

(b) Scenario 2 (2C).

Figure 5.16: Velocity magnitude vectors in the $x - z$ plane ($y = 1.04\,\mathrm{m}$) half-way through the cubicle for 1.5 ACH.

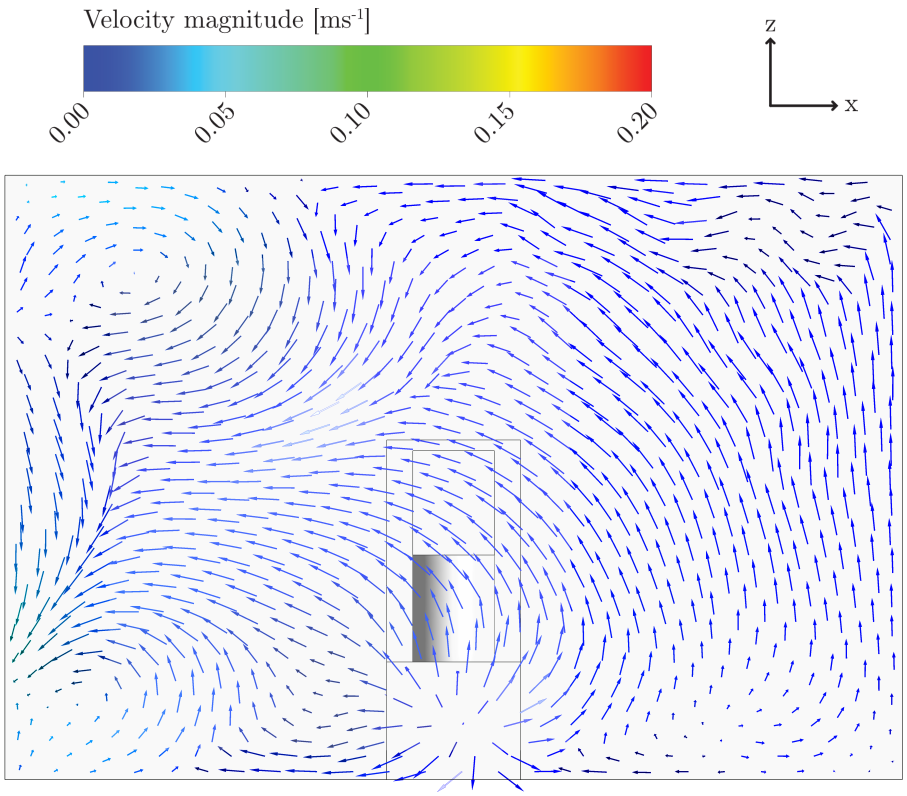

(a) Scenario 1 (NC).

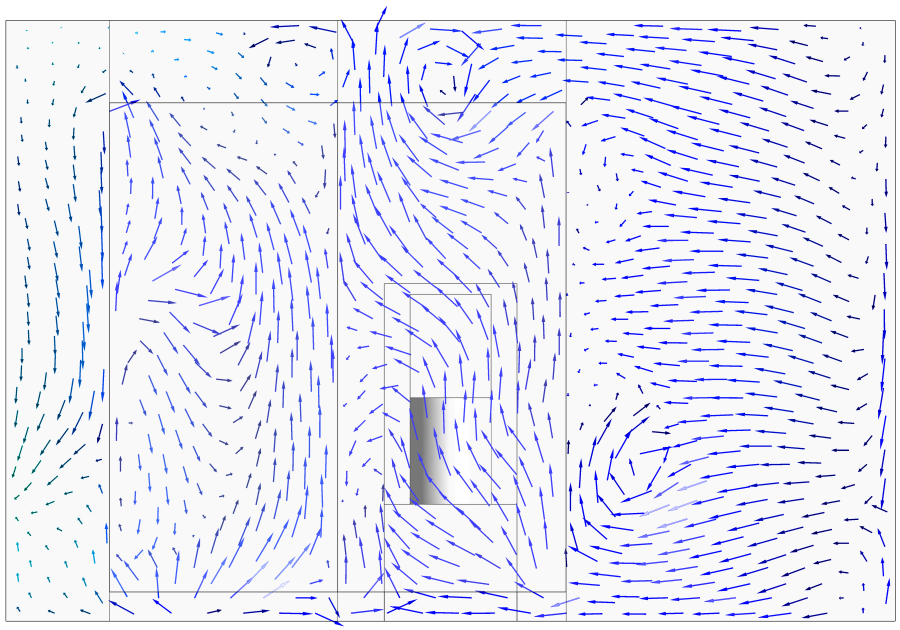

(b) Scenario 2 (2C).

Figure 5.17: Velocity magnitude vectors in the $x - z$ plane ($y = 1.04\,\mathrm{m}$) half-way through the cubicle for 3 ACH.

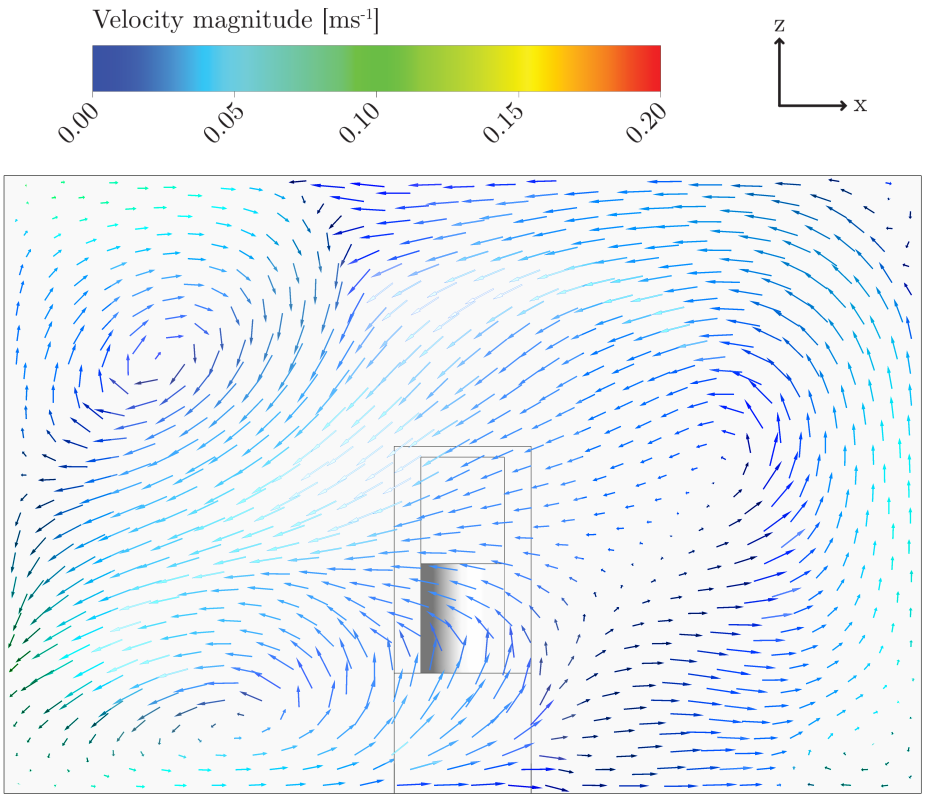

(a) Scenario 1 (NC).

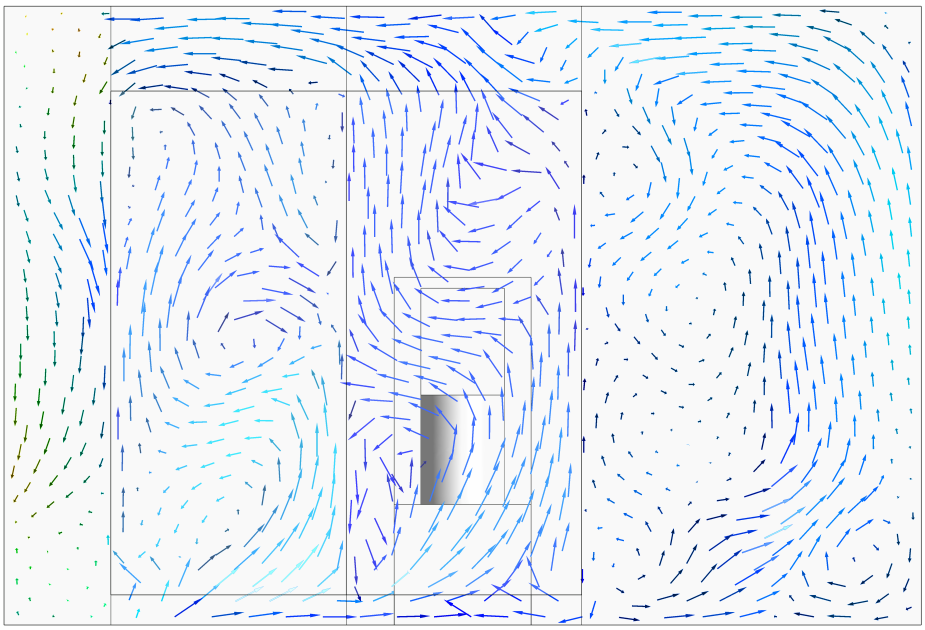

(b) Scenario 2 (2C).

Figure 5.18: Velocity magnitude vectors in the $x - z$ plane ($y = 1.04\,\mathrm{m}$) half-way through the cubicle for 6 ACH.

and over the top of both cubicles. At 1.5 ACH and 3 ACH, a portion of the airflow is recirculated back into the first cubicle. Across all ventilation rates, air is pulled from underneath the cubicle and from above and to the right of the enclosure. The presence of cubicles in scenario 2 (2C) obstructs airflow, requiring it to travel a greater distance before reaching the outlet. This increased path length suggests that airborne contaminants carried by airflow may have a higher likelihood of interacting with surfaces, leading to greater deposition compared to scenario 1 (NC). However, further analysis is required to quantify these effects.

These results highlight that, while increasing ventilation generally enhances air circulation, its effect on aerosol transport is strongly influenced by the layout of the space and the presence of obstructions such as cubicles.

Particle Dispersion

The spatial distribution of particles at six time intervals following a flush (immediately after flushing, at 30 s, 1 min, 3 min, 5 min, and 10 min) is illustrated in Figs. 5.19 - 5.21 for scenario 1. Each particle diameter is represented by a distinct colour, but all particles are displayed at the same visual size. Scaling their actual sizes was not feasible, as the smallest particles would be too difficult to visualise. To improve clarity and allow qualitative comparisons across different ventilation regimes and scenarios, approximately half of the total particles released during the flush, as detailed in Table 3.4, are displayed. The initial injection consisted of 35,606 particles (the sum of column 2 in Table 3.4), but for visualisation purposes, only 15,252 particles are shown in Figs. 5.19 - 5.21. As ventilation removes or particles deposit over time, their displayed quantity is adjusted accordingly.

For scenario 1, at all ventilation rates, the visualised particle distribution is dominated by particle sizes 0.3 µm and 0.5 µm particles. The toilet plume initially rises before being dispersed by the airflow in the room. A comparison of particle dispersion in the aerobiology chamber at 1.5 and 6 ACH reveals distinct differences. At 6 ACH, the higher ventilation rate leads to increased velocities, which disperse particles more widely throughout the room. In contrast, at 1.5 ACH, particles are less dispersed and are drawn more directly toward the ventilation outlet. This

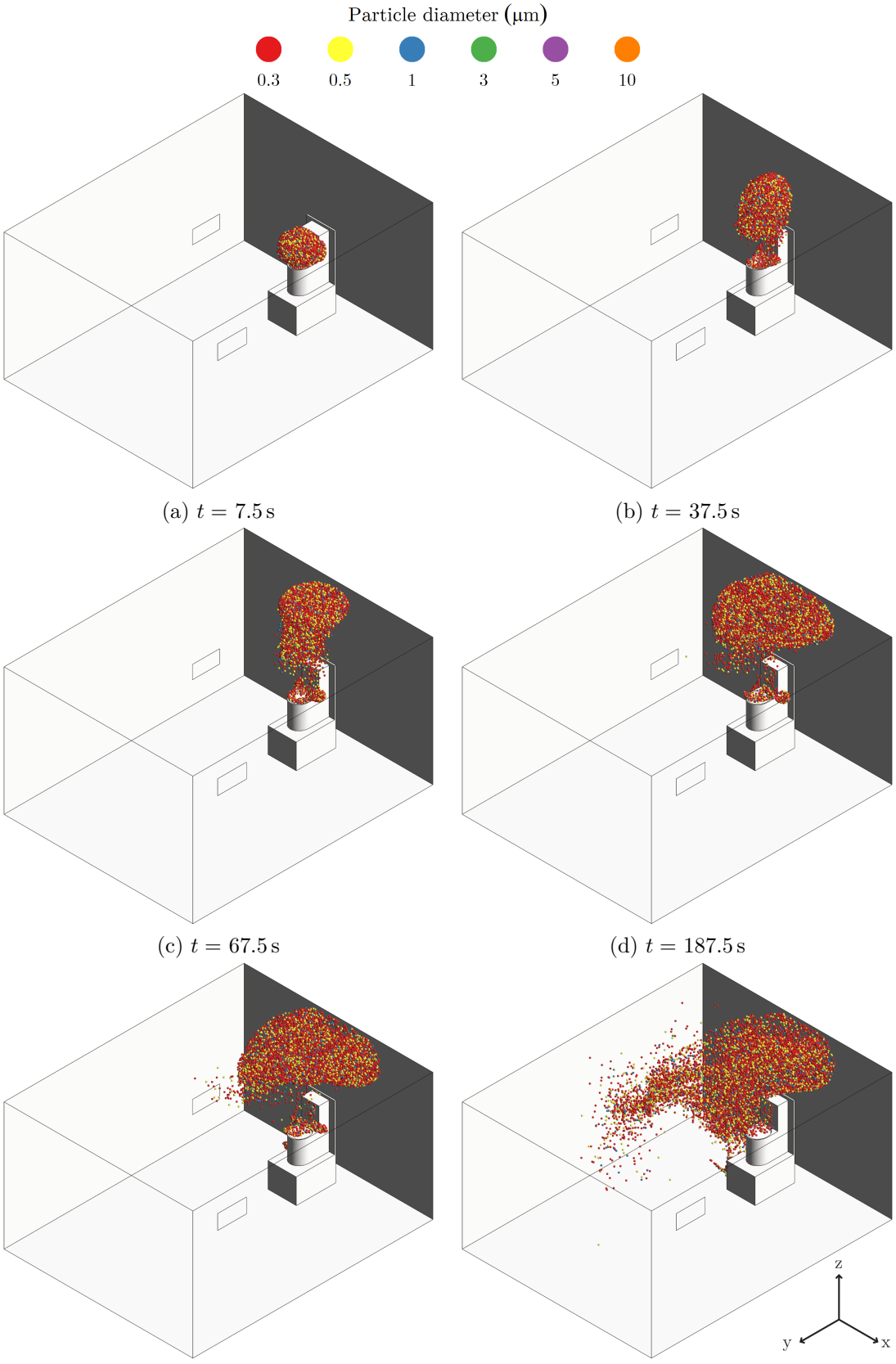

(a) $t = 7.5\,\mathrm{s}$ (b) $t = 37.5\,\mathrm{s}$

(c) $t = 67.5\,\mathrm{s}$ (d) $t = 187.5\,\mathrm{s}$

(e) $t = 307.5\,\mathrm{s}$ (f) $t = 607.5\,\mathrm{s}$

Figure 5.19: Particle locations for scenario 1 (NC) at 1.5 ACH.

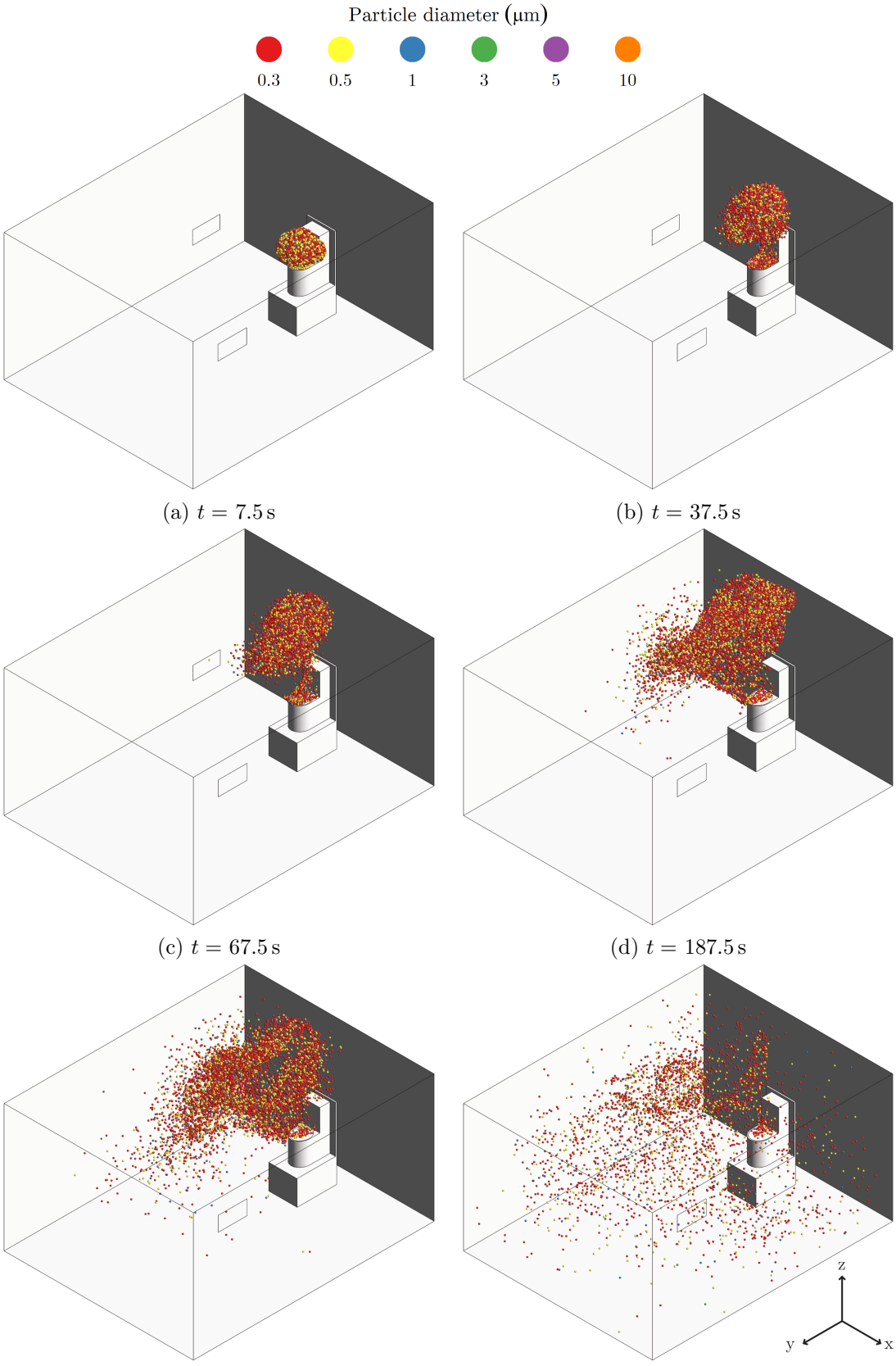

(a) $t = 7.5\,\mathrm{s}$ (b) $t = 37.5\,\mathrm{s}$

(c) $t = 67.5\,\mathrm{s}$ (d) $t = 187.5\,\mathrm{s}$

(e) $t = 307.5\,\mathrm{s}$ (f) $t = 607.5\,\mathrm{s}$

Figure 5.20: Particle locations for scenario 1 (NC) at 3 ACH.

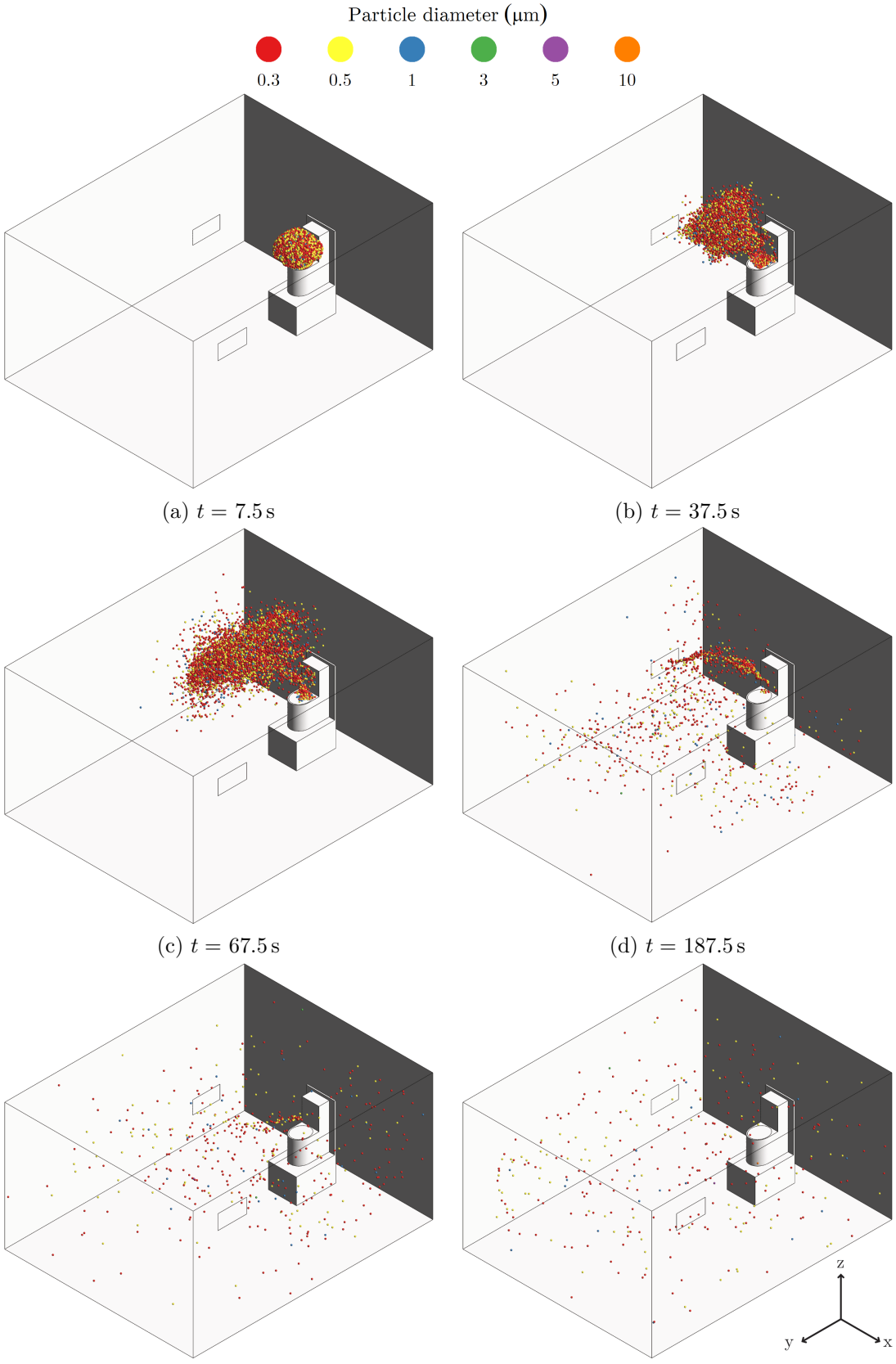

(a) $t = 7.5\,\mathrm{s}$ (b) $t = 37.5\,\mathrm{s}$

(c) $t = 67.5\,\mathrm{s}$ (d) $t = 187.5\,\mathrm{s}$

(e) $t = 307.5\,\mathrm{s}$ (f) $t = 607.5\,\mathrm{s}$

Figure 5.21: Particle locations for scenario 1 (NC) at 6 ACH.

indicates that at lower ventilation rates, particles tend to remain concentrated in a specific region, rather than being distributed.

This has implications for the risk of exposure. In a lower ventilation environment (1.5 ACH), particles are more likely to remain near the toilet. However, in higher ventilation scenarios (3 or 6 ACH), particles become more evenly distributed throughout the room, but at a lower concentration. As a result, a person who enters the toilet facility to use the toilet and thus spends time in the region of the toilet would have a higher infection risk in the lower ventilation rate scenario. However, a person entering the toilet facility for activities that are unrelated to toilet use, such as washing their hands or looking in the mirror, could experience a greater exposure risk in higher ventilation regimes (6 ACH) than in lower ones (1.5 ACH), depending on where the particles have been transported and the time since they were released.

The spatial distribution of particles at the same six time intervals following a flush in scenario 2 (2C) are shown in Figs. 5.22 - 5.24. For scenario 2 (2C), a similar pattern to scenario 1 (NC) is observed such that at higher ventilation rates, particles are more widely dispersed throughout the room.

A comparison of particle dispersion at a specific time step in both scenarios, for example, 3 min after flushing at 6 ACH (Fig. 5.21d vs. Fig. 5.24d), reveals a key difference. When cubicles are introduced in the chamber, the particles tend to remain more concentrated in the toilet region (inside the cubicle), rather than dispersing throughout the room. The presence of cubicles creates a localised airflow restriction, leading to reduced particle transport across the chamber. As a result, a larger amount of particles remain in the cubicle for a longer period compared to scenario 1 (NC).

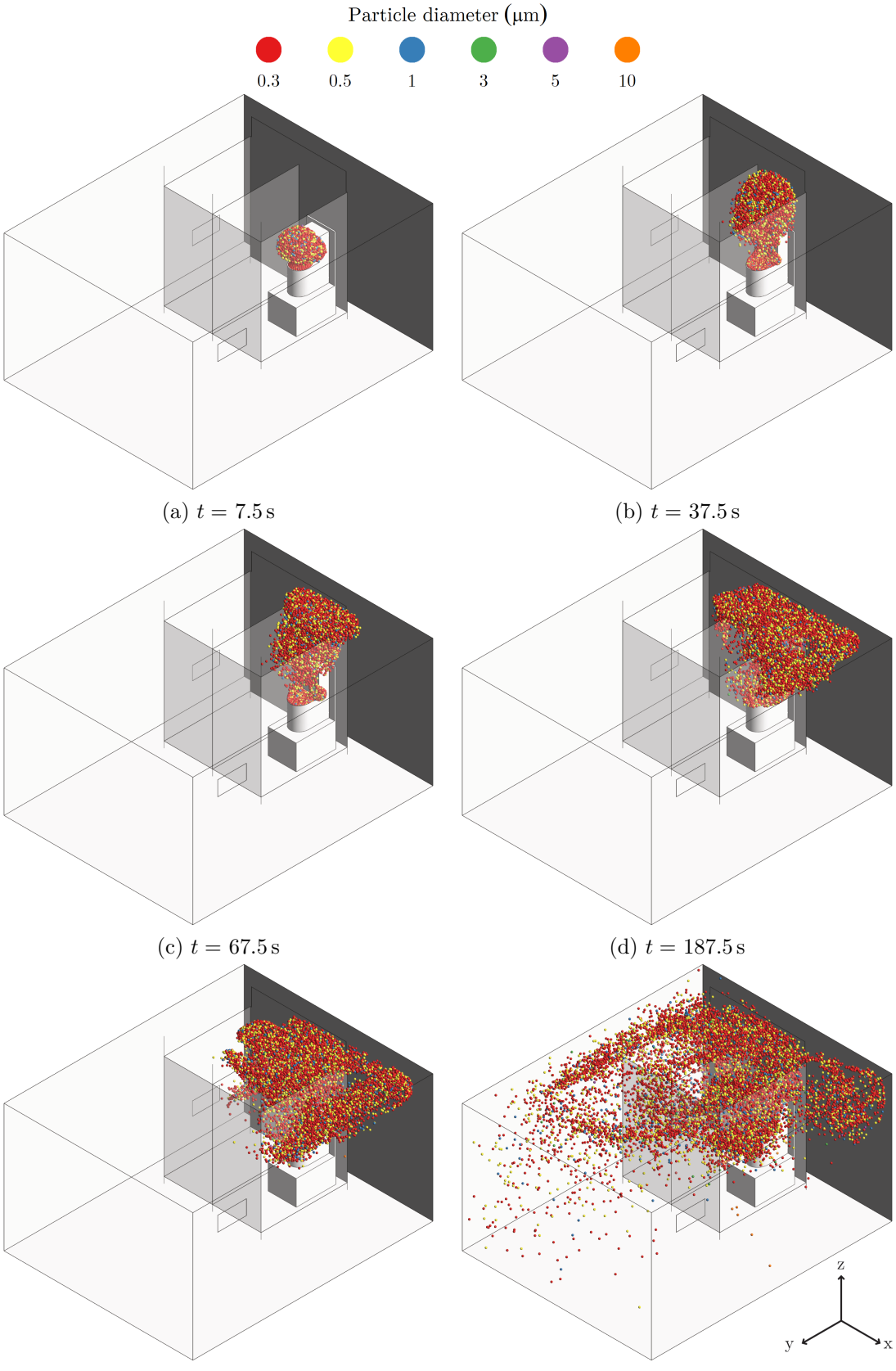

(a) $t = 7.5\,\mathrm{s}$ (b) $t = 37.5\,\mathrm{s}$

(c) $t = 67.5\,\mathrm{s}$ (d) $t = 187.5\,\mathrm{s}$

(e) $t = 307.5\,\mathrm{s}$ (f) $t = 607.5\,\mathrm{s}$

Figure 5.22: Particle locations for scenario 2 (2C) at 1.5 ACH.

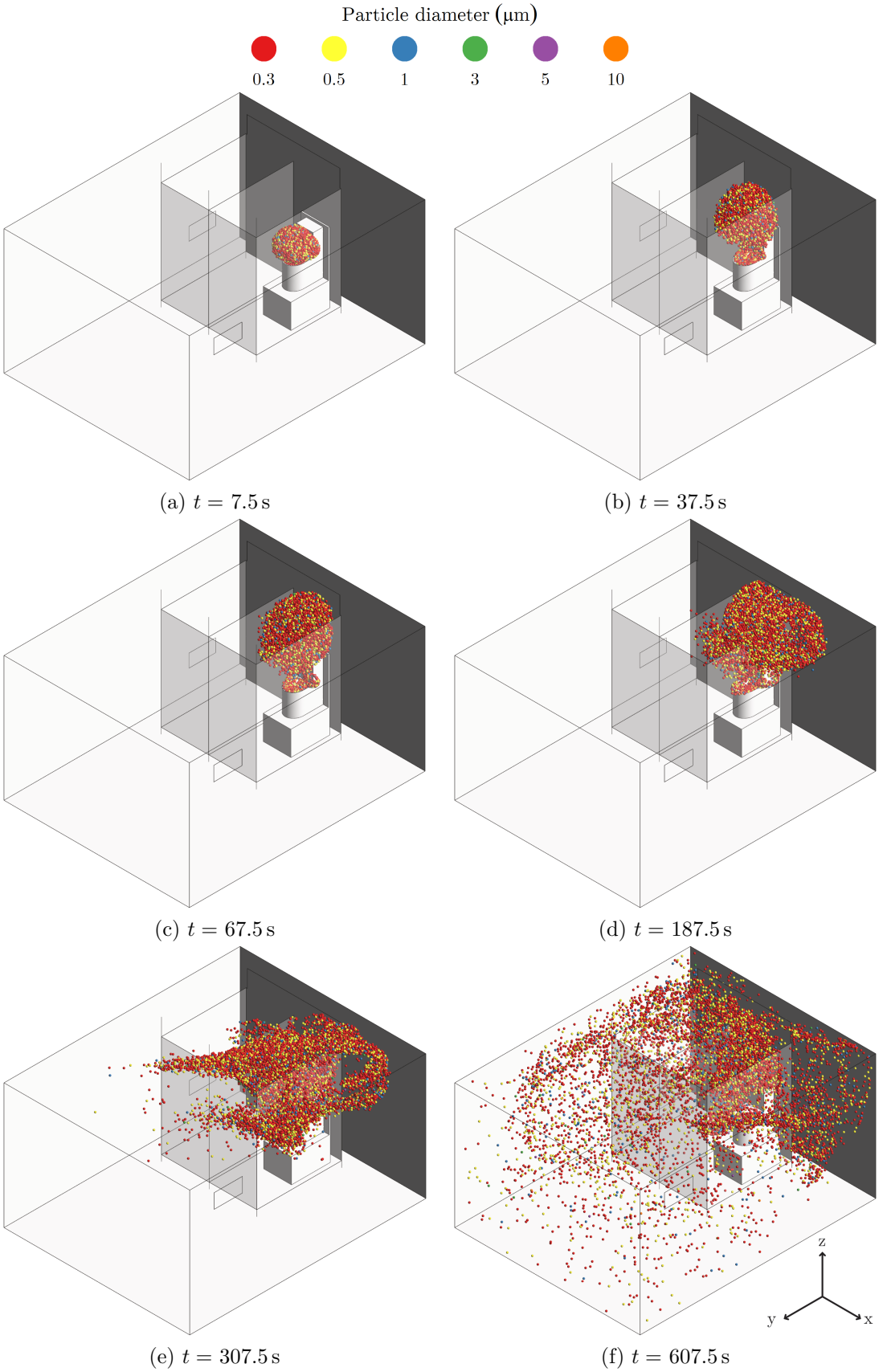

(a) $t = 7.5\,\mathrm{s}$ (b) $t = 37.5\,\mathrm{s}$

(c) $t = 67.5\,\mathrm{s}$ (d) $t = 187.5\,\mathrm{s}$

(e) $t = 307.5\,\mathrm{s}$ (f) $t = 607.5\,\mathrm{s}$

Figure 5.23: Particle locations for scenario 2 (2C) at 3 ACH.

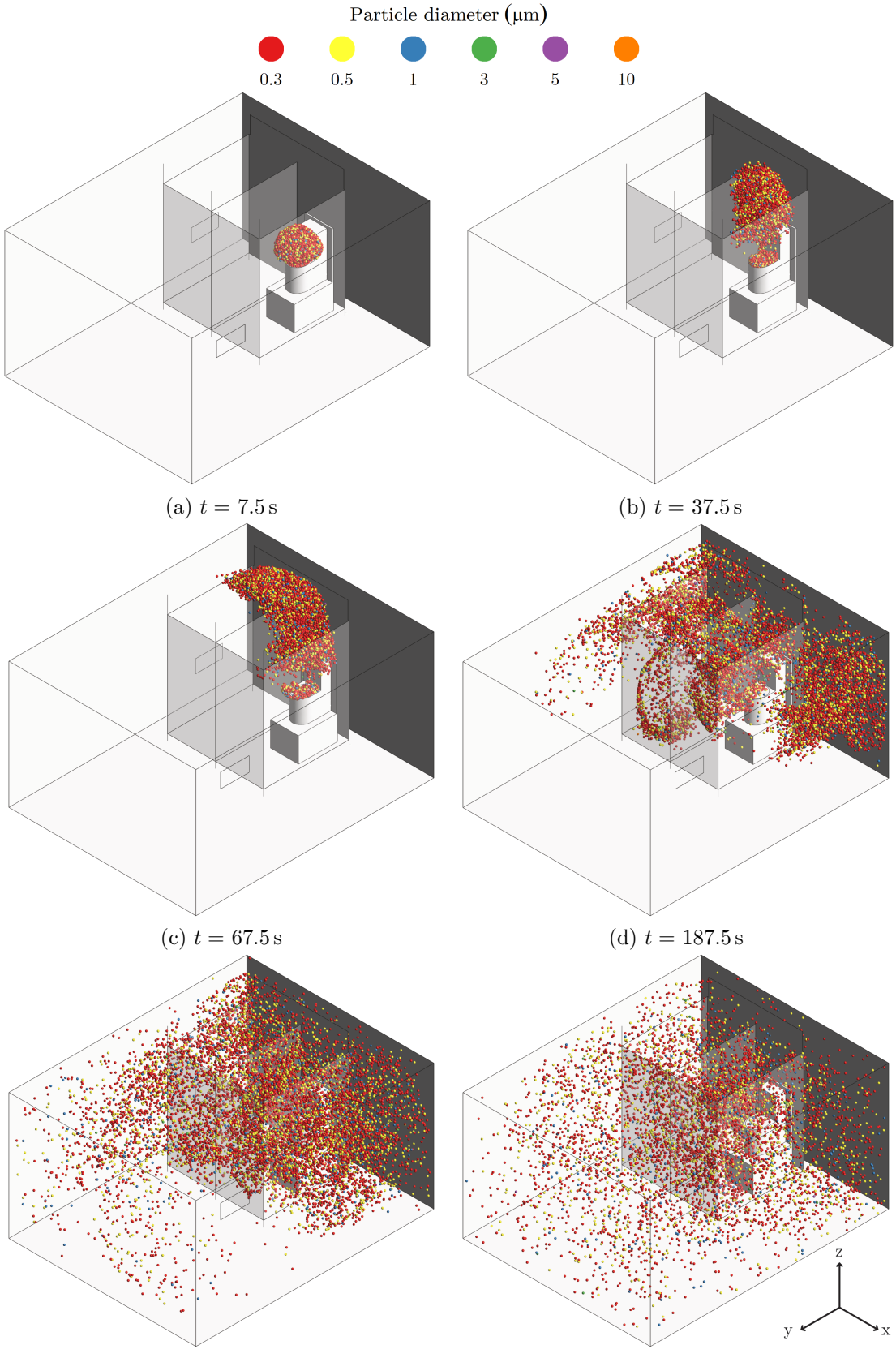

(a) $t = 7.5\,\mathrm{s}$ (b) $t = 37.5\,\mathrm{s}$

(c) $t = 67.5\,\mathrm{s}$ (d) $t = 187.5\,\mathrm{s}$

(e) $t = 307.5\,\mathrm{s}$ (f) $t = 607.5\,\mathrm{s}$

Figure 5.24: Particle locations for scenario 2 (2C) at 6 ACH.

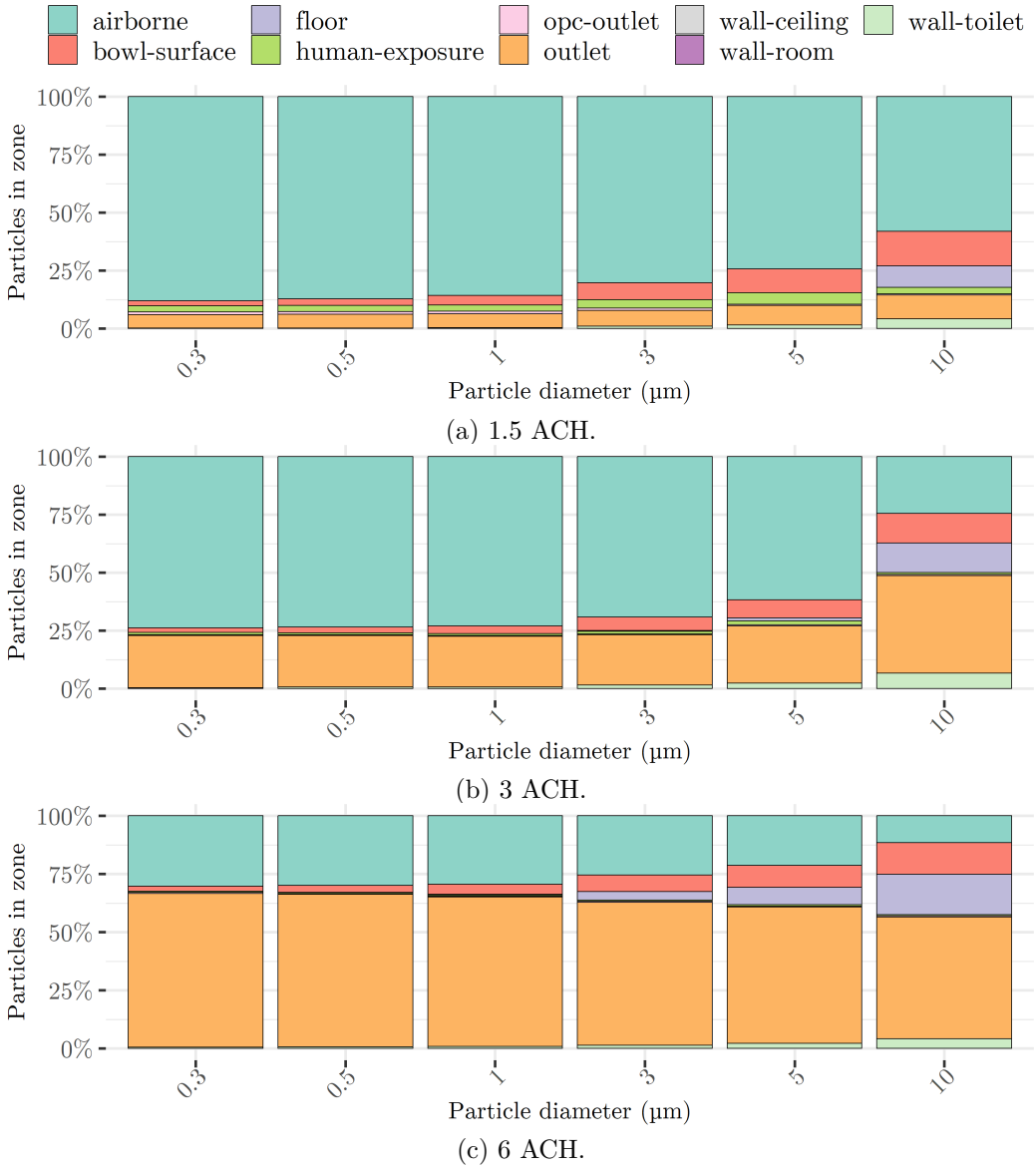

(a) 1.5 ACH.

(b) 3 ACH.

(c) 6 ACH.

Figure 5.25: Particle fate data for scenario 1 (NC) 10 min after flushing.

This effect is further illustrated in Fig. 5.25 and Fig. 5.26, which show the particle fate after a period of 10 min as a proportion of the total number injected. At a given ventilation rate, a higher proportion of particles are removed from the ventilation outlet in scenario 1 (NC) compared to scenario 2 (2C). This corresponds to fewer particles remaining airborne (and thus visible in Figs. 5.22, 5.23 and 5.24 compared to Figs. 5.19, 5.20 and 5.21).

The impact of cubicles becomes more pronounced as ventilation rates increase. At 6 ACH, considering all particle sizes and their initial quantities from Table 3.4, 66 % of particles are removed at the aerobiology chamber ventilation outlet in scenario 1 (NC). This drops to 48 % in scenario 2 (2C) when cubicles are present. At 1.5

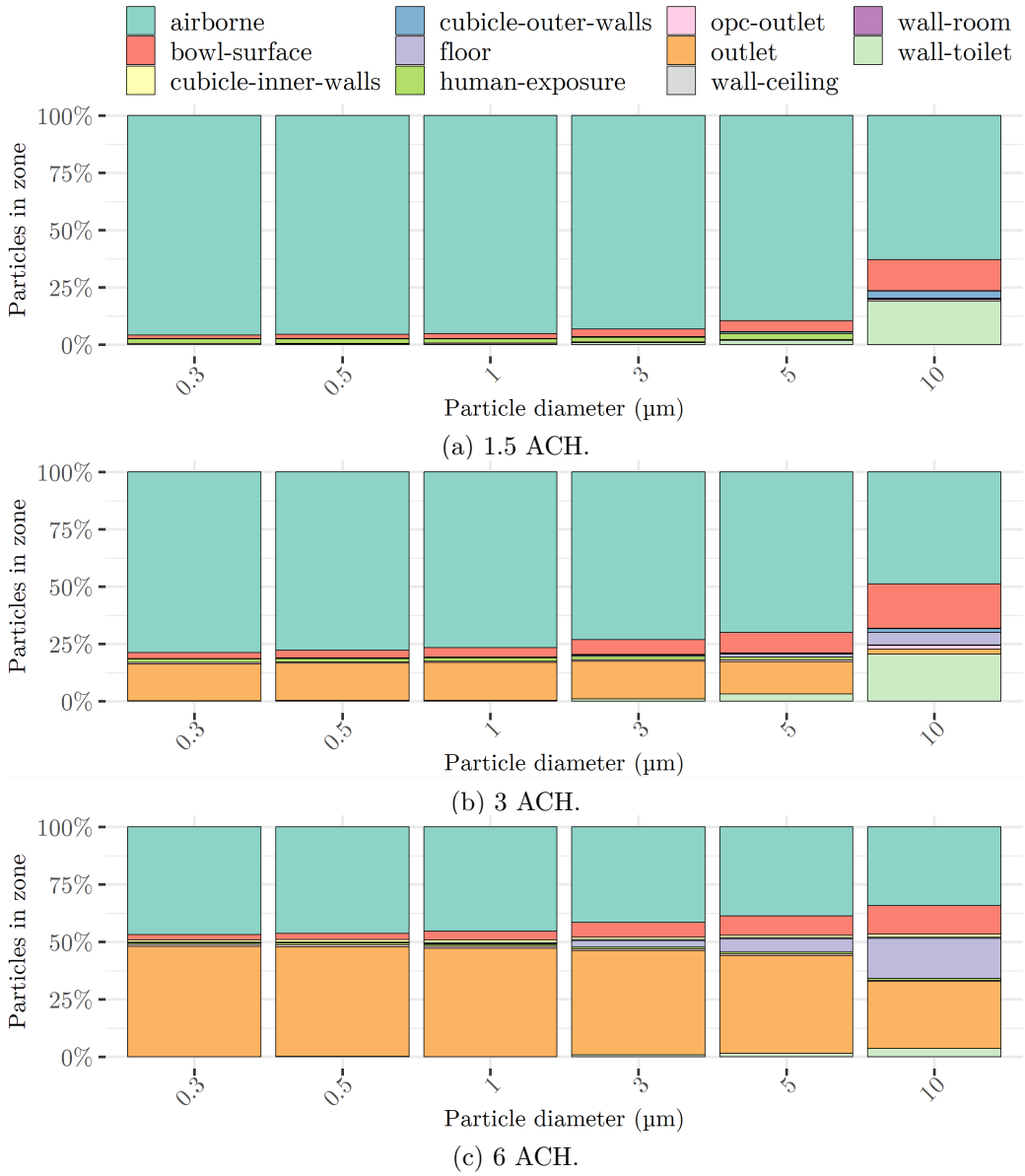

(a) 1.5 ACH.

(b) 3 ACH.

(c) 6 ACH.

Figure 5.26: Particle fate data for scenario 2 (2C) 10 min after flushing.

ACH, the difference is smaller, with 5.9 % of particles removed in scenario 1 (NC), compared to just 0.1 % in scenario 2 (2C). These results indicate that the introduction of cubicles reduces ventilation-driven particle removal for all ventilation rates, as the airflow becomes more obstructed by the partitions. At higher ventilation rates, this difference is greater than at lower ventilation rates. For lower ventilation rates, the difference between the two scenarios is minimal, suggesting that the layout of the toilet facility plays a less critical role when the ventilation rate is already low. In this low ventilation case, prioritising an increase in ventilation rates may be more effective in reducing airborne particle concentrations than modifications to the toilet facility layout.

Figs. 5.25 and 5.26 show that as the particle size increases, a greater proportion of particles settle on the surfaces. The primary contaminated surfaces, depending on the ventilation regime and scenario type, are the toilet walls (including the plinth), the floor, and the surface injection area.

If the walls of the toilet become contaminated, direct contact with these surfaces, such as flushing the toilet, opening or closing the lid, or cleaning the toilet, could result in hand contamination, leading to the risk of contact transmission [48]. For floor contamination, transmission could occur if a person comes into contact with the floor, which may be of particular concern for small children accompanying parents to the toilet. Furthermore, indirect transmission could occur if shoes become contaminated, potentially carrying pathogens into environments such as homes or public spaces [336], or if bags are placed on the floor and then handled.

Considering surface injection contamination to represent particles settling back into the toilet bowl, this could contribute to re-aerosolisation during a subsequent flush, further increasing airborne transmission risks. The persistence of contamination of the toilet bowl water from sequential flushing has previously been shown [44] and this could be a contributing factor to this persistence.

5.5.2 Adaptation of Experimental Scenario 2 (2C*)

Airflow Patterns

Fig. 5.27 shows the velocity magnitude contours for the adapted scenario 2 (2C*), where the original ventilation outlet has been replaced by two outlets, one above each cubicle. The most noticeable difference compared to the original scenario 2 (2C) is the higher velocities near the ceiling in the region of the two new ventilation outlets. The airflow is now directed towards these ceiling-mounted ventilation outlets as it enters the room. This effect is further illustrated by the velocity vectors in Fig. 5.28. The velocity vectors confirm that the highest airflow velocities occur near the new ventilation outlets. Consequently, any contaminants near the toilet will predominantly follow the upward airflow path and be removed more efficiently at the ceiling outlets, potentially reducing the concentration of airborne contaminants

in the cubicle.

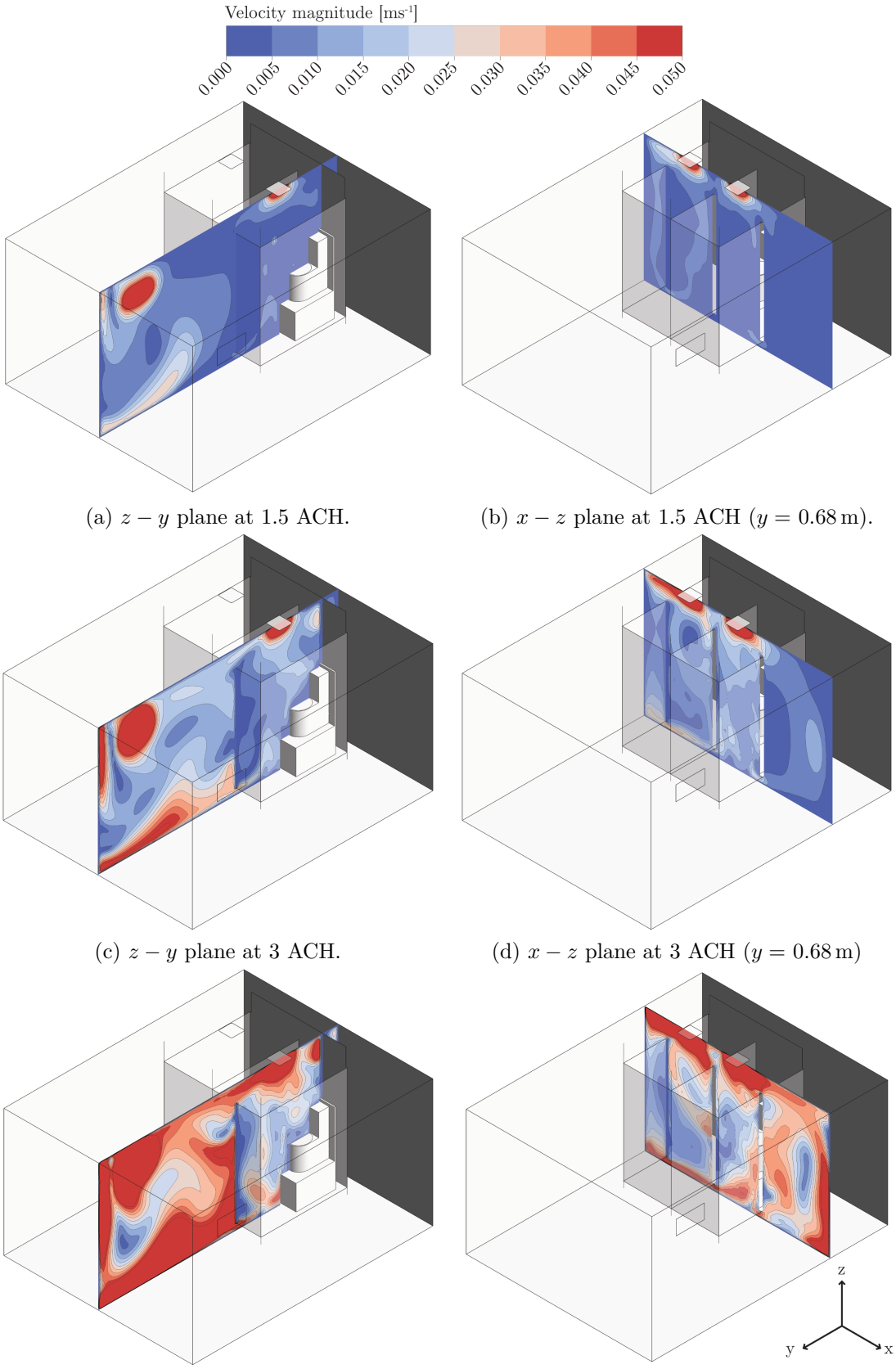

(a) $z-y$ plane at 1.5 ACH.

(b) $x-z$ plane at 1.5 ACH ($y = 0.68\,\mathrm{m}$).

(c) $z-y$ plane at 3 ACH.

(d) $x-z$ plane at 3 ACH ($y = 0.68\,\mathrm{m}$)

(e) $z-y$ plane at 6 ACH.

(f) $x-z$ plane at 6 ACH ($y = 0.68\,\mathrm{m}$)

Figure 5.27: Velocity magnitude contours for adapted scenario 2 (2C*). The range is clipped to $0.05\,\mathrm{m\,s^{-1}}$.

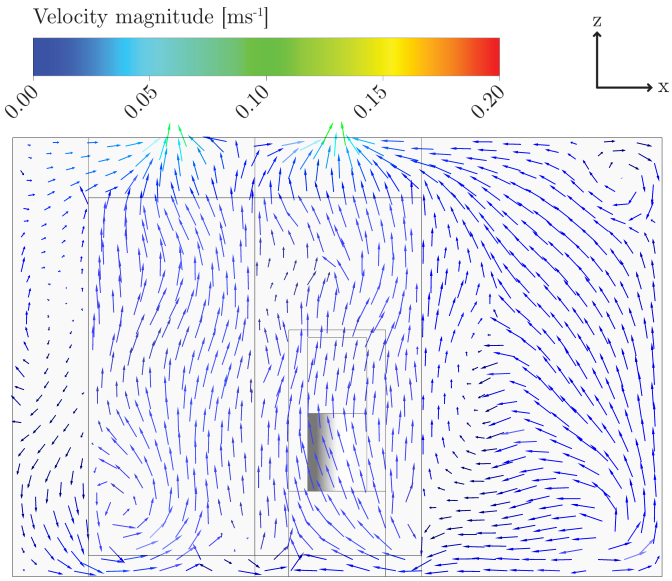

(a) 1.5 ACH.

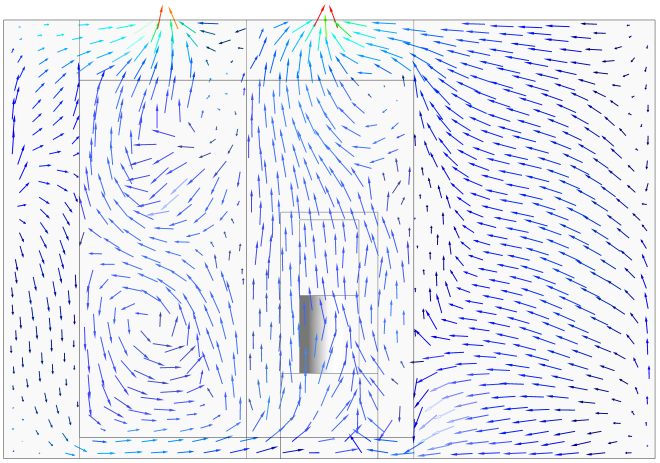

(b) 3 ACH.

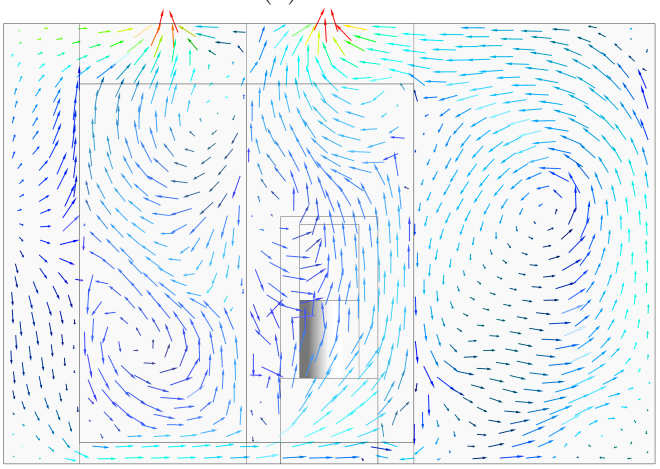

(c) 6 ACH.

Figure 5.28: Velocity magnitude vectors in the $x - z$ plane at mid-cubicle height ($y = 1.04\,\mathrm{m}$) for adapted scenario 2 (2C*).

Particle Dispersion

Figs. 5.29 - 5.31 illustrate particle locations at various time steps.

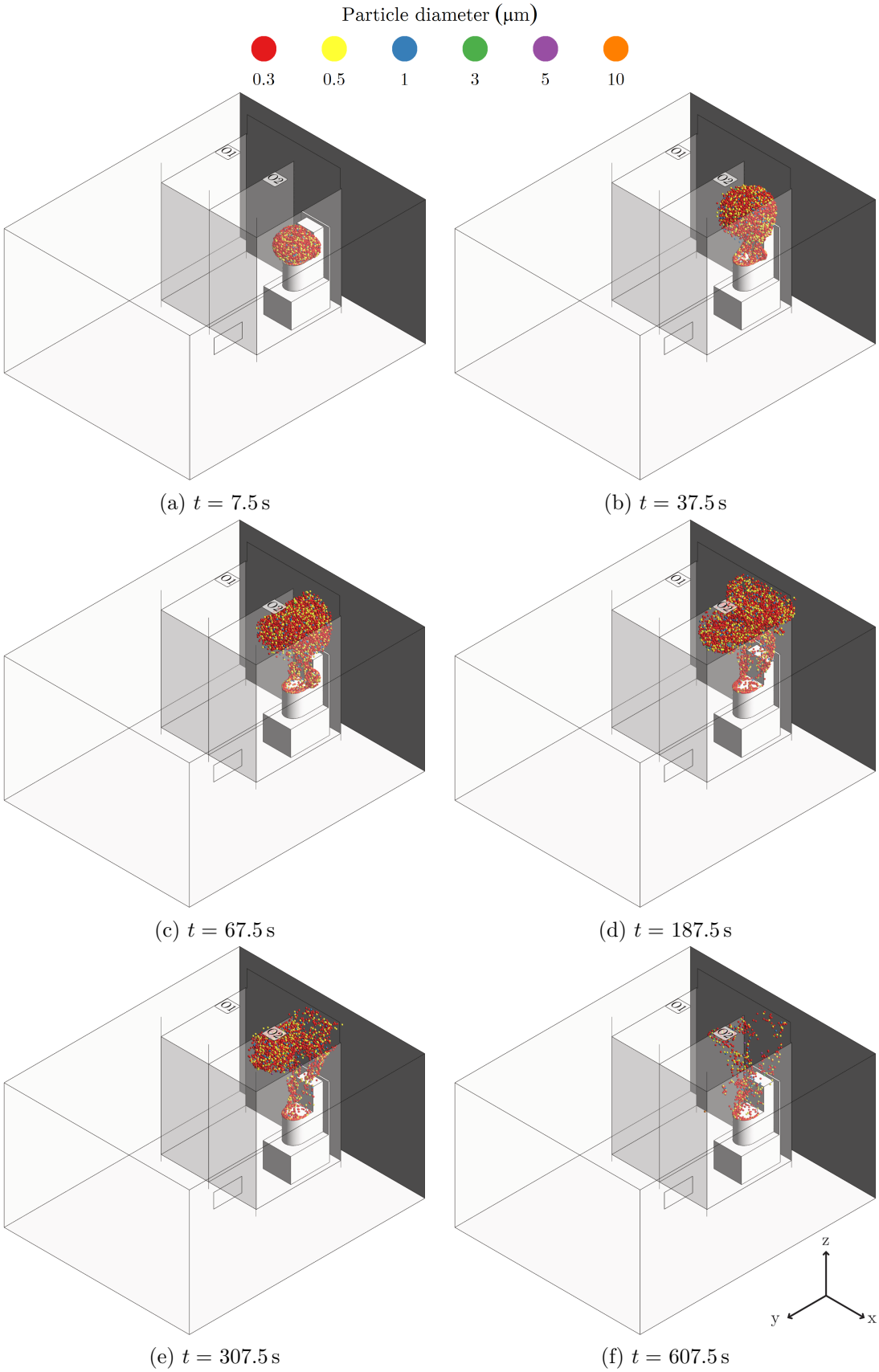

(a) $t = 7.5\,\mathrm{s}$ (b) $t = 37.5\,\mathrm{s}$

(c) $t = 67.5\,\mathrm{s}$ (d) $t = 187.5\,\mathrm{s}$

(e) $t = 307.5\,\mathrm{s}$ (f) $t = 607.5\,\mathrm{s}$

Figure 5.29: Particle locations for adapted scenario 2 (2C*) at 1.5 ACH.

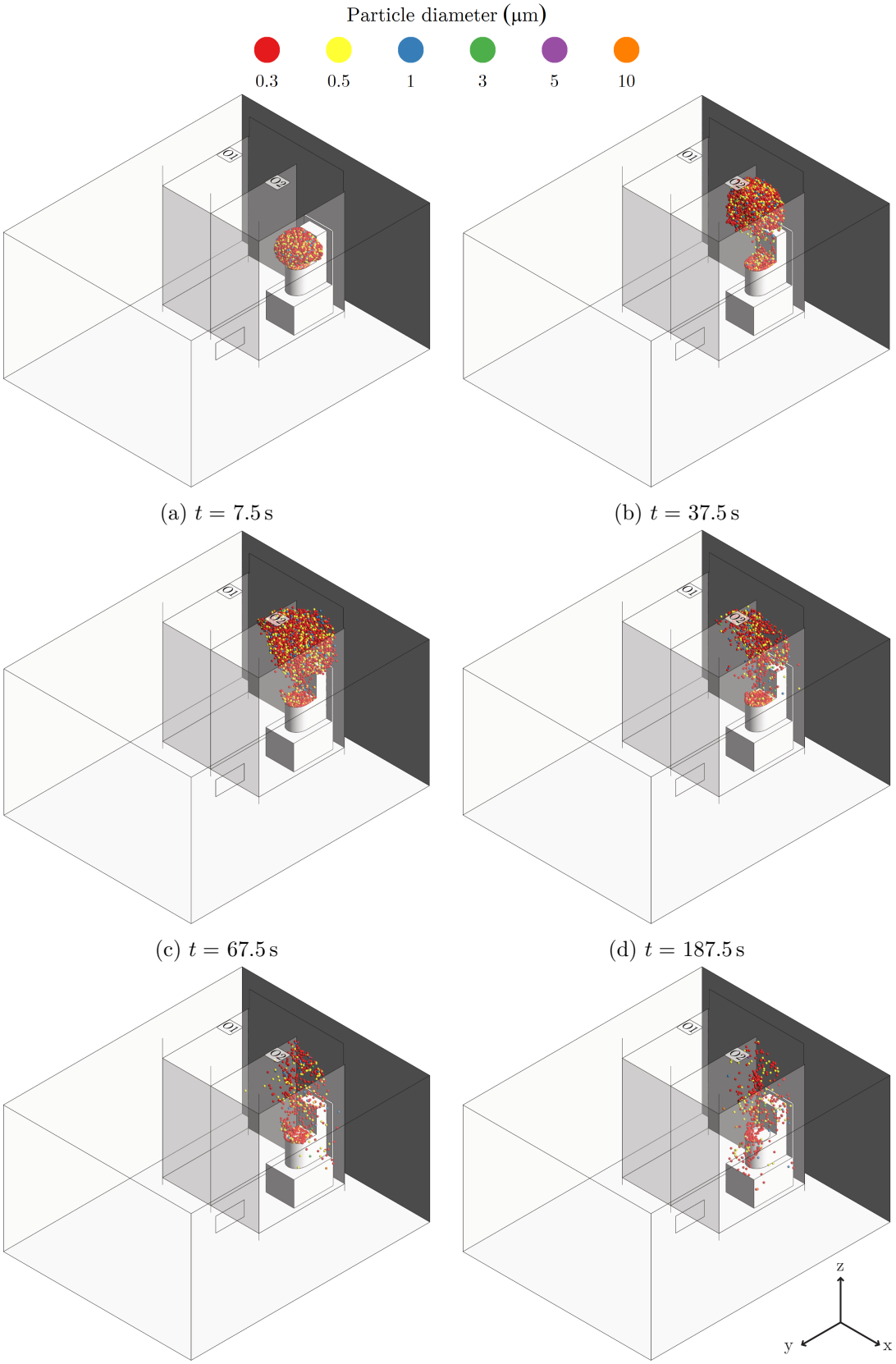

(a) $t = 7.5\,\mathrm{s}$ (b) $t = 37.5\,\mathrm{s}$

(c) $t = 67.5\,\mathrm{s}$ (d) $t = 187.5\,\mathrm{s}$

(e) $t = 307.5\,\mathrm{s}$ (f) $t = 607.5\,\mathrm{s}$

Figure 5.30: Particle locations for adapted scenario 2 (2C*) at 3 ACH.

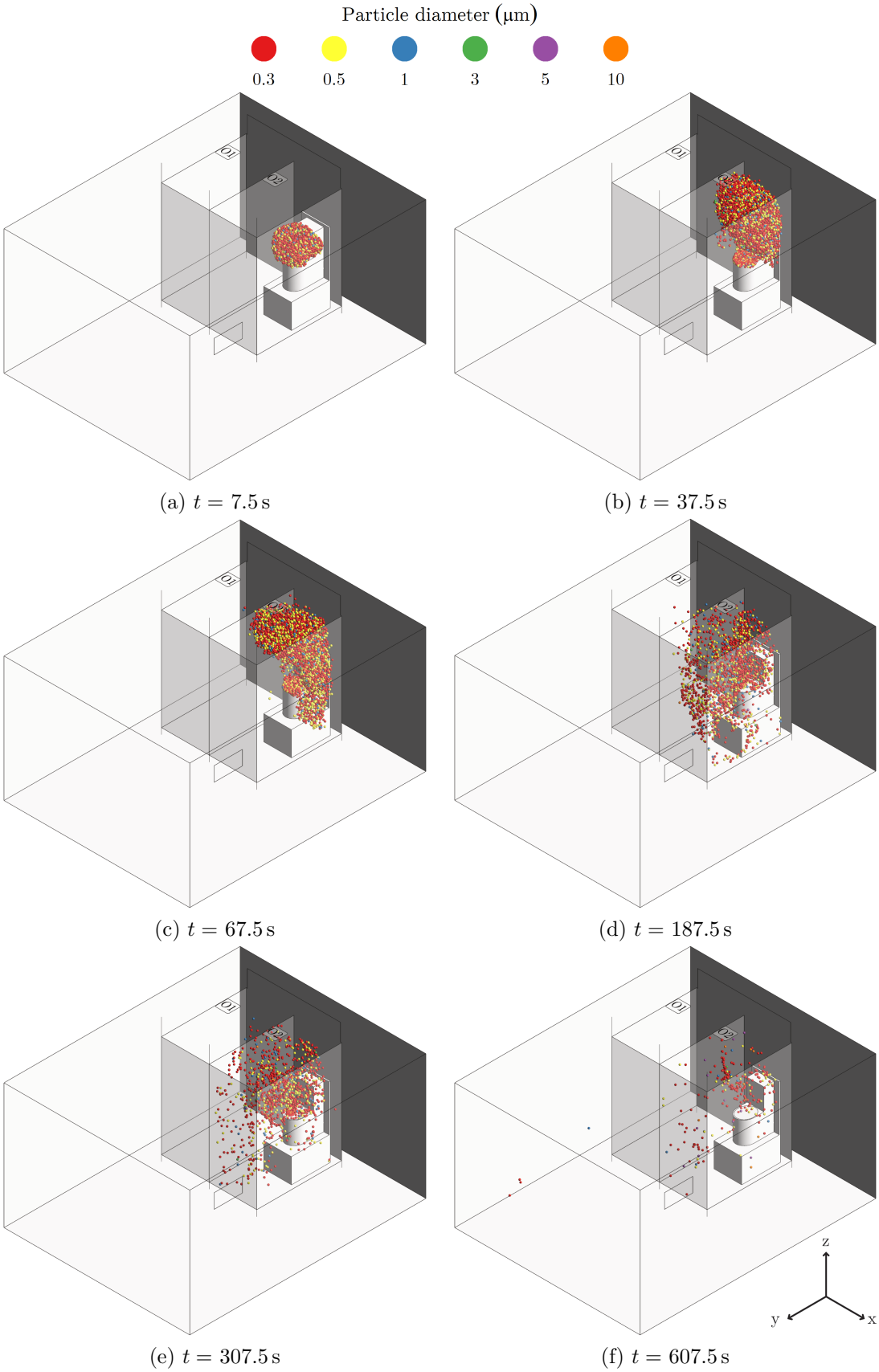

(a) $t = 7.5\,\mathrm{s}$ (b) $t = 37.5\,\mathrm{s}$

(c) $t = 67.5\,\mathrm{s}$ (d) $t = 187.5\,\mathrm{s}$

(e) $t = 307.5\,\mathrm{s}$ (f) $t = 607.5\,\mathrm{s}$

Figure 5.31: Particle locations for adapted scenario 2 (2C*) at 6 ACH.

In all cases, very few particles leave cubicle 1, with dispersion contained within the cubicle. Particles released during the toilet flush are drawn upward towards the ventilation outlet (O1) and removed. This change in the location of the ventilation outlet highlights the importance of studying airflow patterns. A high ventilation rate alone does not guarantee efficient particle removal, and the airflow path is also crucial.

Particle Fate

Fig. 5.32 shows particle locations after a 10 min period for adapted scenario 2 (2C*). Compared to scenario 2 (Fig. 5.26), the proportion of particles removed at the ven-

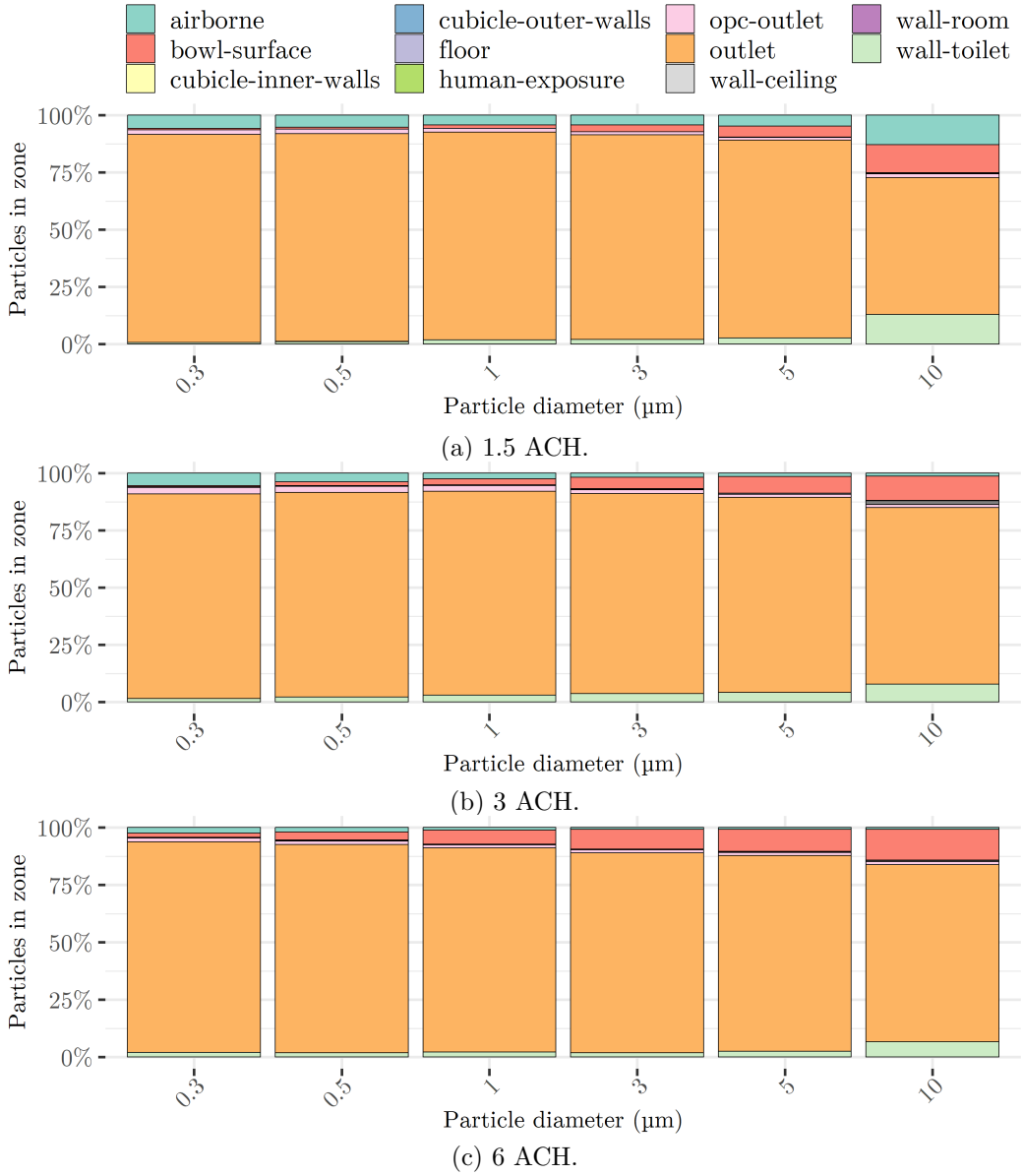

(a) 1.5 ACH.

(b) 3 ACH.

(c) 6 ACH.

Figure 5.32: Particle fate data for adapted scenario 2 (2C*) 10 min after flushing.

tilation outlet is greater across all ventilation rates. For example, across all particle sizes, the proportion of particles removed at the ventilation outlet for adapted scenario 2 (2C*) at 1.5 ACH is 89 %, and at 6 ACH, it is 91 %. In contrast, for scenario 2 (2C), these values are 0.10 % at 1.5 ACH and 48 % at 6 ACH. When the ventilation outlet location is changed, the difference in particle removal quantity is less pronounced with increased ventilation rates. This is because even at low ventilation rates, a large number of particles have already been removed, so improving the ventilation rate has less impact. If increasing ventilation rates is challenging due to constraints such as cost or power, the location of the ventilation outlet becomes extremely important.

5.5.3 Human Exposure Outlet

The number of particles that "escaped" through the human exposure outlet was monitored over a 10 min period. This analysis was carried out for scenario 1 (NC), scenario 2 (2C) and adapted scenario 2 (2C*) to assess the influence of ventilation and airflow dynamics on aerosol transport.

Fig. 5.33 presents a time series of the cumulative number of particles that escape at the human exposure outlet across the two scenarios and the ventilation rates. Fig. 5.34 shows the total number of particles exiting through the human exposure outlet over the full 10 min period.

For scenario 1 (NC), Fig. 5.34a shows that the total number of particles escaping through the human exposure outlet over the 10 min period is greatest at 1.5 ACH. However, examining the time series in Fig. 5.33a, the cumulative number of particles for 6 ACH is greater than the lower ventilation rates at the 5 min mark. This indicates that while higher ventilation rates may reduce exposure over longer periods, shorter-term exposure may be greater for higher ventilation rates, depending on the exposure time. A similar trend is observed for scenario 2 (2C) in Fig. 5.34b. During the 10 min period, 1.5 ACH results in the highest total exposure. However, by 5 min in Fig. 5.33a, the exposure at 3 ACH is greater than at 1.5 ACH. This suggests that ventilation may initially increase the transport of particles towards the breathing zone before subsequently removing them more efficiently.

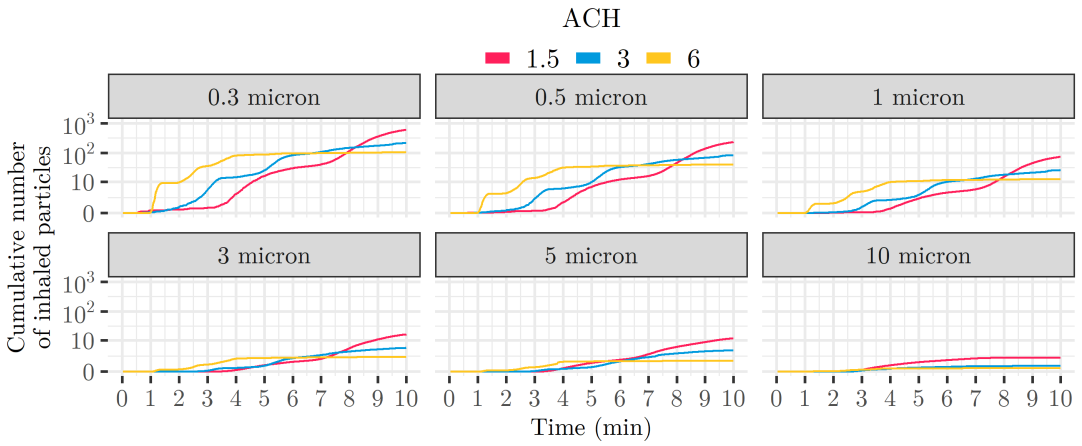

(a) Scenario 1 (NC).

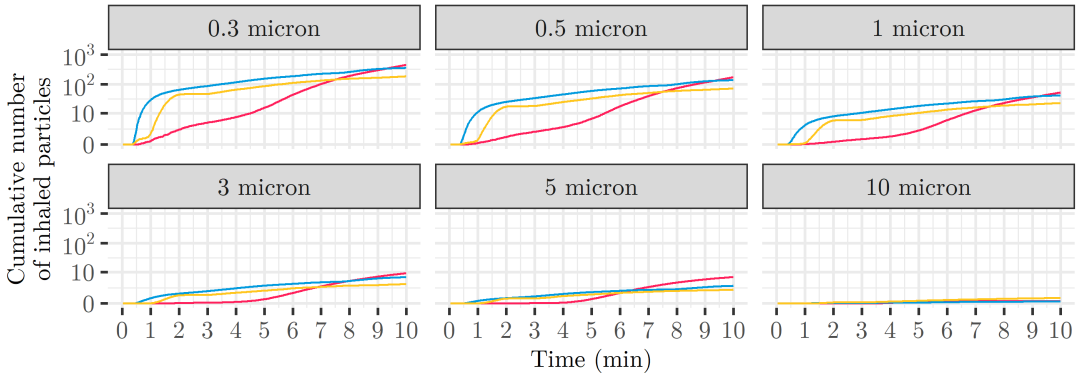

(b) Scenario 2 (2C).

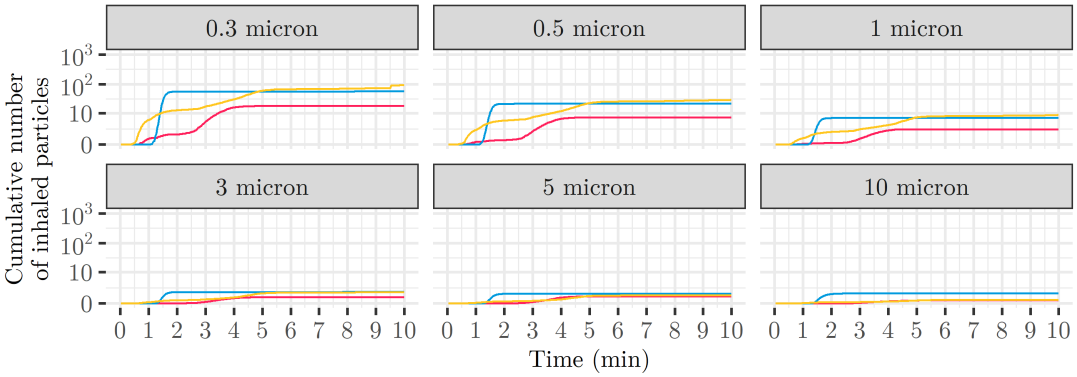

(c) Adapted scenario 2 (2C*).

Figure 5.33: The cumulative number of particles escaping through the human exposure outlet in the CFD simulations over 10 min after flushing.

Similar findings have been reported in experimental studies, such as Pantelic and Tham [394], who demonstrated that increasing ventilation rates from 6 ACH to 12 ACH led to increased exposure to aerosols released from a cough under certain conditions. Their study, conducted in an environmental chamber using particle image velocimetry and aerosol measurements, found that local airflow patterns significantly influenced dispersion, and higher supply flow rates could direct particles towards susceptible individuals rather than away from them. This reinforces that

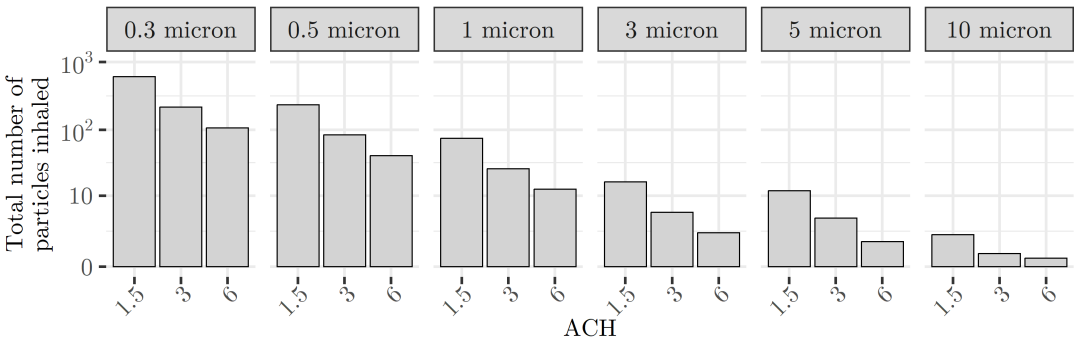

(a) Scenario 1 (NC).

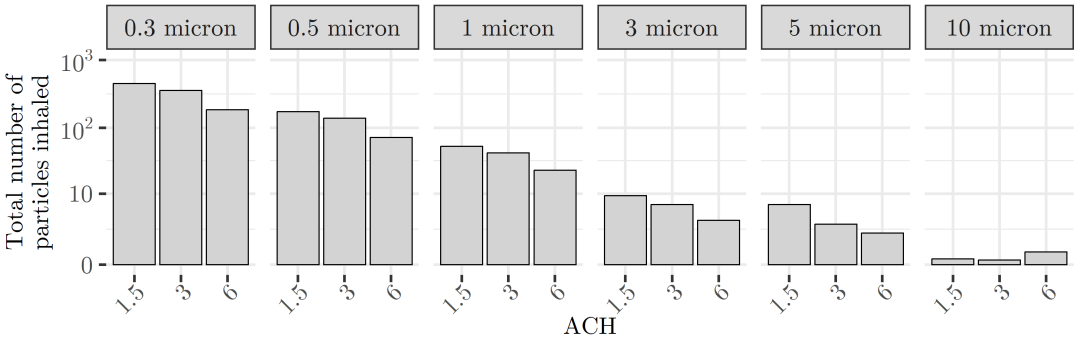

(b) Scenario 2 (2C).

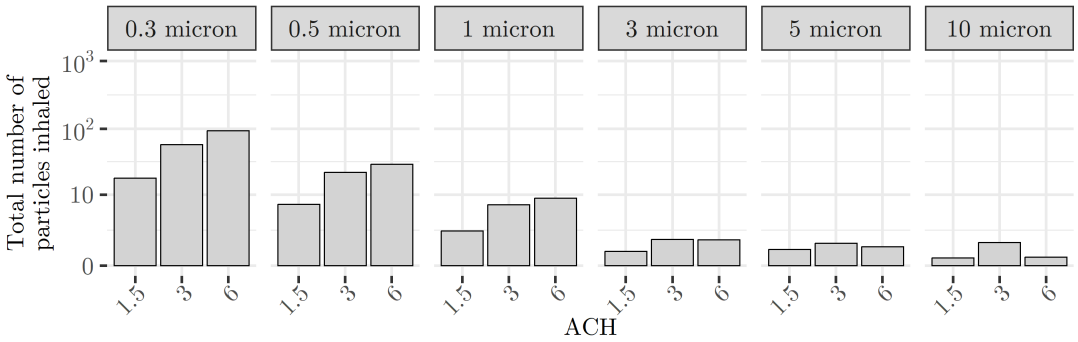

(c) Adapted scenario 2 (2C*).

Figure 5.34: The total number of particles escaping through the human exposure outlet in the CFD simulations over 10 min after flushing.

ventilation rate is not always a sufficient indicator of exposure reduction, as airflow dynamics play a crucial role in particle transport. The results of the present study further support this, indicating that ventilation design and airflow distribution should be carefully considered in shared toilet facilities to minimise exposure risk.

The differences between the ventilation rates for the total number of inhaled particles at the human exposure outlet narrow for scenario 2 (2C) compared to to scenario 1 (NC). This highlights that with the introduction of cubicles to the simulation, although there is an increase in ventilation rate, this does not reflect an

equivalent difference in ventilation rate inside the cubicle.

The results indicate that fewer particles escape through the human exposure outlet in scenario 1 (NC) compared to scenario 2 (2C) at ventilation rates of 3 ACH and 6 ACH. Across all particle sizes, there was a difference of 210 particles for 3 ACH and a decrease of 123 particles for 6 ACH between scenario 2 (2C) and scenario 1 (NC). This difference can be attributed to variations in airflow patterns between the two scenarios. As shown in Figs. 5.17b and 5.18b, the airflow in scenario 2 (2C) tends to flow upward, leading to the possibility of a higher concentration of particles persisting within the human exposure area for an extended period. This is evident in Figs. 5.23 and 5.24, where more particles remain near the human exposure outlet, increasing the likelihood of being drawn into it.

In contrast, in scenario 1 (NC), particles are more likely to be transported directly to the ventilation outlet rather than lingering near the human exposure outlet, as seen in Figs. 5.20 and 5.21. The absence of cubicle partitions allows for a more direct and unobstructed airflow path, facilitating the removal of contaminants from the breathing zone. This results in fewer particles accumulating near the human exposure outlet, reducing the potential for inhalation exposure.

At 1.5 ACH, however, the opposite trend is observed, with more particles sampled by the human exposure outlet in scenario 1 (NC) compared to scenario 2 (2C), as shown in Fig. 5.34a and Fig. 5.34b. Across all particle sizes, this difference was 254 particles. This may be due to the airflow patterns at this ventilation rate. In Fig. 5.16a, the airflow was initially directed upward before being drawn towards the ventilation outlet, potentially allowing more particles to be retained near the human exposure outlet. In contrast, in Fig. 5.16b, the airflow was angled slightly towards the left, which may have influenced the transport and dispersion of the particles differently.

For the adapted scenario 2 (2C*), where the original extract was removed and additional extracts were introduced above the cubicles, the total number of particles escaping through the human exposure outlet is lower for all ventilation rates compared to scenario 2, as shown in Fig. 5.34c. The only exception is for 10 µm

particles at 3 ACH, where a slight increase is observed. This suggests that the additional extract effectively reduces the overall exposure by enhancing particle removal.

Examining the gradient of the cumulative number of particles that escape through the exposure outlet provides additional insight into the potential exposure. In Fig. 5.33c, the cumulative number of particles plateaus after 5 min, suggesting that exposure risk is negligible beyond this point. In contrast, Fig. 5.33a shows that for 1.5 ACH, particularly for smaller particle sizes, the gradient remains non zero even after 9 min after flushing. This indicates that particles are still being inhaled at a low but continuous rate. A similar pattern is observed in Fig. 5.33b, where 1.5 ACH continues to show an increasing particle count at the exposure outlet beyond 9 min.

These results highlight the importance of considering how exposure risk evolves over time. Most particle inhalation can occur in a short window after flushing, when the gradient of the cumulative exposure curve is steepest. Even though higher ventilation rates can reduce total exposure over a 10 min period, they may initially increase exposure by rapidly transporting aerosols to the breathing zone. This reinforces the need to assess risk over shorter time frames rather than rely solely on cumulative exposure over longer periods.

Compared with the experimental measurements, the number of particles that escaped through the OPC outlet was lower in the CFD model than in the experimental data. Additionally, the CFD model exhibited a more rapid decay in particle concentration at the OPC location. This suggests that the model may underestimate exposure risks at the human breathing outlet, as fewer particles were predicted to remain airborne over time. However, despite this potential underestimation, the results still allow meaningful comparisons between different ventilation rates and room configurations.

Despite these discrepancies, the qualitative trends observed in both the CFD simulations and the experimental measurements reinforce the critical role of ventilation design in mitigating exposure risks. Both approaches indicate that increasing ventilation rates generally reduces cumulative exposure over time, but can also introduce short-term peaks in inhalation risk, likely due to airflow-driven particle transport.

The infection risk estimates from the experimental measurements in Chapter 4, Sections 4.3, found that the highest infection risk occurred within the first 1 min. However, these measurements were taken from a fixed location above the toilet, which limits the spatial resolution of the exposure assessment. The CFD findings suggest that the exposure risk can vary between different locations within the room, with peaks occurring at different positions depending on ventilation rates and airflow patterns. This highlights the importance of considering spatial variability in exposure assessment and ventilation design strategies.

5.6 Implications and Limitations

The number of particles reaching the human exposure outlet in the CFD model provides an upper estimate of what an individual might inhale in a confined toilet space based on the modelled emission rate. As ventilation rates increase, the maximum potential inhaled dose decreases, lowering the risk of infection. However, the presence of cubicles increases the concentration of localised particles, which could lead to higher inhalation exposure within these areas. This suggests that toilet facility design and ventilation strategies should focus not only on overall particle removal but also on preventing high-risk breathing zones where particles can accumulate.

The experimental results showed a sharp increase in particle concentration within the first 1 min when sampling near the toilet, consistent with the expected peak in aerosol release at this location after a flush [2]. However, the CFD results suggest that the highest risk of inhalation may not always occur within this first 1 min. Instead, airflow patterns and ventilation rates influence when human exposure risk is highest, with sharp increases at the human exposure outlet occurring at varying times depending on ventilation conditions. This highlights the importance of considering airflow dynamics when assessing exposure risk, as relying solely on measurements taken immediately after flushing may not fully capture peak inhalation risk.

The CFD model also reproduced the sharp increase in particle concentrations observed at particle counter A in the experiments. However, in the experiments at

particle counter B, background concentration fluctuations dominated, making it difficult to distinguish toilet plume aerosols from natural variations in ambient particle counts. For example, at 1.5 ACH in the CFD model, the estimated number of 0.3 µm particles sampled by the human exposure outlet over 10 min was 107. Even if all of these particles were captured by the OPC within a 10 s sampling period, this would correspond to a concentration of approximately $10^5\,\mathrm{m}^{-3}$. Since background count fluctuations at particle counter B were also of this order, it becomes challenging to determine whether the observed increases in the experimental data were due to toilet aerosolisation or natural variations. This underscores the difficulty in accurately quantifying toilet plume aerosols in real-world environments where ambient conditions introduce noise into measurements.

The placement of ventilation outlets plays a crucial role in reducing inhalation exposure. If ventilation effectively removes airborne particles at the source, the overall dispersion of aerosols in the room is reduced. The findings here reinforce previous work by Liu et al. [326], who demonstrated that the position of the ventilation outlet significantly influences particle dispersion. Their study recommended that ventilation outlets avoid through-draughts, be positioned near secondary fresh air sources, and induce turbulence patterns that promote efficient aerosol removal. Their results showed that strategic ventilation outlet placement could reduce indoor droplet residence time by up to 4 %. The findings of the current study suggest that optimising ventilation outlet positioning may be a more effective mitigation measure than simply increasing the overall ventilation rate, as it allows more efficient removal of airborne particles before they spread throughout the room. When designing new toilet facilities, the placement of the ventilation outlet should be a primary consideration to minimise exposure risks.

This study does not account for multiple users or the dynamic airflows introduced by door openings and occupant movement, which can significantly alter dispersion patterns. This is particularly relevant in high-occupancy settings, such as concerts or conferences, where frequent entry and exit generate additional airflow disturbances. Malki-Epshtein et al. [40] took carbon dioxide measurements at a

high-capacity event in Wembley Stadium and found that elevated concentrations persist for up to an hour due to high-occupancy and crowd density. In addition, door openings contribute to mass exchange between zones, creating airflow disturbances driven by large-scale vortices [395]. This applies to both the internal cubicle doors and to the external doors leading to adjacent external rooms. Temperature gradients between the toilet facility and the surrounding external areas could also drive buoyancy-driven flow, further influencing particle dispersion [396]. During these high-occupancy periods, contaminant emission is also greater than during off-peak hours. Rather than maintaining a uniformly high ventilation rate at all times, an adaptive ventilation strategy could be implemented, where ventilation rates are increased only during peak occupancy. This approach would allow energy-efficient and cost-effective operation while ensuring adequate ventilation when most needed.

In toilet facilities that contain cubicle arrangements, the CFD results indicate that within the first 5 min after a flush, the particles remain concentrated primarily within the first cubicle. This suggests that if multiple cubicles are available, individuals should be encouraged to use a vacant cubicle rather than one that was recently occupied. This simple behavioural recommendation could help reduce the risk of exposure in shared toilet facilities.

Both the experimental and the CFD results demonstrate that the sampling location significantly influences the measured aerosol concentrations. Near the toilet, particle concentrations increase rapidly within the first 30 s, reflecting the peak in aerosol generation. Further away, increases are smaller, occur later, and become difficult to distinguish from background fluctuations. This is consistent with the findings of Liu et al. [326], who observed that droplet counts decreased as the sampling height increased. These findings suggest that studies relying on measurements taken far from the toilet may underestimate true exposure risks near the source, while measurements taken too close may overestimate exposure. Future research should carefully consider sampler placement to ensure that measurements capture peak exposure conditions.

This study assumes idealised boundary conditions in a controlled environment,

which may not fully represent the complexities of real-world toilet facilities. Variations in toilet types, such as different flushing mechanisms, were not modelled, despite their known influence on aerosol generation. Additionally, toilet designs vary internationally, meaning that models may need to be adapted for different configurations.

The particle injection model was based on rescaled experimental data, which introduces some level of uncertainty. Although validated against previous studies [2, 52], the injection velocity profile may require refinement. Factors such as humidity and temperature fluctuations, which can affect aerosol behaviour, were not explicitly incorporated and should be considered in future work.

The water in the bowl was modelled as inert water droplets. However, in reality, toilet plumes may contain faecal matter, which could influence particle transport once released into the environment. Future studies could explore the role of droplet composition in aerosol dispersion in toilet facilities.

To refine inhalation risk assessments, future work could incorporate a full-scale human model with a transient breathing pattern to simulate realistic aerosol intake under different ventilation conditions. Furthermore, including human heat generation in CFD simulations would improve the representation of thermal plumes, which significantly affect airflow and aerosol transport. However, implementing such models presents considerable challenges as they require capturing detailed human movement and transient breathing patterns over short timescales, making both computational modelling and experimental validation complex. Despite these challenges, incorporating these refinements would provide a more comprehensive assessment of exposure risks and help to develop improved ventilation guidelines and mitigation strategies to reduce airborne disease transmission in shared toilet facilities.

5.7 Conclusions

This study highlights the critical role of ventilation strategies, airflow dynamics, and room layout in mitigating exposure to airborne particles generated by toilet flushing. The key findings from the CFD simulations are as follows:

- The CFD model was able to replicate the general trends in particle dispersion observed in experiments, demonstrating its utility to predict aerosol transport over time. However, exact agreement in particle concentrations remains challenging due to uncertainties in representing the toilet flushing source and the OPC.
- Increasing the ventilation rate of the controlled chamber reduces the number of toilet plume aerosol particles that remain airborne in all scenarios, this may lower the risk of secondary exposure.
- Physical obstructions, such as cubicle partitions, disrupt airflow patterns and hinder the effective removal of particles, demonstrating that room layout is also important as well as ventilation rate in determining exposure risk.
- The position of the ventilation outlets strongly influences the aerosol removal efficiency, with ceiling-mounted outlets above cubicles improving the removal efficiency from 48 % to 91 % at 6 ACH.
- Higher ventilation rates generally improve particle removal but can also temporarily increase the exposure risk by drawing aerosols into the breathing zone before removal.
- In lower ventilation environments, airborne particles remain concentrated in the region of the toilet longer, potentially increasing the risk to a second individual using the toilet soon after flushing.
- A more effective mitigation strategy than simply increasing ventilation rates may be optimising the placement of ventilation outlets to remove aerosols before they disperse throughout the room.
- The findings have direct implications for the design of public toilet facilities in workplaces, entertainment venues, and other shared spaces, highlighting the need for ventilation strategies that minimise airborne exposure risks.

Chapter 6

Conclusions

6.1 Summary of Key Findings

This thesis has investigated the mechanisms by which toilet plume aerosols contribute to disease transmission, combining experimental, risk assessment, and computational approaches to better understand exposure risks in shared toilet facilities. The key objectives were to quantify the generation of aerosols and bioaerosols during toilet flushing, develop models to estimate associated infection risks, and assess the influence of ventilation strategies, occupancy duration, and room layout on exposure.

The research presented in this thesis has added further evidence that toilet flushing produces large quantities of aerosols, many of which are small enough to remain airborne and potentially transport pathogens. Controlled chamber experiments have provided insight on the temporal characteristics of toilet flush aerosols, while QMRA has allowed infection risks to be estimated. CFD simulations further contributed by modelling aerosol dispersion in different ventilation and room layout scenarios, revealing important interactions between airflow, particle dispersion and infection risks.

Through these combined approaches, this work has addressed several gaps in the literature, improving understanding of the role of the toilet plume on transmission and informing mitigation strategies. The major conclusions from this thesis are:

- Flushing a gravity-flow close-coupled toilet produces a large number of aerosols, with 99 % of measured particles smaller than 5 µm and 90 % smaller than 1 µm. CFD modelling showed that these smaller particles can remain airborne for extended periods, highlighting their potential for exposure through inhalation. The transient nature of the release means that exposure is highest in the first few minutes after flushing in the region of the toilet .
- The impact of ventilation and room layout on aerosol dispersion is complex. Although ventilation slightly reduced airborne *E. coli* concentrations, room layout also had an influence, with unexpectedly higher bioaerosol concentrations in the no cubicle scenario compared to the two cubicle scenario. This suggests airflow patterns within the cubicle space alter aerosol dispersion.
- QMRA analysis showed that exposure to toilet plume aerosols can lead to

non-negligible infection risks, particularly for pathogens with high faecal concentrations, such as norovirus. The probability of infection varied considerably depending on the ventilation conditions and the timing of subsequent toilet use. Allowing even a short delay (e.g. 60 s) before entering a recently flushed toilet can reduce the risk of infection.

- CFD simulations revealed that ventilation strategy and room layout strongly affect the fate of aerosols. Higher ventilation rates (6 ACH compared to 1.5 ACH) substantially reduced the number of airborne aerosols after a 10 min period from flushing. The presence of cubicle partitions altered airflow patterns, which impacted particle removal. The placement of ventilation outlets also played a crucial role, with outlets placed inside the cubicle reducing exposure by more than 90 %.
- Bacterial deposition from the toilet plume was found to occur at low levels but can accumulate over time. While individual flushes did not produce significant surface contamination, repeated use of a facility without proper cleaning could allow pathogens to build up, increasing the risk of contact transmission.

These findings reinforce the importance of considering ventilation, room layout and human behaviour mitigation strategies (delays between toilet use) to minimise exposure in shared toilet facilities.

6.2 Contributions to Current Knowledge

This research has made several key contributions to the field of indoor air research and risk assessment when considering toilet flushing:

- The first controlled chamber study to investigate both particle and bioaerosol dispersion from a toilet plume under different ventilation regimes and room layouts. Previous experimental studies have focused on individual toilet types or uncontrolled real-world settings. The study provided data in a carefully controlled environment.
- The development of a stochastic QMRA framework specifically tailored to airborne toilet plume exposure per toilet flushing event. This approach provides a

quantitative estimate of the risk of infection, incorporating occupancy factors, which has not been explored in previous studies.

- The integration of CFD modelling with experimental approaches to assess exposure risk. The CFD model captured airflow dynamics, demonstrating how ventilation rate, cubicle presence, and ventilation outlet placement influence aerosol transport and exposure. The combined use of experimental and computational modelling provides a more comprehensive understanding of toilet plume behaviour.
- Identification of practical mitigation strategies, including optimised ventilation placement and the effectiveness of human behaviour (delays between toilet use), which can inform policy decisions for public health and building design.

6.3 Future Work

While this research has significantly improved understanding of aerosol behaviour in toilet facilities, several areas require further investigation.

Expanding the QMRA model to use for other pathogens.

This study focused on norovirus, SARS-CoV-2 and *E. coli* pathogens, but the model framework could be extended to assess other airborne and faecal pathogens. This includes adenovirus, rotavirus, and any emerging pathogens. By using pathogen-specific dose-response data, the model could provide broader infection risk estimates for different disease scenarios.

Applying QMRA modelling to CFD results.

The CFD model provided detailed particle dispersion data, but risk estimates were based primarily on experimental data. Future studies could integrate CFD aerosol concentrations into the QMRA framework. Instead of using experimental measurements to estimate the number of inhaled particles, the particle counts recorded at the human exposure outlet in the CFD simulations can be used to estimate inhaled pathogen doses. This approach isolates aerosols produced by the toilet plume and removes the effect of background fluctuations on infection risk results caused by

external contaminants in the experimental work. This also allows infection risk estimates to be generated in a wider range of ventilation and room layouts than those tested experimentally.

Investigating the role of human heat sources and thermal plumes in CFD and experimental modelling.

Human occupants generate thermal plumes as a result of body heat, which could significantly influence particle transport and deposition patterns. Future CFD studies may consider including heat sources representative of human occupants to better model real-world scenarios. This could also be experimentally validated by incorporating human heat sources into particle dispersion measurements.

Further experimental research on pathogen viability in aerosolised faecal matter.

Although the current study confirmed the presence of bacterial bioaerosols, the viability of airborne pathogens over time remains a major uncertainty. Future research could focus on pathogen viability, allowing for direct measurement of whether pathogens remain infectious after aerosolisation and airborne transport and if so for what period of time.

Exploring additional mitigation strategies.

The study identified ventilation strategies and time delays as mitigation measures, but further work could examine the effect of toilet lid closure, air purification technologies (e.g. HEPA filtration, UVGI), and antimicrobial surface coatings on reducing exposure risks. In particular, there is debate regarding the effectiveness of toilet lid closure upon contamination, so further work is necessary in this field.

Assessing real-world implications for different toilet facility types.

This research was conducted in a controlled chamber setting, providing valuable baseline data on aerosol and bioaerosol dispersion from toilet flushing. However, more studies are needed to investigate real-world environments such as hospitals, workplaces, transportation hubs, and public event venues to translate these findings

into practical public health recommendations. The QMRA methodology using particle concentration data offers a straightforward approach that could be applied in these settings to estimate infection risks under different occupancy and ventilation conditions.

Currently, there is limited data on the effectiveness of ventilation in toilet facilities. While building regulations provide recommendations for ventilation rates, there is little evidence on the degree to which these standards are met in practice. Understanding the variability in ventilation compliance and performance across different facilities would help identify potential gaps in exposure mitigation and inform more effective design and policy interventions.

6.4 Final Remarks

This thesis has provided new insight on the generation, dispersion, and potential risk of infection associated with airborne exposure to toilet plume aerosols. The integration of experimental data, risk modelling, and computational simulations has improved the understanding of exposure risks in shared toilet facilities. The findings reinforce the importance of ventilation, facility design, and exposure time management to reduce transmission risks.

While challenges remain in fully quantifying the infection risks posed by toilet plume aerosols, this research provides a robust foundation for future work in bioaerosol transmission, infection risk modelling, and indoor air quality interventions. The integration of experimental, computational, and risk assessment approaches offers a scalable framework that can be applied to other pathogens, environments, and mitigation strategies, ultimately contributing to safer and healthier public spaces.

References

[1] World Health Organization. *Global technical consultation report on proposed terminology for pathogens that transmit through the air*. [Online]. 2024. [Accessed 15 March 2025]. Available from: https://www.who.int/publications/m/item/global-technical-consultation-report-on-proposed-terminology-for-pathogens-that-transmit-through-the-air.

[2] Johnson, D., Lynch, R., Marshall, C., Mead, K., and Hirst, D. Aerosol Generation by Modern Flush Toilets. [Online]. *Aerosol Science and Technology*. 2013, **47**(9), pp.1047–1057. [Accessed 14 November 2023]. Available from: https://doi.org/10.1080/02786826.2013.814911.

[3] Henning, D. N. *Use of public washrooms in an enclosed, suburban shopping plaza*. [Online]. National Research Council of Canada, 1977. [Accessed 4 January 2024]. Available from: https://doi.org/10.4224/20359222.

[4] King, M.-F., Noakes, C., Sleigh, A., and Camargo-Valero, M. Bioaerosol deposition in single and two-bed hospital rooms: A numerical and experimental study. [Online]. *Building and Environment*. 2013, **59**, pp.436–447. [Accessed 4 April 2024]. Available from: https://doi.org/10.1016/j.buildenv.2012.09.011.

[5] Lopez, G. U., Gerba, C. P., Tamimi, A. H., Kitajima, M., Maxwell, S. L., and Rose, J. B. Transfer efficiency of bacteria and viruses from porous and nonporous fomites to fingers under different relative humidity conditions. [Online]. *Applied and Environmental Microbiology*. 2013, **79**(18), pp.5728–5734. [Accessed 9 January 2023]. Available from: https://doi.org/10.1128/AEM.01030-13.

[6] Lai, A. C. K., Tan, T. F., Li, W. S., and Ip, D. K. M. Emission strength of airborne pathogens during toilet flushing. [Online]. *Indoor Air*. 2018, **28**(1), pp.73–79. [Accessed 3 September 2024]. Available from: https://doi.org/10.1111/ina.12406.

[7] Zhang, T., Yao, L., Gao, Z., and Wang, F. Particle exposure risk to a lavatory user after flushing a squat toilet. [Online]. *Scientific Reports*. 2022, **12**(1),

article no: 21088 [no pagination]. [Accessed 26 February 2025]. Available from: https://doi.org/10.1038/s41598-022-25106-4.

[8] Li, P., Zhang, T., and Zhang, Y. Measuring the flushing-generated flow and aerosols in lavatory of commercial aircraft. [Online]. *Building and Environment*. 2022, **214**, article no: 108948 [no pagination]. [Accessed 26 February 2025]. Available from: https://doi.org/10.1016/j.buildenv.2022.108948.

[9] Cai, C., Kim, P., Connor, T. H., Liu, Y., and Floyd, E. L. Reducing the particles generated by flushing institutional toilets. [Online]. *Journal of Occupational and Environmental Hygiene*. 2022, **19**(5), pp.318–326. [Accessed 25 February 2025]. Available from: https://doi.org/10.1080/15459624.2022.2053693.

[10] Gerba, C. P., Wallis, C., and Melnick, J. L. Microbiological Hazards of Household Toilets: Droplet Production and the Fate of Residual Organisms. [Online]. *Applied Microbiology*. 1975, **30**(2), pp.229–237. [Accessed 13 November 2023]. Available from: https://doi.org/10.1128/am.30.2.229-237.1975.

[11] Darlow, H. M. and Bale, W. R. Infective hazards of water-closets. [Online]. *The Lancet*. 1959, **273**(7084), pp.1196–1200. [Accessed 13 November 2023]. Available from: https://doi.org/10.1016/S0140-6736(59)91201-2.

[12] Knowlton, S. D., Boles, C. L., Perencevich, E. N., Diekema, D. J., Nonnenmann, M. W., and CDC Epicenters Program. Bioaerosol concentrations generated from toilet flushing in a hospital-based patient care setting. [Online]. *Antimicrobial Resistance & Infection Control*. 2018, **7**(1), article no: 16 [no pagination]. [Accessed 26 February 2025]. Available from: https://doi.org/10.1186/s13756-018-0301-9.

[13] Paddy, E. N., Afolabi, O. O. D., and Sohail, M. Exploring toilet plume bioaerosol exposure dynamics in public toilets using a Design of Experiments approach. [Online]. *Scientific Reports*. 2024, **14**(1), article no: 10665 [no pagination]. [Accessed 21 February 2025]. Available from: https://doi.org/10.1038/s41598-024-61039-w.

[14] Haas, C. N., Rose, J. B., and Gerba, C. P. *Quantitative Microbial Risk Assessment*. [Online]. 2nd ed. Wiley, 2014. [Accessed 15 March 2024]. Available from: https://doi.org/10.1002/9781118910030.

[15] Rangel, J. M., Sparling, P. H., Crowe, C., Griffin, P. M., and Swerdlow, D. L. Epidemiology of Escherichia coli O157:H7 Outbreaks, United States, 1982–2002. [Online]. *Emerging Infectious Diseases*. 2005, **11**(4), pp.603–609. [Accessed 27 February 2025]. Available from: https://doi.org/10.3201/eid1104.040739.

[16] Czepiel, J., Dróżdż, M., Pituch, H., Kuijper, E. J., Perucki, W., Mielimonka, A., Goldman, S., Wultańska, D., Garlicki, A., and Biesiada, G. Clostridium difficile infection: review. [Online]. *European Journal of Clinical Microbiology & Infectious Diseases*. 2019, **38**(7), pp.1211–1221. [Accessed 5 November 2024]. Available from: https://doi.org/10.1007/s10096-019-03539-6.

[17] Teunis, P. F. M., Sukhrie, F. H. A., Vennema, H., Bogerman, J., Beersma, M. F. C., and Koopmans, M. P. G. Shedding of norovirus in symptomatic and asymptomatic infections. [Online]. *Epidemiology and Infection*. 2015, **143**(8), pp.1710–1717. [Accessed 20 November 2024]. Available from: https://doi.org/10.1017/S095026881400274X.

[18] Crawford, S. E., Ramani, S., Tate, J. E., Parashar, U. D., Svensson, L., Hagbom, M., Franco, M. A., Greenberg, H. B., O'Ryan, M., Kang, G., Desselberger, U., and Estes, M. K. Rotavirus infection. [Online]. *Nature Reviews Disease Primers*. 2017, **3**(1), pp.1–16. [Accessed 27 February 2025]. Available from: https://doi.org/10.1038/nrdp.2017.83.

[19] McKinney, K. R., Gong, Y. Y., and Lewis, T. G. Environmental transmission of SARS at Amoy Gardens. [Online]. *Journal of Environmental Health*. 2006, **68**(9), pp.26–52. [Accessed 6 February 2023]. Available from: https://pubmed.ncbi.nlm.nih.gov/32569870/.

[20] Termansen, M. B. and Frische, S. Fecal-oral transmission of SARS-CoV-2: A systematic review of evidence from epidemiological and experimental studies. [Online]. *American Journal of Infection Control*. 2023, **51**(12), pp.1430–1437. [Accessed 19 November 2024]. Available from: https://doi.org/10.1016/j.ajic.2023.04.170.

[21] Tan, M., Tian, Y., Zhang, D., Wang, Q., and Gao, Z. Aerosol Transmission of Norovirus. [Online]. *Viruses*. 2024, **16**(1), article no: 151 [no pagination]. [Accessed 16 May 2024]. Available from: https://doi.org/10.3390/v16010151.

[22] Ahmed, S. M., Hall, A. J., Robinson, A. E., Verhoef, L., Premkumar, P., Parashar, U. D., Koopmans, M., and Lopman, B. A. Global prevalence of norovirus in cases of gastroenteritis: a systematic review and meta-analysis. [Online]. *The Lancet. Infectious Diseases*. 2014, **14**(8), pp.725–730. [Accessed 9 February 2023]. Available from: https://doi.org/10.1016/S1473-3099(14)70767-4.

[23] Sandmann, F. G., Shallcross, L., Adams, N., Allen, D. J., Coen, P. G., Jeanes, A., Kozlakidis, Z., Larkin, L., Wurie, F., Robotham, J. V., Jit, M., and Deeny, S. R. Estimating the Hospital Burden of Norovirus-Associated Gastroenteritis in England and Its Opportunity Costs for Nonadmitted Patients. [Online]. *Clinical Infectious Diseases*. 2018, **67**(5), pp.693–700. [Accessed 11 March 2025]. Available from: https://doi.org/10.1093/cid/ciy167.

[24] Robilotti, E., Deresinski, S., and Pinsky, B. A. Norovirus. [Online]. *Clinical Microbiology Reviews*. 2015, **28**(1), pp.134–164. [Accessed 21 January 2025]. Available from: https://doi.org/10.1128/CMR.00075-14.

[25] UK Health Security Agency. *National norovirus and rotavirus surveillance reports: 2024 to 2025 season*. [Online]. 2025. [Accessed 11 February 2025]. Available from: https://www.gov.uk/government/statistics/national-norovirus-and-rotavirus-surveillance-reports-2024-to-2025-season/national-norovirus-and-rotavirus-report-week-10-report-data-to-week-8-data-up-to-23-february-2025.

[26] NHS England. *NHS norovirus pressure hits winter high*. [Online]. 2025. [Accessed 18 March 2025]. Available from: https://www.england.nhs.uk/2025/01/nhs-norovirus-pressure-hits-winter-high/.

[27] Alsved, M., Nyström, K., Thuresson, S., Nygren, D., Patzi-Churqui, M., Hussein, T., Fraenkel, C.-J., Medstrand, P., and Löndahl, J. Infectivity of exhaled SARS-CoV-2 aerosols is sufficient to transmit COVID-19 within minutes. [Online]. *Scientific Reports*. 2023, **13**(1), article no: 21245 [no pagination]. [Accessed 24 February 2025]. Available from: https://doi.org/10.1038/s41598-023-47829-8.

[28] Hungerford, D., Vivancos, R., Read, J. M., Iturriza-Gomara, M., French, N., and Cunliffe, N. A. Rotavirus vaccine impact and socioeconomic deprivation: an interrupted time-series analysis of gastrointestinal disease outcomes across primary and secondary care in the UK. [Online]. *BMC Medicine*. 2018, **16**(1), article no: 10 [no pagination]. [Accessed 11 March 2025]. Available from: https://doi.org/10.1186/s12916-017-0989-z.

[29] Sadiq, A., Bostan, N., Yinda, K. C., Naseem, S., and Sattar, S. Rotavirus: Genetics, pathogenesis and vaccine advances. [Online]. *Reviews in Medical Virology*. 2018, **28**(6), article no: e2003 [no pagination]. [Accessed 12 March 2024]. Available from: https://doi.org/10.1002/rmv.2003.

[30] Wilde, J., Van, R., Pickering, L., Eiden, J., and Yolken, R. Detection of rotaviruses in the day care environment by reverse transcriptase polymerase chain reaction. [Online]. *The Journal of Infectious Diseases*. 1992, **166**(3), pp.507–511. [Accessed 12 April 2024]. Available from: https://doi.org/10.1093/infdis/166.3.507.

[31] Bager, P., Svalgaard, I. B., Lomholt, F. K., Emborg, H.-D., Christiansen, L. E., Soborg, B., Hviid, A., and Vestergaard, L. S. The hospital and mortality burden of COVID-19 compared with influenza in Denmark: a national observational cohort study, 2022–24. [Online]. *The Lancet Infectious Diseases*. 2025, **0**(0). [Accessed 11 March 2025]. Available from: https://doi.org/10.1016/S1473-3099(24)00806-5.

[32] Liu, E., Dean, C. A., and Elder, K. T. Editorial: The impact of COVID-19 on vulnerable populations. [Online]. *Frontiers in Public Health*. 2023, **11**, article no: 1267723 [no pagination]. [Accessed 12 March 2025]. Available from: https://doi.org/10.3389/fpubh.2023.1267723.

[33] Wu, Y., Guo, C., Tang, L., Hong, Z., Zhou, J., Dong, X., Yin, H., Xiao, Q., Tang, Y., Qu, X., Kuang, L., Fang, X., Mishra, N., Lu, J., Shan, H., Jiang, G., and Huang, X. Prolonged presence of SARS-CoV-2 viral RNA in faecal samples. [Online]. *The Lancet Gastroenterology & Hepatology*. 2020, **5**(5), pp.434–435. [Accessed 11 March 2025]. Available from: https://doi.org/10.1016/S2468-1253(20)30083-2.

[34] Kaper, J. B., Nataro, J. P., and Mobley, H. L. T. Pathogenic Escherichia coli. [Online]. *Nature Reviews Microbiology*. 2004, **2**(2), pp.123–140. [Accessed 11 March 2025]. Available from: https://doi.org/10.1038/nrmicro818.

[35] UK Health Security Agency. *Annual epidemiological commentary: Gram-negative, MRSA, MSSA bacteraemia and C. difficile infections, up to and including financial year 2023 to 2024*. [Online]. 2024. [Accessed 11 March 2025]. Available from: https://www.gov.uk/government/statistics/mrsa-mssa-and-e-coli-bacteraemia-and-c-difficile-infection-annual-epidemiological-commentary/annual-epidemiological-commentary-gram-negative-mrsa-mssa-bacteraemia-and-c-difficile-infections-up-to-and-including-financial-year-2023-to-2024.

[36] Ludden, C., Coll, F., Gouliouris, T., Restif, O., Blane, B., Blackwell, G. A., Kumar, N., Naydenova, P., Crawley, C., Brown, N. M., Parkhill, J., and Peacock, S. J. Defining nosocomial transmission of Escherichia coli and antimicrobial resistance genes: a genomic surveillance study. [Online]. *The Lancet Microbe*. 2021, **2**(9), pp.e472–e480. [Accessed 11 March 2025]. Available from: https://doi.org/10.1016/S2666-5247(21)00117-8.

[37] Manning, S., Alcamo, I., and Heymann, D. *Escherichia Coli Infections*. [Online]. 3rd ed. Chelsea House, 2020. [Accessed 17 March 2025]. Available from: https://books.google.co.uk/books?id=UWmLEAAAQBAJ.

[38] Yu, I. T. S., Li, Y., Wong, T. W., Tam, W., Chan, A. T., Lee, J. H. W., Leung, D. Y. C., and Ho, T. Evidence of Airborne Transmission of the Severe Acute Respiratory Syndrome Virus. [Online]. *New England Journal of Medicine*. 2004, **350**(17), pp.1731–1739. [Accessed 4 March 2025]. Available from: https://doi.org/10.1056/NEJMoa032867.

[39] Kang, M., Wei, J., Yuan, J., Guo, J., Zhang, Y., Hang, J., Qu, Y., Qian, H., Zhuang, Y., Chen, X., Peng, X., Shi, T., Wang, J., Wu, J., Song, T., He, J., Li, Y., and Zhong, N. Probable Evidence of Fecal Aerosol Transmission of SARS-CoV-2 in a High-Rise Building. [Online]. *Annals of Internal Medicine*. 2020,

173(12), pp.974–980. [Accessed 3 February 2023]. Available from: https://doi.org/10.7326/M20-0928.

[40] Malki-Epshtein, L., Adzic, F., Roberts, B. M., Hathway, E. A., Iddon, C., Mustafa, M., and Cook, M. Measurement and rapid assessment of indoor air quality at mass gathering events to assess ventilation performance and reduce aerosol transmission of SARS-CoV-2. [Online]. *Building Services Engineering Research & Technology*. 2023, **44**(2), pp.113–133. [Accessed 19 February 2025]. Available from: https://doi.org/10.1177/01436244221137995.

[41] Ali, W., Hu, Z., Tang, Z.-R., Liu, S.-Y., Nasir, Z. A., Coulon, F., Liu, P., and Yan, C. Quantitative microbial risk assessment of bioaerosol emissions from squat and bidet toilets during flushing. [Online]. *Risk Analysis*. 2025. [Accessed 6 June 2024]. Available from: https://doi.org/10.1111/risa.70000.

[42] Denpetkul, T., Pumkaew, M., Sittipunsakda, O., Leaungwutiwong, P., Mongkolsuk, S., and Sirikanchana, K. Effects of face masks and ventilation on the risk of SARS-CoV-2 respiratory transmission in public toilets: a quantitative microbial risk assessment. [Online]. *Journal of Water and Health*. 2022, **20**(2), pp.300–313. [Accessed 1 March 2025]. Available from: https://doi.org/10.2166/wh.2022.190.

[43] Goforth, M. P., Boone, S. A., Clark, J., Valenzuela, P. B., McKinney, J., Ijaz, M. K., and Gerba, C. P. Impacts of lid closure during toilet flushing and of toilet bowl cleaning on viral contamination of surfaces in United States restrooms. [Online]. *American Journal of Infection Control*. 2024, **52**(2), pp.141–146. [Accessed 8 March 2024]. Available from: https://doi.org/10.1016/j.ajic.2023.11.020.

[44] Johnson, D. L., Lynch, R. A., Villanella, S. M., Jones, J. F., Fang, H., Mead, K. R., and Hirst, D. V. L. Persistence of Bowl Water Contamination during Sequential Flushes of Contaminated Toilets. [Online]. *Journal of environmental health*. 2017, **80**(3), pp.34–49. [Accessed 31 January 2025]. Available from: https://pubmed.ncbi.nlm.nih.gov/29651169/.

[45] Best, E. L., Sandoe, J. A. T., and Wilcox, M. H. Potential for aerosolization of *Clostridium difficile* after flushing toilets: the role of toilet lids in reducing environmental contamination risk. [Online]. *Journal of Hospital Infection*. 2012, **80**(1), pp.1–5. [Accessed 13 February 2024]. Available from: https://doi.org/10.1016/j.jhin.2011.08.010.

[46] Abney, S., Bright, K., McKinney, J., Ijaz, M. K., and Gerba, C. Toilet hygiene—review and research needs. [Online]. *Journal of Applied Microbiology*. 2021, **131**(6), pp.2705–2714. [Accessed 22 February 2025]. Available from: https://doi.org/10.1111/jam.15121.

[47] Barker, J. and Bloomfield, S. F. Survival of Salmonella in bathrooms and toilets in domestic homes following salmonellosis. [Online]. *Journal of Applied Microbiology*. 2000, **89**(1), pp.137–144. [Accessed 4 April 2023]. Available from: https://doi.org/10.1046/j.1365-2672.2000.01091.x.

[48] Abney, S. E., Higham, C. A., Wilson, A. M., Ijaz, M. K., McKinney, J., Reynolds, K. A., and Gerba, C. P. Transmission of Viruses from Restroom Use: A Quantitative Microbial Risk Assessment. [Online]. *Food and Environmental Virology*. 2024, **16**(1), pp.65–78. [Accessed 13 September 2024]. Available from: https://doi.org/10.1007/s12560-023-09580-1.

[49] Barker, J. and Jones, M. V. The potential spread of infection caused by aerosol contamination of surfaces after flushing a domestic toilet. [Online]. *Journal of Applied Microbiology*. 2005, **99**(2), pp.339–347. [Accessed 3 February 2024]. Available from: https://doi.org/10.1111/j.1365-2672.2005.02610.x.

[50] Ali, W., An, D.-z., Yang, Y.-f., Cui, B.-b., Ma, J.-x., Zhu, H., Li, M., Ai, X.-J., and Yan, C. Comparing bioaerosol emission after flushing in squat and bidet toilets: Quantitative microbial risk assessment for defecation and hand washing postures. [Online]. *Building and Environment*. 2022, **221**, article no: 109284 [no pagination]. [Accessed 1 March 2025]. Available from: https://doi.org/10.1016/j.buildenv.2022.109284.

[51] Amoah, I. D., Pillay, L., Deepnarian, N., Awolusi, O., Pillay, K., Ramlal, P., Kumari, S., and Bux, F. Detection of SARS-CoV-2 RNA on contact surfaces within shared sanitation facilities. [Online]. *International Journal of Hygiene and Environmental Health*. 2021, **236**, article no: 113807 [no pagination]. [Accessed 1 March 2025]. Available from: https://doi.org/10.1016/j.ijheh.2021.113807.

[52] Crimaldi, J. P., True, A. C., Linden, K. G., Hernandez, M. T., Larson, L. T., and Pauls, A. K. Commercial toilets emit energetic and rapidly spreading aerosol plumes. [Online]. *Scientific Reports*. 2022, **12**(1), article no: 20493 [no pagination]. [Accessed 1 October 2023]. Available from: https://doi.org/10.1038/s41598-022-24686-5.

[53] Jessen, C. U. Airborne Microorganisms: Occurrance and Control. [Online]. *G.E.C. Gad Forlag, Copenhagen*. 1955. [Accessed 2 February 2023].

[54] Newsom, S. W. B. Microbiology of hospital toilets. [Online]. *The Lancet*. 1972, **300**(7779), pp.700–703. [Accessed 24 February 2025]. Available from: https://doi.org/10.1016/S0140-6736(72)92102-2.

[55] Flügge, C. Ueber Luftinfection. [Online]. *Zeitschrift für Hygiene und Infectionskrankheiten*. 1897, **25**(1), pp.179–224. [Accessed 3 March 2023]. Available from: https://doi.org/10.1007/BF02220473.

[56] Morawska, L., Johnson, G. R., Ristovski, Z. D., Hargreaves, M., Mengersen, K., Corbett, S., Chao, C. Y. H., Li, Y., and Katoshevski, D. Size distribution and sites of origin of droplets expelled from the human respiratory tract during expiratory activities. [Online]. *Journal of Aerosol Science*. 2009, **40**(3), pp.256–269. [Accessed 15 January 2025]. Available from: https://doi.org/10.1016/j.jaerosci.2008.11.002.

[57] Johnson, G. R., Morawska, L., Ristovski, Z. D., Hargreaves, M., Mengersen, K., Chao, C. Y. H., Wan, M. P., Li, Y., Xie, X., Katoshevski, D., and Corbett, S. Modality of human expired aerosol size distributions. [Online]. *Journal of Aerosol Science*. 2011, **42**(12), pp.839–851. [Accessed 24 February 2025]. Available from: https://doi.org/10.1016/j.jaerosci.2011.07.009.

[58] Foat, T. G., Higgins, B., Abbs, C., Maishman, T., Coldrick, S., Kelsey, A., Ivings, M. J., Parker, S. T., and Noakes, C. J. Modeling the effect of temperature and relative humidity on exposure to SARS-CoV-2 in a mechanically ventilated room. [Online]. *Indoor Air*. 2022, **32**(11), article no: e13146 [no pagination]. [Accessed 24 February 2025]. Available from: https://doi.org/10.1111/ina.13146.

[59] Stettler, M. E. J., Nishida, R. T., Oliveira, P. M. de, Mesquita, L. C. C., Johnson, T. J., Galea, E. R., Grandison, A., Ewer, J., Carruthers, D., Sykes, D., Kumar, P., Avital, E., Obeysekara, A. I. B., Doorly, D., Hardalupas, Y., Green, D. C., Coldrick, S., Parker, S., and Boies, A. M. Source terms for benchmarking models of SARS-CoV-2 transmission via aerosols and droplets. [Online]. *Royal Society Open Science*. 2022, **9**(5), article no: 212022 [no pagination]. [Accessed 24 February 2025]. Available from: https://doi.org/10.1098/rsos.212022.

[60] Calmet, H., Inthavong, K., Both, A., Surapaneni, A., Mira, D., Egukitza, B., and Houzeaux, G. Large eddy simulation of cough jet dynamics, droplet transport, and inhalability over a ten minute exposure. [Online]. *Physics of Fluids*. 2021, **33**(12), article no: 125122 [no pagination]. [Accessed 24 February 2025]. Available from: https://doi.org/10.1063/5.0072148.

[61] Coldrick, S., Kelsey, A., Ivings, M. J., Foat, T. G., Parker, S. T., Noakes, C. J., Bennett, A., Rickard, H., and Moore, G. Modeling and experimental study of dispersion and deposition of respiratory emissions with implications for disease transmission. [Online]. *Indoor Air*. 2022, **32**(2), article no: e13000 [no pagination]. [Accessed 13 November 2024]. Available from: https://doi.org/10.1111/ina.13000.

[62] Oliveira, P. M. de, Mesquita, L. C. C., Gkantonas, S., Giusti, A., and Mastorakos, E. Evolution of spray and aerosol from respiratory releases: theoretical estimates for insight on viral transmission. [Online]. *Proceedings of the Royal Society A: Mathematical, Physical and Engineering Sciences*. 2021, **477**(2245), article no: 20200584 [no pagination]. [Accessed 15 January 2025]. Available from: https://doi.org/10.1098/rspa.2020.0584.

[63] Bake, B., Larsson, P., Ljungkvist, G., Ljungström, E., and Olin, A.-C. Exhaled particles and small airways. [Online]. *Respiratory Research*. 2019, **20**(1), article no: 8 [no pagination]. [Accessed 15 January 2025]. Available from: https://doi.org/10.1186/s12931-019-0970-9.

[64] Fennelly, K. P. Particle sizes of infectious aerosols: implications for infection control. [Online]. *The Lancet. Respiratory Medicine*. 2020, **8**(9), pp.914–924. [Accessed 1 March 2025]. Available from: https://doi.org/10.1016/S2213-2600(20)30323-4.

[65] Gregson, F. K., Watson, N. A., Orton, C. M., Haddrell, A. E., McCarthy, L. P., Finnie, T. J., Gent, R., Donaldson, G. C., Shah, P. L., Calder, J. D., Bzdek, B. R., Costello, D., and Reid, J. P. Comparing aerosol concentrations and particle size distributions generated by singing, speaking and breathing. [Online]. *Aerosol Science and Technology*. 2021, **55**(6), pp.681–691. [Accessed 15 January 2025]. Available from: https://doi.org/10.1080/02786826.2021.1883544.

[66] Yan, J., Grantham, M., Pantelic, J., Bueno de Mesquita, P. J., Albert, B., Liu, F., Ehrman, S., Milton, D. K., and EMIT Consortium. Infectious virus in exhaled breath of symptomatic seasonal influenza cases from a college community. [Online]. *Proceedings of the National Academy of Sciences*. 2018, **115**(5), pp.1081–1086. [Accessed 24 February 2025]. Available from: https://doi.org/10.1073/pnas.1716561115.

[67] Lindsley, W. G., Noti, J. D., Blachere, F. M., Thewlis, R. E., Martin, S. B., Othumpangat, S., Noorbakhsh, B., Goldsmith, W. T., Vishnu, A., Palmer, J. E., Clark, K. E., and Beezhold, D. H. Viable Influenza A Virus in Airborne Particles from Human Coughs. [Online]. *Journal of Occupational and Environmental Hygiene*. 2015, **12**(2), pp.107–113. [Accessed 24 February 2025]. Available from: https://doi.org/10.1080/15459624.2014.973113.

[68] Coleman, K. K., Tay, D. J. W., Tan, K. S., Ong, S. W. X., Than, T. S., Koh, M. H., Chin, Y. Q., Nasir, H., Mak, T. M., Chu, J. J. H., Milton, D. K., Chow, V. T. K., Tambyah, P. A., Chen, M., and Tham, K. W. Viral Load of Severe Acute Respiratory Syndrome Coronavirus 2 (SARS-CoV-2) in Respiratory Aerosols Emitted by Patients With Coronavirus Disease 2019 (COVID-19) While Breathing, Talking, and Singing. [Online]. *Clinical Infectious Diseases*.

2022, **74**(10), pp.1722–1728. [Accessed 8 July 2024]. Available from: https://doi.org/10.1093/cid/ciab691.

[69] Malik, M. and Kunze, T. Detection of SARS-CoV-2 RNA in exhaled breath and its potential for prevention measures. [Online]. *Infection Prevention in Practice*. 2023, **5**(3), article no: 100299 [no pagination]. [Accessed 24 February 2025]. Available from: https://doi.org/10.1016/j.infpip.2023.100299.

[70] Lane, G., Zhou, G., Hultquist, J. F., Simons, L. M., Redondo, R. L., Ozer, E. A., McCarthy, D. M., Ison, M. G., Achenbach, C. J., Wang, X., Wai, C. M., Wyatt, E., Aalsburg, A., Yang, Q., Noto, T., Alisoltani, A., Ysselstein, D., Awatramani, R., Murphy, R., Theron, G., and Zelano, C. [Pre-print] Quantity of SARS-CoV-2 RNA copies exhaled per minute during natural breathing over the course of COVID-19 infection. [Online]. *eLife*. 2024. [Accessed 24 February 2025]. Available from: https://doi.org/10.7554/eLife.91686.1.

[71] Leung, N. H. L., Chu, D. K. W., Shiu, E. Y. C., Chan, K.-H., McDevitt, J. J., Hau, B. J. P., Yen, H.-L., Li, Y., Ip, D. K. M., Peiris, J. S. M., Seto, W.-H., Leung, G. M., Milton, D. K., and Cowling, B. J. Respiratory virus shedding in exhaled breath and efficacy of face masks. [Online]. *Nature Medicine*. 2020, **26**(5), pp.676–680. [Accessed 24 February 2025]. Available from: https://doi.org/10.1038/s41591-020-0843-2.

[72] Fabian, P., Brain, J., Houseman, E. A., Gern, J., and Milton, D. K. Origin of exhaled breath particles from healthy and human rhinovirus-infected subjects. [Online]. *Journal of Aerosol Medicine and Pulmonary Drug Delivery*. 2011, **24**(3), pp.137–147. [Accessed 10 October 2024]. Available from: https://doi.org/10.1089/jamp.2010.0815.

[73] Ghumra, D. P., Shetty, N., McBrearty, K. R., Puthussery, J. V., Sumlin, B. J., Gardiner, W. D., Doherty, B. M., Magrecki, J. P., Brody, D. L., Esparza, T. J., O'Halloran, J. A., Presti, R. M., Bricker, T. L., Boon, A. C. M., Yuede, C. M., Cirrito, J. R., and Chakrabarty, R. K. Rapid Direct Detection of SARS-CoV-2 Aerosols in Exhaled Breath at the Point of Care. [Online]. *ACS Sensors*. 2023, **8**(8), pp.3023–3031. [Accessed 24 February 2025]. Available from: https://doi.org/10.1021/acssensors.3c00512.

[74] Lai, J., Coleman, K. K., Tai, S. H. S., German, J., Hong, F., Albert, B., Esparza, Y., Srikakulapu, A. K., Schanz, M., Maldonado, I. S., Oertel, M., Fadul, N., Gold, T. L., Weston, S., Mullins, K., McPhaul, K. M., Frieman, M., and Milton, D. K. Exhaled Breath Aerosol Shedding of Highly Transmissible Versus Prior Severe Acute Respiratory Syndrome Coronavirus 2 Variants. [Online]. *Clinical Infectious Diseases*. 2022, **76**(5), pp.786–794. [Accessed 24 February 2025]. Available from: https://doi.org/10.1093/cid/ciac846.

[75] Adenaiye, O. O., Lai, J., Bueno de Mesquita, P. J., Hong, F., Youssefi, S., German, J., Tai, S. H. S., Albert, B., Schanz, M., Weston, S., Hang, J., Fung, C., Chung, H. K., Coleman, K. K., Sapoval, N., Treangen, T., Berry, I. M., Mullins, K., Frieman, M., Ma, T., and Milton, D. K. Infectious Severe Acute Respiratory Syndrome Coronavirus 2 (SARS-CoV-2) in Exhaled Aerosols and Efficacy of Masks During Early Mild Infection. [Online]. *Clinical Infectious Diseases*. 2021, **75**(1), pp.e241–e248. [Accessed 24 February 2025]. Available from: https://doi.org/10.1093/cid/ciab797.

[76] Zheng, Y., Chen, H., Yao, M., and Li, X. Bacterial pathogens were detected from human exhaled breath using a novel protocol. [Online]. *Journal of Aerosol Science*. 2018, **117**, pp.224–234. [Accessed 24 February 2025]. Available from: https://doi.org/10.1016/j.jaerosci.2017.12.009.

[77] Anisuzzaman, n., Hossain, M. S., Hatta, T., Labony, S. S., Kwofie, K. D., Kawada, H., Tsuji, N., and Alim, M. A. Food- and vector-borne parasitic zoonoses: Global burden and impacts. [Online]. *Advances in Parasitology*. 2023, **120**, pp.87–136. [Accessed 15 March 2025]. Available from: https://doi.org/10.1016/bs.apar.2023.02.001.

[78] Abney, S. E., Ijaz, M. K., McKinney, J., and Gerba, C. P. Laundry Hygiene and Odor Control: State of the Science. [Online]. *Applied and Environmental Microbiology*. 2021, **87**(14), article no: e03002-20 [no pagination]. [Accessed 24 February 2025]. Available from: https://doi.org/10.1128/AEM.03002-20.

[79] Rashid, T., VonVille, H., Hasan, I., and Garey, K. Shoe soles as a potential vector for pathogen transmission: a systematic review. [Online]. *Journal of Applied Microbiology*. 2016, **121**(5), pp.1223–1231. [Accessed 24 February 2025]. Available from: https://doi.org/10.1111/jam.13250.

[80] Wells, W. F. On Air-borne infection Study II. Droplets and Droplet Nuclei. [Online]. *American Journal of Epidemiology*. 1934, **20**(3), pp.611–618. [Accessed 14 December 2023]. Available from: https://doi.org/10.1093/oxfordjournals.aje.a118097.

[81] Randall, K., Ewing, E. T., Marr, L. C., Jimenez, J. L., and Bourouiba, L. How did we get here: what are droplets and aerosols and how far do they go? A historical perspective on the transmission of respiratory infectious diseases. [Online]. *Interface Focus*. 2021, **11**(6), article no: 20210049 [no pagination]. [Accessed 25 February 2025]. Available from: https://doi.org/10.1098/rsfs.2021.0049.

[82] Sayers, R. R. and Jones, R. R. Silicosis and Similar Dust Diseases: Medical Aspects and Control. [Online]. *Public Health Reports (1896-1970)*. 1938, **53**(33), pp.1453–1472. [Accessed 25 February 2025]. Available from: https://doi.org/10.2307/4582633.

[83] Wijk, A. M. V. and Patterson, H. S. The Percentage of Particles of Different Sizes Removed from Dust-Laden Air by Breathing. [Online]. *Journal of Industrial Hygiene*. 1940, **22**, pp.31–35. [Accessed 25 February 2025]. Available from: https://www.cabdirect.org/cabdirect/abstract/19422200462.

[84] Langmuir, A. D. The Potentialities of Biological Warfare against Man: An Epidemiological Appraisal. [Online]. *Public Health Reports (1896-1970)*. 1951, **66**(13), pp.387–399. [Accessed 15 January 2025]. Available from: https://doi.org/10.2307/4587679.

[85] Wells, W. F. Airborne Contagion and Air Hygiene: An Ecological Study of Droplet Infections. [Online]. *Journal of the American Medical Association*. 1955, **159**(1), p.90. [Accessed 15 January 2025]. Available from: https://doi.org/10.1001/jama.1955.02960180092033.

[86] Bourouiba, L. Turbulent Gas Clouds and Respiratory Pathogen Emissions: Potential Implications for Reducing Transmission of COVID-19. [Online]. *JAMA*. 2020, **323**(18), pp.1837–1838. [Accessed 18 December 2024]. Available from: https://doi.org/10.1001/jama.2020.4756.

[87] Hou, Y. J., Okuda, K., Edwards, C. E., Martinez, D. R., Asakura, T., Dinnon, K. H., Kato, T., Lee, R. E., Yount, B. L., Mascenik, T. M., Chen, G., Olivier, K. N., Ghio, A., Tse, L. V., Leist, S. R., Gralinski, L. E., Schäfer, A., Dang, H., Gilmore, R., Nakano, S., Sun, L., Fulcher, M. L., Livraghi-Butrico, A., Nicely, N. I., Cameron, M., Cameron, C., Kelvin, D. J., Silva, A. de, Margolis, D. M., Markmann, A., Bartelt, L., Zumwalt, R., Martinez, F. J., Salvatore, S. P., Borczuk, A., Tata, P. R., Sontake, V., Kimple, A., Jaspers, I., O'Neal, W. K., Randell, S. H., Boucher, R. C., and Baric, R. S. SARS-CoV-2 Reverse Genetics Reveals a Variable Infection Gradient in the Respiratory Tract. [Online]. *Cell*. 2020, **182**(2), pp.429–446. [Accessed 15 March 2025]. Available from: https://doi.org/10.1016/j.cell.2020.05.042.

[88] Chin, A. W. H., Chu, J. T. S., Perera, M. R. A., Hui, K. P. Y., Yen, H.-L., Chan, M. C. W., Peiris, M., and Poon, L. L. M. Stability of SARS-CoV-2 in different environmental conditions. [Online]. *The Lancet Microbe*. 2020, **1**(1), p.e10. [Accessed 15 January 2025]. Available from: https://doi.org/10.1016/S2666-5247(20)30003-3.

[89] Biryukov, J., Boydston, J. A., Dunning, R. A., Yeager, J. J., Wood, S., Reese, A. L., Ferris, A., Miller, D., Weaver, W., Zeitouni, N. E., Phillips, A., Freeburger, D., Hooper, I., Ratnesar-Shumate, S., Yolitz, J., Krause, M., Williams, G., Dawson, D. G., Herzog, A., Dabisch, P., Wahl, V., Hevey, M. C., and Altamura, L. A. Increasing Temperature and Relative Humidity Accelerates Inactivation of SARS-CoV-2 on Surfaces. [Online]. *mSphere*. 2020, **5**(4),

article no: e00441-20 [no pagination]. [Accessed 15 January 2025]. Available from: https://doi.org/10.1128/msphere.00441-20.

[90] McEldowney, S. and Fletcher, M. The effect of temperature and relative humidity on the survival of bacteria attached to dry solid surfaces. [Online]. *Letters in Applied Microbiology*. 1988, **7**(4), pp.83–86. [Accessed 25 February 2025]. Available from: https://doi.org/10.1111/j.1472-765X.1988.tb01258.x.

[91] Pal, R., Sarkar, S., and Mukhopadhyay, A. Influence of ambient conditions on evaporation and transport of respiratory droplets in indoor environment. [Online]. *International Communications in Heat and Mass Transfer*. 2021, **129**, article no: 105750 [no pagination]. [Accessed 15 January 2025]. Available from: https://doi.org/10.1016/j.icheatmasstransfer.2021.105750.

[92] Walker, M. D., Vincent, J. C., Benson, L., Stone, C. A., Harris, G., Ambler, R. E., Watts, P., Slatter, T., López-García, M., King, M.-F., Noakes, C. J., and Thomas, R. J. Effect of Relative Humidity on Transfer of Aerosol-Deposited Artificial and Human Saliva from Surfaces to Artificial Finger-Pads. [Online]. *Viruses*. 2022, **14**(5), article no: 1048 [no pagination]. [Accessed 2 January 2025]. Available from: https://doi.org/10.3390/v14051048.

[93] Liu, F., Qian, H., Luo, Z., Wang, S., and Zheng, X. A laboratory study of the expiratory airflow and particle dispersion in the stratified indoor environment. [Online]. *Building and Environment*. 2020, **180**, article no: 106988 [no pagination]. [Accessed 12 March 2025]. Available from: https://doi.org/10.1016/j.buildenv.2020.106988.

[94] Qian, H., Li, Y., Nielsen, P. V., Hyldgaard, C. E., Wong, T. W., and Chwang, A. T. Y. Dispersion of exhaled droplet nuclei in a two-bed hospital ward with three different ventilation systems. [Online]. *Indoor Air*. 2006, **16**(2), pp.111–128. [Accessed 12 March 2025]. Available from: https://doi.org/10.1111/j.1600-0668.2005.00407.x.

[95] Sze To, G. N., Wan, M. P., Chao, C. Y. H., Fang, L., and Melikov, A. Experimental Study of Dispersion and Deposition of Expiratory Aerosols in Aircraft Cabins and Impact on Infectious Disease Transmission. [Online]. *Aerosol Science and Technology*. 2009, **43**(5), pp.466–485. [Accessed 18 March 2025]. Available from: https://doi.org/10.1080/02786820902736658.

[96] Sun, S., Li, J., and Han, J. How human thermal plume influences near-human transport of respiratory droplets and airborne particles: a review. [Online]. *Environmental Chemistry Letters*. 2021, **19**(3), pp.1971–1982. [Accessed 12 March 2025]. Available from: https://doi.org/10.1007/s10311-020-01178-4.

[97] Hobday, R. A. and Dancer, S. J. Roles of sunlight and natural ventilation for controlling infection: historical and current perspectives. [Online]. *Journal of Hospital Infection*. 2013, **84**(4), pp.271–282. [Accessed 12 March 2025]. Available from: https://doi.org/10.1016/j.jhin.2013.04.011.

[98] Raiteux, J., Eschlimann, M., Marangon, A., Rogée, S., Dadvisard, M., Taysse, L., and Larigauderie, G. Inactivation of SARS-CoV-2 by Simulated Sunlight on Contaminated Surfaces. [Online]. *Microbiology Spectrum*. 2021, **9**(1), article no: e0033321 [no pagination]. [Accessed 13 March 2025]. Available from: https://doi.org/10.1128/spectrum.00333-21.

[99] Schuit, M., Gardner, S., Wood, S., Bower, K., Williams, G., Freeburger, D., and Dabisch, P. The Influence of Simulated Sunlight on the Inactivation of Influenza Virus in Aerosols. [Online]. *The Journal of Infectious Diseases*. 2020, **221**(3), pp.372–378. [Accessed 11 August 202]. Available from: https://doi.org/10.1093/infdis/jiz582.

[100] West, R., Michie, S., Rubin, G. J., and Amlôt, R. Applying principles of behaviour change to reduce SARS-CoV-2 transmission. [Online]. *Nature Human Behaviour*. 2020, **4**(5), pp.451–459. [Accessed 15 January 2025]. Available from: https://doi.org/10.1038/s41562-020-0887-9.

[101] Mousa, A., Winskill, P., Watson, O. J., Ratmann, O., Monod, M., Ajelli, M., Diallo, A., Dodd, P. J., Grijalva, C. G., Kiti, M. C., Krishnan, A., Kumar, R., Kumar, S., Kwok, K. O., Lanata, C. F., Waroux, O. L. P. de, Leung, K., Mahikul, W., Melegaro, A., Morrow, C. D., Mossong, J., Neal, E. F., Nokes, D. J., Pan-ngum, W., Potter, G. E., Russell, F. M., Saha, S., Sugimoto, J. D., Wei, W. I., Wood, R. R., Wu, J., Zhang, J., Walker, P., and Whittaker, C. Social contact patterns and implications for infectious disease transmission – a systematic review and meta-analysis of contact surveys. [Online]. *eLife*. 2021, **10**, article no: e70294 [no pagination]. [Accessed 12 March 2025]. Available from: https://doi.org/10.7554/eLife.70294.

[102] Marks, M., Millat-Martinez, P., Ouchi, D., Roberts, C. h., Alemany, A., Corbacho-Monné, M., Ubals, M., Tobias, A., Tebé, C., Ballana, E., Bassat, Q., Baro, B., Vall-Mayans, M., G-Beiras, C., Prat, N., Ara, J., Clotet, B., and Mitjà, O. Transmission of COVID-19 in 282 clusters in Catalonia, Spain: a cohort study. [Online]. *The Lancet Infectious Diseases*. 2021, **21**(5), pp.629–636. [Accessed 15 January 2025]. Available from: https://doi.org/10.1016/S1473-3099(20)30985-3.

[103] Marc, A., Kerioui, M., Blanquart, F., Bertrand, J., Mitjà, O., Corbacho-Monné, M., Marks, M., and Guedj, J. Quantifying the relationship between SARS-CoV-2 viral load and infectiousness. [Online]. *eLife*. 2021, **10**, arti-

cle no: e69302 [no pagination]. [Accessed 2 February 2025]. Available from: https://doi.org/10.7554/eLife.69302.

[104] Memoli, M. J., Czajkowski, L., Reed, S., Athota, R., Bristol, T., Proudfoot, K., Fargis, S., Stein, M., Dunfee, R. L., Shaw, P. A., Davey, R. T., and Taubenberger, J. K. Validation of the Wild-type Influenza A Human Challenge Model H1N1pdMIST: An A(H1N1)pdm09 Dose-Finding Investigational New Drug Study. [Online]. *Clinical Infectious Diseases*. 2015, **60**(5), pp.693–702. [Accessed 25 February 2025]. Available from: https://doi.org/10.1093/cid/ciu924.

[105] Mayer, B. T., Krantz, E. M., Wald, A., Corey, L., Casper, C., Gantt, S., and Schiffer, J. T. Estimating the Risk of Human Herpesvirus 6 and Cytomegalovirus Transmission to Ugandan Infants from Viral Shedding in Saliva by Household Contacts. [Online]. *Viruses*. 2020, **12**(2), article no: 171 [no pagination]. [Accessed 25 February 2025]. Available from: https://doi.org/10.3390/v12020171.

[106] Boucoiran, I., Mayer, B. T., Krantz, E. M., Marchant, A., Pati, S., Boppana, S., Wald, A., Corey, L., Casper, C., Schiffer, J. T., and Gantt, S. Non-Primary Maternal CMV Infection Following Viral Shedding in Infants. [Online]. *The Pediatric infectious disease journal*. 2018, **37**(7), pp.627–631. [Accessed 25 February 2025]. Available from: https://doi.org/10.1097/INF.0000000000001877.

[107] Zeng, L., Li, J., Lv, M., Li, Z., Yao, L., Gao, J., Wu, Q., Wang, Z., Yang, X., Tang, G., Qu, G., and Jiang, G. Environmental Stability and Transmissibility of Enveloped Viruses at Varied Animate and Inanimate Interfaces. [Online]. *Environment & Health*. 2023, **1**(1), pp.15–31. [Accessed 12 March 2025]. Available from: https://doi.org/10.1021/envhealth.3c00005.

[108] Vasickova, P., Pavlik, I., Verani, M., and Carducci, A. Issues Concerning Survival of Viruses on Surfaces. [Online]. *Food and Environmental Virology*. 2010, **2**(1), pp.24–34. [Accessed 12 March 2025]. Available from: https://doi.org/10.1007/s12560-010-9025-6.

[109] Katzenberger, R. H., Rösel, A., and Vonberg, R.-P. Bacterial survival on inanimate surfaces: a field study. [Online]. *BMC Research Notes*. 2021, **14**(1), article no: 97 [no pagination]. [Accessed 12 March 2025]. Available from: https://doi.org/10.1186/s13104-021-05492-0.

[110] Kreider, J., Curtiss, P., and Rabl, A. *Heating and Cooling of Buildings: Design for Efficiency*. [Online]. 3rd ed. CRC Press, 2016. [Accessed 17 March 2025]. Available from: https://doi.org/10.1201/9781315374567-24.

[111] Scientific Advisory Group for Emergencies. *Environmental Modelling Group: Role of ventilation in controlling SARS-CoV-2 transmission*. [Online]. 2020. [Accessed 15 March 2025]. Available from: https://www.gov.uk/government/publications/emg-role-of-ventilation-in-controlling-sars-cov-2-transmission-30-september-2020.

[112] Lipinski, T., Ahmad, D., Serey, N., and Jouhara, H. Review of ventilation strategies to reduce the risk of disease transmission in high occupancy buildings. [Online]. *International Journal of Thermofluids*. 2020, **7-8**, article no: 100045 [no pagination]. [Accessed 25 February 2025]. Available from: https://doi.org/10.1016/j.ijft.2020.100045.

[113] Department for Levelling Up, Housing and Communities. *The Building Regulations 2010. Approved Document F: Ventilation*. [Online]. HM Government, 2021. [Accessed 3 December 2025]. Available from: https://www.gov.uk/government/publications/ventilation-approved-document-f.

[114] Roberts, B. M., Adzic, F., Hathway, E. A., Iddon, C., Jones, B., Cook, M. J., and Malki-Epshtein, L., Measurement of ventilation effectiveness and indoor air quality in toilets at mass gathering events. In: *43rd AIVC, 11th TightVent Conference and 9th Venticool Conference 2023, 4 - 5 October 2023, Copenhagen*. [Online]. AIVC, 2023, pp.575–584. [Accessed 13 March 2025]. Available from: https://www.aivc.org/resource/measurement-ventilation-effectiveness-and-indoor-air-quality-toilets-mass-gathering-events?volume=39582.

[115] Lee, M. C. J. and Tham, K. W. Public toilets with insufficient ventilation present high cross infection risk. [Online]. *Scientific Reports*. 2021, **11**(1), article no: 20623 [no pagination]. [Accessed 13 March 2025]. Available from: https://doi.org/10.1038/s41598-021-00166-0.

[116] Jung, J., Lee, J., Jo, S., Bae, S., Kim, J. Y., Cha, H. H., Lim, Y.-J., Kwak, S. H., Hong, M. J., Kim, E. O., Bae, J.-Y., Kang, C., Sung, M., Park, M.-S., and Kim, S.-H. Nosocomial Outbreak of COVID-19 in a Hematologic Ward. [Online]. *Infection & Chemotherapy*. 2021, **53**(2), pp.332–341. [Accessed 8 March 2024]. Available from: https://doi.org/10.3947/ic.2021.0046.

[117] Li, T., Katz, A., Osei-Twum, J.-A., James, L., Leung, V., Bozek, P., Persaud, N., O'Campo, P., and Siegel, J. A. Science tells us that portable air filters reduce infection risk. It's time for public health authorities to make this clear. [Online]. *Journal of Infection and Public Health*. 2025, **18**(3), article no: 102650 [no pagination]. [Accessed 26 February 2025]. Available from: https://doi.org/10.1016/j.jiph.2024.102650.

[118] Buising, K. L., Schofield, R., Irving, L., Keywood, M., Stevens, A., Keogh, N., Skidmore, G., Wadlow, I., Kevin, K., Rismanchi, B., Wheeler, A. J., Humphries, R. S., Kainer, M., Monty, J., McGain, F., and Marshall, C. Use of portable air cleaners to reduce aerosol transmission on a hospital coronavirus disease 2019 (COVID-19) ward. [Online]. *Infection Control and Hospital Epidemiology*. 2022, **43**(8), pp.987–992. [Accessed 17 March 2025]. Available from: https://doi.org/10.1017/ice.2021.284.

[119] Derk, R. C., Coyle, J. P., Lindsley, W. G., Blachere, F. M., Lemons, A. R., Service, S. K., Martin, S. B., Mead, K. R., Fotta, S. A., Reynolds, J. S., McKinney, W. G., Sinsel, E. W., Beezhold, D. H., and Noti, J. D. Efficacy of Do-It-Yourself air filtration units in reducing exposure to simulated respiratory aerosols. [Online]. *Building and Environment*. 2023, **229**, article no: 109920 [no pagination]. [Accessed 17 March 2025]. Available from: https://doi.org/10.1016/j.buildenv.2022.109920.

[120] Coyle, J. P., Derk, R. C., Lindsley, W. G., Blachere, F. M., Boots, T., Lemons, A. R., Martin, S. B., Mead, K. R., Fotta, S. A., Reynolds, J. S., McKinney, W. G., Sinsel, E. W., Beezhold, D. H., and Noti, J. D. Efficacy of Ventilation, HEPA Air Cleaners, Universal Masking, and Physical Distancing for Reducing Exposure to Simulated Exhaled Aerosols in a Meeting Room. [Online]. *Viruses*. 2021, **13**(12), article no: 2536 [no pagination]. [Accessed 17 March 2025]. Available from: https://doi.org/10.3390/v13122536.

[121] Fennelly, M., Hellebust, S., Wenger, J., O'Connor, D., Griffith, G. W., Plant, B. J., and Prentice, M. B. Portable HEPA filtration successfully augments natural-ventilation-mediated airborne particle clearance in a legacy design hospital ward. [Online]. *Journal of Hospital Infection*. 2023, **131**, pp.54–57. [Accessed 26 February 2025]. Available from: https://doi.org/10.1016/j.jhin.2022.09.017.

[122] Rutala, W. A., Jones, S. M., Worthington, J. M., Reist, P. C., and Weber, D. J. Efficacy of portable filtration units in reducing aerosolized particles in the size range of Mycobacterium tuberculosis. [Online]. *Infection Control and Hospital Epidemiology*. 1995, **16**(7), pp.391–398. [Accessed 17 March 2025]. Available from: https://doi.org/10.1086/647136.

[123] Conway Morris, A., Sharrocks, K., Bousfield, R., Kermack, L., Maes, M., Higginson, E., Forrest, S., Pereira-Dias, J., Cormie, C., Old, T., Brooks, S., Hamed, I., Koenig, A., Turner, A., White, P., Floto, R. A., Dougan, G., Gkrania-Klotsas, E., Gouliouris, T., Baker, S., and Navapurkar, V. The Removal of Airborne Severe Acute Respiratory Syndrome Coronavirus 2 (SARS-CoV-2) and Other Microbial Bioaerosols by Air Filtration on Coronavirus Disease 2019 (COVID-19) Surge Units. [Online]. *Clinical Infectious Diseases*.

2022, **75**(1), pp.e97–e101. [Accessed 17 March 2025]. Available from: https://doi.org/10.1093/cid/ciab933.

[124] Thuresson, S., Fraenkel, C. J., Sasinovich, S., Soldemyr, J., Widell, A., Medstrand, P., Alsved, M., and Löndahl, J. Airborne Severe Acute Respiratory Syndrome Coronavirus 2 (SARS-CoV-2) in Hospitals: Effects of Aerosol-Generating Procedures, HEPA-Filtration Units, Patient Viral Load, and Physical Distance. [Online]. *Clinical Infectious Diseases*. 2022, **75**(1), pp.e89–e96. [Accessed 17 March 2025]. Available from: https://doi.org/10.1093/cid/ciac161.

[125] Ueki, H., Ujie, M., Komori, Y., Kato, T., Imai, M., and Kawaoka, Y. Effectiveness of HEPA Filters at Removing Infectious SARS-CoV-2 from the Air. [Online]. *mSphere*. 2022, **7**(4), article no: e0008622 [no pagination]. [Accessed 17 March 2025]. Available from: https://doi.org/10.1128/msphere.00086-22.

[126] Myers, N. T., Laumbach, R. J., Black, K. G., Ohman-Strickland, P., Alimokhtari, S., Legard, A., De Resende, A., Calderon, L., Lu, F. T., Mainelis, G., and Kipen, H. M. Portable air cleaners and residential exposure to SARS-CoV-2 aerosols: A real-world study. [Online]. *Indoor Air*. 2022, **32**(4), article no: e13029 [no pagination]. [Accessed 17 March 2025]. Available from: https://doi.org/10.1111/ina.13029.

[127] Boswell, T. C. and Fox, P. C. Reduction in MRSA environmental contamination with a portable HEPA-filtration unit. [Online]. *The Journal of Hospital Infection*. 2006, **63**(1), pp.47–54. [Accessed 17 March 2025]. Available from: https://doi.org/10.1016/j.jhin.2005.11.011.

[128] Kowalski, W. *UVGI Disinfection Theory*. [Online]. Springer, 2009. [Accessed 26 February 2025]. Available from: https://doi.org/10.1007/978-3-642-01999-9_2.

[129] Buonanno, M., Ponnaiya, B., Welch, D., Stanislauskas, M., Randers-Pehrson, G., Smilenov, L., Lowy, F. D., Owens, D. M., and Brenner, D. J. Germicidal Efficacy and Mammalian Skin Safety of 222-nm UV Light. [Online]. *Radiation research*. 2017, **187**(4), pp.483–491. [Accessed 26 February 2025]. Available from: https://doi.org/10.1667/RR0010CC.1.

[130] Tavares, R. S. N., Adamoski, D., Girasole, A., Lima, E. N., Silva Justo-Junior, A. da, Domingues, R., Silveira, A. C. C., Marques, R. E., Carvalho, M. de, Ambrosio, A. L. B., Leme, A. F. P., and Dias, S. M. G. Different biological effects of exposure to far-UVC (222 nm) and near-UVC (254 nm) irradiation. [Online]. *Journal of Photochemistry and Photobiology B: Biology*. 2023, **243**, article no: 112713 [no pagination]. [Accessed 26 February 2025]. Available from: https://doi.org/10.1016/j.jphotobiol.2023.112713.

[131] Bueno de Mesquita, P. J., Sokas, R. K., Rice, M. B., and Nardell, E. A. Far-UVC: Technology Update with an Untapped Potential to Mitigate Airborne Infections. [Online]. *Annals of the American Thoracic Society*. 2023, **20**(12), pp.1700–1702. [Accessed 26 February 2025]. Available from: https://doi.org/10.1513/AnnalsATS.202305-460VP.

[132] Eadie, E., Hiwar, W., Fletcher, L., Tidswell, E., O'Mahoney, P., Buonanno, M., Welch, D., Adamson, C. S., Brenner, D. J., Noakes, C., and Wood, K. Far-UVC (222 nm) efficiently inactivates an airborne pathogen in a room-sized chamber. [Online]. *Scientific Reports*. 2022, **12**(1), article no: 4373 [no pagination]. [Accessed 17 March 2025]. Available from: https://doi.org/10.1038/s41598-022-08462-z.

[133] Welch, D., Buonanno, M., Grilj, V., Shuryak, I., Crickmore, C., Bigelow, A. W., Randers-Pehrson, G., Johnson, G. W., and Brenner, D. J. Far-UVC light: A new tool to control the spread of airborne-mediated microbial diseases. [Online]. *Scientific Reports*. 2018, **8**(1), article no: 2752 [no pagination]. [Accessed 17 March 2025]. Available from: https://doi.org/10.1038/s41598-018-21058-w.

[134] Kitagawa, H., Nomura, T., Nazmul, T., Omori, K., Shigemoto, N., Sakaguchi, T., and Ohge, H. Effectiveness of 222-nm ultraviolet light on disinfecting SARS-CoV-2 surface contamination. [Online]. *American Journal of Infection Control*. 2021, **49**(3), pp.299–301. [Accessed 17 March 2025]. Available from: https://doi.org/10.1016/j.ajic.2020.08.022.

[135] Kaple, C. E., Memic, S., Cadnum, J. L., and Donskey, C. J. Evaluation of an automated far ultraviolet-C light technology for decontamination of surfaces and aerosolized viruses in bathrooms. [Online]. *Antimicrobial Resistance & Infection Control*. 2024, **13**(1), article no: 114 [no pagination]. [Accessed 26 February 2025]. Available from: https://doi.org/10.1186/s13756-024-01473-7.

[136] Bang, J.-I., Jo, Y.-L., Lee, E.-T., and Sung, M. Far-UVC (222 nm) disinfection performance in residential spaces: Experimental study on *Bacillus subtilis* contamination. [Online]. *Results in Engineering*. 2025, **25**, article no: 103642 [no pagination]. [Accessed 26 February 2025]. Available from: https://doi.org/10.1016/j.rineng.2024.103642.

[137] Kitagawa, H., Kaiki, Y., Tadera, K., Nomura, T., Omori, K., Shigemoto, N., Takahashi, S., and Ohge, H. Pilot study on the decontamination efficacy of an installed 222-nm ultraviolet disinfection device (Care222™), with a motion sensor, in a shared bathroom. [Online]. *Photodiagnosis and Photodynamic Therapy*. 2021, **34**, article no: 102334 [no pagination]. [Accessed 26 February 2025]. Available from: https://doi.org/10.1016/j.pdpdt.2021.102334.

[138] Browne, K. and Mitchell, B. G. Multimodal environmental cleaning strategies to prevent healthcare-associated infections. [Online]. *Antimicrobial Resistance & Infection Control*. 2023, **12**(1), article no: 83 [no pagination]. [Accessed 26 February 2025]. Available from: https://doi.org/10.1186/s13756-023-01274-4.

[139] Donskey, C. J. Does improving surface cleaning and disinfection reduce health care-associated infections? [Online]. *American Journal of Infection Control*. 2013, **41**(5), pp.S12–S19. [Accessed 17 March 2025]. Available from: https://doi.org/10.1016/j.ajic.2012.12.010.

[140] Sassi, H. P., Reynolds, K. A., Pepper, I. L., and Gerba, C. P. Evaluation of hospital-grade disinfectants on viral deposition on surfaces after toilet flushing. [Online]. *American Journal of Infection Control*. 2018, **46**(5), pp.507–511. [Accessed 17 March 2025]. Available from: https://doi.org/10.1016/j.ajic.2017.11.005.

[141] Kollepara, P. K., Siegenfeld, A. F., Taleb, N. N., and Bar-Yam, Y. Unmasking the mask studies: why the effectiveness of surgical masks in preventing respiratory infections has been underestimated. [Online]. *Journal of Travel Medicine*. 2021, article no: taab144 [no pagination]. [Accessed 25 February 2025]. Available from: https://doi.org/10.1093/jtm/taab144.

[142] Das, S., Sarkar, S., Das, A., Das, S., Chakraborty, P., and Sarkar, J. A comprehensive review of various categories of face masks resistant to Covid-19. [Online]. *Clinical Epidemiology and Global Health*. 2021, **12**, article no: 100835 [no pagination]. [Accessed 13 March 2025]. Available from: https://doi.org/10.1016/j.cegh.2021.100835.

[143] MacIntyre, C. R. and Chughtai, A. A. A rapid systematic review of the efficacy of face masks and respirators against coronaviruses and other respiratory transmissible viruses for the community, healthcare workers and sick patients. [Online]. *International Journal of Nursing Studies*. 2020, **108**, article no: 103629 [no pagination]. [Accessed 25 February 2025]. Available from: https://doi.org/10.1016/j.ijnurstu.2020.103629.

[144] Barasheed, O., Almasri, N., Badahdah, A.-M., Heron, L., Taylor, J., McPhee, K., Ridda, I., Haworth, E., Dwyer, D. E., and Rashid, H. Pilot Randomised Controlled Trial to Test Effectiveness of Facemasks in Preventing Influenza-like Illness Transmission among Australian Hajj Pilgrims in 2011. [Online]. *Infectious Disorders - Drug Targets*. 2014, pp.110–116. [Accessed 25 February 2025]. Available from: https://doi.org/10.2174/1871526514666141021112855.

[145] Canini, L., Andréoletti, L., Ferrari, P., D'Angelo, R., Blanchon, T., Lemaitre, M., Filleul, L., Ferry, J.-P., Desmaizieres, M., Smadja, S., Valleron, A.-J., and Carrat, F. Surgical Mask to Prevent Influenza Transmission in Households: A Cluster Randomized Trial. [Online]. *PLOS ONE*. 2010, **5**(11), article no: e13998 [no pagination]. [Accessed 25 February 2025]. Available from: https://doi.org/10.1371/journal.pone.0013998.

[146] Johnson, D. F., Druce, J. D., Birch, C., and Grayson, M. L. A Quantitative Assessment of the Efficacy of Surgical and N95 Masks to Filter Influenza Virus in Patients with Acute Influenza Infection. [Online]. *Clinical Infectious Diseases*. 2009, **49**(2), pp.275–277. [Accessed 25 February 2025]. Available from: https://doi.org/10.1086/600041.

[147] MacIntyre, C. R., Zhang, Y., Chughtai, A. A., Seale, H., Zhang, D., Chu, Y., Zhang, H., Rahman, B., and Wang, Q. Cluster randomised controlled trial to examine medical mask use as source control for people with respiratory illness. [Online]. *BMJ Open*. 2016, **6**(12), article no: e012330 [no pagination]. [Accessed 25 February 2025]. Available from: https://doi.org/10.1136/bmjopen-2016-012330.

[148] Liang, M., Gao, L., Cheng, C., Zhou, Q., Uy, J. P., Heiner, K., and Sun, C. Efficacy of face mask in preventing respiratory virus transmission: A systematic review and meta-analysis. [Online]. *Travel Medicine and Infectious Disease*. 2020, **36**, article no: 101751 [no pagination]. [Accessed 17 March 2025]. Available from: https://doi.org/10.1016/j.tmaid.2020.101751.

[149] Jumaa, P. A. Hand hygiene: simple and complex. [Online]. *International Journal of Infectious Diseases*. 2005, **9**(1), pp.3–14. [Accessed 26 February 2025]. Available from: https://doi.org/10.1016/j.ijid.2004.05.005.

[150] Aiello, A. E., Coulborn, R. M., Perez, V., and Larson, E. L. Effect of Hand Hygiene on Infectious Disease Risk in the Community Setting: A Meta-Analysis. [Online]. *American Journal of Public Health*. 2008, **98**(8), pp.1372–1381. [Accessed 26 February 2025]. Available from: https://doi.org/10.2105/AJPH.2007.124610.

[151] Girou, E., Loyeau, S., Legrand, P., Oppein, F., and Brun-Buisson, C. Efficacy of handrubbing with alcohol based solution versus standard handwashing with antiseptic soap: randomised clinical trial. [Online]. *BMJ*. 2002, **325**(7360), article no: 362 [no pagination]. [Accessed 26 February 2025]. Available from: https://doi.org/10.1136/bmj.325.7360.362.

[152] Mouajou, V., Adams, K., DeLisle, G., and Quach, C. Hand hygiene compliance in the prevention of hospital-acquired infections: a systematic review. [Online]. *The Journal of Hospital Infection*. 2022, **119**, pp.33–48. [Accessed

17 March 2025]. Available from: https://doi.org/10.1016/j.jhin.2021.09.016.

[153] Sickbert-Bennett, E. E., DiBiase, L. M., Willis, T. M. S., Wolak, E. S., Weber, D. J., and Rutala, W. A. Reduction of Healthcare-Associated Infections by Exceeding High Compliance with Hand Hygiene Practices. [Online]. *Emerging Infectious Diseases*. 2016, **22**(9), pp.1628–1630. [Accessed 26 February 2025]. Available from: https://doi.org/10.3201/eid2209.151440.

[154] Gammon, J., Hunt, J., Duffy, L., Humphreys, I., Hinkin, J., and Watkins, A. Impact of an educational intervention on hand hygiene practice among nursing students, with a focus on hand drying efficacy. [Online]. *Journal of Infection Prevention*. 2024, **25**(1), pp.3–10. [Accessed 26 February 2025]. Available from: https://doi.org/10.1177/17571774231224695.

[155] Carter, W. H. *Flushed: How the Plumber Saved Civilization.* [Online]. Atria Books, 2006. [Accessed 17 March 2025]. Available from: https://books.google.co.uk/books?id=QiGdMafoOUkC.

[156] Allen, E. and Swoboda, D. *How Buildings Work: The Natural Order of Architecture*. [Online]. Oxford University Press, 2005. [Accessed 17 March 2025]. Available from: https://doi.org/10.1093/oso/9780195161984.001.0001.

[157] Ritchie, L. *Toilet*. [Online]. 2012. [Accessed 26 February 2025]. Available from: https://flic.kr/p/cSuKFf.

[158] Gugleta, L. *Beautiful and modern bathroom seat*. [Online]. 2019. [Accessed 27 February 2025]. Available from: https://unsplash.com/photos/white-flush-toilet-8mMUnl_exqY.

[159] Acabashi. *City of London Cemetery and Crematorium permissive lavatory block cubicle 1*. [Online]. 2020. [Accessed 26 February 2025]. Available from: https://flic.kr/p/2jhBHfu.

[160] Beltz, G. *Toilet*. [Online]. 2017. [Accessed 26 February 2025]. Available from: https://flic.kr/p/TV7Czj.

[161] Miller, D. K. *Crazy Flushmate 2*. [Online]. 2008. [Accessed 26 February 2025]. Available from: https://flic.kr/p/5faAve.

[162] Kecko. *Swiss SBB Train Toilet*. [Online]. 2010. [Accessed 26 February 2025]. Available from: https://flic.kr/p/88Aiqw.

[163] United States General Accounting Office. *Water Infrastructure: Water-efficient Plumbing Fixtures Reduce Water Consumption and Wastewater Flows*. [Online]. 2000. [Accessed 17 March 2025]. Available from: https://www.gao.gov/assets/rced-00-232.pdf.

[164] U.S. Department of Housing and Urban Development. *The Rehab Guide: Kitchens & baths*. [Online]. 2000. [Accessed 17 March 2025]. Available from: https://books.google.co.uk/books?id=1r86ejmwQzQC.

[165] United Nations Environment Programme. *Every Drop Counts: Environmentally Sound Technologies for Urban and Domestic Water Use Efficiency*. [Online]. 2008. [Accessed 17 March 2025]. Available from: http://digitallibrary.un.org/record/644388.

[166] Li, Y.-Y., Wang, J.-X., and Chen, X. Can a toilet promote virus transmission? From a fluid dynamics perspective. [Online]. *Physics of Fluids*. 2020, **32**(6), article no: 065107 [no pagination]. [Accessed 17 March 2025]. Available from: https://doi.org/10.1063/5.0013318.

[167] LaNasa, P. J. and Upp, E. L. Basic Flow Measurement Laws. In: LaNasa, P. J. and Upp, E. L., eds. *Fluid Flow Measurement*. [Online]. 2nd ed. Gulf Professional Publishing, 2002, pp.19–29. [Accessed 27 February 2025]. Available from: https://doi.org/10.1016/b978-0-12-409524-3.00002-2.

[168] Rapp, B. E. Fluids. In: Rapp, B. E., ed. *Microfluidics: Modelling, Mechanics and Mathematics*. [Online]. Elsevier, 2017, pp.243–263. [Accessed 27 February 2025]. Available from: https://doi.org/10.1016/b978-1-4557-3141-1.50009-5.

[169] Dandekar, R., Shen, N., Naar, B., and Bourouiba, L. Splash on a liquid pool: coupled cavity–sheet unsteady dynamics. [Online]. *Journal of Fluid Mechanics*. 2025, **1002**, article no: A13 [no pagination]. [Accessed 27 February 2025]. Available from: https://doi.org/10.1017/jfm.2024.1105.

[170] Zhang, H., Zhang, X., Yi, X., He, F., Niu, F., and Hao, P. Effect of wettability on droplet impact: Spreading and splashing. [Online]. *Experimental Thermal and Fluid Science*. 2021, **124**, article no: 110369 [no pagination]. [Accessed 27 February 2025]. Available from: https://doi.org/10.1016/j.expthermflusci.2021.110369.

[171] Zhang, H., Su, X., Xiao, Q., and Lai, A. C. K. Experimental study on droplet and bioaerosol emissions from flushing a squat toilet. [Online]. *Building and Environment*. 2024, **250**, p.v. [Accessed 21 February 2025]. Available from: https://doi.org/10.1016/j.buildenv.2024.111162.

[172] Macher, J. M. Positive-hole correction of multiple-jet impactors for collecting viable microorganisms. [Online]. *American Industrial Hygiene Association Journal*. 1989, **50**(11), pp.561–568. [Accessed 17 March 2025]. Available from: https://doi.org/10.1080/15298668991375164.

[173] Halkman, H. B. D. and Halkman, A. K. Indicator Organisms. In: Batt, C. A. and Tortorello, M. L., eds. *Encyclopedia of Food Microbiology*. [Online]. 2nd ed. Academic Press, 2014, pp.358–363. [Accessed 27 February 2025]. Available from: https://doi.org/10.1016/B978-0-12-384730-0.00396-7.

[174] Eden, R. ENTEROBACTERIACEAE, COLIFORMS AND E. COLI | Classical and Modern Methods for Detection and Enumeration. In: Batt, C. A. and Tortorello, M. L., eds. *Encyclopedia of Food Microbiology*. [Online]. 2nd ed. Academic Press, 2014, pp.667–673. [Accessed 27 February 2025]. Available from: https://doi.org/10.1016/B978-0-12-384730-0.00097-5.

[175] Price, R. G., Wildeboer, D., Price, R. G., and Wildeboer, D. *E. coli* as an Indicator of Contamination and Health Risk in Environmental Waters. In: *Escherichia coli - Recent Advances on Physiology, Pathogenesis and Biotechnological Applications*. [Online]. InTech, 2017. [Accessed 27 February 2025]. Available from: https://doi.org/10.5772/67330.

[176] Holcomb, D. A. and Stewart, J. R. Microbial Indicators of Fecal Pollution: Recent Progress and Challenges in Assessing Water Quality. [Online]. *Current Environmental Health Reports*. 2020, **7**(3), pp.311–324. [Accessed 27 February 2025]. Available from: https://doi.org/10.1007/s40572-020-00278-1.

[177] Riemann, H. and Cliver, D. O. *Foodborne Infections and Intoxications*. [Online]. 2011. [Accessed 27 February 2025]. Available from: https://doi.org/10.1016/B978-0-12-416041-5.00037-8.

[178] Im, J., Nichols, C., Bjerregaard-Andersen, M., Sow, A. G., Løfberg, S., Tall, A., Pak, G. D., Aaby, P., Baker, S., Clemens, J. D., Espinoza, L. M. C., Konings, F., May, J., Monteiro, M., Niang, A., Panzner, U., Park, S. E., Schütt-Gerowitt, H., Wierzba, T. F., Marks, F., and Kalckreuth, V. von. Prevalence of Salmonella Excretion in Stool: A Community Survey in 2 Sites, Guinea-Bissau and Senegal. [Online]. *Clinical Infectious Diseases*. 2016, **62**, pp.S50–S55. [Accessed 27 February 2025]. Available from: https://doi.org/10.1093/cid/civ789.

[179] Hale, T. L. and Keusch, G. T. *Medical Microbiology*. [Online]. 4th ed. University of Texas Medical Branch at Galveston, 1996. [Accessed 27 February 2025]. Available from: https://www.ncbi.nlm.nih.gov/books/NBK7627/.

[180] Guh, A. Y. and Kutty, P. K. Clostridioides difficile Infection. [Online]. *Annals of Internal Medicine*. 2018, **169**(7), pp.ITC49–ITC64. [Accessed 27 February 2025]. Available from: https://doi.org/10.7326/AITC201810020.

[181] Lee, N., Chan, M. C. W., Wong, B., Choi, K. W., Sin, W., Lui, G., Chan, R. C. W., Lai, R. W. M., Cockram, C. S., Sung, J. J. Y., and Leung, W. K. Fecal Viral Concentration and Diarrhea in Norovirus Gastroenteritis. [Online].

Emerging Infectious Diseases. 2007, **13**(9), pp.1399–1401. [Accessed 25 January 2024]. Available from: https://doi.org/10.3201/eid1309.061535.

[182] Brown, D. M., Butler, D., Orman, N. R., and Davies, J. W. Gross solids transport in small diameter sewers. [Online]. *Water Science and Technology*. 1996, **33**(9), pp.25–30. [Accessed 26 January 2024]. Available from: https://doi.org/10.1016/0273-1223(96)00366-6.

[183] Flewett, T. H. Rotavirus in the home and hospital nursery. [Online]. *British Medical Journal (Clinical Research Ed.)* 1983, **287**(6392), pp.568–569. [Accessed 17 March 2025]. Available from: https://doi.org/10.1136/bmj.287.6392.568.

[184] Dennehy, P. H. Transmission of rotavirus and other enteric pathogens in the home. [Online]. *The Pediatric Infectious Disease Journal*. 2000, **19**(10), S103–S105. [Accessed 27 February 2025]. Available from: https://doi.org/10.1097/00006454-200010001-00003.

[185] Zhu, N., Zhang, D., Wang, W., Li, X., Yang, B., Song, J., Zhao, X., Huang, B., Shi, W., Lu, R., Niu, P., Zhan, F., Ma, X., Wang, D., Xu, W., Wu, G., Gao, G. F., and Tan, W. A Novel Coronavirus from Patients with Pneumonia in China, 2019. [Online]. *New England Journal of Medicine*. 2020, **382**(8), pp.727–733. [Accessed 15 January 2025]. Available from: https://doi.org/10.1056/NEJMoa2001017.

[186] Foladori, P., Cutrupi, F., Segata, N., Manara, S., Pinto, F., Malpei, F., Bruni, L., and La Rosa, G. SARS-CoV-2 from faeces to wastewater treatment: What do we know? A review. [Online]. *Science of The Total Environment*. 2020, **743**, article no: 140444 [no pagination]. [Accessed 23 January 2024]. Available from: https://doi.org/10.1016/j.scitotenv.2020.140444.

[187] Dada, A. C. and Gyawali, P. Quantitative microbial risk assessment (QMRA) of occupational exposure to SARS-CoV-2 in wastewater treatment plants. [Online]. *Science of The Total Environment*. 2021, **763**, article no: 142989 [no pagination]. [Accessed 12 January 2024]. Available from: https://doi.org/10.1016/j.scitotenv.2020.142989.

[188] Barroso-Arévalo, S., Rivera, B., Domínguez, L., and Sánchez-Vizcaíno, J. M. First Detection of SARS-CoV-2 B.1.1.7 Variant of Concern in an Asymptomatic Dog in Spain. [Online]. *Viruses*. 2021, **13**(7), article no: 1379 [no pagination]. [Accessed 17 March 2025]. Available from: https://doi.org/10.3390/v13071379.

[189] Gortázar, C., Barroso-Arévalo, S., Ferreras-Colino, E., Isla, J., Fuente, G. d. l., Rivera, B., Domínguez, L., Fuente, J. d. l., and Sánchez-Vizcaíno, J. M. Natural SARS-CoV-2 Infection in Kept Ferrets, Spain. [Online]. *Emerging*

Infectious Diseases. 2021, **27**(7), article no: 1994 [no pagination]. [Accessed 19 November 2024]. Available from: https://doi.org/10.3201/eid2707.210096.

[190] Dergham, J., Delerce, J., Bedotto, M., La Scola, B., and Moal, V. Isolation of Viable SARS-CoV-2 Virus from Feces of an Immunocompromised Patient Suggesting a Possible Fecal Mode of Transmission. [Online]. *Journal of Clinical Medicine*. 2021, **10**(12), article no: 2696 [no pagination]. [Accessed 19 November 2024]. Available from: https://doi.org/10.3390/jcm10122696.

[191] Zhou, J., Li, C., Liu, X., Chiu, M. C., Zhao, X., Wang, D., Wei, Y., Lee, A., Zhang, A. J., Chu, H., Cai, J.-P., Yip, C. C.-Y., Chan, I. H.-Y., Wong, K. K.-Y., Tsang, O. T.-Y., Chan, K.-H., Chan, J. F.-W., To, K. K.-W., Chen, H., and Yuen, K. Y. Infection of bat and human intestinal organoids by SARS-CoV-2. [Online]. *Nature Medicine*. 2020, **26**(7), pp.1077–1083. [Accessed 17 March 2025]. Available from: https://doi.org/10.1038/s41591-020-0912-6.

[192] Yao, H., Lu, X., Chen, Q., Xu, K., Chen, Y., Cheng, L., Liu, F., Wu, Z., Wu, H., Jin, C., Zheng, M., Wu, N., Jiang, C., and Li, L. Patient-derived mutations impact pathogenicity of SARS-CoV-2. [Online]. 2020. [Accessed 19 November 2024]. Available from: https://doi.org/10.1101/2020.04.14.20060160.

[193] Das Adhikari, U., Eng, G., Farcasanu, M., Avena, L. E., Choudhary, M. C., Triant, V. A., Flagg, M., Schiff, A. E., Gomez, I., Froehle, L. M., Diefenbach, T. J., Ronsard, L., Lingwood, D., Lee, G. C., Rabi, S. A., Erstad, D., Velmahos, G., Li, J. Z., Hodin, R., Stone, J. R., Honko, A. N., Griffiths, A., Yilmaz, Ö. H., and Kwon, D. S. Fecal Severe Acute Respiratory Syndrome Coronavirus 2 (SARS-Cov-2) RNA Is Associated With Decreased Coronavirus Disease 2019 (COVID-19) Survival. [Online]. *Clinical Infectious Diseases*. 2022, **74**(6), pp.1081–1084. [Accessed 17 March 2025]. Available from: https://doi.org/10.1093/cid/ciab623.

[194] Audsley, J. M., Holmes, N. E., Mordant, F. L., Douros, C., Zufan, S. E., Nguyen, T. H. O., Kedzierski, L., Rowntree, L. C., Hensen, L., Subbarao, K., Kedzierska, K., Nicholson, S., Sherry, N., Thevarajan, I., Tran, T., and Druce, J. Temporal differences in culturable severe acute respiratory coronavirus virus 2 (SARS-CoV-2) from the respiratory and gastrointestinal tracts in a patient with moderate coronavirus disease 2019 (COVID-19). [Online]. *Infection Control and Hospital Epidemiology*. 2022, **43**(9), pp.1286–1288. [Accessed 17 March 2025]. Available from: https://doi.org/10.1017/ice.2021.223.

[195] Jeong, H. W., Kim, S.-M., Kim, H.-S., Kim, Y.-I., Kim, J. H., Cho, J. Y., Kim, S.-h., Kang, H., Kim, S.-G., Park, S.-J., Kim, E.-H., and Choi, Y. K. Viable SARS-CoV-2 in various specimens from COVID-19 patients. [Online]. *Clinical Microbiology and Infection*. 2020, **26**(11), pp.1520–1524. [Accessed 19 November 2024]. Available from: https://doi.org/10.1016/j.cmi.2020.07.020.

[196] Jiao, L., Li, H., Xu, J., Yang, M., Ma, C., Li, J., Zhao, S., Wang, H., Yang, Y., Yu, W., Wang, J., Yang, J., Long, H., Gao, J., Ding, K., Wu, D., Kuang, D., Zhao, Y., Liu, J., Lu, S., Liu, H., and Peng, X. The Gastrointestinal Tract Is an Alternative Route for SARS-CoV-2 Infection in a Nonhuman Primate Model. [Online]. *Gastroenterology*. 2021, **160**(5), pp.1647–1661. [Accessed 17 March 2025]. Available from: https://doi.org/10.1053/j.gastro.2020.12.001.

[197] Xiao, F., Sun, J., Xu, Y., Li, F., Huang, X., Li, H., Zhao, J., Huang, J., and Zhao, J. Infectious SARS-CoV-2 in Feces of Patient with Severe COVID-19. [Online]. *Emerging Infectious Diseases*. 2020, **26**(8), pp.1920–1922. [Accessed 17 March 2025]. Available from: https://doi.org/10.3201/eid2608.200681.

[198] Bartlett, S. L., Diel, D. G., Wang, L., Zec, S., Laverack, M., Martins, M., Caserta, L. C., Killian, M. L., Terio, K., Olmstead, C., Delaney, M. A., Stokol, T., Ivančić, M., Jenkins-Moore, M., Ingerman, K., Teegan, T., McCann, C., Thomas, P., McAloose, D., Sykes, J. M., and Calle, P. P. SARS-CoV-2 Infection And Longitudinal Fecal Screening In Malayan Tigers (Panthera tigris jacksoni), Amur Tigers (Panthera tigris altaica), And African Lions (Panthera leo krugeri) At The Bronx Zoo, New York, USA. [Online]. *Journal of Zoo and Wildlife Medicine*. 2021, **51**(4), pp.733–744. [Accessed 17 March 2025]. Available from: https://doi.org/10.1638/2020-0171.

[199] Wang, W., Xu, Y., Gao, R., Lu, R., Han, K., Wu, G., and Tan, W. Detection of SARS-CoV-2 in Different Types of Clinical Specimens. [Online]. *JAMA*. 2020, **323**(18), article no: 1843 [no pagination]. [Accessed 19 November 2024]. Available from: https://doi.org/10.1001/jama.2020.3786.

[200] Zhang, Y., Chen, C., Song, Y., Zhu, S., Wang, D., Zhang, H., Han, G., Weng, Y., Xu, J., Xu, J., Yu, P., Jiang, W., Yang, X., Lang, Z., Yan, D., Wang, Y., Song, J., Gao, G. F., Wu, G., and Xu, W. Excretion of SARS-CoV-2 through faecal specimens. [Online]. *Emerging Microbes & Infections*. 2020, **9**(1), pp.2501–2508. [Accessed 17 March 2025]. Available from: https://doi.org/10.1080/22221751.2020.1844551.

[201] Riley, E. C., Murphy, G., and Riley, R. L. Airborne spread of measles in a suburban elementary school. [Online]. *American Journal of Epidemiology*.

1978, **107**(5), pp.421–432. [Accessed 17 March 2025]. Available from: https://doi.org/10.1093/oxfordjournals.aje.a112560.

[202] Buonanno, G., Stabile, L., and Morawska, L. Estimation of airborne viral emission: Quanta emission rate of SARS-CoV-2 for infection risk assessment. [Online]. *Environment International*. 2020, **141**, article no: 105794 [no pagination]. [Accessed 13 March 2025]. Available from: https://doi.org/10.1016/j.envint.2020.105794.

[203] Noakes, C. J. and Sleigh, A., Applying the Wells-Riley equation to the risk of airborne infection in hospital environments : The importance of stochastic and proximity effects. In: *Indoor Air 2008: the 11th International Conference on Indoor Air Quality and Climate, 17 - 18 August 2008, Copenhagen*. [Online]. ISIAQ, 2008, pp.161–168. [Accessed 15 March 2025]. Available from: https://eprints.whiterose.ac.uk/7702/1/Noakes-indoorair2008.pdf.

[204] Edwards, A. J., King, M.-F., Noakes, C. J., Peckham, D., and López-García, M. The Wells–Riley model revisited: Randomness, heterogeneity, and transient behaviours. [Online]. *Risk Analysis*. 2024, **44**(9), pp.2125–2147. [Accessed 28 February 2025]. Available from: https://doi.org/10.1111/risa.14295.

[205] Gammaitoni, L. and Nucci, M. C. Using a mathematical model to evaluate the efficacy of TB control measures. [Online]. *Emerging Infectious Diseases*. 1997, **3**(3), pp.335–342. [Accessed 28 February 2025]. Available from: https://doi.org/10.3201/eid0303.970310.

[206] Nardell, E. A., Keegan, J., Cheney, S. A., and Etkind, S. C. Airborne infection. Theoretical limits of protection achievable by building ventilation. [Online]. *The American Review of Respiratory Disease*. 1991, **144**(2), pp.302–306. [Accessed 17 March 2025]. Available from: https://doi.org/10.1164/ajrccm/144.2.302.

[207] Escombe, A. R., Oeser, C. C., Gilman, R. H., Navincopa, M., Ticona, E., Pan, W., Martínez, C., Chacaltana, J., Rodríguez, R., Moore, D. A. J., Friedland, J. S., and Evans, C. A. Natural Ventilation for the Prevention of Airborne Contagion. [Online]. *PLOS Medicine*. 2007, **4**(2), article no: e68 [no pagination]. [Accessed 28 February 2025]. Available from: https://doi.org/10.1371/journal.pmed.0040068.

[208] Gao, N. P., Niu, J. L., Perino, M., and Heiselberg, P. The airborne transmission of infection between flats in high-rise residential buildings: Tracer gas simulation. [Online]. *Building and Environment*. 2008, **43**(11), pp.1805–1817. [Accessed 28 February 2025]. Available from: https://doi.org/10.1016/j.buildenv.2007.10.023.

[209] Qian, H., Li, Y., Nielsen, P. V., and Huang, X. Spatial distribution of infection risk of SARS transmission in a hospital ward. [Online]. *Building and Environment*. 2009, **44**(8), pp.1651–1658. [Accessed 28 February 2025]. Available from: https://doi.org/10.1016/j.buildenv.2008.11.002.

[210] Tung, Y.-C. and Hu, S.-C. Infection Risk of Indoor Airborne Transmission of Diseases in Multiple Spaces. [Online]. *Architectural Science Review*. 2008, **51**(1), pp.14–20. [Accessed 28 February 2025]. Available from: https://doi.org/10.3763/asre.2008.5103.

[211] Wang, Z., Galea, E. R., Grandison, A., Ewer, J., and Jia, F. A coupled Computational Fluid Dynamics and Wells-Riley model to predict COVID-19 infection probability for passengers on long-distance trains. [Online]. *Safety Science*. 2022, **147**, article no: 105572 [no pagination]. [Accessed 28 February 2025]. Available from: https://doi.org/10.1016/j.ssci.2021.105572.

[212] Pantelic, J. and Tham, K. W. Assessment of the mixing air delivery system ability to protect occupants from the airborne infectious disease transmission using Wells–Riley approach. [Online]. *HVAC&R Research*. 2012, **18**(4), pp.562–574. [Accessed 28 February 2025]. Available from: https://doi.org/10.1080/10789669.2012.647230.

[213] Guo, Y., Qian, H., Sun, Z., Cao, J., Liu, F., Luo, X., Ling, R., Weschler, L. B., Mo, J., and Zhang, Y. Assessing and controlling infection risk with Wells-Riley model and spatial flow impact factor (SFIF). [Online]. *Sustainable Cities and Society*. 2021, **67**, article no: 102719 [no pagination]. [Accessed 28 February 2025]. Available from: https://doi.org/10.1016/j.scs.2021.102719.

[214] Lau, Z., Griffiths, I. M., English, A., and Kaouri, K. Predicting the spatio-temporal infection risk in indoor spaces using an efficient airborne transmission model. [Online]. *Proceedings of the Royal Society A: Mathematical, Physical and Engineering Sciences*. 2022, **478**(2259), article no: 20210383 [no pagination]. [Accessed 28 February 2025]. Available from: https://doi.org/10.1098/rspa.2021.0383.

[215] Ding, S., Lee, J. S., Mohamed, M. A., and Ng, B. F. Infection risk of SARS-CoV-2 in a dining setting: Deposited droplets and aerosols. [Online]. *Building and Environment*. 2022, **213**, article no: 108888 [no pagination]. [Accessed 28 February 2025]. Available from: https://doi.org/10.1016/j.buildenv.2022.108888.

[216] Li, J., Cheng, Z., Zhang, Y., Mao, N., Guo, S., Wang, Q., Zhao, L., and Long, E. Evaluation of infection risk for SARS-CoV-2 transmission on university campuses. [Online]. *Science and Technology for the Built Environment*. 2021,

27(9), pp.1165–1180. [Accessed 28 February 2025]. Available from: https://doi.org/10.1080/23744731.2021.1948762.

[217] Li, H., Shankar, S. N., Witanachchi, C. T., Lednicky, J. A., Loeb, J. C., Alam, M. M., Fan, Z. H., Mohamed, K., Eiguren-Fernandez, A., and Wu, C.-Y. Environmental Surveillance and Transmission Risk Assessments for SARS-CoV-2 in a Fitness Center. [Online]. *Aerosol and Air Quality Research*. 2021, **21**(11), article no: 210106 [no pagination]. [Accessed 28 February 2025]. Available from: https://doi.org/10.4209/aaqr.210106.

[218] Timpitak, W. and Pochai, N. A Mathematical Model of Risk Assessment on Airborne Infection in a Room with an Outlet Ventilation System. [Online]. *Engineering Letters*. 2022, **30**(2). [Accessed 19 January 2025]. Available from: https://www.engineeringletters.com/issues_v30/issue_2/EL_30_2_56.pdf.

[219] Boonmeemapasuk, W. and Pochai, N. A Risk Model of Airborne Transmission and Vaccine Efficacy in an Outpatient Room with a Ventilation System. [Online]. *Engineering Letters*. 2022, **30**(2). [Accessed 17 March 2025]. Available from: https://www.engineeringletters.com/issues_v30/issue_2/EL_30_2_28.pdf.

[220] Wood, S. G. A., Craske, J., and Burridge, H. C. Relating quanta conservation and compartmental epidemiological models of airborne disease outbreaks in buildings. [Online]. *Scientific Reports*. 2023, **13**(1), article no: 17335 [no pagination]. [Accessed 28 February 2025]. Available from: https://doi.org/10.1038/s41598-023-44527-3.

[221] Haas, C. N., Rose, J. B., and Gerba, C. P. *Quantitative Microbial Risk Assessment*. [Online]. Wiley, 1999. [Accessed 18 March 2025]. Available from: https://books.google.co.uk/books?id=vjVhhwQh9N8C.

[222] Rose, J. B., Haas, C. N., and Regli, S. Risk assessment and control of waterborne giardiasis. [Online]. *American Journal of Public Health*. 1991, **81**(6), pp.709–713. [Accessed 28 February 2025]. Available from: https://doi.org/10.2105/ajph.81.6.709.

[223] Schmid-Hempel, P. Immune defence, parasite evasion strategies and their relevance for 'macroscopic phenomena' such as virulence. [Online]. *Philosophical Transactions of the Royal Society B: Biological Sciences*. 2009, **364**(1513), pp.85–98. [Accessed 28 February 2025]. Available from: https://doi.org/10.1098/rstb.2008.0157.

[224] Haas, C. N. Estimation of risk due to low doses of microorganisms: a comparison of alternative methodologies. [Online]. *American Journal of Epidemi-*

ology. 1983, **118**(4), pp.573–582. [Accessed 17 March 2025]. Available from: https://doi.org/10.1093/oxfordjournals.aje.a113662.

[225] Sze To, G. N. and Chao, C. Y. H. Review and comparison between the Wells-Riley and dose-response approaches to risk assessment of infectious respiratory diseases. [Online]. *Indoor Air*. 2010, **20**(1), pp.2–16. [Accessed 17 March 2025]. Available from: https://doi.org/10.1111/j.1600-0668.2009.00621.x.

[226] Williams, M. S., Baker, M. R., Guina, T., Hewitt, J. A., Lanning, L., Hill, H., May, J. M., Fogtman, B., and Pittman, P. R. Retrospective Analysis of Pneumonic Tularemia in Operation Whitecoat Human Subjects: Disease Progression and Tetracycline Efficacy. [Online]. *Frontiers in Medicine*. 2019, **6**, article no: 229 [no pagination]. [Accessed 13 March 2025]. Available from: https://doi.org/10.3389/fmed.2019.00229.

[227] Killingley, B., Mann, A. J., Kalinova, M., Boyers, A., Goonawardane, N., Zhou, J., Lindsell, K., Hare, S. S., Brown, J., Frise, R., Smith, E., Hopkins, C., Noulin, N., Löndt, B., Wilkinson, T., Harden, S., McShane, H., Baillet, M., Gilbert, A., Jacobs, M., Charman, C., Mande, P., Nguyen-Van-Tam, J. S., Semple, M. G., Read, R. C., Ferguson, N. M., Openshaw, P. J., Rapeport, G., Barclay, W. S., Catchpole, A. P., and Chiu, C. Safety, tolerability and viral kinetics during SARS-CoV-2 human challenge in young adults. [Online]. *Nature Medicine*. 2022, **28**(5), pp.1031–1041. [Accessed 15 January 2025]. Available from: https://doi.org/10.1038/s41591-022-01780-9.

[228] McCullogh, N. B. and Eisele, C. W. Experimental human salmonellosis. I. Pathogenicity of strains of Salmonella meleagridis and Salmonella anatum obtained from spray-dried whole egg. [Online]. *The Journal of Infectious Diseases*. 1951, **88**(3), pp.278–289. [Accessed 17 March 2025]. Available from: https://doi.org/10.1093/infdis/88.3.278.

[229] DuPont, H. L., Hornick, R. B., Dawkins, A. T., Snyder, M. J., and Formal, S. B. The Response of Man to Virulent Shigella flexneri 2a. [Online]. *The Journal of Infectious Diseases*. 1969, **119**(3), pp.296–299. [Accessed 3 March 2025]. Available from: https://doi.org/10.1093/infdis/119.3.296.

[230] Ward, R. L., Bernstein, D. I., Young, E. C., Sherwood, J. R., Knowlton, D. R., and Schiff, G. M. Human rotavirus studies in volunteers: determination of infectious dose and serological response to infection. [Online]. *The Journal of Infectious Diseases*. 1986, **154**(5), pp.871–880. [Accessed 17 March 2025]. Available from: https://doi.org/10.1093/infdis/154.5.871.

[231] Zhang, X. and Wang, J. Dose-response Relation Deduced for Coronaviruses From Coronavirus Disease 2019, Severe Acute Respiratory Syndrome, and Middle East Respiratory Syndrome: Meta-analysis Results and its Application for Infection Risk Assessment of Aerosol Transmission. [Online]. *Clinical Infectious Diseases*. 2021, **73**(1), pp.e241–e245. [Accessed 17 March 2025]. Available from: https://doi.org/10.1093/cid/ciaa1675.

[232] Dediego, M. L., Pewe, L., Alvarez, E., Rejas, M. T., Perlman, S., and Enjuanes, L. Pathogenicity of severe acute respiratory coronavirus deletion mutants in hACE-2 transgenic mice. [Online]. *Virology*. 2008, **376**(2), pp.379–389. [Accessed 17 March 2025]. Available from: https://doi.org/10.1016/j.virol.2008.03.005.

[233] Koprowski, H. Immunization against poliomyelitis with living attenuated virus. [Online]. *The American Journal of Tropical Medicine and Hygiene*. 1956, **5**(3), pp.440–452. [Accessed 17 March 2025]. Available from: https://doi.org/10.4269/ajtmh.1956.5.440.

[234] Cliver, D. O. Experimental Infection by Waterborne Enteroviruses. [Online]. *Journal of Food Protection*. 1981, **44**(11), pp.861–865. [Accessed 17 March 2025]. Available from: https://doi.org/10.4315/0362-028X-44.11.861.

[235] Toth, D. J. A., Gundlapalli, A. V., Schell, W. A., Bulmahn, K., Walton, T. E., Woods, C. W., Coghill, C., Gallegos, F., Samore, M. H., and Adler, F. R. Quantitative models of the dose-response and time course of inhalational anthrax in humans. [Online]. *PLoS pathogens*. 2013, **9**(8), article no: e1003555 [no pagination]. [Accessed 17 March 2025]. Available from: https://doi.org/10.1371/journal.ppat.1003555.

[236] Murphy, B. R., Clements, M. L., Madore, H. P., Steinberg, J., O'Donnell, S., Betts, R., Demico, D., Reichman, R. C., Dolin, R., and Maassab, H. F. Dose Response of Cold-Adapted, Reassortant Influenza A/California/10/78 Virus (H1N1) in Adult Volunteers. [Online]. *The Journal of Infectious Diseases*. 1984, **149**(5), p.816. [Accessed 15 January 2025]. Available from: https://doi.org/10.1093/infdis/149.5.816.

[237] Hendley, J. O., Edmondson, W. P., and Gwaltney, J. M. Relation between naturally acquired immunity and infectivity of two rhinoviruses in volunteers. [Online]. *The Journal of Infectious Diseases*. 1972, **125**(3), pp.243–248. [Accessed 17 March 2025]. Available from: https://doi.org/10.1093/infdis/125.3.243.

[238] DuPont, H. L., Formal, S. B., Hornick, R. B., Snyder, M. J., Libonati, J. P., Sheahan, D. G., LaBrec, E. H., and Kalas, J. P. Pathogenesis of Escherichia coli diarrhea. [Online]. *The New England Journal of Medicine*. 1971, **285**(1),

pp.1–9. [Accessed 17 March 2025]. Available from: https://doi.org/10.1056/NEJM197107012850101.

[239] Allen, L. J. S. *An introduction to stochastic processes with applications to biology*. [Online]. 2nd ed. CRC Press, 2003. [Accessed 15 January 2025]. Available from: https://doi.org/10.1201/b12537.

[240] King, M.-F., Noakes, C. J., and Sleigh, P. A. Modeling environmental contamination in hospital single- and four-bed rooms. [Online]. *Indoor Air*. 2015, **25**(6), pp.694–707. [Accessed 15 January 2025]. Available from: https://doi.org/10.1111/ina.12186.

[241] Pessoa-Silva, C. L., Dharan, S., Hugonnet, S., Touveneau, S., Posfay-Barbe, K., Pfister, R., and Pittet, D. Dynamics of bacterial hand contamination during routine neonatal care. [Online]. *Infection Control and Hospital Epidemiology*. 2004, **25**(3), pp.192–197. [Accessed 17 March 2025]. Available from: https://doi.org/10.1086/502376.

[242] Wilson, A. M., Mussio, I., Verhougstraete, M. P., Jung, Y., Ashraf, A., Chilton, S., and Hamilton, K. A. A risk-risk tradeoff approach for incorporating the public's risk perceptions into quantitative microbial risk assessment. [Online]. *Journal of Occupational and Environmental Hygiene*. 2025, **0**(0), pp.1–17. [Accessed 20 January 2025]. Available from: https://doi.org/10.1080/15459624.2024.2423756.

[243] Environmental Protection Agency (EPA). National primary drinking water regulations: Long Term 1 Enhanced Surface Water Treatment Rule. Final rule. [Online]. *Federal Register*. 2002, **67**(9), pp.1811–1844. [Accessed 17 March 2025]. Available from: https://www.federalregister.gov/d/02-409.

[244] Reynolds, K. A., Verhougstraete, M. P., Mena, K. D., Sattar, S. A., Scott, E. A., and Gerba, C. P. Quantifying pathogen infection risks from household laundry practices. [Online]. *Journal of Applied Microbiology*. 2022, **132**(2), pp.1435–1448. [Accessed 20 January 2025]. Available from: https://doi.org/10.1111/jam.15273.

[245] Ryan, M. O., Haas, C. N., Gurian, P. L., Gerba, C. P., Panzl, B. M., and Rose, J. B. Application of quantitative microbial risk assessment for selection of microbial reduction targets for hard surface disinfectants. [Online]. *American Journal of Infection Control*. 2014, **42**(11), pp.1165–1172. [Accessed 17 March 2025]. Available from: https://doi.org/10.1016/j.ajic.2014.07.024.

[246] King, M.-F., Wilson, A. M., Weir, M. H., López-García, M., Proctor, J., Hiwar, W., Khan, A., Fletcher, L. A., Sleigh, P. A., Clifton, I., Dancer, S. J., Wilcox, M., Reynolds, K. A., and Noakes, C. J. Modeling fomite-mediated

SARS-CoV-2 exposure through personal protective equipment doffing in a hospital environment. [Online]. *Indoor Air*. 2022, **32**(1), article no: e12938 [no pagination]. [Accessed 1 March 2025]. Available from: https://doi.org/10.1111/ina.12938.

[247] Mizukoshi, A., Nakama, C., Okumura, J., and Azuma, K. Assessing the risk of COVID-19 from multiple pathways of exposure to SARS-CoV-2: Modeling in health-care settings and effectiveness of nonpharmaceutical interventions. [Online]. *Environment International*. 2021, **147**, article no: 106338 [no pagination]. [Accessed 17 March 2025]. Available from: https://doi.org/10.1016/j.envint.2020.106338.

[248] Schijven, J. F., Wind, M., Todt, D., Howes, J., Tamele, B., and Steinmann, E. Risk assessment of banknotes as a fomite of SARS-CoV-2 in cash payment transactions. [Online]. *Risk Analysis*. 2023, **43**(4), pp.700–708. [Accessed 1 March 2025]. Available from: https://doi.org/10.1111/risa.13935.

[249] Zhang, X., Wu, J., Smith, L. M., Li, X., Yancey, O., Franzblau, A., Dvonch, J. T., Xi, C., and Neitzel, R. L. Monitoring SARS-CoV-2 in air and on surfaces and estimating infection risk in buildings and buses on a university campus. [Online]. *Journal of Exposure Science & Environmental Epidemiology*. 2022, **32**(5), pp.751–758. [Accessed 1 March 2025]. Available from: https://doi.org/10.1038/s41370-022-00442-9.

[250] Bate, A. M., Miller, D., King, M.-F., Moseley, K.-A., Xu, J., Hall, I., López-García, M., Parker, S. T., and Noakes, C. J. A quantitative microbial risk assessment approach to estimate exposure to SARS-CoV-2 on a bus. [Online]. *Journal of Transport & Health*. 2024, **38**, article no: 101829 [no pagination]. [Accessed 1 March 2025]. Available from: https://doi.org/10.1016/j.jth.2024.101829.

[251] Wilson, A. M., Reynolds, K. A., Sexton, J. D., and Canales, R. A. Modeling Surface Disinfection Needs To Meet Microbial Risk Reduction Targets. [Online]. *Applied and Environmental Microbiology*. 2018, **84**(18), article no: e00709–18 [no pagination]. [Accessed 1 March 2025]. Available from: https://doi.org/10.1128/AEM.00709-18.

[252] Wilson, A. M., Reynolds, K. A., and Canales, R. A. Estimating the effect of hand hygiene compliance and surface cleaning timing on infection risk reductions with a mathematical modeling approach. [Online]. *American Journal of Infection Control*. 2019, **47**(12), pp.1453–1459. [Accessed 1 March 2025]. Available from: https://doi.org/10.1016/j.ajic.2019.05.023.

[253] Wilson, A. M., King, M.-F., López-García, M., Clifton, I. J., Proctor, J., Reynolds, K. A., and Noakes, C. J. Effects of patient room layout on viral accruement on healthcare professionals' hands. [Online]. *Indoor Air*. 2021, **31**(5), pp.1657–1672. [Accessed 17 March 2025]. Available from: https://doi.org/10.1111/ina.12834.

[254] Armstrong, T. W. and Haas, C. N. A Quantitative Microbial Risk Assessment Model for Legionnaires' Disease: Animal Model Selection and Dose-Response Modeling. [Online]. *Risk Analysis*. 2007, **27**(6), pp.1581–1596. [Accessed 1 March 2025]. Available from: https://doi.org/10.1111/j.1539-6924.2007.00990.x.

[255] Madera-García, V., Mraz, A. L., Lopez-Galvez, N., Weir, M. H., Werner, J., Beamer, P. I., and Verhougstraete, M. P. Legionella pneumophila as a Health Hazard to Miners: A Pilot Study of Water Quality and QMRA. [Online]. *Water*. 2019, **11**(8), article no: 1528 [no pagination]. [Accessed 1 March 2025]. Available from: https://doi.org/10.3390/w11081528.

[256] Pepper, I. L. and Gerba, C. P. Risk of infection from *Legionella* associated with spray irrigation of reclaimed water. [Online]. *Water Research*. 2018, **139**, pp.101–107. [Accessed 1 March 2025]. Available from: https://doi.org/10.1016/j.watres.2018.04.001.

[257] Xu, P.-C., Zhang, C.-M., and Wang, X. C. Numerical simulation for spatial distribution of water aerosol produced from nozzle spray and health risk related to *Legionella pneumophila* in spray scenarios. [Online]. *Water Research*. 2022, **216**, article no: 118304 [no pagination]. [Accessed 1 March 2025]. Available from: https://doi.org/10.1016/j.watres.2022.118304.

[258] Hamilton, K. A., Kuppravalli, A., Heida, A., Joshi, S., Haas, C. N., Verhougstraete, M., and Gerrity, D. Legionnaires' disease in dental offices: Quantifying aerosol risks to dental workers and patients. [Online]. *Journal of Occupational and Environmental Hygiene*. 2021, **18**(8), pp.378–393. [Accessed 1 March 2025]. Available from: https://doi.org/10.1080/15459624.2021.1939878.

[259] Hamilton, K. A., Hamilton, M. T., Johnson, W., Jjemba, P., Bukhari, Z., LeChevallier, M., and Haas, C. N. Health risks from exposure to *Legionella* in reclaimed water aerosols: Toilet flushing, spray irrigation, and cooling towers. [Online]. *Water Research*. 2018, **134**, pp.261–279. [Accessed 1 March 2025]. Available from: https://doi.org/10.1016/j.watres.2017.12.022.

[260] Hamilton, K. A., Hamilton, M. T., Johnson, W., Jjemba, P., Bukhari, Z., LeChevallier, M., Haas, C. N., and Gurian, P. L. Risk-Based Critical Concentrations of Legionella pneumophila for Indoor Residential Water Uses. [Online]. *Environmental Science & Technology*. 2019, **53**(8), pp.4528–4541.

[Accessed 17 March 2025]. Available from: https://doi.org/10.1021/acs.est.8b03000.

[261] Ahmed, W., Vieritz, A., Goonetilleke, A., and Gardner, T. Health risk from the use of roof-harvested rainwater in Southeast Queensland, Australia, as potable or nonpotable water, determined using quantitative microbial risk assessment. [Online]. *Applied and Environmental Microbiology*. 2010, **76**(22), pp.7382–7391. [Accessed 17 March 2025]. Available from: https://doi.org/10.1128/AEM.00944-10.

[262] Blanky, M., Sharaby, Y., Rodríguez-Martínez, S., Halpern, M., and Friedler, E. Greywater reuse - Assessment of the health risk induced by Legionella pneumophila. [Online]. *Water Research*. 2017, **125**, pp.410–417. [Accessed 17 March 2025]. Available from: https://doi.org/10.1016/j.watres.2017.08.068.

[263] Bouwknegt, M., Schijven, J. F., Schalk, J. A. C., and Roda Husman, A. M. de. Quantitative risk estimation for a Legionella pneumophila infection due to whirlpool use. [Online]. *Risk Analysis*. 2013, **33**(7), pp.1228–1236. [Accessed 17 March 2025]. Available from: https://doi.org/10.1111/j.1539-6924.2012.01909.x.

[264] Chen, M., Shi, L., Liu, G., Wu, X., and Lu, Y. Aerosol exposure assessment during reclaimed water utilization in China and risk evaluation in case of Legionella. [Online]. *Frontiers of Environmental Science & Engineering*. 2021, **16**(7), article no: 95 [no pagination]. [Accessed 1 March 2025]. Available from: https://doi.org/10.1007/s11783-021-1516-1.

[265] Kusumawardhana, A., Zlatanovic, L., Bosch, A., and Hoek, J. P. van der. Microbiological Health Risk Assessment of Water Conservation Strategies: A Case Study in Amsterdam. [Online]. *International Journal of Environmental Research and Public Health*. 2021, **18**(5), article no: 2595 [no pagination]. [Accessed 1 March 2025]. Available from: https://doi.org/10.3390/ijerph18052595.

[266] Massiot, G., Courault, D., Jacob, P., and Albert, I. Monitoring the risk of Legionella infection using a general Bayesian network updated from temporal measurements in agricultural irrigation with reclaimed wastewater. [Online]. *Environmental Science: Water Research & Technology*. 2022, **9**(1), pp.176–192. [Accessed 1 March 2025]. Available from: https://doi.org/10.1039/D2EW00311B.

[267] Ali, W., Yang, Y.-f., Gong, L., Yan, C., and Cui, B.-b. Emission characteristics and quantitative health risk assessment of bioaerosols in an indoor toilet after flushing under various ventilation scenarios. [Online]. *Building and En-*

vironment. 2022, **207**, article no: 108463 [no pagination]. [Accessed 1 March 2025]. Available from: https://doi.org/10.1016/j.buildenv.2021.108463.

[268] Chen, Y.-h., Yan, C., Yang, Y.-f., and Ma, J.-x. Quantitative microbial risk assessment and sensitivity analysis for workers exposed to pathogenic bacterial bioaerosols under various aeration modes in two wastewater treatment plants. [Online]. *The Science of the Total Environment*. 2021, **755**, article no: 142615 [no pagination]. [Accessed 1 March 2025]. Available from: https://doi.org/10.1016/j.scitotenv.2020.142615.

[269] Ma, J., An, D., Cui, B., Liu, M., Zhu, H., Li, M., Ai, X., Ali, W., and Yan, C. What are the disease burden and its sensitivity analysis of workers exposing to Staphylococcus aureus bioaerosol during warm and cold periods in a wastewater treatment plant? [Online]. *Environmental Science and Pollution Research*. 2022, **29**(55), pp.82938–82947. [Accessed 1 March 2025]. Available from: https://doi.org/10.1007/s11356-022-21447-9.

[270] Wu, J.-t., Song, X.-q., Liang, L.-w., and Yan, C. Estimating acceptable exposure time for bioaerosols emission in a wastewater treatment plant by reverse quantitative microbial risk assessment based on various risk benchmarks. [Online]. *Environmental Science and Pollution Research*. 2022, **29**(9), pp.13345–13355. [Accessed 1 March 2025]. Available from: https://doi.org/10.1007/s11356-021-16699-w.

[271] Yan, C., Leng, Y.-L., and Wu, J.-T. Quantitative microbial risk assessment for occupational health of temporary entrants and staffs equipped with various grade PPE and exposed to microbial bioaerosols in two WWTPs. [Online]. *International Archives of Occupational and Environmental Health*. 2021, **94**(6), pp.1327–1343. [Accessed 17 March 2025]. Available from: https://doi.org/10.1007/s00420-021-01663-5.

[272] Yan, C., Zhao, X.-y., Luo, X., An, D.-z., Zhu, H., Li, M., Ai, X.-j., and Ali, W. Quantitative microbial risk assessment with nasal/oral breathing pattern for S. aureus bioaerosol emission from aeration tanks and residual sludge storage yard in a wastewater treatment plant. [Online]. *Environmental Science and Pollution Research*. 2023, **30**(8), pp.21252–21262. [Accessed 1 March 2025]. Available from: https://doi.org/10.1007/s11356-022-23621-5.

[273] Dean, K. and Mitchell, J. Reverse QMRA for *Pseudomonas aeruginosa* in Premise Plumbing to Inform Risk Management. [Online]. *Journal of Environmental Engineering*. 2020, **146**(3). [Accessed 1 March 2025]. Available from: https://doi.org/10.1061/(ASCE)EE.1943-7870.0001641.

[274] Augenbraun, B. L., Lasner, Z. D., Mitra, D., Prabhu, S., Raval, S., Sawaoka, H., and Doyle, J. M. Assessment and mitigation of aerosol airborne SARS-CoV-2 transmission in laboratory and office environments. [Online]. *Journal of Occupational and Environmental Hygiene*. 2020, **17**(10), pp.447–456. [Accessed 17 March 2025]. Available from: https://doi.org/10.1080/15459624.2020.1805117.

[275] Wagner, J., Sparks, T. L., Miller, S., Chen, W., Macher, J. M., and Waldman, J. M. Modeling the impacts of physical distancing and other exposure determinants on aerosol transmission. [Online]. *Journal of Occupational and Environmental Hygiene*. 2021, **18**(10), pp.495–509. [Accessed 1 March 2025]. Available from: https://doi.org/10.1080/15459624.2021.1963445.

[276] Bale, R., Iida, A., Yamakawa, M., Li, C., and Tsubokura, M. Quantifying the COVID19 infection risk due to droplet/aerosol inhalation. [Online]. *Scientific Reports*. 2022, **12**(1), article no: 11186 [no pagination]. [Accessed 1 March 2025]. Available from: https://doi.org/10.1038/s41598-022-14862-y.

[277] Cortellessa, G., Stabile, L., Arpino, F., Faleiros, D. E., Bos, W. van den, Morawska, L., and Buonanno, G. Close proximity risk assessment for SARS-CoV-2 infection. [Online]. *Science of The Total Environment*. 2021, **794**, article no: 148749 [no pagination]. [Accessed 1 March 2025]. Available from: https://doi.org/10.1016/j.scitotenv.2021.148749.

[278] Domino, S. P. A Case Study on Pathogen Transport, Deposition, Evaporation and Transmission: Linking High-Fidelity Computational Fluid Dynamics Simulations to Probability of Infection. [Online]. *International Journal of Computational Fluid Dynamics*. 2021, **35**(9), pp.743–757. [Accessed 1 March 2025]. Available from: https://doi.org/10.1080/10618562.2021.1905801.

[279] Hedworth, H. A., Karam, M., McConnell, J., Sutherland, J. C., and Saad, T. Mitigation strategies for airborne disease transmission in orchestras using computational fluid dynamics. [Online]. *Science Advances*. 2021, **7**(26), article no: eabg4511 [no pagination]. [Accessed 1 March 2025]. Available from: https://doi.org/10.1126/sciadv.abg4511.

[280] Bertone, M., Mikszewski, A., Stabile, L., Riccio, G., Cortellessa, G., d'Ambrosio, F. R., Papa, V., Morawska, L., and Buonanno, G. Assessment of SARS-CoV-2 airborne infection transmission risk in public buses. [Online]. *Geoscience Frontiers*. 2022, **13**(6), article no: 101398 [no pagination]. [Accessed 1 March 2025]. Available from: https://doi.org/10.1016/j.gsf.2022.101398.

[281] Rocha-Melogno, L., Crank, K., Bergin, M. H., Gray, G. C., Bibby, K., and Deshusses, M. A. Quantitative risk assessment of COVID-19 aerosol transmission indoors: a mechanistic stochastic web application. [Online]. *Envi-*

ronmental Technology. 2023, **44**(9), pp.1201–1212. [Accessed 1 March 2025]. Available from: https://doi.org/10.1080/09593330.2021.1998228.

[282] Buonanno, G., Morawska, L., and Stabile, L. Quantitative assessment of the risk of airborne transmission of SARS-CoV-2 infection: Prospective and retrospective applications. [Online]. *Environment International*. 2020, **145**, article no: 106112 [no pagination]. [Accessed 1 March 2025]. Available from: https://doi.org/10.1016/j.envint.2020.106112.

[283] Dhawan, S. and Biswas, P. Aerosol Dynamics Model for Estimating the Risk from Short-Range Airborne Transmission and Inhalation of Expiratory Droplets of SARS-CoV-2. [Online]. *Environmental Science & Technology*. 2021, **55**(13), pp.8987–8999. [Accessed 1 March 2025]. Available from: https://doi.org/10.1021/acs.est.1c00235.

[284] Henriques, A., Mounet, N., Aleixo, L., Elson, P., Devine, J., Azzopardi, G., Andreini, M., Rognlien, M., Tarocco, N., and Tang, J. Modelling airborne transmission of SARS-CoV-2 using CARA: risk assessment for enclosed spaces. [Online]. *Interface Focus*. 2022, **12**(2), article no: 20210076 [no pagination]. [Accessed 1 March 2025]. Available from: https://doi.org/10.1098/rsfs.2021.0076.

[285] Parhizkar, H., Van Den Wymelenberg, K. G., Haas, C. N., and Corsi, R. L. A Quantitative Risk Estimation Platform for Indoor Aerosol Transmission of COVID-19. [Online]. *Risk Analysis*. 2022, **42**(9), pp.2075–2088. [Accessed 1 March 2025]. Available from: https://doi.org/10.1111/risa.13844.

[286] Carducci, A., Donzelli, G., Cioni, L., Federigi, I., Lombardi, R., and Verani, M. Quantitative Microbial Risk Assessment for Workers Exposed to Bioaerosol in Wastewater Treatment Plants Aimed at the Choice and Setup of Safety Measures. [Online]. *International Journal of Environmental Research and Public Health*. 2018, **15**(7), article no: 1490 [no pagination]. [Accessed 17 March 2025]. Available from: https://doi.org/10.3390/ijerph15071490.

[287] Carducci, A., Donzelli, G., Cioni, L., and Verani, M. Quantitative Microbial Risk Assessment in Occupational Settings Applied to the Airborne Human Adenovirus Infection. [Online]. *International Journal of Environmental Research and Public Health*. 2016, **13**(7), article no: 733 [no pagination]. [Accessed 17 March 2025]. Available from: https://doi.org/10.3390/ijerph13070733.

[288] Xu, C., Wei, X., Liu, L., Su, L., Liu, W., Wang, Y., and Nielsen, P. V. Effects of personalized ventilation interventions on airborne infection risk and transmission between occupants. [Online]. *Building and Environment*. 2020, **180**, article no: 107008 [no pagination]. [Accessed 1 March 2025]. Available from: https://doi.org/10.1016/j.buildenv.2020.107008.

[289] Nicas, M. and Jones, R. M. Relative Contributions of Four Exposure Pathways to Influenza Infection Risk. [Online]. *Risk Analysis*. 2009, **29**(9), pp.1292–1303. [Accessed 1 March 2025]. Available from: https://doi.org/10.1111/j.1539-6924.2009.01253.x.

[290] Lim, K.-Y., Hamilton, A. J., and Jiang, S. C. Assessment of public health risk associated with viral contamination in harvested urban stormwater for domestic applications. [Online]. *Science of The Total Environment*. 2015, **523**, pp.95–108. [Accessed 5 March 2025]. Available from: https://doi.org/10.1016/j.scitotenv.2015.03.077.

[291] Mousavi, E. and Bhattacharya, A. Event based approach for modeling indoor airflow patterns. [Online]. *Journal of Building Engineering*. 2022, **51**, p.104244. [Accessed 3 March 2025]. Available from: https://doi.org/10.1016/j.jobe.2022.104244.

[292] Ye, W., Pan, Y., He, L., Chen, B., Liu, J., Gao, J., Wang, Y., and Yang, Y. Design with modeling techniques. In: Goodfellow, H. D. and Wang, Y., eds. *Industrial Ventilation Design Guidebook*. [Online]. 2nd ed. Elsevier, 2021, pp.109–183. [Accessed 27 February 2025]. Available from: https://doi.org/10.1016/b978-0-12-816673-4.00008-0.

[293] Noakes, C. J. and Sleigh, P. A. Mathematical models for assessing the role of airflow on the risk of airborne infection in hospital wards. [Online]. *Journal of the Royal Society, Interface*. 2009, **6**, pp.S791–S800. [Accessed 17 March 2025]. Available from: https://doi.org/10.1098/rsif.2009.0305.focus.

[294] López-García, M., King, M.-F., and Noakes, C. J. A Multicompartment SIS Stochastic Model with Zonal Ventilation for the Spread of Nosocomial Infections: Detection, Outbreak Management, and Infection Control. [Online]. *Risk Analysis*. 2019, **39**(8), pp.1825–1842. [Accessed 3 March 2025]. Available from: https://doi.org/10.1111/risa.13300.

[295] National Institute of Standards and Technology (NIST), *CONTAM*. [Software]. [Accessed 17 March 2025]. Available from: https://www.nist.gov/services-resources/software/contam.

[296] Edwards, A. J., Benson, L., Guo, Z., López-García, M., Noakes, C. J., Peckham, D., and King, M.-F. A mathematical model for assessing transient airborne infection risks in a multi-zone hospital ward. [Online]. *Building and Environment*. 2023, **238**, article no: 110344 [no pagination]. [Accessed 3 March 2025]. Available from: https://doi.org/10.1016/j.buildenv.2023.110344.

[297] Yan, S., Wang, L., Birnkrant, M. J., Zhai, J., and Miller, S. L. Evaluating SARS-CoV-2 airborne quanta transmission and exposure risk in a mechanically ventilated multizone office building. [Online]. *Building and Environ-*

ment. 2022, **219**, article no: 109184 [no pagination]. [Accessed 3 March 2025]. Available from: https://doi.org/10.1016/j.buildenv.2022.109184.

[298] Shrestha, P., DeGraw, J. W., Zhang, M., and Liu, X. Multizonal modeling of SARS-CoV-2 aerosol dispersion in a virtual office building. [Online]. *Building and Environment*. 2021, **206**, article no: 108347 [no pagination]. [Accessed 3 March 2025]. Available from: https://doi.org/10.1016/j.buildenv.2021.108347.

[299] Cheong, C. H., Park, B., and Lee, S. Design Method to Prevent Airborne Infection in an Emergency Department. [Online]. *Journal of Asian Architecture and Building Engineering*. 2018, **17**(3), pp.573–579. [Accessed 3 March 2025]. Available from: https://doi.org/10.3130/jaabe.17.581.

[300] Emmerich, S. J., Heinzerling, D., Choi, J.-i., and Persily, A. K. Multizone modeling of strategies to reduce the spread of airborne infectious agents in healthcare facilities. [Online]. *Building and Environment*. 2013, **60**, pp.105–115. [Accessed 3 March 2025]. Available from: https://doi.org/10.1016/j.buildenv.2012.11.013.

[301] Navthar, R. R., Kotakar, S. G., and Khire, M. Y., Computational Fluid Dynamics: Computer Simulation. In: *2011 3rd International Conference on Computer Technology and Development, 25 - 27 November 2011, Chengdu*. [Online]. ASME Press, 2011. [Accessed 15 January 2025]. Available from: https://doi.org/10.1115/1.859919.paper190.

[302] Hathway, E., Noakes, C., Sleigh, P., and Fletcher, L. CFD simulation of airborne pathogen transport due to human activities. [Online]. *Building and Environment*. 2011, **46**(12), pp.2500–2511. [Accessed 3 March 2025]. Available from: https://doi.org/10.1016/j.buildenv.2011.06.001.

[303] Wang, J. and Chow, T.-T. Influence of human movement on the transport of airborne infectious particles in hospital. [Online]. *Journal of Building Performance Simulation*. 2015, **8**(4), pp.205–215. [Accessed 3 March 2025]. Available from: https://doi.org/10.1080/19401493.2014.905636.

[304] Jo, S., Hong, J., Lee, S.-E., Ki, M., Choi, B. Y., and Sung, M. Airflow analysis of Pyeongtaek St Mary's Hospital during hospitalization of the first Middle East respiratory syndrome patient in Korea. [Online]. *Royal Society Open Science*. 2019, **6**(3), article no: 181164 [no pagination]. [Accessed 3 March 2025]. Available from: https://doi.org/10.1098/rsos.181164.

[305] Li, Y., Huang, X., Yu, I. T. S., Wong, T. W., and Qian, H. Role of air distribution in SARS transmission during the largest nosocomial outbreak in Hong Kong. [Online]. *Indoor Air*. 2005, **15**(2), pp.83–95. [Accessed 17 March

2025]. Available from: https://doi.org/10.1111/j.1600-0668.2004.00317.x.

[306] ANSYS, Inc., *ANSYS Fluent* (version 2023 R2). [Software]. 2023. [Accessed 3 January 2025]. Available from: https://www.ansys.com/products.

[307] Siemens Digital Industries Software, *STAR CCM+*. [Software]. [Accessed 17 March 2025]. Available from: https://plm.sw.siemens.com/en-US/simcenter/fluids-thermal-simulation/star-ccm/.

[308] Mirzaie, M., Lakzian, E., Khan, A., Warkiani, M. E., Mahian, O., and Ahmadi, G. COVID-19 spread in a classroom equipped with partition – A CFD approach. [Online]. *Journal of Hazardous Materials*. 2021, **420**, article no: 126587 [no pagination]. [Accessed 21 January 2025]. Available from: https://doi.org/10.1016/j.jhazmat.2021.126587.

[309] Abuhegazy, M., Talaat, K., Anderoglu, O., and Poroseva, S. V. Numerical investigation of aerosol transport in a classroom with relevance to COVID-19. [Online]. *Physics of Fluids*. 2020, **32**(10), article no: 103311 [no pagination]. [Accessed 3 March 2025]. Available from: https://doi.org/10.1063/5.0029118.

[310] Foster, A. and Kinzel, M. Estimating COVID-19 exposure in a classroom setting: A comparison between mathematical and numerical models. [Online]. *Physics of Fluids*. 2021, **33**(2), article no: 021904 [no pagination]. [Accessed 17 March 2025]. Available from: https://doi.org/10.1063/5.0040755.

[311] Pei, G., Azimi, P., Rim, D., and Allen, J. G. A CFD study on the effect of portable air cleaner placement on airborne infection control in a classroom. [Online]. *Environmental science. Processes & impacts*. 2024, **26**(9), pp.1476–1488. [Accessed 3 March 2025]. Available from: https://doi.org/10.1039/d4em00114a.

[312] Firatoglu, Z. A. The effect of natural ventilation on airborne transmission of the COVID-19 virus spread by sneezing in the classroom. [Online]. *The Science of the Total Environment*. 2023, **896**, article no: 165113 [no pagination]. [Accessed 17 March 2025]. Available from: https://doi.org/10.1016/j.scitotenv.2023.165113.

[313] ElShimi, M., Morcos, S. M., Mostafa, G. M., Khalil, E. E., El-Hariry, G. A., and ElDegwy, A. A novel transparent cabin used in the classroom during the coronavirus pandemic: a CFD analysis. [Online]. *Journal of Engineering and Applied Science*. 2024, **71**(1), article no: 19 [no pagination]. [Accessed 3 March 2025]. Available from: https://doi.org/10.1186/s44147-023-00316-3.

[314] Yan, W., Zhang, Y., Sun, Y., and Li, D. Experimental and CFD study of unsteady airborne pollutant transport within an aircraft cabin mock-up. [Online]. *Building and Environment*. 2009, **44**(1), pp.34–43. [Accessed 3 March 2025]. Available from: https://doi.org/10.1016/j.buildenv.2008.01.010.

[315] Webner, F., Shishkin, A., Schmeling, D., and Wagner, C. A Direct Infection Risk Model for CFD Predictions and Its Application to SARS-CoV-2 Aircraft Cabin Transmission. [Online]. *Indoor Air*. 2024, **2024**(1), article no: 9927275 [no pagination]. [Accessed 3 March 2025]. Available from: https://doi.org/10.1155/2024/9927275.

[316] Zee, M., Davis, A. C., Clark, A. D., Wu, T., Jones, S. P., Waite, L. L., Cummins, J. J., and Olson, N. A. Computational fluid dynamics modeling of cough transport in an aircraft cabin. [Online]. *Scientific Reports*. 2021, **11**(1), article no: 23329 [no pagination]. [Accessed 3 March 2025]. Available from: https://doi.org/10.1038/s41598-021-02663-8.

[317] ANSYS, Inc. *ANSYS Fluent Theory Guide*. [Online]. 2021. [Accessed 22 January 2025]. Available from: https://www.afs.enea.it/project/neptunius/docs/fluent/html/th/main_pre.htm.

[318] Ge, X., Wang, H., Liu, S., Li, Z., Tong, X., and Pu, J. Application of Fibonacci Sequence and Lucas Sequence on the Design of the Toilet Siphon Pipe Shape. [Online]. *Journal of Engineering and Technological Sciences*. 2019, **51**(4), pp.463–478. [Accessed 18 February 2025]. Available from: https://doi.org/10.5614/j.eng.technol.sci.2019.51.4.2.

[319] Li, Z., Ge, X., Li, K., and Tong, X. Siphon pipe parameter optimization of the toilet using CFD-DEM coupling method. [Online]. *International Journal of Numerical Methods for Calculation and Design in Engineering*. 2021, **37**(1). [Accessed 18 February 2025]. Available from: https://doi.org/10.23967/j.rimni.2020.10.003.

[320] Yang, S., Zhang, Y., Hemida, H., Wang, Y., and Ren, D. Flow Field Simulation Analysis of Train Siphon Toilet with Variable Pipe Diameter Based on the Investigation of Siphon Performance. [Online]. *Journal of Physics: Conference Series*. 2020, **1626**(1), p.012099. [Accessed 18 February 2025]. Available from: https://doi.org/10.1088/1742-6596/1626/1/012099.

[321] Wang, Y., Xiu, G., and Tan, H. CAD and CAE Analysis for Siphon Jet Toilet. [Online]. *Physics Procedia*. 2011, **19**, pp.472–476. [Accessed 3 March 2025]. Available from: https://doi.org/10.1016/j.phpro.2011.06.194.

[322] Wu, S.-C., Guo, M.-Y., Wang, J.-X., Yao, S., Chen, J., and Li, Y.-y. Liquid-curtain-based strategy to restrain plume during flushing. [Online]. *Physics of*

Fluids. 2020, **32**(11), article no: 111707 [no pagination]. [Accessed 11 February 2025]. Available from: https://doi.org/10.1063/5.0033836.

[323] Wan, J., Wei, J., Lin, Y., and Zhang, T. Numerical Investigation of Bioaerosol Transport in a Compact Lavatory. [Online]. *Buildings*. 2021, **11**(11), article no: 526 [no pagination]. [Accessed 22 January 2025]. Available from: https://doi.org/10.3390/buildings11110526.

[324] Li, P., Liu, W., and Zhang, T. T. CFD modeling of dynamic airflow and particle transmission in an aircraft lavatory. [Online]. *Building Simulation*. 2023, **16**(8), pp.1375–1390. [Accessed 18 February 2025]. Available from: https://doi.org/10.1007/s12273-023-1031-3.

[325] COMSOL, Inc., *COMSOL*. [Software]. 2024. [Accessed 17 March 2025]. Available from: https://www.comsol.com/.

[326] Liu, H., Zhang, Z., Zhang, Y., and Zhou, X. Impact of ventilation efficiency on restraining hazardous toilet plume post-flushing in indoor environments. [Online]. *Indoor and Built Environment*. 2024, **33**(10), pp.1897–1911. [Accessed 21 January 2025]. Available from: https://doi.org/10.1177/1420326X241262650.

[327] Ho, M. S., Glass, R. I., Monroe, S. S., Madore, H. P., Stine, S., Pinsky, P. F., Cubitt, D., Ashley, C., and Caul, E. O. Viral gastroenteritis aboard a cruise ship. [Online]. *Lancet (London, England)*. 1989, **2**(8669), pp.961–965. [Accessed 17 March 2025]. Available from: https://doi.org/10.1016/s0140-6736(89)90964-1.

[328] Widdowson, M.-A., Glass, R., Monroe, S., Beard, R. S., Bateman, J. W., Lurie, P., and Johnson, C. Probable Transmission of Norovirus on an Airplane. [Online]. *JAMA*. 2005, **293**(15), pp.1855–1860. [Accessed 15 January 2025]. Available from: https://doi.org/10.1001/jama.293.15.1859.

[329] National Research Council (US) Subcommittee on Microbiological Criteria. *An Evaluation of the Role of Microbiological Criteria for Foods and Food Ingredients*. [Online]. National Academies Press, 1985. [Accessed 24 February 2025]. Available from: https://doi.org/10.17226/372.

[330] Percival, S. L., Yates, M. V., Williams, D. D., Chalmers, R., and Gray, N. *Microbiology of Waterborne Diseases: Microbiological Aspects and Risks*. [Online]. 2nd ed. Elsevier, 2014. [Accessed 17 March 2025]. Available from: https://doi.org/10.1016/C2010-0-67101-X.

[331] Seidman, L., Kraus, M., Brandner, D., and Mowery, J. *Laboratory Manual for Biotechnology and Laboratory Science*. [Online]. CRC Press, 2022. [Accessed 17 March 2025]. Available from: https://doi.org/10.1201/9781003360742.

[332] Noakes, C. J., Fletcher, L. A., Sleigh, P. A., Booth, W. B., Beato-Arribas, B., and Tomlinson, N., Comparison of tracer techniques for evaluating the behaviour of bioaerosols in hospital isolation rooms. In Proceedings of the Healthy Buildings, Kuala Lumpur, Malaysia, 13–17 September 2009. In: *9th International Conference and Exhibition on Healthy Buildings 2009, 13 - 17 September 2009, Syracuse*. [Online]. ISIAQ, 2009, pp.1642–1645. [Accessed 17 March 2025]. Available from: https://www.proceedings.com/17570.html.

[333] King, M.-F., Camargo-Valero, M., Matamoros-Veloza, A., Sleigh, P., and Noakes, C. J. An Effective Surrogate Tracer Technique for S. aureus Bioaerosols in a Mechanically Ventilated Hospital Room Replica Using Dilute Aqueous Lithium Chloride. [Online]. *Atmosphere*. 2017, **8**(12), article no: 238 [no pagination]. [Accessed 23 May 2024]. Available from: https://doi.org/10.3390/atmos8120238.

[334] Huang, H.-L., Lee, M.-K., and Shih, H.-W. Assessment of Indoor Bioaerosols in Public Spaces by Real-Time Measured Airborne Particles. [Online]. *Aerosol and Air Quality Research*. 2017, **17**(9), pp.2276–2288. [Accessed 24 February 2025]. Available from: https://doi.org/10.4209/aaqr.2017.02.0089.

[335] Božić, J., Ilić, P., and Ilić, S. Indoor Air Quality in the Hospital: The Influence of Heating, Ventilating and Conditioning Systems. [Online]. *Brazilian Archives of Biology and Technology*. 2019, **62**, article no: p.e19180295 [no pagination]. [Accessed 24 February 2025]. Available from: https://doi.org/https://doi.org/10.1590/1678-4324-2019180295.

[336] Boone, S. A., Ijaz, M. K., McKinney, J., and Gerba, C. P. Resuspension and Dissemination of MS2 Virus from Flooring After Human Activities in Built Environment: Impact of Dust Particles. [Online]. *Microorganisms*. 2024, **12**(12), article no: 2564 [no pagination]. [Accessed 31 January 2025]. Available from: https://doi.org/10.3390/microorganisms12122564.

[337] Wanger, A., Chavez, V., Huang, R. S. P., Wahed, A., Actor, J. K., and Dasgupta, A. Media for the Clinical Microbiology Laboratory. In: Wanger, A., Chavez, V., Huang, R. S. P., Wahed, A., Actor, J. K., and Dasgupta, A., eds. *Microbiology and Molecular Diagnosis in Pathology*. [Online]. Elsevier, 2017, pp.51–60. [Accessed 17 March 2025]. Available from: https://doi.org/10.1016/b978-0-12-805351-5.00004-1.

[338] Hiwar, W., Kharrufa, H., King, M.-F., Salman, N., Fletcher, L., and Noakes, C., Multiplate air passive sampler to measure deposition rate of airborne microorganisms over time. In: *16th Conference of the International Society of Indoor Air Quality & Climate, 1 - 5 November 2020, Online*. [Online]. ISIAQ, 2021, pp.708–713. [Accessed 17 March 2025]. Available from: https://www.proceedings.com/57711.html.

[339] Hiwar, W., King, M.-F., Kharrufa, H., Tidswell, E., Fletcher, L. A., and Noakes, C. J. The impact of ventilation rate on reducing the microorganisms load in the air and on surfaces in a room-sized chamber. [Online]. *Indoor Air*. 2022, **32**(11), article no: e13161 [no pagination]. [Accessed 20 February 2025]. Available from: https://doi.org/10.1111/ina.13161.

[340] Hathway, A., Sleigh, A., and Noakes, C., CFD modelling of transient pathogen release in indoor environments due to human activity. In: *International Conference on Room Air Distribution RoomVent 2007, 13 - 15 June 2007, Finland*. [Online]. FINVAC, 2007. [Accessed 17 March 2025]. Available from: https://eprints.whiterose.ac.uk/7699/1/Hathway_Roomvent07.pdf.

[341] NHS England. *Health Technical Memorandum 03-01: Specialised ventilation for healthcare premises*. [Online]. 2021. [Accessed 17 March 2025]. Available from: https://www.england.nhs.uk/publication/specialised-ventilation-for-healthcare-buildings/.

[342] Cantium Scientific. *Correction of sample counts*. [Online]. [Accessed 7 March 2025]. Available from: https://confluence.external-share.com/content/685314/countcorrection.

[343] The British Standards Institution. *BS 6465-2:2017: Sanitary installations: Space recommendations. Code of practice*. [Online]. 2017. [Accessed 17 March 2025]. Available from: https://knowledge.bsigroup.com/products/sanitary-installations-space-recommendations-code-of-practice.

[344] R Foundation for Statistical Computing, *R: A Language and Environment for Statistical Computing*. [Software]. 2023. [Accessed 17 March 2025]. Available from: https://www.R-project.org/.

[345] Schmid-Hempel, P. and Frank, S. A. Pathogenesis, Virulence, and Infective Dose. [Online]. *PLoS Pathogens*. 2007, **3**(10), article no: e147 [no pagination]. [Accessed 23 February 2025]. Available from: https://doi.org/10.1371/journal.ppat.0030147.

[346] Ramlal, P. S., Lin, J., Buckley, C. A., Stenström, T. A., and Amoah, I. D. An assessment of the health risks associated with shared sanitation: a case study of the community ablution blocks in Durban, South Africa. [Online]. *Environmental Monitoring and Assessment*. 2022, **194**(3), article no: 166 [no pagination]. [Accessed 23 February 2025]. Available from: https://doi.org/10.1007/s10661-022-09815-x.

[347] Higham, C. A., López-García, M., Noakes, C. J., Tidswell, E., and Fletcher, L. A Quantitative Microbial Risk Assessment (QMRA) framework for exposure from toilet flushing using experimental aerosol concentration measurements. [Online]. *Indoor Environments*. 2025, **2**(1), article no: 100069 [no pagination].

[Accessed 10 March 2025]. Available from: https://doi.org/10.1016/j.indenv.2024.100069.

[348] Rawls, S. K. *Restroom usage in selected public buildings and facilities: a comparison of females and males*. Ph.D thesis. Virginia Polytechnic Institute and State University, 1988.

[349] Gwynne, S. M. V., Hunt, A. L. E., Thomas, J. R., Thompson, A. J. L., and Séguin, L. The toilet paper: Bathroom dwell time observations at an airport. [Online]. *Journal of Building Engineering*. 2019, **24**, article no: 100751 [no pagination]. [Accessed 21 May 2024]. Available from: https://doi.org/10.1016/j.jobe.2019.100751.

[350] Baillie, M. A., Fraser, S., and Brown, M. J. Do women spend more time in the restroom than men? [Online]. *Psychological Reports*. 2009, **105**(3), pp.789–790. [Accessed 8 September 2024]. Available from: https://doi.org/10.2466/PR0.105.3.789-790.

[351] Johnson, H. D., Sholcosky, D., Gabello, K., Ragni, R., and Ogonosky, N. Sex Differences in Public Restroom Handwashing Behavior Associated with Visual Behavior Prompts. [Online]. *Perceptual and Motor Skills*. 2003, **97**(3), pp.805–810. [Accessed 15 May 2024].

[352] Davidson, P. J. and Courtney, R. G. Revised scales for sanitary accommodation in offices. [Online]. *Building and Environment*. 1976, **11**(1), pp.51–56. [Accessed 3 January 2024]. Available from: https://doi.org/10.1016/0360-1323(76)90019-6.

[353] Miura, F., Kitajima, M., and Omori, R. Duration of SARS-CoV-2 viral shedding in faeces as a parameter for wastewater-based epidemiology: Re-analysis of patient data using a shedding dynamics model. [Online]. *Science of The Total Environment*. 2021, **769**, article no: 144549 [no pagination]. [Accessed 20 November 2024]. Available from: https://doi.org/10.1016/j.scitotenv.2020.144549.

[354] U.S. Environmental Protection Agency, Washington, DC. *Exposure Factors Handbook 2011 Edition (Final Report)*. [Online]. 2011. [Accessed 17 March 2025]. Available from: https://cfpub.epa.gov/ncea/risk/recordisplay.cfm?deid=236252.

[355] Wilson, A. M., Canter, K., Abney, S. E., Gerba, C. P., Myers, E. R., Hanlin, J., and Reynolds, K. A. An application for relating Legionella shower water monitoring results to estimated health outcomes. [Online]. *Water Research*. 2022, **221**, article no: 118812 [no pagination]. [Accessed 4 January 2024]. Available from: https://doi.org/10.1016/j.watres.2022.118812.

[356] McBride, G. B., Stott, R., Miller, W., Bambic, D., and Wuertz, S. Discharge-based QMRA for estimation of public health risks from exposure to stormwater-borne pathogens in recreational waters in the United States. [Online]. *Water Research*. 2013, **47**(14), pp.5282–5297. [Accessed 17 March 2025]. Available from: https://doi.org/10.1016/j.watres.2013.06.001.

[357] McBride, G. B. *Using Statistical Methods for Water Quality Management: Issues, Problems and Solutions*. [Online]. Wiley, 2005. [Accessed 17 March 2025]. Available from: https://doi.org/10.1002/0471733199.

[358] Pitol, A. K. and Julian, T. R. Community Transmission of SARS-CoV-2 by Surfaces: Risks and Risk Reduction Strategies. [Online]. *Environmental Science & Technology Letters*. 2021, **8**(3), pp.263–269. [Accessed 25 January 2024]. Available from: https://doi.org/10.1021/acs.estlett.0c00966.

[359] Black, R. E., Levine, M. M., Clements, M. L., Cisneros, L., and Daya, V. Treatment of Experimentally Induced Enterotoxigenic Escherichia coli Diarrhea with Trimethoprim, Trimethoprim-Sulfamethoxazole, or Placebo. [Online]. *Reviews of Infectious Diseases*. 1982, **4**(2), pp.540–545. [Accessed 11 January 2024]. Available from: https://doi.org/10.1093/clinids/4.2.540.

[360] Božič, A. and Kanduč, M. Relative humidity in droplet and airborne transmission of disease. [Online]. *Journal of Biological Physics*. 2021, **47**(1), pp.1–29. [Accessed 31 January 2024]. Available from: https://doi.org/10.1007/s10867-020-09562-5.

[361] Wang, C. C., Prather, K. A., Sznitman, J., Jimenez, J. L., Lakdawala, S. S., Tufekci, Z., and Marr, L. C. Airborne transmission of respiratory viruses. [Online]. *Science*. 2021, **373**(6558), article no: eabd9149 [no pagination]. [Accessed 23 May 2024]. Available from: https://doi.org/10.1126/science.abd9149.

[362] Haas, C. N. Action Levels for SARS-CoV-2 in Air: Preliminary Approach. [Online]. *Risk Analysis*. 2021, **41**(5), pp.705–709. [Accessed 17 March 2025]. Available from: https://doi.org/10.1111/risa.13728.

[363] Van Abel, N., Schoen, M. E., Kissel, J. C., and Meschke, J. S. Comparison of Risk Predicted by Multiple Norovirus Dose Response Models and Implications for Quantitative Microbial Risk Assessment. [Online]. *Risk Analysis*. 2017, **37**(2), pp.245–264. [Accessed 29 April 2024]. Available from: https://doi.org/10.1111/risa.12616.

[364] Viau, E., Bibby, K., Paez-Rubio, T., and Peccia, J. Toward a Consensus View on the Infectious Risks Associated with Land Application of Sewage Sludge. [Online]. *Environmental Science & Technology*. 2011, **45**(13), pp.5459–5469.

[Accessed 27 November 2024]. Available from: https://doi.org/10.1021/es200566f.

[365] Adhikari, U., Esfahanian, E., Mitchell, J., Charbonneau, D., Song, X., and Lu, Y. Quantitation of Risk Reduction of E. coli Transmission after Using Antimicrobial Hand Soap. [Online]. *Pathogens*. 2020, **9**(10), article no: 778 [no pagination]. [Accessed 17 January 2025]. Available from: https://doi.org/10.3390/pathogens9100778.

[366] Nag, R., Monahan, C., Whyte, P., Markey, B. K., O'Flaherty, V., Bolton, D., Fenton, O., Richards, K. G., and Cummins, E. Risk assessment of *Escherichia coli* in bioaerosols generated following land application of farmyard slurry. [Online]. *Science of The Total Environment*. 2021, **791**, article no: 148189 [no pagination]. [Accessed 17 January 2025]. Available from: https://doi.org/10.1016/j.scitotenv.2021.148189.

[367] Shi, K.-W., Wang, C.-W., and Jiang, S. C. Quantitative microbial risk assessment of Greywater on-site reuse. [Online]. *The Science of the Total Environment*. 2018, **635**, pp.1507–1519. [Accessed 17 March 2025]. Available from: https://doi.org/10.1016/j.scitotenv.2018.04.197.

[368] Nam, G. W., Jeong, M., Heo, E. J., Chang, O. K., Kim, M.-G., Kwak, H.-S., and Suh, S. H. Quantitative microbial risk assessment of pathogenic Escherichia coli in commercial kimchi in South Korea. [Online]. *Food Science and Biotechnology*. 2021, **30**(11), pp.1455–1464. [Accessed 17 March 2025]. Available from: https://doi.org/10.1007/s10068-021-00997-7.

[369] Wilson, A. M., Weir, M. H., Bloomfield, S. F., Scott, E. A., and Reynolds, K. A. Modeling COVID-19 infection risks for a single hand-to-fomite scenario and potential risk reductions offered by surface disinfection. [Online]. *American Journal of Infection Control*. 2021, **49**(6), pp.846–848. [Accessed 20 January 2025]. Available from: https://doi.org/10.1016/j.ajic.2020.11.013.

[370] Verbyla, M. E., Pitol, A. K., Navab-Daneshmand, T., Marks, S. J., and Julian, T. R. Safely Managed Hygiene: A Risk-Based Assessment of Handwashing Water Quality. [Online]. *Environmental Science & Technology*. 2019, **53**(5), pp.2852–2861. [Accessed 20 January 2025]. Available from: https://doi.org/10.1021/acs.est.8b06156.

[371] Pillay, K., Marr, L. C., Henriques, A., Martin, A. R., Prussin, A. J., Aleixo, L., Andreini, M., Mounet, N., Finlay, W. H., and Tang, J. W. Can we use viral receptor mapping and particle deposition models to predict the clinical severity of novel airborne pathogens? [Online]. *Clinical Microbiology and Infection*. 2024, **0**(0), pp.P503–505. [Accessed 27 November 2024]. Available from: https://doi.org/10.1016/j.cmi.2024.11.005.

[372] Azimi, P., Keshavarz, Z., Cedeno Laurent, J. G., Stephens, B., and Allen, J. G. Mechanistic transmission modeling of COVID-19 on the Diamond Princess cruise ship demonstrates the importance of aerosol transmission. [Online]. *Proceedings of the National Academy of Sciences of the United States of America*. 2021, **118**(8), article no: e2015482118 [no pagination]. [Accessed 17 March 2025]. Available from: https://doi.org/10.1073/pnas.2015482118.

[373] Lei, H., Li, Y., Xiao, S., Lin, C.-H., Norris, S. L., Wei, D., Hu, Z., and Ji, S. Routes of transmission of influenza A H1N1, SARS CoV, and norovirus in air cabin: Comparative analyses. [Online]. *Indoor Air*. 2018, **28**(3), pp.394–403. [Accessed 17 March 2025]. Available from: https://doi.org/10.1111/ina.12445.

[374] Kolli, A. R., Semren, T. Z., Bovard, D., Majeed, S., Toorn, M. van der, Scheuner, S., Guy, P. A., Kuczaj, A., Mazurov, A., Frentzel, S., Calvino-Martin, F., Ivanov, N. V., O'Mullane, J., Peitsch, M. C., and Hoeng, J. Pulmonary Delivery of Aerosolized Chloroquine and Hydroxychloroquine to Treat COVID-19: In Vitro Experimentation to Human Dosing Predictions. [Online]. *The AAPS Journal*. 2022, **24**(1), article no: 33 [no pagination]. [Accessed 27 November 2024]. Available from: https://doi.org/10.1208/s12248-021-00666-x.

[375] Olsen, M., Lohning, A., Campos, M., Jones, P., McKirdy, S., Alghafri, R., and Tajouri, L. Mobile phones of paediatric hospital staff are never cleaned and commonly used in toilets with implications for healthcare nosocomial diseases. [Online]. *Scientific Reports*. 2021, **11**(1), article no: 12999 [no pagination]. [Accessed 21 May 2024]. Available from: https://doi.org/10.1038/s41598-021-92360-3.

[376] Zhi-wei, P. Optimized design of the toilet siphon pipeline based on CFD flow-field analysis. [Online]. *Mechanics in Engineering*. 2007. [Accessed 18 February 2025].

[377] ANSYS, Inc., *ANSYS DesignModeler* (version 2023 R2). [Software]. 2023. [Accessed 17 March 2025]. Available from: https://www.ansys.com/products.

[378] Khoa, N. D., Li, S., Phuong, N. L., Kuga, K., Yabuuchi, H., Kan-O, K., Matsumoto, K., and Ito, K. Computational fluid-particle dynamics modeling of ultrafine to coarse particles deposition in the human respiratory system, down to the terminal bronchiole. [Online]. *Computer Methods and Programs in Biomedicine*. 2023, **237**, article no: 107589 [no pagination]. [Accessed 21 January 2025]. Available from: https://doi.org/10.1016/j.cmpb.2023.107589.

[379] Zore, K., Sasanapuri, B., Parkhi, G., and Varghese, A., Ansys mosaic poly-hexcore mesh for high-lift aircraft configuration. In: *21st AeSI Annual CFD Symposium, 8 - 9 August 2019, Bangalore*. [Online]. 2019. [Accessed 17 February 2025]. Available from: https://www.nal.res.in/themes/stark/cfdimgs/FullPaper/P41-ANSYS-Mosaic-Poly-Hexcore-Mesh-For-High-Lift-Aircraft-Configuration.pdf.

[380] Karami, S., Lakzian, E., and Ahmadi, G. Prediction of COVID-19 infection in dental clinic by CFD and Wells-Riley model, identifying safe area and proper ventilation velocity. [Online]. *International Journal of Refrigeration*. 2023, **151**, pp.112–124. [Accessed 21 January 2025]. Available from: https://doi.org/10.1016/j.ijrefrig.2023.03.013.

[381] Salati, H., Fletcher, D. F., Khamooshi, M., Dong, J., Ito, K., Vahaji, S., and Inthavong, K. Exhaled Jet and Viral-Laden Aerosol Transport from Nasal Sneezing. [Online]. *Aerosol and Air Quality Research*. 2022, **22**(4), article no: 210338 [no pagination]. [Accessed 21 January 2025]. Available from: https://doi.org/10.4209/aaqr.210338.

[382] Rahvard, A. J., Karami, S., and Lakzian, E. Finding the proper position of supply and return registers of air condition system in a conference hall in term of COVID-19 virus spread. [Online]. *International Journal of Refrigeration*. 2023, **145**, pp.78–89. [Accessed 21 January 2025]. Available from: https://doi.org/10.1016/j.ijrefrig.2022.10.010.

[383] Khodadadi, R., Pournasr, A., Hataysal, E., and Tabarra, M., Investigation of Airborne Particle Spread in an Underground Station. In: *19th International Symposium on Aerodynamics, Ventilation & Fire in Tunnels, 18 September 2022, Brighton*. [Online]. 2022. [Accessed 15 March 2025]. Available from: https://www.researchgate.net/publication/364309671_Investigation_of_Airborne_Particle_Spread_in_an_Underground_Station.

[384] Menter, F. R. Two-equation eddy-viscosity turbulence models for engineering applications. [Online]. *AIAA Journal*. 1994, **32**(8), pp.1598–1605. [Accessed 13 February 2025]. Available from: https://doi.org/10.2514/3.12149.

[385] Stamou, A. and Katsiris, I. Verification of a CFD model for indoor airflow and heat transfer. [Online]. *Building and Environment*. 2006, **41**(9), pp.1171–1181. [Accessed 14 January 2025]. Available from: https://doi.org/10.1016/j.buildenv.2005.06.029.

[386] Sheikhnejad, Y., Aghamolaei, R., Fallahpour, M., Motamedi, H., Moshfeghi, M., Mirzaei, P. A., and Bordbar, H. Airborne and aerosol pathogen transmission modeling of respiratory events in buildings: An overview of computational fluid dynamics. [Online]. *Sustainable Cities and Society*. 2022, **79**,

article no: 103704 [no pagination]. [Accessed 14 January 2025]. Available from: https://doi.org/10.1016/j.scs.2022.103704.

[387] Gilani, S., Montazeri, H., and Blocken, B. CFD simulation of stratified indoor environment in displacement ventilation: Validation and sensitivity analysis. [Online]. *Building and Environment*. 2016, **95**, pp.299–313. [Accessed 14 January 2025]. Available from: https://doi.org/10.1016/j.buildenv.2015.09.010.

[388] Zhang, T., Lee, K., and Chen, Q. A simplified approach to describe complex diffusers in displacement ventilation for CFD simulations. [Online]. *Indoor Air*. 2009, **19**(3), pp.255–267. [Accessed 14 January 2025]. Available from: https://doi.org/10.1111/j.1600-0668.2009.00590.x.

[389] Zhai, Z. J., Zhang, Z., Zhang, W., and Chen, Q. Y. Evaluation of Various Turbulence Models in Predicting Airflow and Turbulence in Enclosed Environments by CFD: Part 1 - Summary of Prevalent Turbulence Models. [Online]. *HVAC&R Research*. 2007, **13**(6), pp.853–870. [Accessed 14 January 2025]. Available from: https://doi.org/10.1080/10789669.2007.10391459.

[390] Hussain, S. and Oosthuizen, P. H. Validation of numerical modeling of conditions in an atrium space with a hybrid ventilation system. [Online]. *Building and Environment*. 2012, **52**, pp.152–161. [Accessed 14 January 2025]. Available from: https://doi.org/10.1016/j.buildenv.2011.12.016.

[391] Hussain, S., Oosthuizen, P. H., and Kalendar, A. Evaluation of various turbulence models for the prediction of the airflow and temperature distributions in atria. [Online]. *Energy and Buildings*. 2012, **48**, pp.18–28. [Accessed 14 January 2025]. Available from: https://doi.org/10.1016/j.enbuild.2012.01.004.

[392] Graham, D. I. and Moyeed, R. A. How many particles for my Lagrangian simulations? [Online]. *Powder Technology*. 2002, **125**(2), pp.179–186. [Accessed 24 January 2025]. Available from: https://doi.org/10.1016/S0032-5910(01)00504-6.

[393] ANSYS, Inc., *ANSYS CFD-Post* (version 2023 R2). [Software]. 2023. [Accessed 17 March 2025]. Available from: https://www.ansys.com/products.

[394] Pantelic, J. and Tham, K. W. Adequacy of air change rate as the sole indicator of an air distribution system's effectiveness to mitigate airborne infectious disease transmission caused by a cough release in the room with overhead mixing ventilation: A case study. [Online]. *HVAC&R Research*. 2013, **19**(8), pp.947–961. [Accessed 17 March 2025]. Available from: https://doi.org/10.1080/10789669.2013.842447.

[395] Hathway, A., Papakonstantis, I., Bruce-Konuah, A., and Brevis, W. Experimental and Modelling Investigations of Air Exchange and Infection Transfer due to Hinged-Door Motion in Office and Hospital Settings. [Online]. *International Journal of Ventilation*. 2015, **14**(2), pp.127–140. [Accessed 19 February 2025]. Available from: https://doi.org/10.1080/14733315.2015.11684075.

[396] Wilson, D. J. and Kiel, D. E. Gravity driven counterflow through an open door in a sealed room. [Online]. *Building and Environment*. 1990, **25**(4), pp.379–388. [Accessed 19 February 2025]. Available from: https://doi.org/10.1016/0360-1323(90)90012-G.